

**DEVELOPMENT OF FERRITIC ROLLING
PROCESS FOR THE PRODUCTION OF
INTERSTITIAL FREE AUTOMOTIVE
STEEL**

Thesis

**Submitted in partial fulfilment of the requirements for the degree of
DOCTOR OF PHILOSOPHY**

by

D. SATISH KUMAR



**DEPARTMENT OF METALLURGICAL AND
MATERIALS ENGINEERING
NATIONAL INSTITUTE OF TECHNOLOGY KARNATAKA,
SURATHKAL, MANGALORE -575025
JULY – 2022**

**DEVELOPMENT OF FERRITIC ROLLING
PROCESS FOR THE PRODUCTION OF
INTERSTITIAL FREE AUTOMOTIVE
STEEL**

Thesis

**Submitted in partial fulfilment of the requirements for the degree of
DOCTOR OF PHILOSOPHY**

by

D. SATISH KUMAR

(Registration Number: 177046MT500)

**Under the Guidance of
Dr. UDAYA BHAT K
&
Dr. S MANJINI**



**DEPARTMENT OF METALLURGICAL AND
MATERIALS ENGINEERING
NATIONAL INSTITUTE OF TECHNOLOGY KARNATAKA,
SURATHKAL, MANGALORE -575025
JULY – 2022**

DECLARATION

I hereby declare that the Research Thesis entitled **DEVELOPMENT OF FERRITIC ROLLING PROCESS FOR THE PRODUCTION OF INTERSTITIAL FREE AUTOMOTIVE STEEL**, which is being submitted to the National Institute of Technology Karnataka, Surathkal in partial fulfilment of the requirements for the award of the Degree of Doctor of Philosophy in Metallurgical and Materials Engineering, is a bonafide report of the research work carried out by me. The material contained in this Research Thesis has not been submitted to any University or Institution for the award of any degree.



D. Satish Kumar

Registration No - 177046-177MT500

Department of Metallurgical and Materials Engineering

Place: NITK-Surathkal

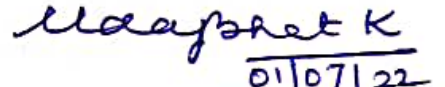
Date: 01/07/2022

CERTIFICATE

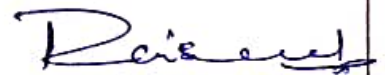
This is to *certify* that the Research Thesis entitled **DEVELOPMENT OF FERRITIC ROLLING PROCESS FOR THE PRODUCTION OF INTERSTITIAL FREE AUTOMOTIVE STEEL**, submitted by D. Satish Kumar, (Register Number: 177MT500) as the record of the research work carried out by him/her, is *accepted as the Research Thesis submission* in partial fulfilment of the requirements for the award of degree of Doctor of Philosophy.



Dr. S Manjini
AVP and Head R&D
JSW Steel Ltd.
Vijayanagar Works



01/07/22
Dr. Udaya Bhat K
Professor
Department of Metallurgical and
Materials Engineering
NITK Surathkal



Chairman - DRPC
Department of Metallurgical and Materials Engineering
NITK Surathkal

Chairman - DRPC
Dept. of Metallurgical and Materials Engineering
National Institute of Technology Karnataka, Surathkal
Post Srinivasnagar, Mangaluru - 575 025
Karnataka, India

ACKNOWLEDGEMENT

Firstly, I would like to express my sincere gratitude to my advisor Prof. Udaya Bhat K for the continuous support to my Ph.D study and related research. His patience, motivation, meticulous observations and immense knowledge, guided me to widen my research from various perspectives. My sincere thanks also go to Dr. Sambandam Manjini, who encouraged me to start the Ph.D through his initiatives at the work place and as co-guide, continued his guidance through insightful comments and encouragement at various stages of work.

Special thanks to Mr. P C Mahapatra, the very first person who wholeheartedly motivated and encouraged me to take-up the doctoral work.

I would also like to sincerely thank my thesis committee members Prof. Shashi Bhushan Arya and Prof. Srikant Bontha for their insightful comments, suggestions and encouragement.

I would like to profoundly thank the management of JSW Steel Ltd, Vijayanagar works, for the permission to carry the research work and use its facilities. I would also like to express my gratitude to my batchmates at NITK and colleagues of R&D at JSW Steel for their love and time, they bestowed with me during discussions, experimentation, testing and leisure. These moments are precious and will cherish all my life.

Last but not the least; I would like to thank my family for supporting me morally and spiritually throughout this PhD work and my life in general.

D. Satish Kumar

ABSTRACT

Interstitial free (IF) grade steels have high transformation temperatures and their production through austenitic rolling, often results in non-uniform rolling, shape defects and lower yields. As a solution, soft hot strip and hard hot strip produced through ferritic rolling is projected as a direct replacement to austenitic cold rolled sheets. However, it is not industrially adopted due to hot rolling thickness limitations and formability variations. In the present work a new intermediate approach, consisting of ferritic hot rolling and subsequent cold rolling and annealing in the existing mills is proposed. However, in this approach, the combination of hot rolling temperature, cold reduction and annealing parameters governs the final microstructure and, texture and hence parameters must be optimized. In this work, the new route was first simulated and optimized for a Ti-Nb interstitial free steel (IF steel) using a thermo-mechanical simulator and hot strip mill model (HSMM) at different operating regimes. The best two ferritic rolling regimes were validated in the industrial hot rolling, cold rolling and annealing mill. Metallurgical and mechanical properties were compared between the ferritic and austenitic regime rolled sheets at each stage for structure-property comparison. Key observation was the gradual transition of recrystallization mechanism from oriented nucleation to oriented growth with the decrease in temperature of deformation in the ferritic region which changed the formability behaviour of the rolled sheets. As formability is an important requirement in auto steels, application-specific formability characteristics such as fracture criterion, stretch-flangeability, deep drawability and stretch formability was studied through the formability limit diagram, hole expansion ratio, earing and Erichsen cupping tests, respectively. High temperature ferritic rolled sheets show improved formability in all tests with higher formability limits in uniaxial tension of FLD, due to better $\dot{\epsilon}$, higher n -value, low Δr and stronger gamma fibre maxima at $111\langle 121 \rangle$. Low temperature ferritic rolled sheets show the lowest Δr and reduced $\dot{\epsilon}$ but improved n -value and higher limits of biaxial tension in the FLD curve due to higher alpha fibre texture. Study established that high temperature ferritic rolled sheets are best suited for deep drawing and stretching applications whereas low temperature ferritic rolled sheets should be preferred for stretch forming applications. This intermediate route produced sheets have uniform and improved properties for all formability applications and lower cost due to reduced energy consumption. This new processing will help in the wider adoption of the ferritic rolling process on an industrial scale for developing high formability sheets in cold-rolled and annealed conditions.

Key words: IF steel, ferritic rolling, thermo-mechanical simulation, texture, formability

CONTENTS

List of Figures	iii
List of Tables	vii
List of Abbreviations	viii
Chapter 1: Introduction	1
1.1 Automotive Steels	2
1.2 Properties of Automotive Steels	3
1.3 Interstitial Free (IF) Steels	5
1.4 Composition and Processing of IF Steels	7
1.5 Issues in Producing IF Steels	10
1.6 Research Gaps	14
Chapter 2: Literature Review	15
2.1 Types of Ferritic Rolling	15
2.2 Studies on Various Aspects of Ferritic Rolling	16
2.3 Objectives of the Study	27
Chapter 3: Methodology and Work Steps	30
3.1 Base Material	30
3.2 Methodology	30
3.3 Work Steps	31
Chapter 4: Mathematical and Thermo-Mechanical Simulation	34
4.1 Selection of Hot Rolling Parameters for Ferritic Rolling	34
4.1.1 Measurement of transformation temperatures	35
4.1.2 Hot rolling simulation	41
4.1.3 HSMM (hot strip mill model) simulation	46
4.2 Selection of Continuous Annealing Parameters Through Simulation	47
Chapter 5: Experimentation and Plant Trials	51
5.1 Selection of Composition/Grade	51
5.2 Industrial Production of IF Steels	52
5.3 Steelmaking and Casting Process	53

5.4 Selection of Steelmaking Parameters for Ferritic Rolling	55
5.5 Hot Rolling Process	55
5.6 Ferritic Hot Rolling Plant Trials	57
5.7 Cold Rolling and Annealing Process	61
5.8 Selection of Cold Rolling Parameters	64
5.9 Cold Rolling and Annealing Plant Trials	66
Chapter 6: Formability Studies on Cold Rolled Sheets	69
6.1 Formability Limit Diagram	71
6.2 Hole Expansion Test	73
6.3 Earing Test	74
6.4 Erichsen Cupping Test	74
Chapter 7: Results and Discussion	76
7.1 Thermo-Mechanical Simulation Results	76
7.2 HSMM (Hot Strip Mill Model) Simulation Results	87
7.3 Plant Hot Rolling Results	87
7.4 Annealing Simulation Results	97
7.5 Plant Cold Rolling (Full Hard) Sheet Results	100
7.6 Continuous Annealed Sheet Results	104
7.7 Formability Study Results	112
Chapter 8: Conclusions	117
Publications from Present Work	121
References	122
Published Papers	

List of Figures

- Fig. 1.1. Steel making process
- Fig. 1.2. Steels used in a commercial vehicle
- Fig. 1.3. Application of IF steels in a vehicle (outer body and doors)
- Fig. 1.4. Comparison of transformation temperatures
- Fig. 1.5. Shape defects in IF steels
- Fig. 1.6. Shape and hole defects in cold rolled IF steels
- Fig. 1.7. Comparison of (a) conventional austenitic and (b) ferritic rolling
- Fig. 1.8. A_3 and A_1 temperature lines in Fe-Fe₃C diagram
- Fig. 2.1. Effect of strain rate and deformation temperature on the critical flow stress
- Fig. 2.2. 3D orientation Euler space at $\phi_2 = 45^\circ$ section (a) common indices (b) ODF of a cold rolled sheet
- Fig. 2.3. IF steel cold-rolling textures
- Fig. 2.4. ODF sections of austenitic rolled IF steel
- Fig. 2.5. ODF sections of ferritic rolled IF steel
- Fig. 2.6. Maximum intensity of three textures at different annealing temperatures
- Fig. 3.1. Sequence of project working steps
- Fig. 4.1. Schematic of a heat flux DSC set-up
- Fig. 4.2. Phase changes identified in IF steel through DSC instrument
- Fig. 4.3. Schematic representation of dilation measurement in Gleeble
- Fig. 4.4. Standard sample geometry in Gleeble for dilatometry
- Fig. 4.5. Experimental setup for dilation measurement in Gleeble
- Fig. 4.6. Dilation plot from Gleeble
- Fig. 4.7. Schematic temperature-time plots indicating simulation of a-austenitic rolling and b-ferritic rolling
- Fig. 4.8. Hot deformation simulation in the thermo-mechanical simulator
- Fig. 4.9. Effect of temperature on flow stress values measured in Gleeble
- Fig. 4.10. HSMM model mill configuration interface
- Fig. 4.11. Specimens for strip annealing simulations in Gleeble
- Fig. 4.12. Thermocouple arrangements during strip annealing simulations set-up in Gleeble
- Fig. 4.13. Simulated annealing cycles
- Fig. 4.14. Strip sample after annealing simulation in Gleeble

- Fig. 4.15. Tensile test specimen punched out and tested from the annealed sample
- Fig. 5.1. Process route for industrial production of the IF steels
- Fig. 5.2. RH-degasser snorkels
- Fig. 5.3. Continuous caster and casting process
- Fig. 5.4. Hot strip mill at JSW Steel, Vijayanagar works
- Fig. 5.5. Schematic of microstructure development during hot rolling
- Fig. 5.6. Reversing roughing mill
- Fig. 5.7. Finishing mill stand controlling strip thickness
- Fig. 5.8. Sampling locations on the coil
- Fig. 5.9. Markings for sample cutting on HR coil
- Fig. 5.10. Schematic of a tandem cold rolling mill
- Fig. 5.11. Cold rolling mill line at JSW steel
- Fig. 5.12. Continuous annealing line
- Fig. 5.13. Comparison of formability indicators
- Fig. 5.14. Variation of average plastic strain ratio with % reduction
- Fig. 5.15. Effect of cold rolling reduction on the r values of Ti, Ti+Nb, and Nb IF steels
- Fig. 5.16. Annealing cycle utilized for the experimental IF steel coils
- Fig. 6.1. Bulging press with 3D camera
- Fig. 6.2. Die and blank holder setup
- Fig. 6.3. Specimens before and after the FLD test
- Fig. 6.4. Sequence of operations in the hole expansion test
- Fig. 6.5. Typical earing behaviour in sheet metals
- Fig. 6.6. Erichsen cupping test
- Fig. 7.1. Variation in flow stress with extent of deformation in Gleeble for IF steels
- Fig. 7.2. Variation in peak flow stress with the extent of deformation in Gleeble for IF steels
- Fig. 7.3. Comparison of hardness on rolling simulated samples
- Fig. 7.4. Variation in grain morphology along with the thickness of the simulated samples
- Fig. 7.5. Microstructures at the centre portion of the simulated samples
- Fig. 7.6. Mechanism of nucleation and grain growth
- Fig. 7.7. Schematic illustration of important texture components for $\phi_2 = 45^\circ$ ODF sections in BCC material

- Fig. 7.8 Comparison of textures developed in rolling simulated samples
- Fig. 7.9. Comparison of residual stress at different locations as measured using Magnetic Barkhausen Emission technique in hot rolled sheets
- Fig. 7.10. Variation in grain morphology along the thickness in hot rolled sheets
- Fig. 7.11. Microstructures of austenitic and ferritic rolled samples in hot rolled sheets
- Fig. 7.12. Comparison of textures developed in austenitic and ferritic hot rolled sheets
- Fig. 7.13. Change in UTS with an increase in temperature in annealing simulated samples
- Fig. 7.14. Change in percentage elongation with an increase in temperature in annealing simulated samples
- Fig. 7.15. Comparison of microstructures and grain size of annealing simulated samples
- Fig. 7.16. Comparison of residual stresses at different locations as measured using Magnetic Barkhausen Emission technique
- Fig. 7.17. Comparison of microstructures of austenitic and ferritic rolled sheets after cold rolling
- Fig. 7.18. Comparison of textures of austenitic and ferritic rolled sheets after cold rolling
- Fig. 7.19. Comparison of residual stresses at different locations as measured using Magnetic Barkhausen Emission technique in cold-rolled and annealed sheets
- Fig. 7.20. Comparison of microstructures of austenitic and ferritic rolled sheets after cold rolling and annealing
- Fig. 7.21. Comparison of textures of austenitic and ferritic rolled sheets after cold rolling and annealing
- Fig. 7.22. Comparison of inverse pole Figure maps from EBSD analysis for austenitic and ferritic rolled sheets
- Fig.7.23. Comparison of grain boundary mis-orientation from EBSD analysis for austenitic and ferritic rolled sheets
- Fig. 7.24. Comparison of major and minor strains for austenitic and ferritic rolled sheets
- Fig. 7.25. Comparison of HER for austenitic and ferritic rolled sheets
- Fig. 7.26. Comparison of ear formation and average earing values for austenitic and ferritic rolled sheets

Fig. 7.27. Specimen after the cupping test

Fig. 7.28. Comparison of thickness variation after the test and Erichsen number values for austenitic and ferritic rolled sheets

List of Tables

- Table 1.1 Mechanical properties of a typical IF steel
- Table 1.2 Typical compositions of Ti-only and Ti-Nb IF steels
- Table 1.3 Typical processing parameters for IF steels
- Table 2.1 Properties of ferritic steel for drawing operation
- Table 3.1 Composition of the IF steel considered for the present study (in wt%)
- Table 3.2 List of the facilities/tools used
- Table 4.1 Comparison of phase change measuring techniques and its results
- Table 4.2 Effect of cooling rate on transformation temperatures of IF grade steel
- Table 5.1 Composition of selected IF grade slab, wt.%
- Table 5.2 Comparison of key hot rolling parameters
- Table 5.3 Comparison of rolling force in each stand (MPa) in hot strip mill
- Table 5.4 Comparison of cold rolling parameters
- Table 7.1 Comparison of process parameters and properties from the HSMM model
- Table 7.2 Comparison of mechanical properties of ferritic and austenitic hot rolled coils
- Table.7.3 Comparison of HSMM predicted and actual plant mechanical properties
- Table 7.4 Comparison of mechanical properties of austenitic and ferritic rolled samples in full hard condition
- Table 7.5. Comparison of mechanical properties of austenitic and ferritic rolled samples after cold rolling and annealing
- Table 7.6 Volume fractions of the three dominant fibres in austenitic and ferritic rolled samples

List of Abbreviations

BOS	-Basic oxygen furnace
EAF	-Electric arc furnace
HSS	-High strength steel
AHSS	-Advanced high strength steel
FLD	-Forming limit diagram
IF Steels	-Interstitial free steels
ELC	-Extra low carbon steels
AlN	-Aluminium nitride
SLA	-High strength low alloy
DDQ	-Deep drawing quality
SFE	-Stacking fault energy
DRX	-Dynamic recrystallization
CRCA	-Cold rolled close annealed
DSC	-Differential scanning calorimetry
HSMM	-Hot strip mill model software
ODF	-Orientation distribution function
ND	-Normal direction
RD	-Rolling direction
HET	-Hole expansion test
FT	-Finishing temperature
CT	-Coiling temperature
MBE	-Magnetic Barkhausen Emission
EBSD	-Electron back scattered diffractometer

CHAPTER 1

INTRODUCTION

Steel has been the most preferred engineering material since its invention and will continue to remain so in the absence of a sustainable alternative. Its variety and availability make it suitable for numerous uses in the domain of machinery, tools, buildings and public works, aeronautics, automotive, medical equipment, etc. contributing to the technological development of industrialized societies (Worldsteel 2011).

The steelmaking process involves two major steps, iron making (converting iron ore into molten iron) and steel making (refining molten iron to steel). Ironmaking involves the raw inputs of iron ore, coke, and lime being melted in a blast furnace. The resulting molten iron, also referred to as hot metal, still contains 4 to 4.5 percent carbon and other impurities (Dipak 2014). This makes it brittle and therefore carbon and impurities are subsequently removed in the primary steelmaking process. Primary steelmaking has two methods: BOS (Basic Oxygen Furnace) and the more modern EAF (Electric Arc Furnace) methods (Fruehan 1998). BOS methods add recycled steel scrap to the molten iron in a converter. At high temperatures, oxygen is blown through the metal, which reduces the carbon content to <0.1 wt%. EAF methods feed primarily recycled steel scrap and use high-power electric arcs to melt the metal, refine it and convert it into a high-quality steel. Secondary steelmaking or ladle refining involves treating the molten steel produced from both BOS and EAF routes to adjust the steel composition. This is done by adding or removing certain elements and/or manipulating the temperature and production environment (David 1999). De-gassing may also be carried out based on the final grade requirement. Molten steel of the desired composition is then sent to the caster for solidification. Continuous casting sees the molten steel cast into a water-cooled mould causing a thin steel shell to solidify. The partially solidified shell is withdrawn using guided rolls with water sprays, during which the cast is fully cooled and solidified. The solidified strand is cut into desired lengths depending on the application. Cast slabs are further rolled into final products in rolling mills. According to shape and dimensions, rolled steel products are classified as (i) flat products, and (ii) long products (Allan 2003). Flat products consist of plate products or sheet and strip products while the long products consist of sectional products like bar and rod. Slab casters are used for producing the slabs which are rolled into flat products in a hot strip mill. Flat products include slabs, hot-rolled coil, cold-rolled coil,

coated steel products, tinplate and heavy plate. They are used in automotive, heavy machinery, pipes and tubes, construction, packaging and appliances (Vladimir 2001). Billet or bloom casters are used for producing billets and blooms which are further rolled in a wire rod mill or bar mill to produce final long products. Long products include billets, blooms, rebars, wire rod, sections, rails, sheet piles and drawn wire. The main markets for these products are construction, mechanical engineering, energy and automotive sectors. The majority of steel applications is in flat form. The complete steel making process is schematically presented in Fig. 1.1 (Worldsteel 2011).

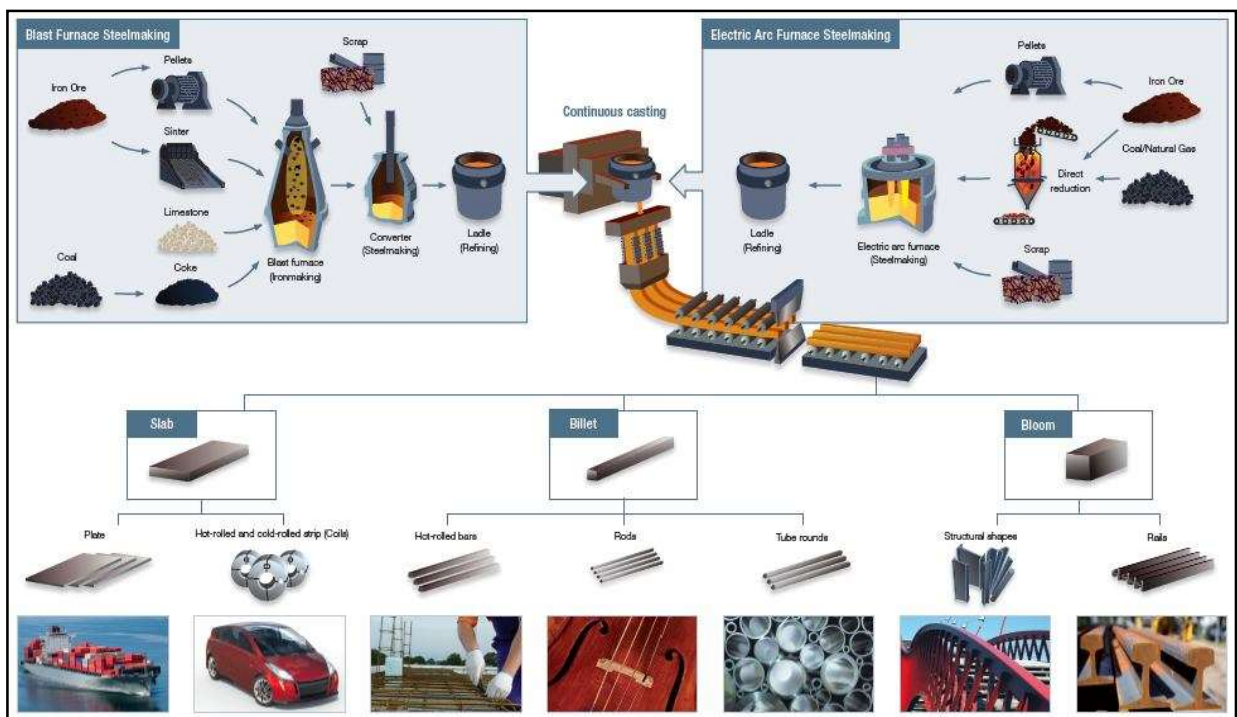


Fig. 1.1. Steelmaking process (Worldsteel 2011)

1.1 Automotive Steels

In recent times, major developments have been made in developing high strength steel in a flat-rolled category, especially in the automotive sector. Despite the emergence of new materials, steel continues to be the material of choice for auto makers with steel contributing to ~50-60% of the total raw material contained in an automobile (Manabu 2015). The automotive industry is always striving for improving fuel economy. One of the factors affecting fuel economy is vehicle weight. To reduce the weight of the auto body, the development of high strength automotive steel sheets has been the prime objective for the steel industry (Manabu 2015).

Automotive steels can be classified in several ways. One is a metallurgical designation where steels are classified as (i) low to high strength steels (i.e., interstitial free and mild steels), (ii) conventional high strength steels (HSS) (i.e., carbon-manganese, bake hardening and high strength low alloy steels), and (iii) the new advanced high strength steels -AHSS (i.e., dual-phase, transformation-induced plasticity, twinning-induced plasticity, ferritic-bainitic, complex phase and martensitic steels) (Miklós 2020). Additional higher strength steels for the automotive industry include hot-formed steels, post-forming heat-treated steels, and steels designed for unique applications that include improved edge stretch and stretch bending (World auto steel - AHSS guidelines 2017). The percentage of these steels being used in a commercial vehicle is shown in Fig. 1.2 (Hardy 2007). Mild steels, bake hardened and interstitial free steels are the major components in any commercial vehicle (Miklós 2020).

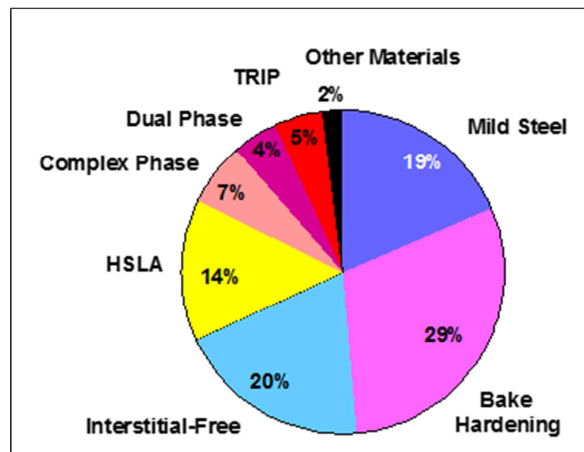


Fig. 1.2. Steels used in a commercial vehicle (Hardy 2007)

1.2 Properties of Auto Steels

These automotive steels are complex, sophisticated materials, with specific chemical compositions and multiphase microstructures resulting from precisely controlled heating and cooling processes. Various strengthening mechanisms are employed to achieve a range of strength, ductility, toughness, and formability properties. Yield strength and ultimate tensile strength are the basic properties required for any steel and are determined by cutting a test specimen from the blank and performing a tensile test. However, automotive steel requires some additional special properties to meet the applications such as *r*-value, *n*-value, stretch-flangeability and formability (Llewellyn and Hudd 1998).

For steels, strain ratio '*r*' or *r*-value is a measure of the ability of sheet metal to resist thinning or thickening when subjected to tensile or compressive forces (World auto steel - AHSS guidelines

2017). The r-value is the ratio of the true strain in the width direction (ϵ_w) to the true strain in the thickness direction (ϵ_t) when a sheet material is pulled in uniaxial tension beyond its elastic limit.

$$r = \epsilon_w / \epsilon_t \dots\dots\dots (1)$$

n-value, also known as the strain hardening exponent, is the measure of a metal’s response to cold working. Cold working is the plastic deformation of metal below its recrystallization temperature and this is used in many manufacturing processes, such as wire drawing, forging and rolling (Vladimir 2001). As ductile metal is plastically deformed during cold working, it becomes harder and stronger while its ductility decreases. The strain hardening exponent gives us an indication of how much the metal hardens or becomes stronger as it is plastically deformed. The strain hardening exponent ‘*n*’ can thus be determined from the slope of the logarithmic form of the true stress versus the true strain curve within the plastic region (Song et al. 2006).

Stretch-flangeability is an important sheet forming property for complicated automotive part applications (World auto steel - AHSS guidelines 2017). The hole expansion ratio (HER) is a key indicator to evaluate the stretch flanging performance of steel sheets, which is obtained by the hole expanding test using a cylindrical or conical punch. This test also characterizes the edge cracking resistance of steel. It is possible to predict the success or failure of real sheet under imposed forming process conditions with high accuracy (Saikat et al. 2011).

Formability is a term applicable to sheet metal forming. Manufacturing automotive components involve sheet metal operations, such as deep drawing, cup drawing, bending, etc. They involve extensive tensile deformation (Nourani et al. 2010). The problems of localized deformation called necking and fracture, due to thinning down are common in many sheet forming operations (World auto steel - AHSS guidelines 2017). Forming limit diagram (FLD) is a very effective way of optimizing sheet metal forming (Nakazima 1968). This test is performed using a bulging press, where a grid of circles is etched on the surface of sheet metal and the sheet is subjected to deformation. Usually, the sheet is deformed by stretching it over a dome-shaped die. Strips of different widths can be taken for the test, to induce a uniaxial or biaxial stress state. The circles deform into elliptic shapes. The strain along two principal directions could be expressed as the percentage change in length of the major and minor axes. The strains as measured near necks or fracture are the strains for failure. A plot of the major strain versus minor strain is then made. This plot is called forming limit diagram (Narayanasamy et al. 2005). This

plot gives the limiting strains corresponding to safe deformations. The FLD is generally a plot of the combinations of major and minor strains which lead to fracture. A combination of strains represented by the region above the limiting curves in the forming limit diagram represents failure, while those below the curves represent safe deformations. Additionally, weldability, bendability, corrosion resistance, fatigue strength, etc. are also determined in some of the automotive steels subjected to special applications (Manabu 2015).

1.3 Interstitial Free (IF) Steels

Interstitial free steels (IF steels) are an important class of automotive steels. IF steels are utilized for broad applications ranging from the automotive body to the electronic components and from enamel wares to household appliances (Barrett 1999). The main automotive application of formable IF steels are the rear roof pan, the spare wheel, and the front and the rear door inners. Outer body and door panels are shown in Fig. 1.3. Interstitial free steels are highly formable due to their very low carbon and nitrogen contents, typically <0.0030 wt.%C and < 0.0040 wt.%N (Hoile 2000). In IF steel manufacturing, ultra-low carbon content, and low dissolved gases (N and H) are achieved by removing them during steelmaking through a vacuum degassing process (Hoile 2000).



Fig. 1.3. Application of IF steels in a vehicle (outer body and doors)

The term ‘Interstitial free steel or IF steel’ refers to the fact, that there are negligible interstitial solute atoms to strain the solid iron lattice, resulting in a very soft structure. These steels normally have low to medium yield strength, high plastic strain ratio (r-value), high strain rate sensitivity and good formability. This is because the carbon is combined as precipitates rather than in the solid-solution. IF steels are also non-ageing. These characteristics are ideal for deep drawn parts. Among all automotive steels, only IF steels can meet the stringent formability standard requirements of extra deep drawing steels (Chang 2020). These steels are designed to provide

an excellent combination of drawability and mechanical strength based on their specific interstitial free (IF) metallurgy. The r-value (or Lankford value) is an important parameter in IF steels and commonly used to compare the deep drawability or its formability as a measure to the resistance to thinning (Lankford et al. 1950). The r-value will be extensively utilised in the following sections for defining the effect of various parameters on the performance of IF steels. The r-value and other typical properties of the IF steels are shown in Table 1.1.

The r-value of a material varies with the testing direction. This is due to the plastic anisotropy arising from the crystallographic texture imparted to the steel during the sheet rolling operation. Since the cold-rolled IF steel strips are anisotropic, normal practice is to test the strip in three directions, at 0, 45 and 90° to the rolling direction. This allows average r-value, \bar{r} to be determined from the equation (Ray et al. 1994).

$$\bar{r} = (r_0 + r_{90} + 2r_{45})/4 \quad \dots\dots\dots (2)$$

Isotropic steels have \bar{r} values around 1, whereas steels suitable for deep drawing applications should have $\bar{r} \geq 1.8$. Factors responsible for the development of a favourable \bar{r} value include chemical composition, the interaction between the constituent elements, the hot rolling schedule (Parera et al. 1991), the degree of cold reduction and the annealing cycles (Wilshynsky et al. 1995).

Similar to \bar{r} the factor, n-value also has significant impact on the IF steels and will be studied in detail in this work. n-value, also known as the strain hardening exponent, is the measure of a metal's response to cold working (World auto steel - AHSS guidelines 2017). As ductile metal is plastically deformed during cold working, it becomes harder and stronger while its ductility decreases. The strain hardening exponent gives us an indication of how much the metal hardens or becomes stronger as it is plastically deformed. Although the yield strength, tensile strength, yield/tensile ratio and percent elongation are commonly compared, while assessing sheet metal formability, for most steels it is the n-value along with the steel thickness that determines the position of the forming limit curve (FLC) on the forming limit diagram (FLD). The n-value is considered as the key parameter when global formability concerns exist (World auto steel - AHSS guidelines 2017). The n value describes the work hardening of the metal. Work hardening of sheet steels is commonly determined through the Holloman power law equation:

$$\sigma = K\varepsilon^n \quad \dots\dots\dots (3)$$

Where, σ is the true flow stress (the strength at the current level of strain), K is a constant known as the strength coefficient, defined as the true strength at a true strain of 1, ε is the true strain, and n is the work hardening exponent. n -value is mathematically defined as the slope or steepness of the true stress – true strain curve. A metal with large strain hardening exponent n responds well to cold working. Plots of n -value against strain define instantaneous n -values, and are helpful in characterizing the stretchability of these newer steels. The n -value is strongly related to the yield strength of the conventional steels. It is worth noting that even though n -value and r -value are two distinct parameters, the test for measuring them is usually conducted at the same time.

Table 1.1. Mechanical properties of a typical IF steel (World auto steel 2017)

0.2 % proof stress, MPa	Tensile Strength, MPa	Total elongation, %	\dot{r}	n
120 - 180	270 – 350	≥ 38	≥ 1.8	0.22

1.4 Composition and Processing of IF Steels

There is a complex relationship between chemical composition, precipitation, recrystallization and grain growth in IF steels. Production and processing of IF steels is more complicated than conventional aluminium killed steels (Dipak 2014). The production process of IF steels is as follows: Steelmaking in basic oxygen furnace → vacuum degassing in RH system → continuous casting → hot-rolling at hot strip tandem mill → pickling → cold-rolling at cold strip tandem mill → annealed by using batch annealing furnace or continuous annealing furnace → skin tempering, oiling and packaging. In the production of IF steel role of different elements and processing parameters is discussed below. IF steels have two compositional categories as Ti only and Ti-Nb IF steels, based on the alloy design. Typical compositions of Ti-only and Ti-Nb IF steels are shown in Table 1.2. (Hoile 2000).

Table 1.2. Typical compositions of Ti-only and Ti-Nb IF steels

Wt. %	C	Mn	Si	P	S	N	Nb	Ti
Ti only IF	0.0030	0.15	0.025	0.015	0.010	0.0030	-	≥ 0.040
Ti-Nb IF	0.0030	0.15	0.025	0.015	0.010	0.0030	≥ 0.020	≥ 0.028

In conventional steels, carbon and nitrogen contribute to the strength of the steel by going into a solid solution. However, in IF steel, increasing C and N content has a deleterious effect on the formability of the steel. This is due to the interstitial elements degrading the beneficial {111} recrystallization texture components and increasing the unfavourable {110} and {100} texture components (Held 1965). After blowing in the basic oxygen furnace, where the tapped steel has 0.03- 0.04 wt. %C, liquid steel is processed through a vacuum degasser to reduce C and N to the desired low values 0.002 – 0.003 wt. %. Even with best of the steel making practices, it is impossible to remove all solutes, i.e., carbon and nitrogen interstitial elements from the solid solution. Hence the micro alloying elements, titanium and niobium are added singly or in combination to scavenge interstitial atoms from solid solution through the formation of carbide, nitride, and carbonitride precipitates (Hutchinson 1994).

Sulphur is preferably maintained below <0.010 wt.%. In IF steels optimization of sulphur content relative to the steel composition is necessary for achieving the elongation and $\dot{\epsilon}$ values. Lowering the sulphur content in IF steel retards precipitation of fine titanium carbides, owing to the reduction of prior precipitation of $Ti_4C_2S_2$ (Tsunoyama et al. 1988) which helps in recrystallization and grain growth.

With such a low C, if strengthening elements were not added to the IF steels, its properties would be similar to that of the pure iron. The three most common solid solution strengthening elements added to the IF steels are phosphorous, manganese and silicon. Yield strength and tensile strength increases linearly with increasing (Si+Mn+10P) whereas elongation decreases linearly (Hasimoto et al. 1981). The largest negative effect is on $\dot{\epsilon}$ values. The addition of phosphorous results in the smallest decrease in $\dot{\epsilon}$, and manganese the greatest. However in practice phosphorous is not preferred as it effects the grain boundary strength and results in cold work embrittlement. Yamada et al. (1995) studied the magnitude of the effect of tramp elements such as copper, nickel, chromium and tin on tensile strength and elongation and found it proportional to the difference between the atomic radius of the alloying additions and that of the iron. These elements reduce the $\dot{\epsilon}$ value. The effect of these elements on $\dot{\epsilon}$ value enhances with slab reheating temperature, hence it is always preferred to keep the tramp elements to a minimum. In a hot strip mill, the major variables for controlling the mechanical properties of IF steels are re-heating, finishing and coiling temperatures. Hot band metallurgical properties (high-temperature properties of steel) govern the final $\dot{\epsilon}$ values in cold rolled and annealed product.

During slab reheating, dissolution of the precipitates occurs and determines the first texture and grain size. Low slab reheating temperatures are preferable if a temperature less than 1150 °C can be employed. A lower slab reheating temperature is especially favourable with low levels of alloying additions of Ti and Nb, as this retard the dissolution of TiC and NbC (Katoh 1985). It is observed that reducing the slab reheating temperature from 1250 to 1100 °C would result in an increase in \bar{r} value by 0.3.

In the next step, the slab is subjected to rough rolling or roughing. The most favourable texture component for good formability is developed when a high initial strain (> 50 %) is applied to the large austenite grains. However, roughing pass for conventionally rolled IF steel is generally < 30 %, hence any crystallographic textures set-up during roughing or finishing are diluted during austenite to ferrite transformation. After roughing, the deformed strip is subjected to a series of finish rolling steps to achieve the final thickness. During finishing, the \bar{r} values increase with an increase in the temperature to a maximum and then decreases (Gupta et al. 1988). It is known that \bar{r} value increases with decreasing hot band grain size, the finest grain size is formed when the finishing temperature is close to the austenite to ferrite transformation temperature. The optimum finishing temperatures in IF steels vary between 910-930 °C. The rolled strips are then coiled at the down coiler at which the coiling temperature is maintained between 600 – 750 °C, based on the composition. Here higher coiling temperature results in higher \bar{r} values (Kino et al. 1990) as the precipitates formed under such conditions are coarse and widely spaced and favour ferrite recrystallization and grain growth during annealing. The hot-rolled coils are then pickled in acid to remove the scale and cold rolled to customer-specific thickness. Maximum cold reductions of 90% give the best \bar{r} values but due to practical limitations, most of the IF steel is cold rolled with 70-80 % reduction. Cold rolling imparts a highly deformed structure from which the recrystallization of grains with favourable textures nucleate and grow during annealing (Vladimir 2001).

Table 1.3. Typical processing parameters for IF steels (World auto steel 2017)

Slab reheating temperature	1250 – 1100 °C
Finishing temperature	910 – 930 °C
Coiling temperature	600 -750 °C
Cold reduction	70 - 80%
Annealing temperature	800 – 830 °C

The cold-rolled sheets are subjected to batch or continuous annealing furnaces where the coil is exposed to 800 – 830 °C to attain the most desired texture. During annealing, r value increases with increasing annealing temperature until ferrite to austenite transformation temperature is reached (Ray et al. 1994). These cold-rolled and annealed sheets are further galvanized or galvannealed to avoid corrosion before being used as auto components. The typical processing parameters for IF steels are shown in Table 1.3.

1.5 Issues in Producing IF Steels

The IF grade steels are conventionally produced through continuous casting, reheating, hot rolling, pickling, cold rolling and annealing route. IF steels are more difficult to manufacture than aluminium killed steels. The very nature of the production and processing of the IF steel makes these grades more expensive than the conventional steels. The low carbon contents required in IF steels necessitate the use of vacuum degassing and special low carbon-containing refractory bricks, covering compounds and mould powders. In addition, care must be taken during processing to avoid unacceptable amounts of carbon pick-up. Longer vacuum degassing times and the use of expensive alloying elements and powders results in a cost increase. In these grades, high coiling temperature is required to optimise the properties but this causes problems during pickling due to excessive scale formation (Hoile 2000). Additionally, higher recrystallization temperatures of IF steels have implications during hot rolling and annealing. Surface roughness control is also an important criterion and is met by temper rolling. Due to these different and conflicting requirements, industrial production of IF steels have lower yields and is not produced by all steel makers. The major yield loss in the production of IF steels is during hot rolling. Similar to other grades, IF steels are also rolled above the austenite to ferrite transformation temperature (A_{r3}). These ultra-low carbon steels have high A_{r1} and A_{r3} temperature and hence are finished and coiled at higher temperatures. The normal finishing temperature is > 900 °C and the coiling temperature > 620 °C. The transformation range is also very narrow as compared to other extra-low carbon steels (ELC) as shown in Fig. 1.4 (Andreas et al. 2000). The reheating temperatures above 1200 °C would be required for thicknesses of 2 - 4 mm. Hot strips thinner than 1.8 mm cannot be produced at all by a conventional “austenitic” hot rolling. To avoid scaling and surface issues these steels are normally rolled just above the recrystallization temperature. While rolling very thin gauge (< 3 mm) IF steels, the control of temperature in a narrow band, across the strip width and along the length becomes difficult due to differential temperature loss. It is not possible to prevent certain areas (edges, etc.) of the strip from entering into a two-phase region (Hai

at al. 2013). Because of the low strip thickness and large surface area, the strip cools more rapidly in the finishing mill and some of its edge parts cool, very fast compared to its centre. Hence, the rolling temperatures can easily drop down below the austenite - ferrite transformation temperature at some parts of the coil, leading to non-uniform transformation along the width of the strip. This non-uniform and uncontrolled rolling in the inter-critical temperature region along the width and length changes the coil tension, resulting in shape defects, such as buckles, cross bow, etc. and also deteriorates the mechanical properties (Hailiang et al. 2021). During hot rolling of IF steels, issues of load variation, hunting, buckling, shape defects arise as shown in Fig. 1.5. During cold rolling, due to the non-uniform temperature profile in hot rolled sheet and its effect on the phase transformation, the strip results in edge slivers, shape defects and holes as shown in Fig. 1.6. These defects are found at any part along the width but predominantly at the head and the tail portions which experiences higher temperature variations.

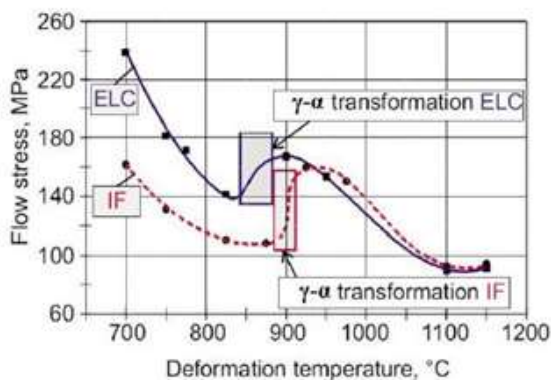


Fig. 1.4. Comparison of transformation temperatures (Andreas et al. 2000)

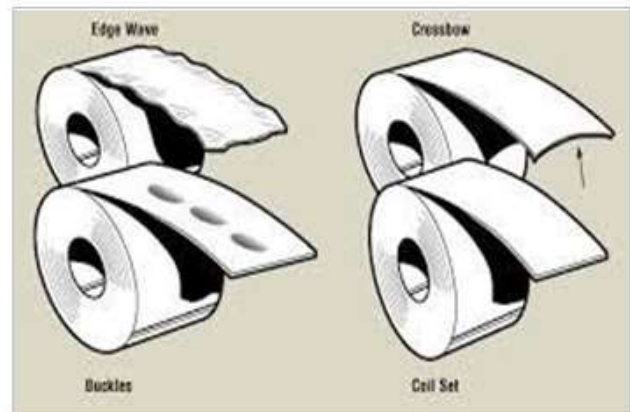


Fig.1.5. Shape defects in IF Steel



Fig. 1.6. Shape and hole defects in cold rolled IF steels

Generally, there is a variation of 10 -30 °C along the width and 30 – 50 °C along the length

of the coil (Ronan et al. 2015). This requires double trimming of the cold-rolled sheets, reducing its yield (Hoile 2000). This makes the production of thin gauge IF steels costly.

A possible solution for this problem is ferritic rolling. Ferritic rolling of deep-drawing steels is a relatively new rolling strategy developed to eliminate temperature control problem during rolling in austenite conditions, which is on its way to the industrial application (Peeped et al. 1997) (Harlet et al. 1993). In the ferritic rolling strategy, the finish rolling temperature is shifted down into the fully ferritic temperature region below A_{r1} temperature with no chance of any two phase rolling. Lower reheating temperatures for ferritic rolling results in a reduced AlN (aluminium nitride) dissolution (enhancing ferrite recrystallization kinetics) and a smaller initial austenite grain size. This low rolling temperature practice is expected to have an improved hot rolled product quality with fewer surface defects. The product will also have improved flatness due to the reduced internal stresses because the steel strips are already transformed before cooling on the run-out table. The difference in the processing routes of a conventional austenitic rolling and a novel ferritic rolling is apparent from Fig. 1.7. (Andreas et al. 2000). The reduction in the temperature below the α/γ transformation allows for the production of the thin hot strip (<2 mm) and even ultra-thin hot strip (<1 mm). In addition to the reduced strip thickness, it becomes possible to produce hot strips with adequate deep-drawing properties (Andreas et al. 2000).

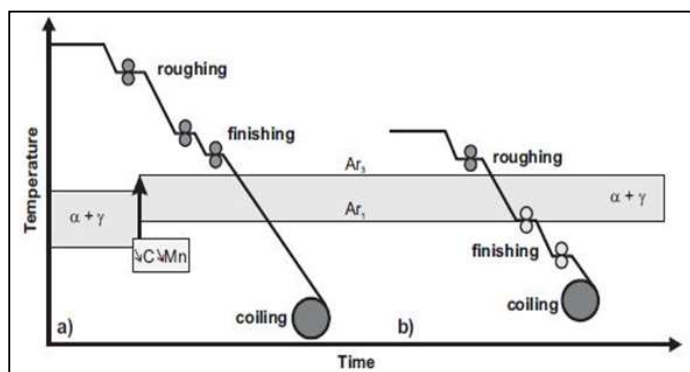


Fig. 1.7. Comparison of (a) conventional austenitic and (b) ferritic rolling (Andreas et al. 2000)

Figure 1.8. shows that transformation temperatures or the critical temperatures in the Fe-C diagram. These temperatures play important role in defining the rolling parameters in the mill. For a given steel, the critical temperatures depend on whether the steel is being heated or cooled. Critical temperatures for the start and completion of the transformation to austenite

during heating are denoted, respectively, by Ac_1 and Ac_3 for hypo-eutectoid steels and by Ac_1 and Ac_{cm} (or simply A_{cm}) for hyper-eutectoid steels. These temperatures are higher than the corresponding critical temperatures for the start and completion of the transformation from austenite during cooling, which are denoted, respectively, by Ar_3 and Ar_1 for hypo-eutectoid steels and by Ar_{cm} and Ar_1 for hyper-eutectoid steels. (The ‘c’ and ‘r’ in the symbols are derived from the French words ‘chauffage’ for heating and ‘refroidissement’ for cooling). The A_3 and A_1 temperature lines are shown in Fig. 1.8. In the rolling process, the property development takes place during cooling and hence Ar_3 and Ar_1 are the relevant critical temperatures. Ar_1 is therefore the temperature at which transformation of austenite to ferrite or to ferrite plus cementite is completed during rolling and the Ar_3 is the temperature at which austenite begins to transform to ferrite during rolling. The temperature of deformation w.r.t to the transformation temperatures determine the final microstructure and the properties (ASM Hand book 2016).

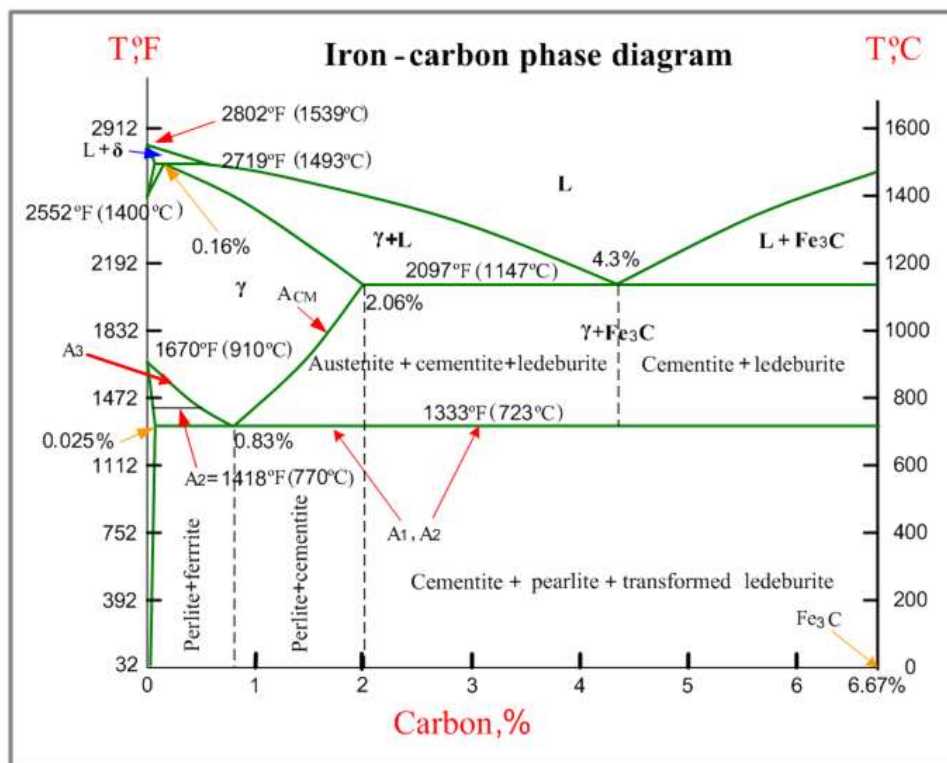


Fig. 1.8. A_3 and A_1 temperature lines in Fe- Fe_3C diagram

Ferritic rolling introduces the possibility of producing thinner hot strips in the range of <2 mm with desirable deep-drawing properties (Barrett et al. 2002). It has also gained interest as means of cutting down costs and of extending the application range of hot rolled products. Therefore, the optimisation of its process parameters is of great interest to steel producers.

1.6 Research Gaps

Despite several claimed benefits, (Herman et al. 1992) (Barrett et al. 2002) (Andreas et al. 2000), ferritic rolling is not in wide practice in the industry as rolling in the ferritic zone or lower temperatures possess many operational problems. It is suspected and proved many times that ferritic rolling requires higher mill-power and rolling loads due to lower finish rolling temperatures. Several attempts (Barrett et al. 2002) (Messien et al. 1993) (Sakai et al. 1988) have claimed poor deep drawability properties caused by a detrimental shear structure formed during the final finishing strands. The results found in the literature for the properties of ferritic rolled hot strips are diverse and not consistent even for similar alloy compositions (Andreas et al. 2000). This is caused by the fact that the production parameters, such as the rolling and coiling temperatures, strongly influence the results obtained. For the design of the rolling schedules in the ferrite region, the determination of the range of the γ - α -transformation temperatures as well as the knowledge of the recrystallization behaviour of ferrite is indispensable. Most importantly, the majority of the studies produced ferritic hot rolled sheets as a replacement for cold-rolled sheets using laboratory mills. They compared the formability of sheets using texture in the hot rolled condition but did not carry out formability tests. New technology of this type requires development work in several fields in order to be used in high production industrial lines (Appell 1978). This does not provide one to one comparison for the users to look for applications.

Additionally, limitations in maximum reduction possible in a hot strip mill and the requirement of surface finish do not promote such practices industrially. Rather, ferritic hot rolled coils if, subsequently, cold-rolled and annealed, can take advantages of reduced defects, better yield, and improved properties and can be adopted in actual practice without any changes in the existing mill. There are very limited studies which, followed ferritic hot rolling and subsequent cold rolling and annealing. These studies are also in laboratory mills and have never been tried in an industrial mill (Grobheim et al. 1996).

Due to the availability of less information on the formability behaviour of different ferritic temperature rolled steels, it is less produced and rarely utilized in industry. Therefore, very specific hot rolling, cold rolling parameters and annealing regime would also be required for ferritic hot rolled coils. At this point, it is relevant to holistically study and optimize process parameters in hot rolling, cold rolling and annealing for developing IF steel through ferritic rolling on an industrial scale for varied applications.

CHAPTER 2

LITERATURE REVIEW

IF (Interstitial Free) steels are widely used in automotive outer panels, in which, solute C and N atoms are fixed as precipitates by Ti and Nb. These are extremely formable steels. These steels have average plastic strain ratio (r-value) varying between 1.8 - 2.5 and work hardening coefficient in between 0.22 - 0.27. These grades have been developed by a combination of grain refinement of ferrite through high reduction hot rolling and accelerated cooling immediately after hot rolling, high reduction cold rolling, and high-temperature annealing (Valdimir 2001). Traditionally, ULC and IF steels are hot rolled in the austenite region. However, hot rolling in the austenite region can lead to a weak, nearly random texture and low r-value because the developed austenitic texture is randomized during the transformation from austenite to ferrite. These grades have rolling issues due to high transformation temperature (Okuda 2013). Recently, a new strategy referred as warm rolling or ferritic rolling was extensively investigated to develop a cheap, soft and ductile hot-rolled strip as a substitute for the conventional cold rolling and annealing. Many studies (Harlet et al. 1993) (Ghosh et al. 2008) have been conducted on the ferrite region rolling, and the results show that hot rolling in the ferrite region is feasible, and the finished materials have pronounced $\{111\} < 110 >$ annealing texture and have good deep drawability. These studies showed that the process of hot rolling in the ferrite region followed by recrystallization annealing results in a much stronger γ -fiber texture ($<111> // ND$, i. e. normal direction) than the conventional austenite rolling process (Leilei et al. 2021). Some concerns were also highlighted (Roberto 2011), where ferritic rolling was suggested only for low yield strength grades. These grades were reported with negative planar anisotropy indicating a tendency to ear formation. The formation of shear texture near the surface region was also observed. Kohsaku (2021) found heterogeneity of the deformation structure in the vicinity of a grain boundary as a result of differences in the plastic deformation of the $ND // <111>$ (γ fiber) grains and the $RD // <011>$ (α fiber) grains. In ferritic rolling understanding and prediction of heterogeneous deformation structures, both experimentally and theoretically, are still insufficient and further advancement is required.

2.1 Types of Ferritic Rolling

The ferritic rolling strategy allows for the production of two different hot strip grades, a "soft" hot strip and a "hard" hot strip (Elsner et al. 2004). The "soft" hot strip is rolled at

higher temperatures in the ferritic region and a sufficiently high coiling temperature ensures a full recrystallization of strip directly in the coil. The "hard" hot strip is rolled and coiled at lower temperatures in the ferritic region so that complete recrystallization in the coil does not occur. Hence, these strips exhibit a strained microstructure after coiling and a subsequent recrystallization annealing is required, to obtain the desired deep-drawing properties. These two products can be used as a cheaper substitute for cold strip for some applications (Barrett et al. 2002). By the measurements of the texture development as well as by computing r -values, the texture formation could be optimized for achieving deep-drawability in the hot strips comparable to that of a cold strip conventional austenitic rolling. Additionally, this concept requires major changes in the hot rolling mill to incorporate thinner sheet rolling capability (Hoile 2000). However, both the hard and soft ferritic hot strip grades can also be used subsequently to produce "cold" strip. In this case, the ferritic rolled strips are used as initial hot strips for a subsequent cold rolling and the hot-rolled texture has a significant effect on the final texture in the steel. The deep drawing behaviour of steels depends on attaining the proper $\{111\}$ texture on the final product which is influenced by hot rolling, cold rolling, and annealing (Zhang et al. 2010). This part of ferritic rolling is less known but can be directly used in existing mills and requires detailed study for implementation. Currently, the steel industries are greatly interested in ferritic rolling due to the better properties and lower cost of the finished product. Additionally, many other benefits (Barrett et al. 2002; Chang et al 2020) also are claimed as enlisted below.

1. Stable rolling without hunting because of one phase rolling at a time
2. Better strip flatness control by rolling of a transformed and homogeneous microstructure
3. Less scale formation, due to the lower finishing temperatures
4. Reduced strip surface defects
5. Reduction of work roll wear, due to lower rolling temperatures in the finishing mill
6. Improvement in the yield of hot rolled and cold rolled products
7. May replace the conventional hot-rolled and cold-rolled products by ferritic-rolled HR products and result in savings in terms of energy, productivity and cost.

2.2 Studies on Various Aspects of Ferrite Rolling

Traditionally, the low carbon and IF grade steels are having good formability and suitable

for complex shapes used in automotive applications (Guo et al. 2014). These steels are hot rolled, cold rolled, and annealed. IF grade steels having very low carbon are hot-rolled in austenitic regime at higher temperatures and frequently results in surface and shape defects and have lower yields. Herman et al. (1992) introduced ferritic-rolled thin strip steel as a low-cost approach for such steels. Andreas et al. (2000) carried out ferritic rolling, below the austenite start temperatures in low carbon steels to produce thin gauge hot-rolled coils with better deep drawability, as a replacement of cold-rolled sheets to reduce the production cost. Later Barrett and Wilshire (2002) manufactured IF grade steels under a ferritic rolling regime at lower temperatures to reduce the defects and increase its yield. But it also reported higher heat loss (lowering coil temperature) and an increase in the rolling loads. These studies produced ferritic hot-rolled sheets as a replacement for cold-rolled sheets and show that thermo-mechanical processing can have a profound effect on the microstructure and mechanical properties of the ferritic rolled steels. Numerous studies have been published on the effect of slab reheating temperature, hot rolling finishing temperature, coiling temperature after rolling, amount of deformation during hot rolling, etc. (Andreas et al. 2000) (Barrett et al. 2002) (Lifeng et al. 2017) and others on the effect of cold rolling, and annealing parameters on the texture and mechanical properties of the ferritic-rolled steels (Chang et al. 2020; Wang et al. 2019). There are also some disagreements in the results presented in the literature. Some of the investigations, where different aspects of the ferritic-rolled steels including hot rolling, cold rolling, annealing and formability testing have been studied and are discussed below.

Barnett and Jonas (1999) reviewed the physical metallurgy aspects of ferritic rolling and found significant variation in concepts of warm rolling from hot and cold rolling. The presence of second phase interferes with deformation and softening mechanisms of the primary phase and literature has less investigations. Inconsistency in the formation of in-grain shear band formation was also reported in many works (Barrett and Wilshire 2002). Many practical issues in industrial rolling have also been enlisted and more specifically, through thickness texture gradient is the most common issue reported. The review highlights a lack of understanding in ferritic rolling under different conditions and specifically under industrial rolling of full length coils.

Lifeng et al. (2017) studied the effect of reduction ratio ranging from 60% to 90% on microstructures and mechanical properties of the AISI 4140 steels produced by warm rolling. It was found that the microstructures of steels were remarkably refined after

heavy warm rolling. Ultrafine grained ferrite formed because of the dynamic recrystallization and ferrite formation. An increase in the YS, UTS and microhardness after warm rolling were attributed to grain refinement and subsequent formation of the martensite. The increase in ferrite and decrease in martensite contents contributed to the decrement of strength and increment of ductility in steels when the warm rolling reduction ratio was increased. No details were presented on other important parameters.

In the work of Kaneharu et al. (2013), one pass hot rolling in the ferrite region was conducted at higher temperatures, using various rolling temperatures and rolling reductions, with two types of ULC steels, 0.016% Nb and 0.023% Ti, and their recrystallization behaviours immediately after hot rolling were investigated. The Ti-bearing steel was easily recrystallized; recrystallization occurred even at 1323 K with a low rolling reduction of 30%. The γ -fiber strength reached its maximum value at around 50% rolling reduction at 1273 K with the Nb-bearing steel and 1323 K with the Ti bearing steel. On the other hand, during high temperature rolling of the Ti-bearing steel, the γ -fiber did not develop, independent of rolling reduction. These changes correspond to the recrystallized fraction, in that the strength of the γ -fiber decreased when recrystallization occurred immediately after rolling.

Asensio et al. (2001) examined the microstructure and the texture of the hot-rolled steel and the cold formability properties (n and r values) of the blanks produced through the cold-rolling and subsequent annealing processes. It enlists the mechanical properties, texture and formability requirements of various steel grades and highlights the role of the recrystallization process to be followed through a mechanism of oriented nucleation and growth. Table 2.1. summarizes the mechanical properties and drawing parameters of the five basic ferritic steel categories for cold formability: interstitial-free, aluminium-killed, rephosphorized, bake-hardened and micro-alloyed (HSLA- high strength low alloy) steels. It is to be noted that their respective r_m (referred as \dot{r} in the present work) values set them in different formability categories.

Table 2.1. Properties of ferritic steels for drawing operations (Asensio et al. 2001)

Steel Type	YS (MPa)	UTS (MPa)	Elongation (%)	n	\dot{r}
Interstitial -free	155	305	42	0.23	2.0
Al-killed	160 -190	300	42	0.22	1.8

Rephosphorized	190-230	345-370	36	0.20	1.5
Bake-hardened	210	320	40	0.22	1.6
HSLA	375	475	27	0.15	1.0

GroBheim et al. (1996), studied differences concerning the deformation behaviour of low carbon steels in the austenite and ferrite region in hot compression tests. The simulation of hot deformation processes was carried out on a hot deformation simulator using a commercially produced low carbon deep drawing steel. As shown in Fig. 2.1., the flow stress in the austenite range or in the ferrite range increases with decrease in deformation temperatures. However, a small temperature band exists, in which the flow stress of the ferrite is less than that of the austenite. The effect of the strain rate on the flow stress is enhanced during very high strain rate deformation. A slight difference in flow stress was found between the ferrite and the austenite region deformed samples. This confirms that there should not be much change in the rolling loads during ferritic rolling.

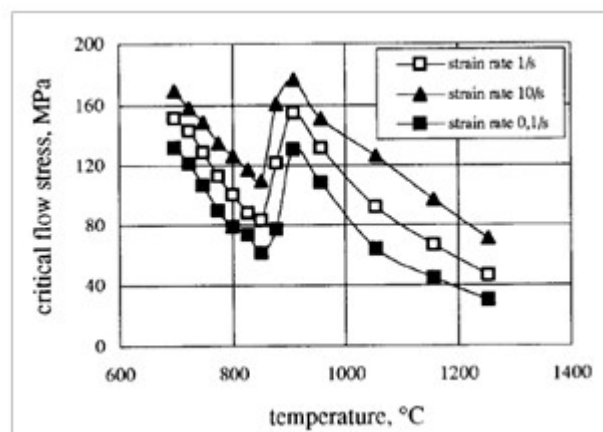


Fig. 2.1. Effect of strain rate and deformation temperature on critical flow stress (GroBheim et al. 1996)

In the work of Elsner et al. (2004), "soft" and "hard" hot strips were produced on a laboratory hot rolling mill and development of the recrystallization texture of the cold-rolled and annealed ferritic-rolled hot strip for different cold reductions was studied. Cold strips produced from the ferritic rolled "soft" or "hard" hot strips exhibit improved deep-drawing properties. The strip produced from a "soft" hot strip reveals slightly higher mean r-values compared to a conventionally produced cold strip, whereas the initially "hard" hot strip exhibits a somewhat lower mean r-value but a drastically improved planar anisotropy. This paper also suggests that the influence of the selective growth mechanism

is less important for lower rolling reductions but becomes more dominant for cold rolling reductions greater than 80%. However, in this work, the annealing parameters were kept constant, which makes this study very specific.

Pawan et al. (2016) studied warm working characteristics of the ferrite for 0.044C-1.51Cu-

1.52Mn-0.064Ti steel by using scanning electron microscopy, energy-dispersive X-ray spectroscopy and transmission electron microscopy. The specimens were subjected to multi-pass hot rolling at 800 °C and 850 °C with a holding time of 10 minutes. The result shows that Cu precipitation takes place during the warm working of the ferrite and results in the formation of the Cu precipitates at the boundaries of newly born ferrite grains. This inhibits the grain boundary movement and the ferrite grains of size 1-4 μm are formed which provides additional strength. In this paper, no discussion has been made on other important properties.

Before we review the studies on textural changes in ferritic rolled sheets, it is important to understand the textural evolution in a conventional IF steel. Drawability is known to depend on the recrystallization textures, and there is a strong correlation between the ratio of near {111} components and near {100} components; the higher this ratio, the better is the drawability (Wilson 1966). Conventionally processed IF steel is rolled at elevated temperatures in the austenitic state, which when cooled produces a randomly textured body centred cubic (BCC) hot band. Cold rolling of this randomly textured material causes the individual crystals to rotate by slip processes towards two sets of orientations, the α fiber set, i.e., where $\langle 110 \rangle$ is parallel to the rolling direction, $\langle 110 \rangle // RD$, and the γ fiber set, where $\langle 111 \rangle$ is parallel to the direction normal to the sheet plane, $\langle 111 \rangle // ND$. These fibers are most clearly shown in the three-dimensional (3D) orientation Euler space defined by Bunge (1969), in the $\phi_2 = 45^\circ$ section, which is shown in Fig. 2.2 (a). This behaviour is common to most BCC metals and alloys, and the textures are rather insensitive to minor alloying additions (Dillamore and Roberts 1965). The strength of these texture components increases with cold rolling reduction. Fig. 2.2 (b) shows the texture results after cold rolling with 85% reduction (Duggan et al. 2011). The α fiber runs from $\{001\} \langle 110 \rangle$ to $\{111\} \langle 110 \rangle$, with clustering of poles at $\{001\} \langle 110 \rangle$ and $\{112\} \langle 110 \rangle$. The γ fiber runs from $\{111\} \langle 110 \rangle$ to $\{111\} \langle 112 \rangle$ and is peaked at $\{111\} \langle 110 \rangle$.

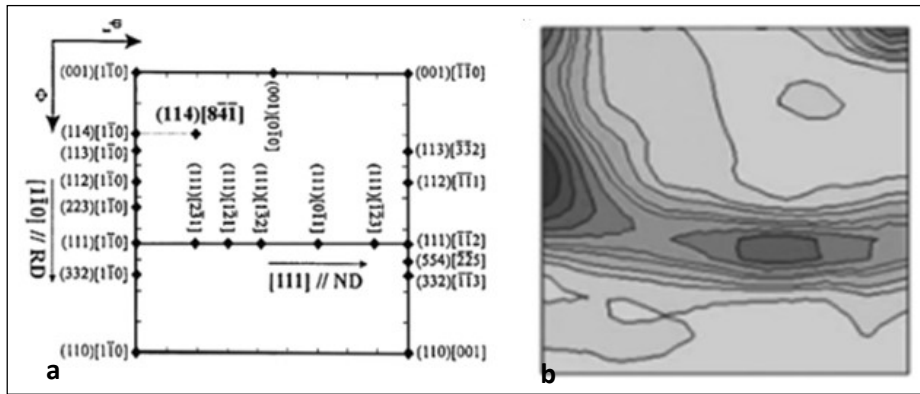


Fig. 2.2. 3D orientation Euler space at $\phi_2 = 45^\circ$ section (a) common indices (b) ODF of a cold-rolled sheet (Duggan et al. 2011).

Pero et al. (1999) studied the influence of the hot rolling conditions, cold reduction rate, and final annealing on the evolution of the steel sheet textures on two grades of steel, low-C steel and extra-low-C steel of the interstitial-free type. The IF steel was hot rolled in the alpha phase, while the low carbon steel was rolled in the gamma phase domain. His results show that the intensity of $\{111\}$ component and drawability is considerably higher in the textures of the cold-rolled and the annealed sheets than in the hot-rolled sheets and among the two experimental grades it was higher in the low carbon steel. However, the structure of the recrystallized alpha grains resulted to be equiaxial in both steels at the end of their respective processing. It was suggested that drawability of sheets annealed after cold rolling improves if greater reduction rates ($> 70\%$) are used during rolling. Figure 2.3. shows the texture evolution with cold rolling in IF steels. For the 70% cold reduction (most common in industrial settings), the ratio of the $\{111\}$ and $\{100\}$ intensities turn out to be substantially smaller whereas it increases as it reaches 90%. In this paper, only the comparison was made and no detailed analysis was presented on improving properties of the ferritic rolled IF steels.

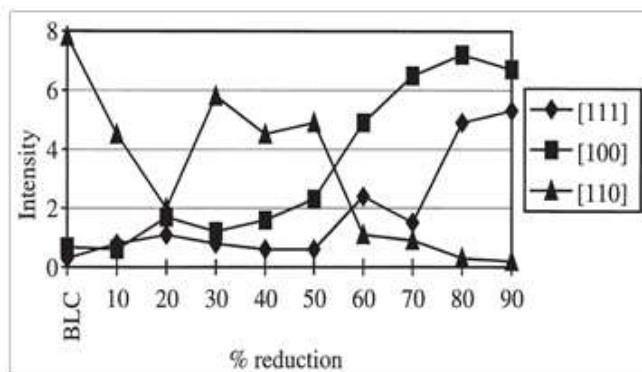


Fig. 2.3. IF steel cold rolling textures (Pero et al. 1999)

Guo et al. (2014) studied the effect of α and γ texture in hot-rolled coils during cold rolling and annealing in Ti-IF steel sheets using X-ray diffraction analysis. Different hot rolling parameters result in different hot rolling texture, leading to different texture evolution during cold rolling and annealing. He reported that an ideal γ fiber texture is beneficial for improving deep drawability. It forms after annealing but only when a well-proportioned γ fiber dominates in the cold-rolled texture. It requires formation of a strong γ fiber in the hot band. He reported that to obtain a beneficial recrystallization texture, the γ fiber should be the most prominent texture in the un-annealed texture. Figure 2.4. and Fig. 2.5. shows the $\phi = 45^\circ$ ODF figures in hot-rolled, cold-rolled, and annealed sheets for austenite and ferrite rolling respectively. The annealed texture in austenite rolling grade is similar to hot rolling texture in ferritic rolling grade indicating that the ferritic rolled HR sheet can be a substitute for the conventional cold-rolled and annealed sheet. This work does explain the methodology to achieve such textures.

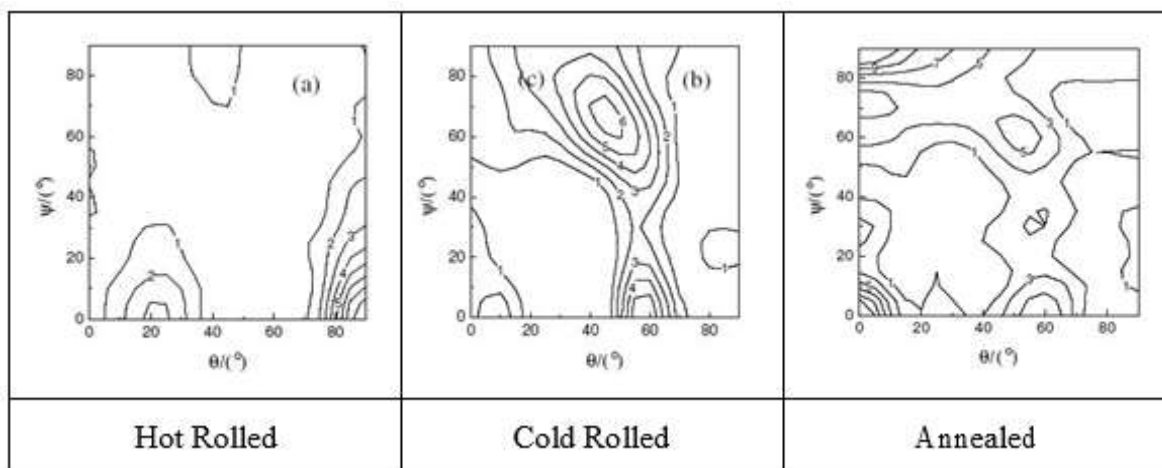


Fig. 2.4. ODF sections of austenitic rolled IF steel (Guo et al. 2014)

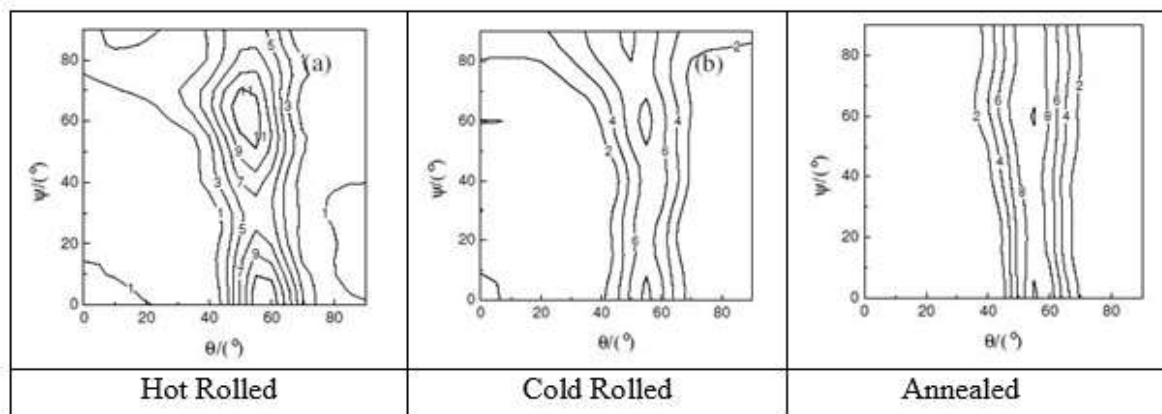


Fig. 2.5. ODF sections of ferritic-rolled IF steel (Guo et al. 2014)

Costa et al. (2000), investigated the microstructure and the texture developed in a Ti microalloyed IF steel by rolling in an intermediate temperature range at 400 °C and 600 °C. Reductions of 40% and 60% were applied to a set of hot-rolled strip specimens, part of which was subsequently annealed at 800 °C for 5 minutes. The textures developed in both cases were reported similar to those obtained by cold rolling, both in orientation and intensity. The deformation temperature does not seem to perturb the rotations that lead to textural definition even for 40% reduction but the recrystallization textures reported better for 60% reduced materials.

Wang et al. (2006), investigated the effects of the rolling conditions and annealing conditions on texture and mechanical properties of an IF steel, and develop a new ferritic rolling and direct annealing process. His studies show that the r -value increases with a decrease in reheating temperature and finish rolling temperature, and the increase in reductions in the ferritic region. His work claims that a high r -value can only be obtained in the low-temperature rolling process with efficient lubrication. By lubricated ferritic rolling and annealing, the r -value is raised to 1.75 and the elongation rate is over 50% at a finish rolling temperature of 650 °C, which is suitable for DDQ (deep drawing quality) grade products. For samples subjected to lubricated rolling and annealing, the strong $\{111\} // ND$ recrystallization texture is distributed homogeneously along the thickness direction, and the intensity of $\{110\}$ recrystallization texture is very low even on the surface. For non-lubricated samples, the $\{111\}$ texture distributes non-uniformly and is weak along the thickness direction, while the $\{110\} // ND$ recrystallization texture is strong, which deteriorates the formability. Barrett et al. (2002) studied the effect of reheating, finishing, coiling temperature, lubrication and hot rolling loads during ferritic rolling of an IF steel. His studies show that coiling and finishing temperature governs the final microstructure and mechanical properties. Higher temperatures (> 800 °C finishing temperature) resulted in more recrystallized grains and better r -values. The use of oils was recommended for improved lubrication but they also reported a higher temperature loss and reduction in the total deformation. Paper also reported an increase in the rolling loads in the final few strands. However, this paper did not present any effect on the formability of hot rolled coils and the effect of subsequent cold rolling operations.

In the work of Ray et al. (2002), the warm rolling and subsequent annealing textures of an extra-low carbon (ELC) and two interstitial free (IF) steels have been investigated using both single pass and multi-pass rolling. The author claims that ELC steels acquire only a

weak texture after finish rolling in the upper ferritic range, for both single and multi-pass rolling whereas much sharper overall texture (and γ fiber) develops in the IF steels during warm rolling, and it generally sharpens after subsequent recrystallization anneal. Authors also claim that among two IF steels, the Ti-containing steel appears to develop a perceptibly sharper γ fiber after warm rolling and annealing as compared to the Nb-containing one. This study only highlights the comparison of extra low carbon and two interstitial free steels and the process for improving the properties to conventional rolling is not explained.

In this work by Roberto (2011), the effect of finishing temperature and coiling temperature on the microstructure, recrystallization behaviour and texture of LC steels rolled under industrial hot and warm rolling conditions were investigated. In this study, during warm rolling, dynamic recovery of ferrite occurs due to its high SFE (stacking fault energy), thus leading to a strained and non-recrystallized ferrite structure after coiling at low temperature whereas an exaggerated grain growth was reported during hot rolling. Additionally, negative planar anisotropy and weak texture were observed in warm rolled samples. No solution has been suggested to improve the texture during warm rolling.

Wang et al. (2006) studied the texture characteristics in two different IF steels after rolling in the ferrite range and coiling at high temperature. The ordinary Ti-IF steel was recrystallized completely and strong $\langle 111 \rangle // ND$ recrystallization texture was formed at the mid-section and 1/4-section after hot rolling in the ferrite region and coiling at high temperature. Due to high content of P in the high-strength Ti-IF steel, most of the grains were still in rolling status after coiling and $\langle 110 \rangle // RD$ texture was in the ascendant at the mid-section and 1/4-section with very weak $\langle 111 \rangle // ND$ recrystallization texture. Textures at the surface in both sheets of steel are very weak with $\langle 001 \rangle // ND$ in ordinary Ti-IF steel and $\langle 110 \rangle // ND$ in high-strength Ti-IF steel.

Guo et al. (2008) studied the texture evolution in a high strength Ti-IF steel simulating hot rolling, cold rolling, and annealing in a laboratory mill. He reported similar texture development in ferritic and austenitic rolling but the texture intensity was found higher in the ferrite-rolled sample. The key difference was found in the texture characteristics at the surface and at the mid-section in both ferritic rolled and austenite- rolled samples under all conditions. Ferritic-rolled samples were found to have better properties compared to the austenitic- rolled sample. This study reported a decrease in α -texture and along with $\{111\}$

$\langle 112 \rangle$ and $\{111\} \langle 110 \rangle$ components of γ -texture, but found improvement in $\{111\} \langle 123 \rangle$ component at the surface. It also found to have increased $\{111\} \langle 112 \rangle$ oriented grains at the centre after annealing. However, this study does not validate formability characteristics.

Yazheng et al. (2019) used Gleeble-3500 thermal simulator to study the plastic deformation behaviour of steel SPHC produced by CSP process (compact strip process) under ferritic rolling condition in a double-pass hot compression test. The results show a non-uniform trend in deformation resistance as the temperature is reduced. Initially, the deformation resistance decreased by about 70 MPa at different strain rates during compression between 870 °C to 820 °C. It remained constant at a lower value between 820 °C to 800 °C and reached its minimum and increased thereafter in the temperature range of < 800 °C. It was correlated to the softening effect of phase transformation which is higher than that of hardening effect of decreasing temperature, which decreased the deformation resistance. This trend is expected to be of different intensity in slab rolling and can also be similarly investigated in the Gleeble simulator.

Wang et al. (2019) simulated the ferritic rolling process of SPHC steel to study the causes for difference in microstructure of low carbon steel for application of endless continuous casting and rolling line that uses ferritic zone rolling technology. This study of thermal simulation reported the microstructure to be ferrite and pearlite in a very small proportion. At lower temperatures (around 780 °C), mixed crystals appear, which is characterized by small grains sandwiched between the coarse grains and the degree of mixed crystals becomes smaller as the strain rate decreases. This varying behaviour needs to be studied in detail and parameters must be optimized for developing an industrial process.

The low carbon steel was produced by using a semi-continuous hot rolling production line with a ferritic rolling process by Zhao et al. (2019) to study the effect on the cold-rolled and annealed plate. The deformation stress of low carbon steel was found larger than that of the interstitial free steel. In addition, the deformation stress of the low carbon steel is reported to be more sensitive to the deformation rate than that of the interstitial free steel, contradicting other studies. The microstructure along the thickness was inhomogeneous with fully recrystallized grains at the surface layer and fibrous grains in the centre layer with more of $\{111\}$ texture component. The low carbon steel deformed by ferritic rolling has shown a lower yield ratio and higher elongation than that of the low carbon steel treated

by normal rolling. This is in line with other studies but the effect on actual formability characteristics of the produced low carbon steel is not studied.

Hao et al. (2019) studied the microstructure development and recrystallization texture of the Ti-IF steel after hot rolling, cold rolling and annealing under ferrite rolling and austenite rolling conditions. The work found that compared to austenite rolling, annealed grains obtained after ferrite rolling are more homogeneous and a little bigger in grain size at mid-section. The intensity of γ -fibers is also reported to be higher after ferrite rolling. Compared to austenite rolling, the yield strength, the tensile strength, the yield ratio and parameter Δr of the annealed samples after ferrite rolling are reported lower, while r and n are higher. This work also does not test the samples for formability.

Qiu et al. (2018) studied the microstructure, mechanical properties, and textures of warm rolled interstitial-free steel annealed at four different temperatures (730, 760, 790, and 820 °C). YS, UTS, and yield ratio reported to decrease with an increase in annealing temperature and the elongation, r value and n value increased with increase in temperature. The sizes of TiN and TiS precipitates did not change but the $Ti_4C_2S_2$ and TiC precipitate size increased with increasing the temperatures from 730 to 820 °C. The intensity of three important textures at different annealing temperatures is shown in Fig. 2.6. It shows that the intensity of $\{001\}$ and $\{111\}$ texture increases with an increase in temperature. It is reported that the difference in $111\} \langle 110 \rangle$ and $\{111\} \langle 112 \rangle$ components is lower at 820 °C compared to a 790 °C resulting in uniform γ texture and expected reduced earing during the stamping process.

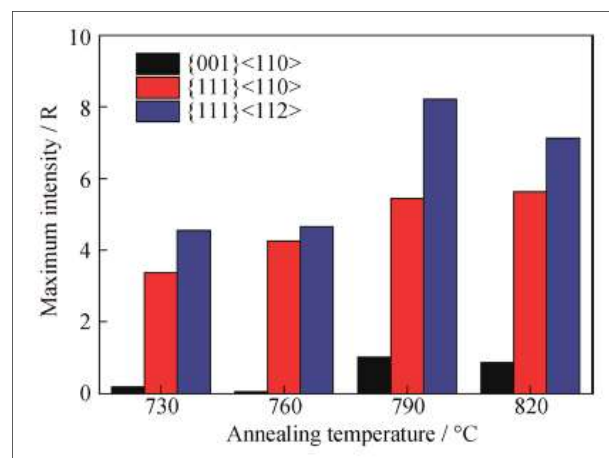


Fig. 2.6. Maximum intensity of three textures at different annealing temperatures (Qiu et al. 2018)

In the present work, Chang et al. (2020) physically simulated hot rolling-coiling, cold rolling and continuous annealing processes for an IF grade billet in the ferritic zone. He reported the hot rolling texture to be hereditary and more γ -fiber recrystallization texture is formed after cold rolling and annealing in coils having higher γ -fiber after hot rolling. This work also confirms recrystallization after hot rolling and coiling in the ferritic region with the formation of weak α -fiber and weak γ -fiber, the strength of which increased with decreasing temperature. Both α -fiber and γ -fiber textures were strengthened after cold rolling but preferentially, γ -fiber was strengthened after annealing. This work also confirms the dependence of uniform grain size and better mechanical properties on rolling temperature. The impact can be different in annealed sheet, rolled out of the actual slab and its formability behaviour must also be studied independently.

To make ferritic rolling industrially feasible, work has also been carried out in many practical aspects. It is also reported (Hai et al. 2013) that with reduced temperature the friction increases. The increased friction has been addressed with use of new lubricants. Kong et al. (2013) studied different lubrication conditions, namely lubricating oil, solid lubricant and dry condition during ferrite rolling of thin interstitial free steel strip. Rolling force, roll roughness and strip oxidation were reported to improve making ferritic rolling possible even at lower temperatures. However, such lubrication practices are still not widely accepted. Recently Leilei et al. (2021) also reported the lubrication effect on the texture formation, and, in turn, affecting the r-value or the deep drawing performance of the IF steel at low temperatures. Study also reported friction generated shear deformation and formation of unwanted goss texture. Hence, temperature optimization becomes very important in ferritic rolling in industrial mills.

2.3 Objectives of the Study

It could be summarized from the literature that the microstructure and texture evolution, in the ferritic rolled IF steel is different from that in the conventional rolled IF steel, thereby affecting the mechanical properties and formability. It is attributed to the mechanism of austenite rolling which is metallurgically different from the ferrite rolling. Stacking fault energy plays an important role during recovery and recrystallization in austenite restoration or ferrite forming mechanisms (Sellars 1986). In metals with low SFE, such as γ -iron and austenitic steels, in which recovery processes are slow, dynamic recrystallization (DRX) during hot rolling may take place when a critical deformation condition is reached (Sellars 1986). In metals with high SFE, such as α -iron and ferritic steels, the phenomenon of

dislocation climb and cross-slip occur readily. In these grades as the dynamic recovery is rapid and extensive, perhaps it is usually the only form of dynamic restoration taking place (Langner et al. 1998).

Most of the research has been on the lab scale simulation of hot ferritic rolling, to produce ferritic-hot-rolled sheets as a replacement for cold-rolled sheets. The work has been focussed on the physical metallurgical aspects of warm rolling, not much is known about the details of this process and its control on an industrial scale. Few studies have dealt with the relation of microstructures and textures with bulk formability (which is an important criterion for industrial production) in ferritic-rolled steel but the variation of microstructure, texture and properties across the strip width and along the length in ferritic-rolled IF steel has never been investigated.

Very few simulations or trials have been reported for subsequent cold rolling and annealing of the hot-rolled, ferritic rolled coils. The texture evolution for achieving desired formability along with other properties in the whole processing system starting from hot rolling to cold rolling and annealing in an industrial set up has also not been experimented or discussed in detail in the literature. Considering the expected benefits and industrial application, it is important to understand the recrystallization behaviour and evolution of texture which affects the formability in industrially rolled ferritic IF steels after subsequent cold rolling and annealing.

Most importantly, the formability is a critical requirement in interstitial free (IF) grade steels used in many automotive components and is affected by processing steps and development of the final grain orientations and texture. None of the literature studied and physically tested the formability in ferritic-rolled sheets either in hot-rolled sheets or annealed sheets. Seldom, ferritic rolling has been carried out by many researchers but a detailed comparison of its formability behaviour for different applications after cold rolling and annealing has not been investigated.

Hence, this work will focus on the development of the mechanical properties, especially bulk formability, through optimization of process parameters in ferritic-rolled IF steel by control of textures at different stages of processing. The above study will provide a theoretical basis for industrial production.

The objectives of the study are as below:

1. To study the effect of ferritic rolling parameters on the microstructure, texture, mechanical properties and bulk formability in hot-rolled coils compared to conventional rolling.
2. To study the variation in microstructure, texture and mechanical properties along the length of the rolled coil in a ferritic-rolled IF steel.
3. To study the effect of cold rolling and annealing on the texture development in ferritic hot rolled coils.
4. To develop optimum rolling (reheating temperature, finishing temperature, coiling temperature) and annealing schedules (speed, annealing temperature, cooling rate, etc.) for industrial production of the ferritic rolled IF steels.
5. To industrially produce IF grade steel sheet through ferritic hot rolling followed by cold rolling and annealing.
6. Compare the suitability of ferritic-rolled IF grade steel vs the austenitic rolled sheet for various formability applications.

CHAPTER 3

METHODOLOGY AND WORK STEPS

3.1 Base Material

The study was carried out on an IF-steel as representative of high formability steels. An industrially produced IF steel, with the chemical composition (wt. %) given in Table 3.1, was used for the rolling experiments. Composition of the steel used in the present investigation was analysed using OES (optical emission spectroscopy – make Spectro) and found to be within the range mentioned here.

Table 3.1. Composition of the IF steel considered for the present study (in wt%)

C	Mn	Si	Al	S	P	Ti	Nb	B	N
0.001– 0.003	0.15 – 0.18	0.006 - .0012	0.030 – 0.040	0.01 max	0.02 max	0.02 – 0.03	0.01 – 0.015	0.000 3 max	0.00 4

3.2 Methodology

In the present work ferritic rolling was carried out on IF steel in an industrial mill and compared it with conventional austenitic rolling for different formability operations. Complete work was divided into 4 major steps.

1. Data collection, sampling and characterization of conventional austenitic rolling of IF steel.
2. Offline simulation and optimization of various processing steps for ferritic rolling of IF steel.
3. Processing, data collection, sampling and characterization of ferritic rolling of IF steel.
4. Formability studies to confirm the suitability of the processed IF steel

Data collection consisted of gathering information of processing parameters affecting the metallurgical characteristics at each step of processing – hot rolling, cold rolling and annealing. This information includes temperatures, rolling loads, speeds, reduction ratios, etc. Sampling include cutting of full width samples from the head and tail end of the coils, after each step of processing. Figure 3.1. shows the sequence of project work steps carried out in this work.

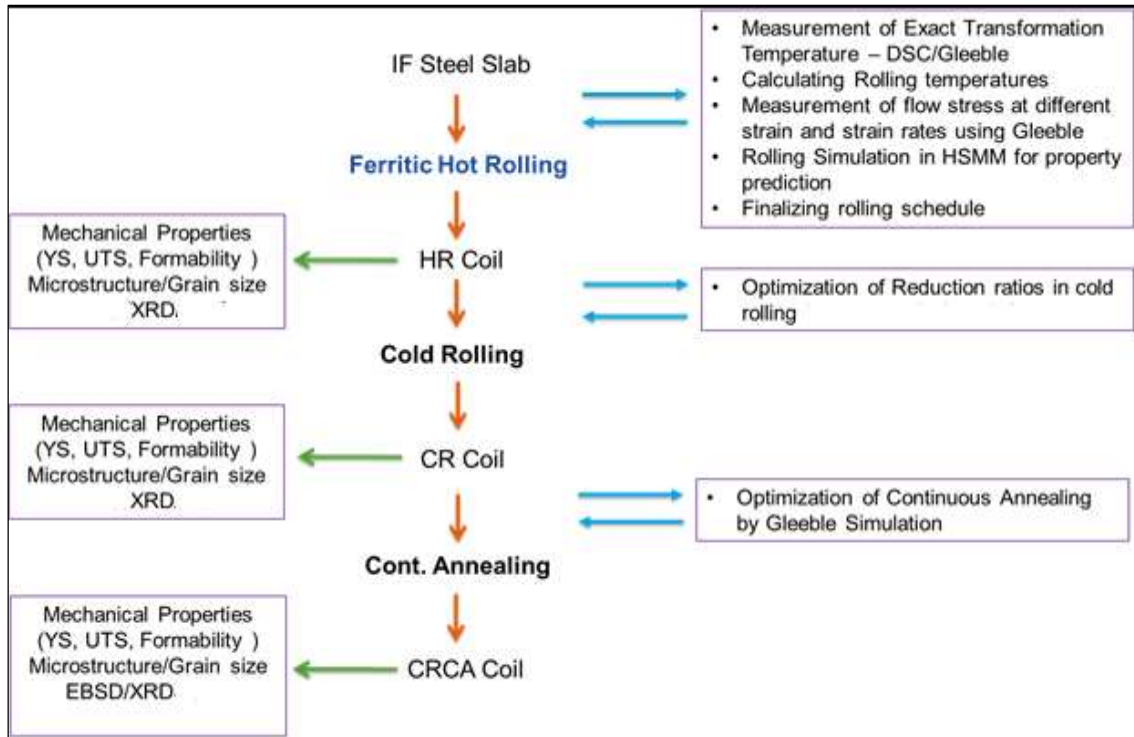


Fig. 3.1. Sequence of project work steps

3.3 Work Steps

Details of the work carried out is explained below.

1. Conventional austenitic rolling of IF steel in a hot strip mill
 - Data collection during the rolling
 - Sample collection at each step
 - Characterization of collected samples
2. Offline simulation and optimization of various processing steps for ferritic rolling
 - Measurement of transformation temperatures for the selected grade using differential scanning calorimetry (DSC) and thermomechanical simulator - Gleeble.
 - Rolling process simulation at different strain and strain rates encountered in the mill using hot deformation studies in Gleeble.
 - Offline rolling simulation in Hot Strip Mill Model software (HSMM) and validation of Gleeble simulation
 - Annealing simulation in Gleeble for optimizing the annealing temperatures for ferritic rolled coils

3. Ferritic hot rolling of IF steel, followed by cold rolling and annealing

- Data collection during the rolling
- Sample collection at each step
- Characterization of collected samples

4. Formability studies on cold rolled and annealed sheets

- Formability limit diagram
- Hole expansion ratio
- Erichsen cupping test
- Earing test

To carry out this research work, many simulation and characterization facilities were used. The facilities/tools used are enlisted in Table 3.2

Table 3.2. List of the facilities/tools used

S. No	Facility/Tool	Purpose
1	Gleeble thermo- mechanical simulator (Model – Gleeble 3800 with pocket jaw and hydrowedge)	For measuring transformation temperature, measurement of flow stress at different stain rates, annealing simulation
2	Hot strip mill model (Model: HSMM V6.5)	For simulating hot rolling process
3	Universal testing machine (Model: Zwick UTM 250)	For YS, UTS and % Elongation
4	Bulging press (Model: Zwick BUP 600)	For formability studies (FLD, earing test , hole expansion ratio, Erichsen cupping test)
5	Optical Microscope (Model: Olympus DSX510)	For grain size and morphology
6	SEM, EBSD (Model: Hitachi –S3400N and Hikari EDAX)	For grain orientation
7	XRD (Model: PANalytical Empyrean)	For texture studies
8	Magnetic Barkhausen Emissions (Model: Rollscan 300)	For residual stress measurement

9	TG-DSC (Model: NETZSCN STA 449 F3 Jupiter)	For determining transformation temperatures
---	--	---

CHAPTER 4

MATHEMATICAL AND THERMO-MECHANICAL SIMULATION

The results found in the literature for the properties of ferritic rolled hot strips are diverse and not consistent even for similar alloy compositions. This is because the production parameters, such as the rolling and coiling temperatures, strongly influence the properties in ferritic rolling (Lifeng et al. 2017) and the impact of these parameters is not studied in detail. This needs customised optimization in each mill by hit and trial. Laboratory facilities and simulation software are generally used to simulate the ferritic hot rolling process for evaluating variables, such as re-heating furnace temperature, finishing and coiling temperature and rolling loads, thereby avoiding costly plant trials. This allows the determination of microstructure/mechanical property for ferritic-rolled IF steel and suggest the optimized rolling schedule for plant rolling. Work in this section includes the selection of process parameters during the processing through off line simulation using Gleeble simulator (Gleeble 3800) or rolling software (HSMM – V 6.5), and incorporate them during the trials. This includes measurement of exact transformation temperatures for the selected composition, finalizing the rolling regime for complete ferritic rolling, validating the physical simulation results with rolling mill software HSMM and simulation of annealing process for temperature optimization.

4.1 Selection of Hot Rolling Parameters for Ferritic Rolling

Literature reports two different types of ferritic rolled coils being produced (Elsner et al. 2004; Kong et al. 2014). First one is, the finishing and coiling temperatures are kept just below A_{r1} , and allow complete recrystallization in the coil. This makes the coil soft and called as the soft hot coil. The second type is called as the hard hot coil where the processing is done at temperatures much lower than A_{r1} . In this case, the coil does not recrystallize and becomes harder and must additionally be recrystallized by annealing (Elsner et al. 2004, Lifeng et al. 2017). In the present work, soft hot coil route is selected as it will not require high loads in a hot strip mill. The rolling schedule to be determined, studied and validated offline, before the plant trials. In the present work, the effect of lower finishing and coiling temperature on an increase in rolling load and expected behaviour is

studied through measurement of transformation temperatures and offline simulations as listed below.

1. Measurement of transformation temperatures through Gleeble
2. Thermo-mechanical simulation of hot rolling process in Gleeble
3. Low-temperature rolling simulation in HSMM software.

4.1.1 Measurement of transformation temperatures

In industrial ferrite rolling, rough rolling or roughing is carried out in the austenite phase above A_{r3} and the finish rolling is carried out in the ferrite phase below A_{r1} (Barrett et al. 2002). The slab is held on the intermediate roller table between the roughing and finishing strands to cool down through the two-phase region and allow complete transformation. The ferrite rolling process requires the finish rolling temperature to be controlled below A_{r1} all along with the coil. The presence of different alloying elements in steel also drastically affects these transformation temperatures (Hoile 2000; Lifeng et al. 2017). Additionally, IF steels have a higher and narrower transformation band and therefore, precise determination of the A_{r3} and A_{r1} temperatures which gives the range of the γ - α transformation temperatures for the experimental cooling rates is important. The knowledge of the recrystallization behaviour of ferrite in absence of a second phase in IF steels are also important to set the ferritic rolling process parameters (Roberto 2011). A phase change is accompanied by dimensional as well as enthalpy change. The phase change phenomenon can be determined by either using differential scanning calorimetry (DSC) equipment or dilation equipment (dilatometer). It is well established that the transformation temperatures are different during heating and cooling (Zhang 2015). In industrial hot rolling process, the phase transformation temperatures in cooling process are the governing parameters, hence transformation temperatures during cooling was measured in this work. A DSC instrument is commonly used to exactly identify the phase transformation temperatures. In the present work, NETZSCH STA 449 F3 Jupiter TGA-DTA-DSC equipment was used for measuring the phase transformation temperatures of IF grade by measuring the amount of energy absorbed/released by the steel sample during phase changes during cooling. Schematic of a DSC set-up is shown in Fig. 4.1. Heat flux DSC comprises the sample and reference holder, the heat resistor, the heat sink, and the heater. Heat required for the heater is supplied into the sample and the reference through heat sink and heat resistor. Heat flow is proportional to the temperature

difference of heat sink and holders. Heat sink has enough heat capacity compared to the sample. In the case of sample showing endothermic or exothermic phenomena, such as phase transition and reaction, this endothermic or exothermic phenomena is compensated by the heat sink. Thus, the temperature difference between the sample and the reference is kept constant. The difference in the amount of heat supplied to the sample and the reference is proportional to the temperature difference of both holders. By calibrating with the standard material, the quantitative measurement of unknown sample is achievable.

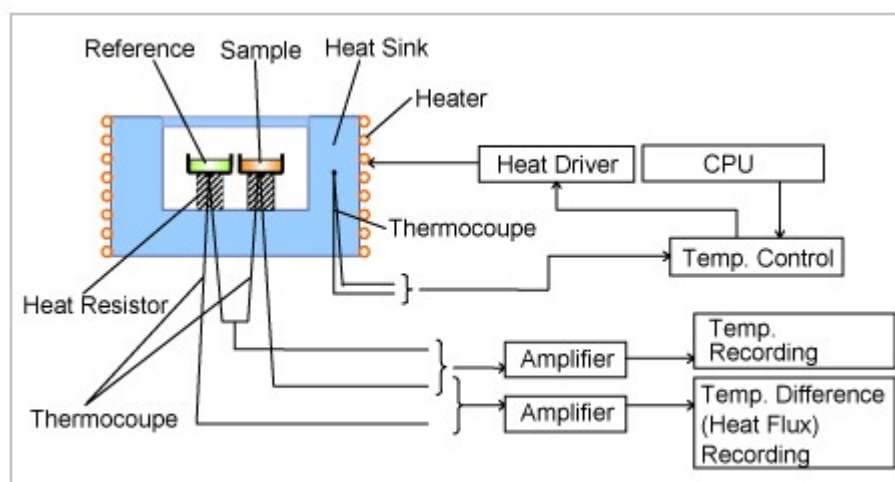


Fig. 4.1. Schematic of a heat flux DSC set-up

In this test, a small sample in the form of a circular disc was prepared to have a diameter of 5 mm and a thickness of 1 mm with a weight of 0.15 g. The sample was placed in a small cylindrical alumina crucible and was heated in a protective nitrogen environment maintained at a flow rate of 40 ml/min. The sample was heated up to 1100 °C at 50 K/min, soaked for 5 minutes and then cooled at 50 K/min till 100 °C.

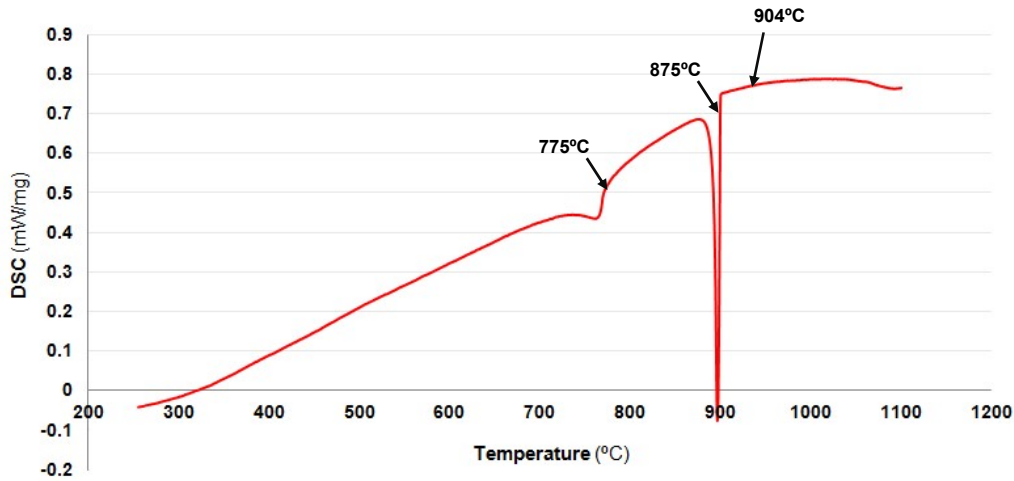


Fig. 4.2. Phase changes identified in IF steel through DSC instrument

The basic principle is that when the sample undergoes phase transformation there is a change in associated heat flow. The result of a DSC experiment is a curve of heat flux versus temperature or versus time. In the DSC curve, during cooling, the first deviation from DSC baseline is observed at the starting temperature of γ to α transformation. Considering that the two-phase region is narrow, the heat flow change per unit time is large which is indicated by a sharp large dip in DSC value. The thermal changes were recorded and were subsequently used to identify the exact upper (Ar_3) and lower (Ar_1) transformation temperatures during slow cooling. Figure 4.2. shows the identified transformation temperatures during cooling. Curve shows 904 °C as Ar_3 , 875 °C as Ar_1 and 775 °C as transition from paramagnetic to ferromagnetic temperature.

Contact type dilatometry is another effective and inexpensive technique for phase change identification. Thermo-mechanical simulator Gleeble is one of the highly precise equipment-available for such measurements and has been used by many researchers (Andres et al. 2002; Yang et al. 2015). In this technique a cylindrical sample is heated to high temperatures and then cooled slowly at controlled heating and cooling rates while recording the dimensional changes using a contact type dilatometer having a low thermal expansion coefficient. The temperature of the specimen is continuously recorded with a set of thermocouples attached to its surface. Figure 4.3. shows the schematic representation of a sample tested for phase change identification in Gleeble.

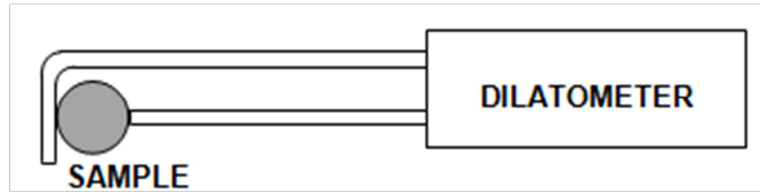


Fig. 4.3. Schematic representation of dilation measurement in Gleeble

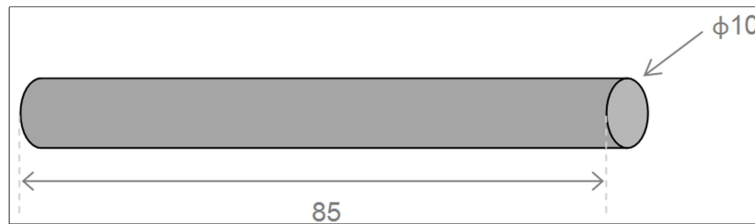


Fig. 4.4. Standard sample geometry in Gleeble for dilatometry

Figure 4.4. shows the standard cylindrical sample used in Gleeble for phase change identification having length 85 mm and diameter 10 mm. Similar to DSC experimentation cycle, the sample was heated at a controlled heating rate of 50 K/min till 1100 °C, soaked for 5 minutes and then cooled at 50 K/min till 100 °C through resistive heating deployed in Gleeble. The testing was carried out in a vacuum to protect the sample from oxidation. A K-type chromel-alumel thermocouple was attached to the sample surface for continuously recording the temperature.

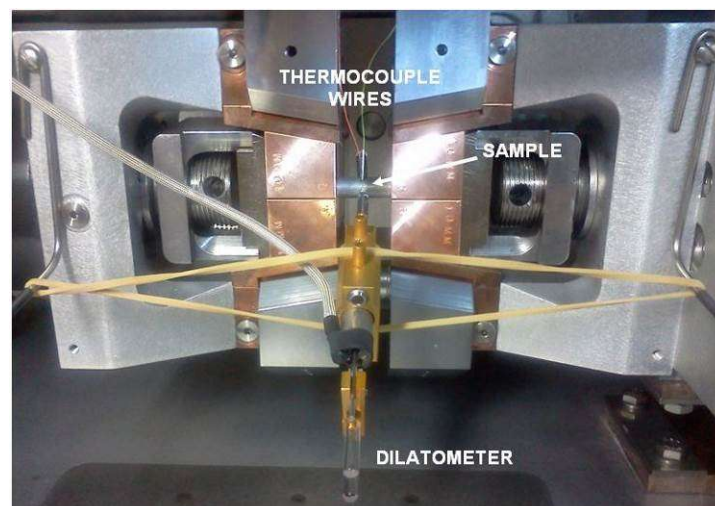


Fig. 4.5. Experimental setup for dilation measurement in Gleeble

The dilation was measured using a contact type LVDT dilatometer at the centre of the

sample (where the thermocouples are also attached) to detect the phase change. Figure 4.5. shows the setup with all the accessories attached. The dilation plot obtained through dilation measurements in Gleeble for IF grade steel is presented in Fig. 4.6. The different transition temperature points or the beginning and end temperatures of the transformed phase were obtained by taking the tangential point of the dilation curve.

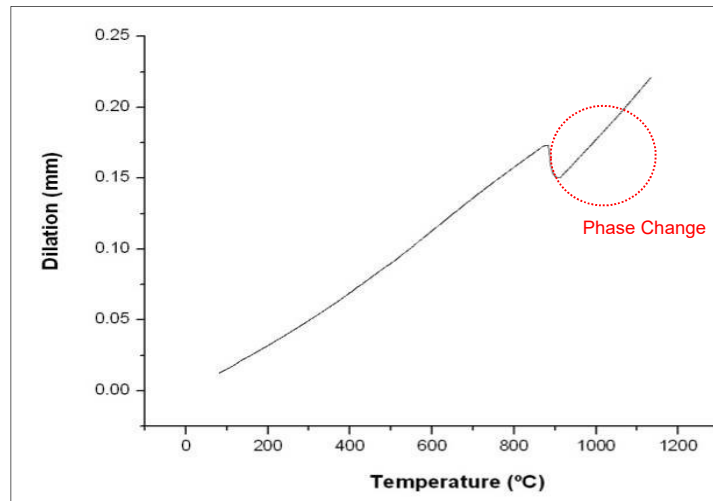


Fig. 4.6. Dilation plot from Gleeble

Table 4.1. Comparison of phase change measuring techniques and their results

Equipment	DSC	Gleeble with contact type Dilatometer
Phase Change Identification Parameter	Thermal Change (Heat absorbed/released)	Volumetric Change (Increase/Decrease in diameter or width)
Atmosphere	Nitrogen	Vacuum
Cooling Rate	1°C/sec	1°C/sec - 30°C/sec
Sample Type	●	▬
Sample Geometry	Circular Disc, dia 5 mm, thickness 1 mm; 0.15 g	Cylinder, 10 mm dia, 15 mm length
Upper Transition Temperature - Ar₃	904 °C	905 °C
Lower Transition Temperature - Ar₁	875 °C	875 °C

The transformation temperatures measured through DSC were compared with those measured through Gleeble using a contact type dilatometer, measured at a similar cooling rate. The comparison of parameters and their corresponding phase transformation temperatures obtained from both techniques are listed in Table 4.1. Transformation temperatures obtained from Gleeble are in good agreement with values measured by using DSC. The above comparison confirms that similar to DSC technique, accurate measurement of transformation temperatures of steel can be carried out by using contact type dilatometry in Gleeble. In industrial scenario, cooling rates frequently encountered during finishing strands are in the range of 5-20 °C/sec. As the phase transformation temperatures are strongly dependent upon heating and cooling rates, it was essential to identify the Ar₃ and Ar₁ temperatures at all these cooling rates, within the limitation of maximum heating and cooling rates possible in the setup. As the DSC equipment used was capable of providing a maximum heating and cooling rate of 50 K/min only (~ 1°C/sec), dilation experiments for identifying Ar₃ and Ar₁ temperatures for IF steel for a wider range of cooling rates were carried out in Gleeble. All the tests were run under vacuum. Different samples of IF grade were heated to 1100 °C, soaked for 1 min and then controlled cooling rates of 1, 2, 5, 10, 15, 20, 25 & 30 °C/sec were deployed and the corresponding phase change temperatures were recorded. The change in the Ar₃ and Ar₁ temperatures at different cooling rates are shown in Table 4.2. The phase transition temperature decreases with increase in cooling rate, but the difference between Ar₃ and Ar₁ temperature increases with increase in the cooling rate. Hence with these experiments, it is concluded that the Ar₁ temperature varies between 875 – 851 °C at the industrial cooling rates of 1-10 °C/s and hence the temperatures of the transfer bar head must be maintained at 40 – 50 °C below this temperature for having the full coil rolling in the ferritic region.

Table 4.2. Effect of cooling rate on the transformation temperatures of IF grade steel

Cooling Rate (°C/s)	Ar ₃ (°C)	Ar ₁ (°C)	Temperature difference, (°C)
1	911	875	36
2	906	871	35
5	902	868	34
10	886	851	35

15	883	837	46
20	873	830	43
25	877	813	64
30	874	807	67

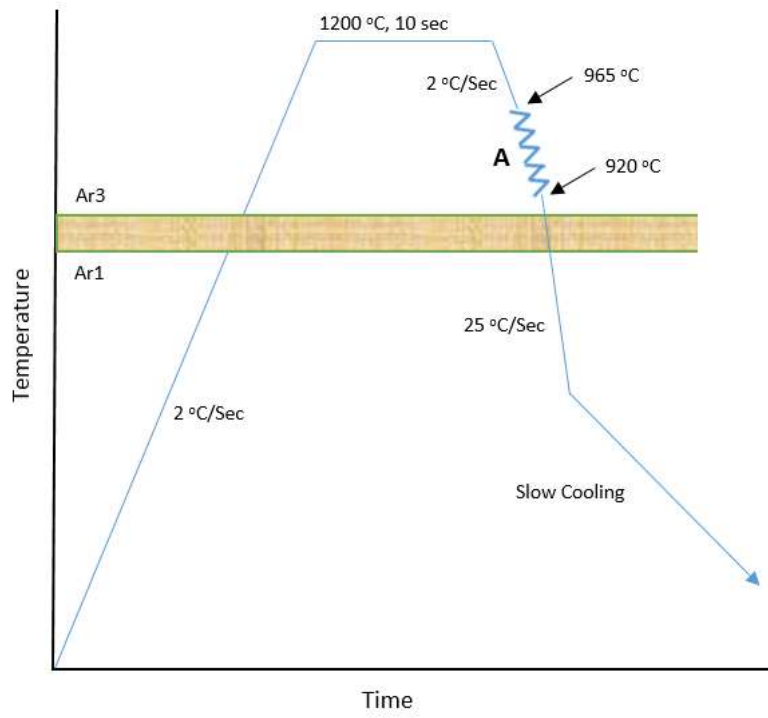
4.1.2 Hot rolling simulation

Rolling load is a critical limitation in any mill and it depends on the temperature of deformation, applied strain in a strand and the corresponding strain rate. Therefore, before industrial rolling, it is necessary to calculate and compare the flow stress of IF grade steel at operating temperatures. The knowledge of the plastic flow behaviour of IF steel at lower temperatures is also required to adjust reduction ratios during rolling. Generally, the flow stress values decrease with increase in temperature and vice versa (Loveday et al. 2006). In ferritic rolling, at lower temperatures, it is expected to have an increase in flow stress and hence it requires higher mill loads. It is also established that the deformation resistance varies non-uniformly with the decrease in temperatures (Guang et al. 2008). Therefore, it is important to choose the range of least deformation resistance to have reduced rolling pressure which brings process stability and will also improve rolling mill availability and productivity during industrial rolling.

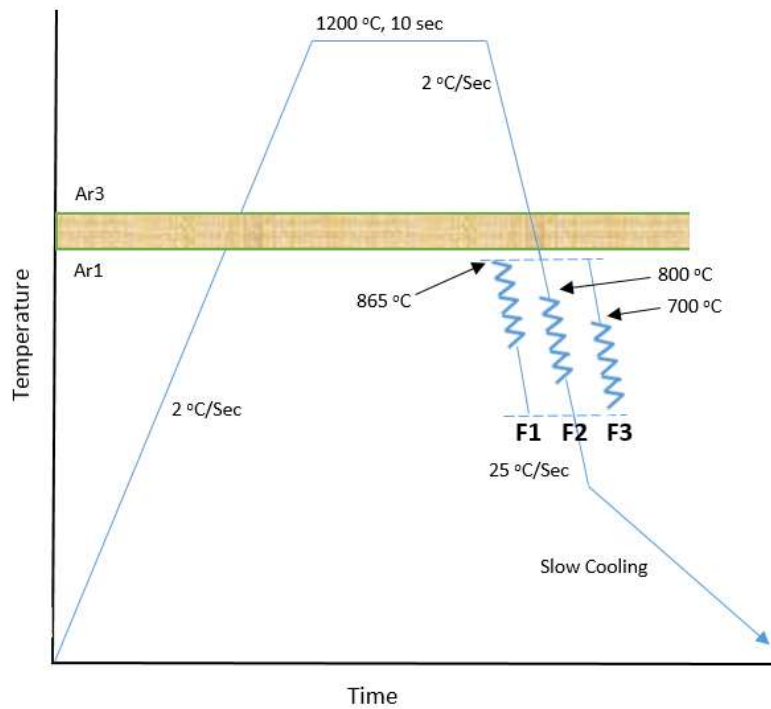
It also becomes imperative to study the impact of low temperature phase transformation on flow stress values and optimize the ferritic rolling temperatures for industrial rolling. In the present time design and optimization of hot deformation processes are no more attempted using costly and time consuming industrial trials (Caleb et al. 2020). Mathematical modelling packages have advantages over plant trials and are regularly used for such simulations but limits its prediction accuracy to the conditions where correlations between strain-controlled deformation and microstructure evolution are known. For the new and complex deformation conditions, flow stress behaviour and microstructural changes can only be experimentally identified using thermomechanical simulators (GroBheim et al. 1996; Leire et al. 2020). In the present work, hot deformation tests under plane strain conditions were performed in Gleeble-3800 thermo-mechanical simulator for simulating hot rolling of IF grade steel in austenitic and ferritic temperatures. As the cast structure suffers from structural inhomogeneities and segregations, the samples were collected from austenitic rolled IF steel transfer bar from the hot strip mill for obtaining a homogeneous initial structure. The samples were cut into smaller pieces and machined into 30 mm × 26 mm × 15

mm cuboid shape for simulations. Multi-hit uniaxial hot deformation tests were carried out using the hydra-wedge module of Gleeble to measure the flow stress values for the selected IF grade under 3 different ferritic temperature regimes. The existing austenitic rolling was also simulated for comparison. The strain and strain rates in each deformation pass during ferritic rolling were kept similar to the values experienced during industrial austenitic hot rolling.

The deformation was carried out in vacuum, using tungsten carbide deformation dies. Nickel paste was used as the lubricant to avoid sticking and ensure uniform deformation along the diameter during hot compression tests. The temperature of the specimens was monitored using a chromel–alumel thermocouple. In industrial rolling, the total reduction ratio for conversion of the slab to hot-rolled coil involving rough rolling and finish rolling is close to 98 %. Such a large reduction is not possible in any regular simulator (Vinod 2016). Rough rolling has to be always carried out above recrystallization temperature and therefore does not have much impact on the final properties and hence can be skipped for a relative comparison study (GroBheim et al. 1996). Therefore, in the present work, finish rolling, run-out table (ROT) cooling and coiling is simulated which has a direct impact on the final properties. The strain, strain rate, finishing temperature (FT) and coiling temperature (CT) programmed for each pass during all four experiments. Due to the strain limitation in Gleeble, all 7 finishing passes of the hot strip mill could not be simulated. Consequently, a total of six passes (deformation passes 2-7) were simulated under plane strain condition (with pass 2 being partially simulated). A maximum strain of 0.5 was given in strand 3 and a minimum strain of 0.16 was given in strand 7.



a: austenitic rolling



b: ferritic rolling

Fig. 4.7. Schematic temperature-time plots indicating simulation of a) austenitic rolling and b) ferritic rolling

During rolling, strip speed is lowest in the initial strands and hence corresponding strain rate of 20 per sec was maintained in the first strand and the highest strain rate of 165 per sec was given in strand 7 where the strip speed is maximum. The schematic temperature-time plots indicating simulating conditions is shown in Fig. 4.7. The specimens were heated to 1100 °C with a rate of 2 °C / sec, held for 10 secs for homogenization. Ar₃ and Ar₁ temperatures were taken corresponding to a cooling rate of 2 °C / sec. Thereafter, the sample was control cooled to the 1st deformation temperature. 3 sec holding time was given to homogenize the temperature in the sample before the deformation in each deformation cycle. The strain and strain rates of each six deformation steps are different and similar to the values set in the industrial rolling of an austenitic IF steel. A delay period of 2 - 4 seconds was given between each deformation step based on the rolling speed. This is to simulate the time taken for the movement of material between each strand. Total four finishing and run-out table cooling sequences were simulated: (1) austenitic rolling – ‘A’ with finishing start at 965 °C, (2) high temp ferritic rolling – ‘F1’ with finishing start at 865 °C, (3) medium temp ferritic rolling – ‘F2’ with finishing start at 800 °C, (4) low temp ferritic rolling – ‘F3’ with finishing start at 700 °C. F1 simulated the industrial rolling just below Ar₁ to see the effect of partial recrystallization, whereas F2 and F3 simulated complete ferritic rolling at lower temperatures within practically possible limits of an industrial rolling setup. Run out table (ROT) cooling of the strip was simulated by spraying mist through the specially designed nozzles onto the specimen surface to provide a cooling rate of 25 °C/sec down to the coiling temperature. Coiling temperatures were varied between 640 °C and 550 °C based on the finishing temperatures. The specimens were then slowly cooled to room temperature in the simulator itself, in 30 minutes to simulate the slow cooling of the coil surface after coiling. The deformation dies, initial sample and the final sample after deformation are shown in Fig. 4.8. The temperature of the specimen, flow stress, time, and strain for each deformation was recorded continuously. The measured temperatures of the sample during the continuous rolling and cooling cycle closely matched with the programmed temperature. Five samples were repeated under each condition and the best three samples having a uniform shape and contact thickness were selected. Precisely cut centre part of these deformed samples were used for further characterization studies.

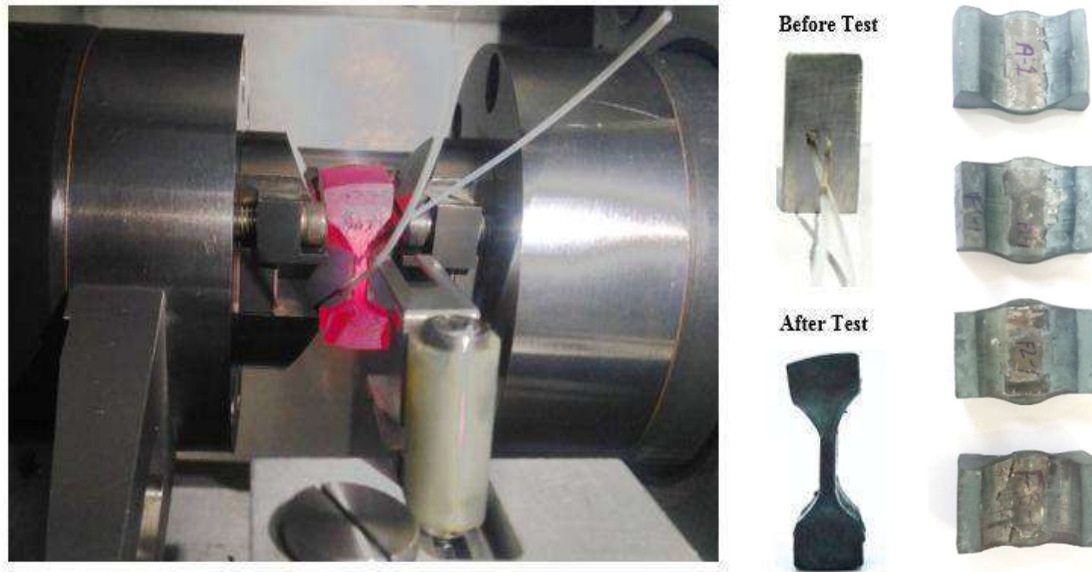


Fig. 4.8. Hot deformation simulation in the thermo-mechanical simulator

A multi-hit deformation simulation was also carried out in Gleeble at different temperatures covering the phase transformation temperature band, as shown in Fig. 4.9. The stress-strain curve shows a change in slope at maximum flow stress by strain accumulation indicating DRX occurring between passes 2 and 3. During rolling, an abrupt drop in flow stress occurs in the fifth pass due to the start of austenite to ferrite transformation. The temperature in this pass is 875 °C which is near the A_{r1} temperature (~ 880 °C). It is found that the flow stress decreases substantially upon phase transformation from the austenite to the ferrite. Hence, it can be safely concluded that the mill load will not increase when finish rolling is carried out in the ferritic phase.

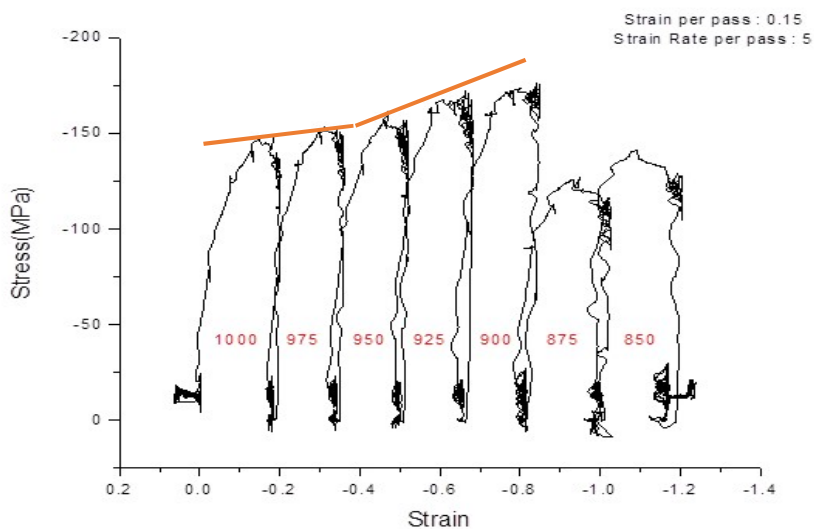


Fig. 4.9. Effect of temperature on flow stress values measured in Gleeble

4.1.3 HSMM (hot strip mill model) simulation

Before carrying out the actual trials in the plant, in addition to the thermomechanical simulation, the proposed rolling schedule was validated offline through a mathematical model also. Such offline simulations are being carried out by many researchers (Millitzer 2000; Sushant 2016) and steel companies using commercial simulation packages such as Hot Strip Mill Model (HSMM). The Hot Strip Mill Model (HSMM) is an invaluable tool to assist cost-effectively, in determining the optimum processing conditions to achieve the desired product properties in the hot and plate rolling process. The HSMM model performs a multitude of calculations to simulate the physical process of rolling steel in a hot strip mill. To model various mechanical and thermodynamic processes during hot rolling, these calculations rely on equations from the basic principles of physics and on equations developed from the theories proposed by researchers of the rolling mill. To properly implement the calculations, an integrated model is provided that includes a user-friendly interface for set-up, configuration, implementation and viewing results. The HSMM contains a completely linked model that allows the user to simulate the processing of the steel from reheat furnace dropout to the coiler or cooling bed. The model's tracking program tracks the head, middle and tail points along the length of the piece, modelling each point as it progresses through the mill. The temperature evolution, rolling forces, microstructure changes and final mechanical properties are calculated for each of these three points. In the present work, HSMM V6.5 is used to simulate the existing austenite rolling process and the proposed ferritic rolling process. The HSMM model was first configured for Hot Strip Mill – 2 of JSW Vijayanagar steel plant where the existing austenitic rolling is being carried out and ferritic rolling is proposed. The user interface of the model is shown in Fig. 4.10. Configuration process includes data input on the furnace area, roughing area (mills, edgers, sprays), heat retention area (coil box, panels), finishing area (mills, edgers, sprays), run out table and mill exit area. It also requires a specific set of coefficients to be used for the grade of steel being processed via a specific rolling mill schedule. The model was also validated for the existing austenitic rolling of IF grade steel.

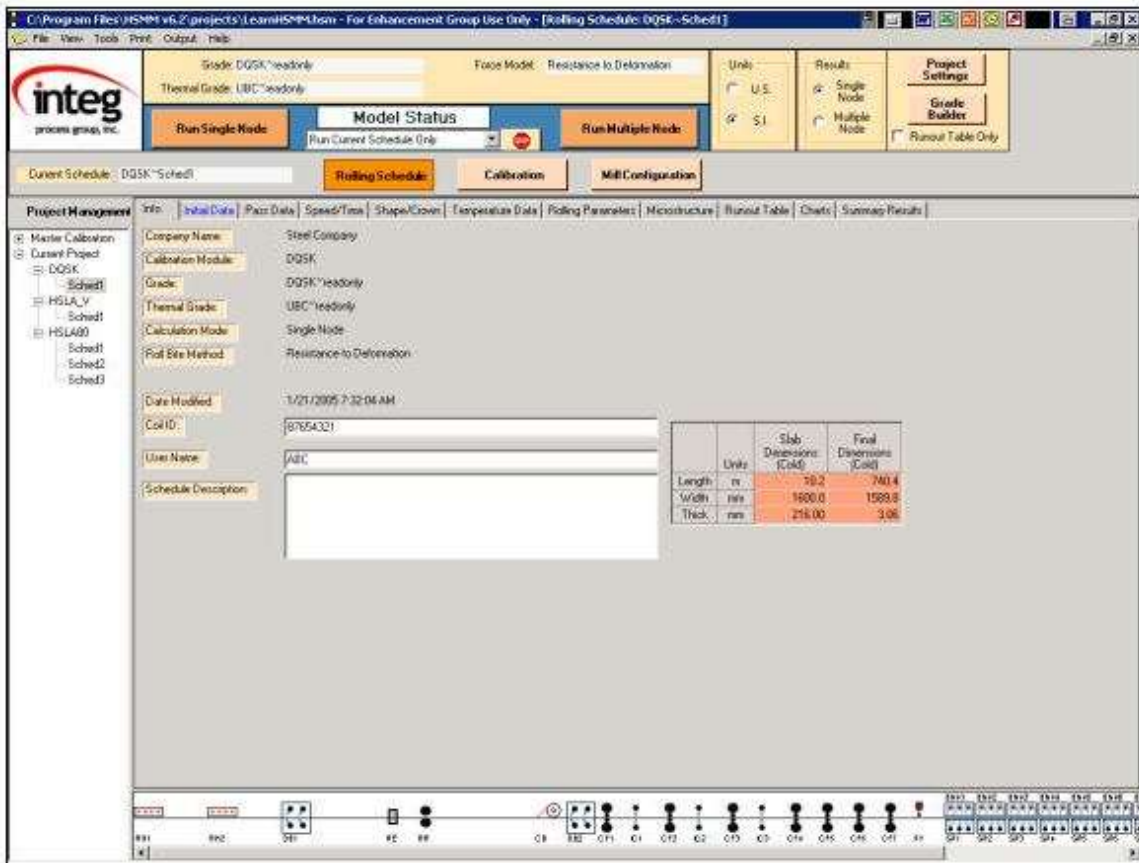


Fig. 4.10. HSM model mill configuration interface

4.2 Selection of Continuous Annealing Parameters Through Simulation

The cold-rolled sheets are continuously annealed for controlled recrystallization and relieving stresses. The heat treatment parameters applied to the cold-rolled strip during continuous annealing are extremely important in determining the final mechanical properties and microstructure of the coils (Ahmad et al. 2014). These parameters are highly grade-specific and include the inter-critical annealing temperature, soaking duration and specific combinations of cooling rates. The continuous annealing lines are divided into specific sections involving preheating, heating, soaking, slow cooling, rapid cooling, over ageing and final cooling in a very short time. The strengthening mechanisms in these processes, such as phase transformation, precipitation, etc. are a strong function of line speed and strip temperatures (Hoile 2000; Zhao 2019). Any change in these parameters causes significant variations in mechanical properties. Hence, it becomes imperative to optimize the process parameters for close control of the mechanical properties of the final product. Since the ferritic-rolled sheets have a different stress concentration and grain morphology, the annealing cycle must be optimized separately (Hao et al. 2019). In the

present study, experiments were carried out to simulate the continuous annealing processes in the thermo-mechanical simulator (Gleeble). Gleeble system offers an excellent platform to simulate any complex cycle involving multistep heating and cooling cycle (Yang et al. 2015). Accurate temperature control makes it the most effective tool to study the microstructural evolution during the annealing process and ultimately optimize it to achieve the desired microstructure and properties. Representative cold rolled full hard sheets of both the ferritic rolled coils and the one austenitic rolled coil of similar thickness were collected, and cut from the tail end of the coil. These sheets were further cut to experimental dimensions of 240 x 50 mm size with 5 mm diameter holes on either side, as shown in Fig. 4.11. All the samples were cleaned with acetone to remove any dirt or scale.



Fig. 4.11. Specimens for strip annealing simulations in Gleeble

On these samples, chromel-alumel thermocouple wires were welded and then fixed inside pocket jaw module with strip annealing grips. Fig. 4.12 shows the arrangement for strip annealing simulation in Gleeble 3800 thermo-mechanical simulator. The continuous annealing process is broadly divided into four stages, heating section, soaking section, rapid cooling section and the over ageing section. These sections are programmed into the simulator in a time-temperature plot.

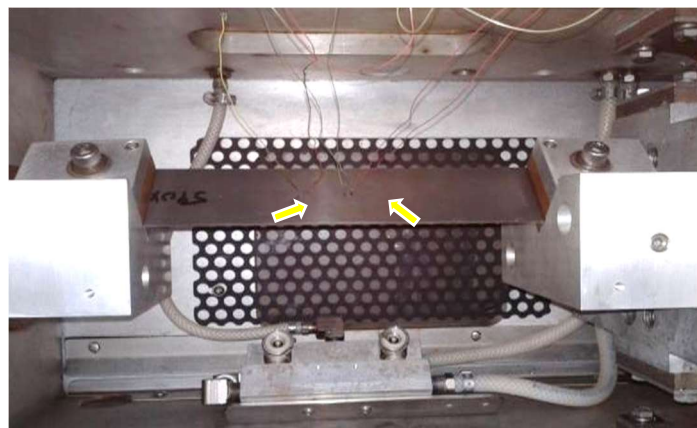


Fig. 4.12. Thermocouple arrangements during strip annealing simulations set-up in Gleeble

In annealing, the soaking temperature is the most critical parameter. Other parameters are optimised as per the production requirement. Hence in this work, simulations were carried out to study the effect of soaking temperature on the ferritic rolled samples compared to the austenitic rolled samples and to identify the optimized temperature band. The conventional austenitic rolled sheet is annealed at 800 - 820 °C during the actual production. Samples from all three coils were subjected to soaking temperatures of 740 °C, 760 °C, 780 °C, 800 °C and 820 °C. The heating rate was programmed at 5 °C/sec and the soaking time was kept for 45 secs. In the rapid cooling section, the strip was cooled at the rate of 14 °C/s till 480 °C. The final over-ageing was done at 397 °C before cooling to room temperature at a speed of 5 °C/s. Other than the soaking temperature all other parameters were kept similar to the conventional austenitic annealing cycle. The annealing cycles simulated are shown in Fig. 4.13.

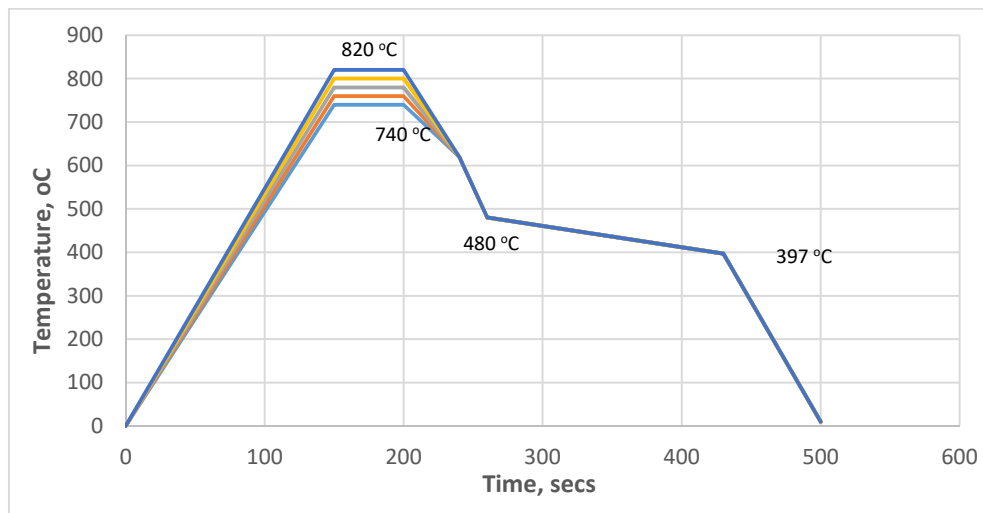


Fig. 4.13. Simulated annealing cycles



Fig. 4.14. Strip sample after annealing simulation in Gleeble

Three samples were tested under each cycle. Figure 4.14. shows the condition of the sample after annealing simulation. Samples does not show any excessive oxidation and uniform surface near the central portion. The simulated specimens were tested for mechanical properties and microstructure to find the optimized cycle producing the largest grains and

highest elongation. The tensile test samples are precisely punched out of the simulated specimens as shown in Fig. 4.15 and subjected to the tensile test for strength and elongation measurements. Two samples were subjected to tensile test and one sample is used for the microscopy study after polishing and etching.

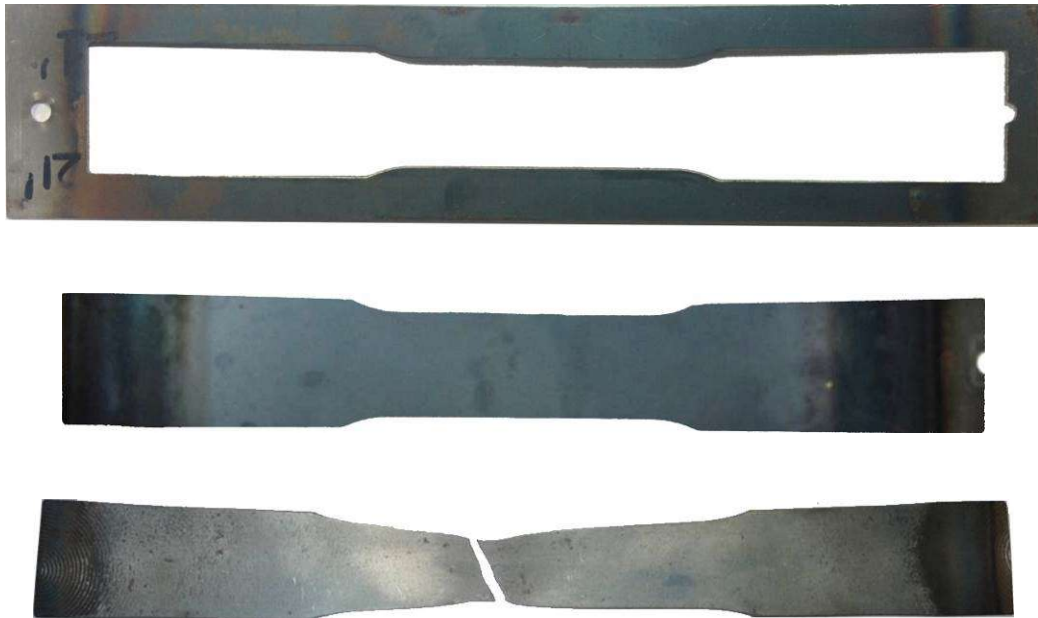


Fig. 4.15. Tensile test specimen punched out and tested from the annealed sample

These simulations helped in studying the effect of various process parameters, optimizing the critical parameters before the plant trials and reducing the number of costly online plant trials.

CHAPTER 5

EXPERIMENTATION AND PLANT TRIALS

Interstitial free (IF) steels are used for very complex products, like inner door panels, side parts or inner wheelhouses. In these steels, by the addition of titanium and/or niobium, a complete fixation of carbon and nitrogen is reached in the form of nitrides (TiN), carbides (TiC), or carbonitrides (TiCN). This gives excellent forming ability, low yield points, and at the same time, high forming characteristics. However, these advantages are accompanied by the variation in properties along the length and the width of these steel sheets. It is arising from the production difficulties during rolling thinner sheets due to temperature loss, some of the areas of the strip enters two phase region. This causes shape defects and a reduction in yield (Andreas et al. 2000). In response to this problem, ferritic rolling is being developed whereby the hot rolling finishing temperature is lowered below the two phase region into the ferritic region, hence avoiding phase transformation during cooling. By ferritic rolling, gauge control for the thin and wide hot strip as well as mechanical properties is expected to be improved. Ferritic rolling, though has many processing advantages, a notable drawback reported is poor deep drawing properties caused by detrimental shear texture formed during final finishing (Sarkar et al. 2010). It was found (Barrett et al. 1999) that (110) shear texture was formed just below the surface of the strip and prevented the formation of (111)/(110) texture ratio greater than unity required for good drawability. Ferritic rolling is also been reported (Barrett et al. 2002) to have a negative effect on productivity. The present work is aimed to develop optimized processing schedules for industrial production of ferritic interstitial free steel. The present work investigates the metallurgical aspects of the process at all stages, whose control is not yet completely understood, and develop parameters for industrial production of ferritic IF steels.

5.1 Selection of Composition/Grade

Many variants of the IF grades are produced in an integrated steel plant. The lower strength variants having tensile strength between 180 – 240 MPa are used to manufacture visible parts, such as door panels. The widely used variant is 270 MPa IF grade designed for more complex structural parts (longitudinal beams, cross members, suspension and chassis components, etc.) (Elaheh 2011). Here the 270 represents the minimum UTS to be

achieved. These are used in the thickness range of 0.5 – 1.5 mm. This grade requires excellent drawability for its mechanical strength level. This behaviour is associated with very good elongation at rupture, very good strain-hardening coefficient and normal anisotropy (Perera et al. 1991). Significant variation in properties along the coil and shape defects are found in this grade leading to lower yields. This can be minimized for better yields through ferritic rolling (Sarkar et al. 2010). For the baseline measurement, a regularly made 270 D IF steel grade steel made at JSW Vijayanagar works (HR grade- JVHC210N00, CR grade - CAU212, Category – DIF) has been selected. The selected grade has Ti-Nb stabilized IF steel composition which is shown in Table 5.1. The selected IF grade is also prone to many surface defects during austenitic rolling and is a best case for comparison with ferritic rolling.

Table 5.1. Composition of selected IF grade slab, wt.%

C	Mn	Si	Al	S	P	Ti	Nb	B	N
0.002	0.17	0.006	0.036	0.007	0.011	0.027	0.011	0.0001	0.0025

The unique feature of this grade is low levels of C and N. IF liquid steel is processed through degassing to reduce C and N to levels low enough that the remainder is ‘stabilized’ by small additions of Ti and Nb. Ti and Nb are strong carbide/nitride formers, taking the remaining C and N out of solution from the liquid iron, after which these latter two elements are no longer available to reside in the interstices between solidified iron atoms. The synergy of these two elements allows complete stabilization to be achieved at lower levels of each element. Depending on the relative amounts of Ti and Nb, the steel needs to be annealed at a higher temperature during galvanizing (Helong et al. 2015).

5.2 Industrial Production of IF Steels

The broad processing steps of IF steels include, steelmaking in basic oxygen furnace → vacuum degassing in RH degasser → continuous casting → hot-rolling → pickling → cold-rolling → annealing by using batch annealing furnace or continuous annealing furnace → skin tempering, oiling and packaging (Hoile 2000). Figure 5.1. shows the process route for the industrial manufacturing of conventional IF grade. The key processing step where the properties are primarily decided by the hot rolling, where the temperature of the slab is raised above the recrystallization temperature and rolled in the austenitic temperature range.

In this work, it is proposed to reduce the hot rolling temperatures below A_{r1} and roll in the ferritic temperature region. Therefore, it is proposed to study each subsequent step in offline condition for optimizing the parameters for a ferritic rolled strip. The first step of the work is to understand the existing austenitic rolling of IF steels and form a baseline for comparison. Work in this part includes a collection of data of all process parameters during the processing and complete characterization of samples collected at various stages. The objective of this part is to develop a full characterization map for the rolled coils at each stage for the austenitic and ferritic rolled coils. During the production of IF steel, the same heat was completely followed from steelmaking to final coiling and samples were cut at each stage for the characterization and off line simulations. The results are shown in terms of microstructures, crystallographic textures and mechanical properties. This section will explain the mechanisms and structure-property correlations for the existing austenitic rolled IF grade coils and ferritic rolled coils.

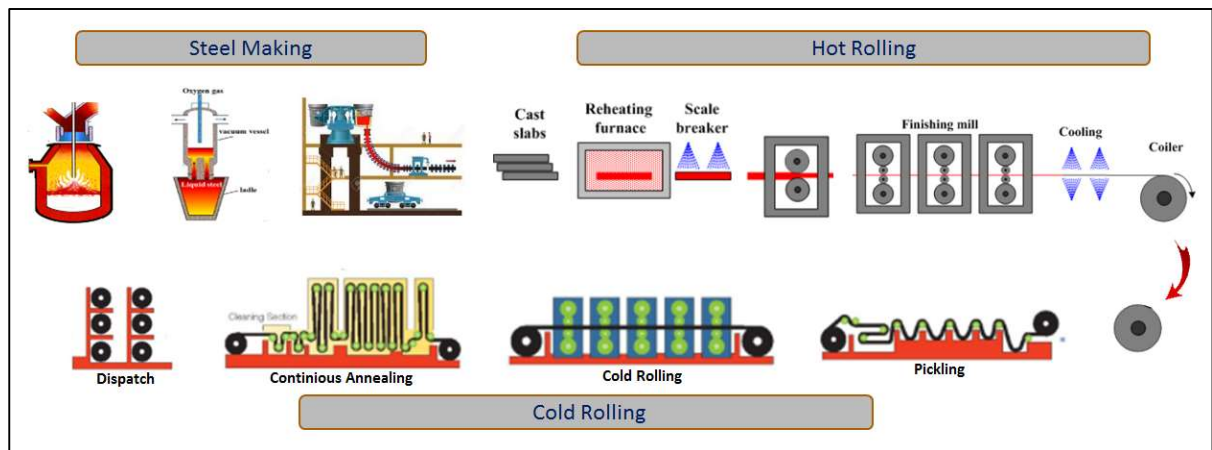


Fig. 5.1. Process route for industrial production of the IF steels

5.3 Steelmaking and Casting Process

Steelmaking process for an IF steel is different from the normal grades due to its low carbon and high cleanliness requirement. Hot metal from iron making is first deep de-sulphurised at the hot metal desulphurisation station through KR process (Kanbara Reactor). KR is a hot metal pre-treatment system for the desulphurization process in which reaction takes place by the addition of reagents and mixing through the mechanical stirred refractory impeller. The hot metal sulphur is brought down from 0.05 % to < 0.005 % during the de-sulphurization process. After raking the De-S slag, the hot metal is charged into the LD converter. In the converter, oxygen is blown into the molten

metal through a top lance which removes the silicon, carbon and phosphorous (Fruehan 1998). The raw steel is tapped into a ladle at a steel temperature of 1650 °C with bath carbon around 0.04 % and bath oxygen at 600 ppm. Only lime and synthetic slag is added at the tapping and no de-oxidation is carried out. This dissolved oxygen is utilized for de- carburization in RH (Ruhrstahl Heraeus) degasser. This is the key difference in the manufacturing of the IF steel compared to other steels where de-oxidation is carried out at tapping itself. The heats are then directly sent to the ladle heating furnace where Al shots are added to kill the slag. The steel is then transported to RH-Degasser. The Ruhrstahl Heraeus (RH) vacuum recirculation process is carried out in a refractory-lined vessel equipped with two snorkels immersed in the steel bath as shown in Fig. 5.2.



Fig. 5.2. RH-degasser snorkels

In this process, oxygen is blown under the vacuum from the top lance for more than 10 mins with intermediate Al addition (Fruehan 1998). The process is for decarburization and degassing and is the best suitable system for the production of ultra-low carbon steel grades with carbon < 0.002%. The purpose of the RH degassing is to remove as much carbon as possible and subsequently precipitate the rest as carbides by the addition of Ti or Nb forming TiC or NbC. These carbides are stable at the subsequent annealing temperature. Alloying elements are added after the degassing and have the advantages of achieving higher yields and high accuracy of chemical analysis of steel due to the absence of air and the avoidance of metal slag reactions (Fruehan 1998). After ensuring the desired composition, the steel is sent to a continuous casting machine as shown in Fig. 5.3. In the continuous casting facility, molten steel is transferred from the ladle to the tundish through a shroud and subsequently poured from the tundish into the water-cooled mold. The partially solidified slab is withdrawn from the bottom of the mold into the water sprayed segments so that the

solidified slab is produced constantly and continuously. The key parameters maintained during continuous casting are superheat in between 20-30 °C, casting speed in between 2-2.5 m/min, sequence length 3-5 heats, and casting with no abnormalities (Allan 2003), The slabs thus produced are hot dispatched for rolling. After casting, the slabs are inspected for any surface defects before sending it to rolling. These parameters will remain same even for the slabs produced for ferritic rolling experiments.



Fig. 5.3. Continuous caster and casting process

5.4 Selection of Steelmaking Parameters for Ferritic Rolling

As the study is based on the commercially produced IF grade steel from JSW steel Vijayanagar works no compositional change is proposed for the ferric rolling trials. The selected grade for ferritic rolling is Ti-Nb stabilized IF grade steel, as shown in Table 5.1, which is regularly rolled in austenitizing conditions. As it is an optimized composition and the parameters selected during steel making are designed to have the best cleanliness possible, no changes have been done in the steel making process parameters.

5.5 Hot Rolling Process

The primary function of the hot rolling process carried out in a hot strip mill is to reheat semi- finished steel slabs above recrystallization temperatures, then roll them thinner and longer through successive rolling mill stands driven by motors and finally coiling up the lengthened steel sheet for transport to the next process. A typical hot strip mill is shown in Fig. 5.4. Hot rolling permits large deformations of the metal to be achieved with a lower number of rolling cycles (Vladimir 2001).



Fig. 5.4. Hot strip mill at JSW Steel, Vijayanagar works

Hot strip mill consists of a re-heating furnace for heating the slab and achieving the recrystallization temperature ($> 1250\text{ }^{\circ}\text{C}$), a de-scaler to remove the scale formed due to oxidation in the furnace, a roughing mill for the initial reduction of the slab (80 % reduction), which then achieves the final ordered thickness through successive reductions in a series of closely coupled mill stands in finishing mill (90 % reduction). After leaving the last finishing stand, the rolled strip is delivered across a run-out table that is equipped with top and bottom cooling sprays. The cooling rate and final coiling temperature are controlled to obtain the desired uniform metallurgical properties. During hot rolling of steel which takes place above the recrystallization temperature, the cast grain structure is broken. Old grain boundaries are destroyed and new grain boundaries are formed along with a more uniform grain structure. Schematic of typical microstructure development during hot rolling is shown in Fig. 5.5.

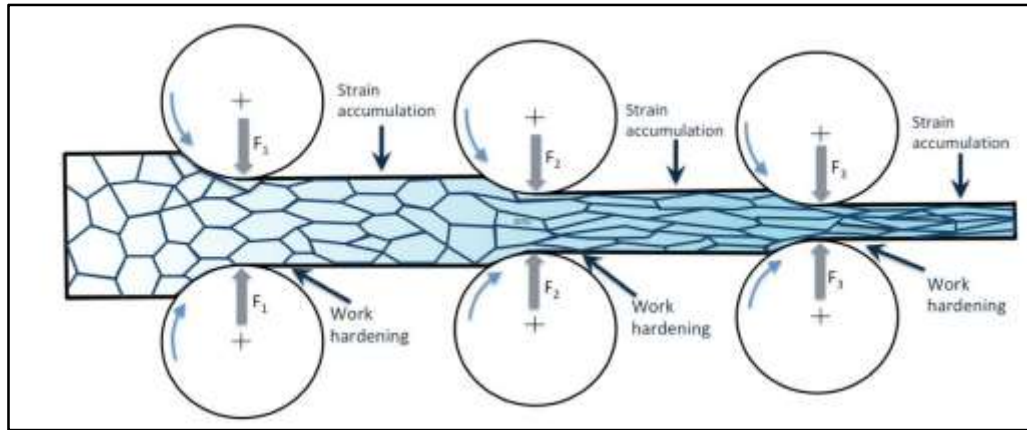


Fig. 5. 5. Schematic of microstructure development during hot rolling

Rolling of steel also closes the vacancies and shrinkage cavities within the steel and breaks the inclusions and distributes them uniformly throughout the work piece. The distinctive mark of hot rolling is not only a crystallized structure but the simultaneous occurrence of dislocation propagation and softening processes (Vladimir 2001). During the process, temperature, strain, and strain rate distributions within the rolled metal play a significant role in the kinetics of metallurgical events such as static, dynamic, and meta dynamic recrystallization during or after hot rolling as well as decomposition of austenite on a run-out table (Barnett et al. 1999).

5.6 Ferritic Hot Rolling Plant Trials

Hot rolling is a complex process and the microstructure evolution during rolling is a function of static, dynamic and meta dynamic recrystallization and grain growth. These processes are interdependent and must be studied in an integrated manner to derive logical conclusions. Based on the thermo-mechanical simulation and HSMM results, two ferritic rolling regimes were considered for plant trails. Plant trails were conducted in a 2-Hi, 2 stand roughing and 7 stand finishing hot rolling mill. Two coils were rolled at 2 different target conditions, namely FR-1 (FT-840 °C, CT-640 °C) and FR-2 (FT-800 °C, CT-600 °C). The industrial trials started with continuously cast 220 mm thick and 1470 mm wide IF grade slabs. Slabs were reheated in a gas-fired reheating furnace for 160 mins to achieve the drop out temperature of 1130 °C. It was followed by descaling, 2 stand roughing and 7 stand finishing to produce a HR coil of 4 mm thickness. The speed of the slab movement was kept lower at 60 mpm (meters per minute) to obtain lower ferritic temperatures. After furnace exit, the slab was descaled and rolled in 2 stand reversing roughing mill with 3 passes in each stand, as shown in Fig. 5.6.



Fig. 5.6. Reversing roughing mill



Fig. 5.7. Finishing mill stand controlling strip thickness

During industrial rolling, it is not feasible to significantly lower the reheating furnace temperatures to the ferritic range and hence the furnace exit temperature was lowered by 100-150 °C. This restricts the rolling temperatures and therefore the rough rolling is carried in the austenite phase above A_{r3} temperature and the slab is held thereafter to cool down through the two phase region before it enters the finishing stands on the transfer table. The finish rolling is carried out in the ferrite phase below A_{r1} temperature. The roughing mill exit thickness was maintained at about 44 mm and temperature at 930 °C to ensure all roughing deformations being carried out, above A_{r3} temperature. The FR-1

and FR-2 transfer bars were air cooled to below 840 °C before entering into finishing stands for ferritic rolling. The speeds were controlled to match the finishing entry temperatures. The intermediate bars were then rolled in 7 passes to 4 mm thickness in the finishing mill. The finishing mill stand controlling the final thickness by roll gap adjustment is shown in Fig. 5.7. The actual finish rolling temperature achieved was 825 °C and 780 °C, marginally lower than the targeted values. The rolled coils were then cooled on the run-out table (ROT) and the coiling temperatures achieved were 625 °C and 575 °C in FR-1 and FR-2 respectively. This shows that whole rolling has been carried in two temperature bands, FR1 at higher temperatures and FR2 at lower temperatures in the ferrite region. This helps in studying the effect of these critical rolling temperatures on the microstructure development. The cooling pattern was kept similar to the IF grade austenitic rolling. All the rolling data and the samples for a similar section austenitic rolling named AR, was also collected from the plant for detailed characterization and process comparison. The comparison of process parameters for the austenitic and both the ferritic rolling coils in the hot strip mill is shown in Table 5.2.

Table 5.2. Comparison of key hot rolling parameters

S. No	Parameters	AR	FR1	FR2
1	Re-heating furnace exit temperature, °C	1247	1130	1128
2	Roughing mill 1 Passes, Nos	3	3	3
3	Roughing mill 2 Passes, Nos	3	3	3
4	Roughing mill exit temperature, °C	1052	930	910
5	Roughing mill exit thickness, mm	44.1	44.6	44.5
6	No of finishing passes, Nos	7	7	7
7	Finishing mill entry temperature, °C	964	860	820
8	Finishing temperature, °C	920	825	780
9	Coiling temperature, °C	641	625	575
10	Final coil thickness, mm	4.1	4.05	4.05

Normally, low temperature rolling increases the roll loads and sticking tendency. Modern mills have temperature, speed and profile sensors which generates alarms in case of any

parameter going out of range. No process abnormality or alarms were observed during these ferritic rolling trials conforming the results of offline simulations. During each rolling pass, strain is imparted to the material which causes an increase in dislocation density and consequently results in work hardening. But simultaneously static and dynamic recrystallization also takes place. The finish rolling parameters also have a strong impact on the microstructure and texture evolution. As it is not possible to measure the microstructural differences of the coil between the stands, it is indirectly compared by measuring the change in the rolling force exerted in each stand. No significant change in rolling force in the finishing stands was observed between austenitic and ferritic rolling. Rolling forces in ferritic rolling were marginally lower than the austenitic rolling (4-8 %). Table 5.3 shows the comparison of rolling force (MPa) in each stand in the finishing mill. At the selected temperatures, the softening effect of phase transformation or ferrite phase is equal to the hardening effect due to a decrease in temperature and applied strain, which keeps the roll force or the deformation resistance close to austenitic rolling conditions. The shape of the fish tail was also normal and similar to the austenitic rolling, hence did not affect the head and tail end. The temperature difference between the head end and tail was ~ 50 °C, marginally higher than the austenitic rolled coils, which is attributed to the slower speeds and resulting in a difference in physical properties.

Table 5.3. Comparison of rolling force in each stand (MPa) in hot strip mill

Stand	F1	F2	F3	F4	F5	F6	F7
AR	22650	23795	21036	18464	14608	12228	10660
FR1	20023	22249	19586	17138	14457	12221	10470
FR2	20077	22307	19631	17176	14498	12267	10542

Full-width samples were collected from both the head end and the tail end of the hot-rolled coil after cooling as shown in Fig. 5.8. To map the variation in properties, samples were cut from the centre at both head and tail ends. The full-width sample was first subjected to residual stress measurement to quantify the relative difference in stresses between the selected areas. This is done on the as-received samples to avoid stress relieving due to cutting. After the residual stress measurement, from each full-width sample, the surface was marked for various testing from similar locations as shown in Fig. 5.9. Complete characterization (residual stress, hardness, mechanical properties, microstructure, texture)

was carried out at two locations in each coil to map the variations in the properties. Customised samples were cut for tensile testing, hole expansion ratio, phase analysis and microscopy. Since the temperature difference between the head and tail (50 - 60 °C) is much higher than the centre and the width (25 - 35 °C), a comparative analysis has been carried out between the head and the tail samples in all the coils.



Fig. 5.8. Sampling locations on the coil



Fig. 5.9. Markings for sample cutting on HR coil

5.7 Cold Rolling and Annealing Process

The hot-rolled sheets were subjected to cold rolling and annealing in a cold rolling mill complex for converting them into thin sheets (4 mm hot rolled sheets to 1 mm cold-rolled sheets) for various applications. In this process, hot-rolled coils were first pickled, cold rolled, annealed and skin passed to get shiny CRCA sheets. Pickling is a metal surface treatment used to remove impurities, such as stains, inorganic contaminants, rust or scale. Scales and oxide layers are harder than the steel and hence hinder the process of cold rolling of the low carbon steel. A solution called pickle liquor, which contains strong acids, is used to remove the surface impurities. It is commonly used to descale or clean steel in various

steelmaking processes. The IF grade, hot-rolled strip is passed through a series of 3 tanks containing hydrochloric acid with varying concentrations wherein the acid dissolves the oxide layer. The strip is then rinsed with water to remove any excess acid, dried and the strip is ready for cold rolling. These hot-rolled and pickled coils are subsequently reduced to the desired thickness by cold rolling. Cold rolling is a metalworking process in which the metal is deformed by passing it through the rollers at a temperature below its recrystallization temperature ($< 1250\text{ }^{\circ}\text{C}$). Cold rolling increases the yield strength and hardness of a metal by introducing defects into the metal's crystal structure. These defects prevent further slip and can reduce the grain size of the metal, resulting in Hall-Petch hardening (Ray et al. 1994; Ejaz et al. 2014). Thickness is achieved by passing the coil through a series of rolling stands in tandem. The tandem rolling mill consists of 5-7 stands having four-high configuration (two large back-up rolls and two small work rolls) as shown in Fig. 5.10. In the present case the hot-rolled and pickled coil is passed through a 5 strand tandem cold rolling mill at JSW Vijayanagar works as shown in Fig. 5.11. The cold-rolled sheet is a highly strained material and also called as a full hard sheet. The average force applied is maximum in strand 1 and it gradually decreases in the subsequent strands as the reduction ratio decreases. The total reduction given here varies from 60 % - 90 %. Steel material hardens after cold rolling due to the dislocation tangling generated by plastic deformation. Annealing is therefore carried out to soften the material. The annealing process comprises heating, holding of the material at an elevated temperature (soaking), and cooling of the material. Heating facilitates the movement of iron atoms, resulting in the disappearance of tangled dislocations and the formation and growth of new grains of various sizes, which depend on the heating and soaking conditions (Ray et al. 1994; Ejaz et al. 2014). Continuous annealing line mainly comprises of three sections, namely entry section, furnace section and delivery section. The annealing is done by passing the strip through a vertical furnace having different heat cycles for different grades. Before annealing, the strip is cleaned in the cleaning section to remove the rolling oil, iron fines, scales, etc. being carried from the rolling mill. After the cleaning process, the strip is annealed by heating it above the recrystallization temperature ($> 750\text{ }^{\circ}\text{C}$) in the heating section, holding on to a particular temperature for a specified time (40-50 sec) in the soaking section. This furnace section comprises a heating zone, soaking zone, and cooling zone. The heating cycle applied to strips by continuous annealing differs from product to product. The cooling zone is divided into three sub-zones so that complex cooling patterns such as cooling-heating-holding-cooling can be performed. The strip is then cooled slowly in the slow

cooling section and rapidly in the rapid cooling section respectively with different cooling rates depending upon the grades of steel to be produced. The annealing line is shown in Fig. 5.12. The strip is then passed through the 6Hi skin pass mill in order to increase its roughness and elongate the grains thus maintaining the good shape of the strip. Many of these process parameters affect the final properties and must be optimized for the ferritic hot-rolled coils (Ejaz et al. 2014; Okan 2020).

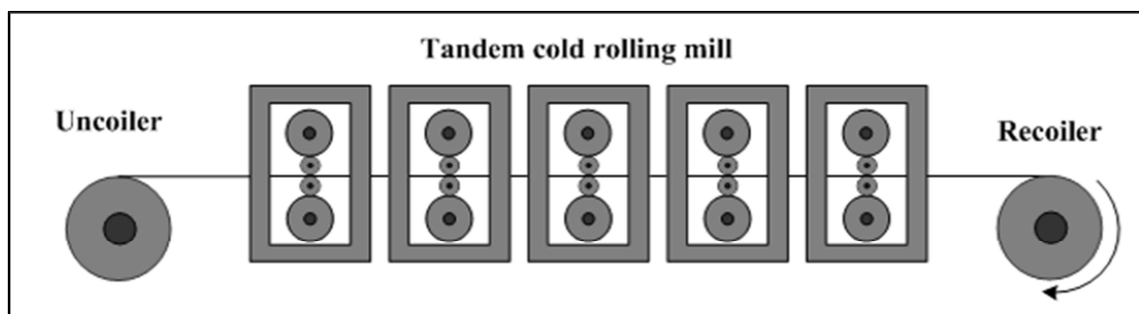


Fig. 5.10. Schematic of a tandem cold rolling mill



Fig. 5.11. Cold rolling mill line at JSW steel



Fig. 5.12. Continuous annealing line

5.8 Selection of Cold Rolling Parameters

The primary purpose of cold rolling is to roll the sheets to the desired thickness and impart uniform deformation to the grains which recrystallize to the favourable gamma texture after annealing. The reduction imparted during cold rolling governs the $\dot{\epsilon}$ and n values of the annealed sheet (Ray et al. 1994). Several studies have been previously made on optimizing the reduction ratios in cold rolling for low carbon and IF grades steels. It is well established that, increasing the reduction ratio during cold rolling increases the formability, especially above 70 %. However cold rolling reductions above 80% is not feasible on an industrial mill due to hot rolling thickness limitations and load requirements at a cold rolling mill. Hence for practical purposes reduction ratios of 70 – 80 % is followed in the industry (Okan 2020). Pero-Sanj et al. (1999) have shown that the intensity of the $\langle 111 \rangle$ component is considerably higher in the textures of cold-rolled and annealed sheets than in hot-rolled sheets. For both low and extra-low carbon steels, cold rolling rates higher than the conventional 70% are advantageous to achieve improved drawability.

Elsner et al. (2004) studied "soft" and "hard" hot strip, for the development of the recrystallization texture of cold-rolled and annealed ferritic-rolled hot strips for different cold reductions. It was found that for cold reductions in the range 65 – 75 %, the r -values for all three directions are in the same order of magnitude, leading to a very low planar anisotropy with a still quite high mean r -value and is expected to exhibit a very good deep drawability together with a low tendency to form ears. Figure 5.13 shows the comparison of Lankford value, r , mean r -value, r_m , planar anisotropy, Δr , of the cold strips produced of

"soft" and "hard" hot strips with the properties of a conventionally produced cold strip (open symbols)

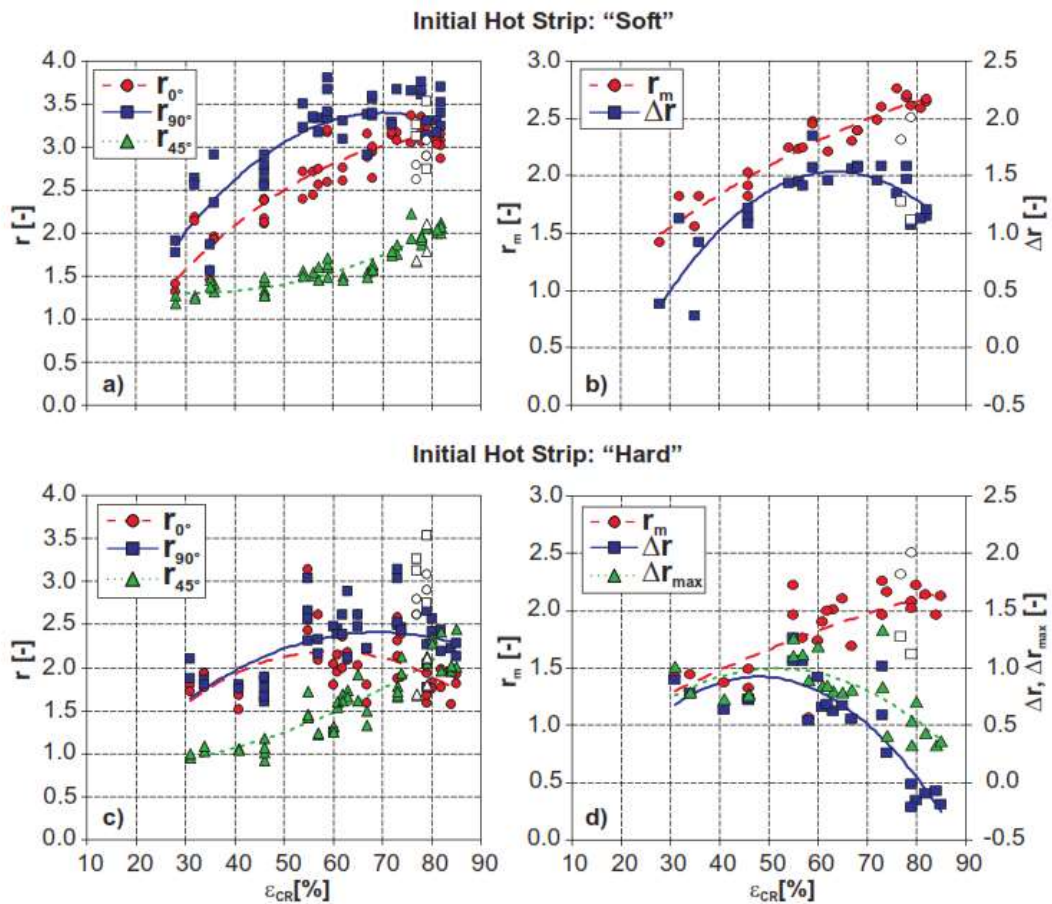


Fig. 5.13. Comparison of formability indicators (Elsner et al. 2004)

Zhang et al (2010) studied the texture evolution of ferritic hot-rolled Ti-IF steel during cold rolling with a reduction in the range of 15% to 85%. The alpha fibre texture is intensified monotonously with increase in the cold rolling reduction, but the gamma fibre changed differently. It is found that the cold rolling reduction of 75 % is suitable for obtaining the best average plastic strain ratio after annealing, as shown in Fig. 5.14.

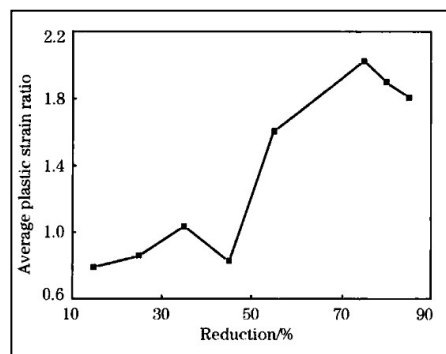


Fig. 5.14. Variation of average plastic strain ratio with % reduction (Zhang et al. 2010)

Figure 5.15 shows the effect of cold rolling reduction on the r_m values of Ti, Ti+Nb, and Nb IF steels from a US patent (Tokunada and Yamada, 1985). It shows that irrespective of composition, the average r-value curve increases with a reduction ratio up to 75% and then flattens. However, it is also reported (Hoile, 2000) that at higher reductions the r_{45} component becomes dominant over the r_{90} thereby affecting the directional properties. As all the previous studies well establishes with microstructural and textural justification, that 70-80% is the most optimized band for the cold rolling. In absence of pilot scale cold rolling simulation facilities, in the present experiments the cold reduction decision will be made based on the literature and plant rolling feasibility.

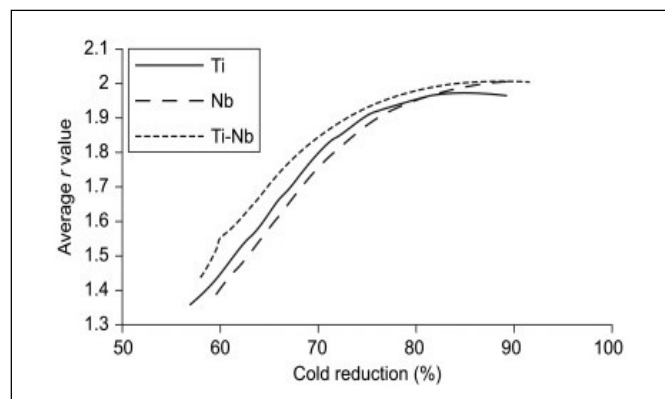


Fig. 5.15. Effect of cold rolling reduction on the r values of Ti, Ti+Nb, and Nb IF steels (Tokunada and Yamada, 1985).

The most widely used IF steel grade product is of 1 mm thickness and 75 % reduction was being followed for the present austenitic sheet rolling in industrial line. Hence, considering the previous studies in literature, in this case, for the industrial trials of the ferritic-rolled sheets, the final thickness of the cold-rolled sheet was fixed at 1 mm through the reduction ratio of 75% for better one to one comparison with the austenitic rolled material. As the hot-rolled sheets were 4.05 mm thickness, the final thickness was set at 1.0 mm to be achieved in 5 reduction passes. 1.0 mm sheets are most widely used material in the industry.

5.9 Cold Rolling and Annealing Plant Trials

Hot rolling at different temperatures is expected to impart different grain morphology and orientations, which on subsequent cold rolling and annealing may result in differences in specific properties (Wang et al. 2019; Zhao et al. 2019). Hence, to study the effect of ferritic regime rolling, hot-rolled coils were further cold-rolled and annealed under conditions

similar to conventional austenitic rolled IF grade coils in an industrial cold rolling mill and continuous annealing furnace.

Ferritic hot-rolled coils were first pickled in hydrochloric acid to remove the oxide layer similar to the parameters maintained for austenitic-rolled coils. The entry and exit temperatures of the 3 pickling tanks were maintained at 83 °C. The HCL acid concentration was lowest in tank 1 (5- 6%), moderate in tank 2 (9-10%) and highest in tank 3 (13 -14 %). The pickled coils were subsequently cold-rolled in a 5 stand tandem cold rolling mill. The total reduction given here was 75%. During the cold rolling, the 4.05 mm hot-rolled coil was rolled to 1 mm cold-rolled coil through a 5 strand mill. The average force applied was maximum in strand 1 and it gradually decreases in the subsequent strands as the reduction ratio decreases. The comparison of key cold rolling parameters for the ferritic rolled IF grades steel sheets and a selected austenitic rolled coil of similar thickness are listed in Table 5.4. The load required for similar reduction is also lower during the cold rolling process.

Table 5.4. Comparison of cold rolling parameters

Total reduction, %	76	75	75
Initial thickness, mm	4.1	4.05	4.05
Reduction C1, %	32.5	31.3	31
Reduction C2, %	33.1	31.1	31
Reduction C3, %	27.4	27.8	28.1
Reduction C4, %	22.2	21.4	21.1
Reduction C5, %	2.1	5.6	5.7
Average force C1, MPa	15614	10793	10784
Average force C2, MPa	14654	10576	10462
Average force C3, MPa	13700	8284	8394
Average force C4, MPa	11505	7658	7579
Average force C5, MPa	7275	6481	6481
Average thickness C1, mm	2.77	2.78	2.79
Average thickness C2, mm	1.85	1.92	1.93
Average thickness C3, mm	1.34	1.38	1.39
Average thickness C4, mm	1.05	1.09	1.09
Average thickness C5, mm	1.02	1.03	1.03

These cold-rolled sheets were further processed through continuous annealing and skin pass mill. The continuous annealing process could be broadly divided into four stages. In the heating stage, the ferritic coils were heated from room temperature to soaking temperature of 780 °C at the heating rate of 5 °C/sec. Coils were then soaked at around 788 °C for 45

secs, however, higher temperatures are preferred for better properties. In the rapid cooling section coil was cooled to 480 °C at the rate of 14 °C/s. The final step over ageing was done at 397 °C before cooling to room temperature at a speed of 5 °C/s. The used annealing cycles for both ferritic-rolled coils and the austenitic-rolled coils are shown in Fig. 5.16.

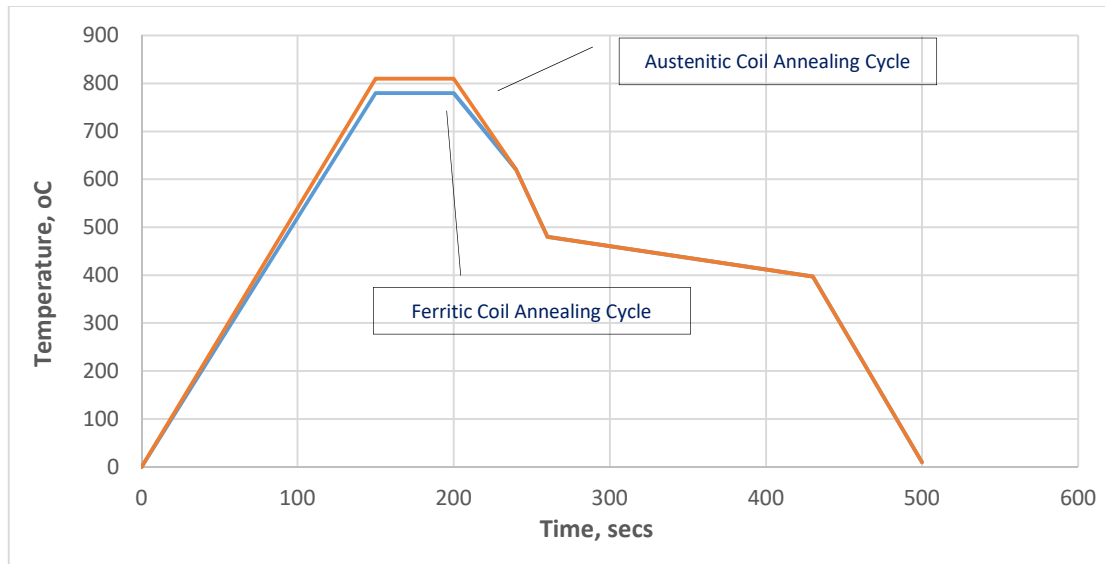


Fig. 5.16. Annealing cycle utilized for the experimental IF steel coils

These annealed coils were subjected to skin pass reduction of 0.9%. Full-width samples were collected from the tail end of both the ferritic-rolled coils (FR1 and FR2) and a representative austenitic-rolled coil (AR). Samples were cut from the centre at both head and tail ends. The full-width sample was first subjected to residual stress measurement to quantify the relative difference of stresses between the selected areas. On each cut sample, marking was done on the surface for various testing from similar locations. Customized samples were cut for complete characterization, which includes tensile testing, formability studies, phase analysis, and microscopy. Samples were cut and mechanically polished and etched using nital for microscopic analysis. Deep drawable steel sheets require higher amount of gamma, γ -fibre ($\{111\} \parallel ND$) textures and alpha, α -fibre ($\langle 110 \rangle \parallel RD$) texture in steel sheets (Ray et al. 1994). Therefore, the texture of the samples was also analysed using an X-ray diffractometer.

CHAPTER 6

FORMABILITY STUDIES ON COLD ROLLED SHEETS

Sheet metal forming in the automotive industry is continuously changing with the introduction of new technologies and complex manufacturing processes to meet the higher safety and quality standards. This also drives the development of newer steel grades and more reliable and quick methods of assessing the formability to avoid product defects. Therefore, the steel grades, especially IF and low carbon grades and their formability testing is also improving and getting customized to applications. Formability by definition is the ability of sheet metal to be formed into the desired shape without necking, thinning or cracking (Reddy et al 2019). Since sheet metal forming operations are diverse in shape, type, extent of load applied, and rate of loading, several formability tests have been proposed for different applications. No single test can provide an accurate indication of the formability for all situations (Behrens et al. 2021). Schey (1992) reported the formability determination techniques in sheet metals and suggested methods that involve extensive tensile deformation and encounter necking and thinning defects during various mechanical tests. Animesh et al. (2013) further explained through their comparative studies that basic mechanical properties such as, hardness, yield strength, tensile strength or elongation, are not sufficient to specify forming limit conditions for different shaping applications. Measurement of application specific formability is now an important aspect for sheet metals which helps in the right selection of material to be formed into the required shape without undergoing localized necking, thinning, or fracture. The forming operation can be deep drawing, stretch forming, stretch flanging, and bending. Manabu (2015) compiled different sheet forming technologies used in the automotive industry and confirm that these operations encounter different nature of stress due to varying loading paths and can be biaxial or triaxial. Therefore, different formability tests are used for quantification of the formability of sheet metals for particular configuration and applications. Very frequently (Nourani et al. 2010; Katerina et al. 2021), designers used FLD (formability limit diagram) - a plot of the combinations of major and minor strains which lead to fracture. Narayanasamy and Sathiya (2005) studied FLD in interstitialfree steel and Ravi (2002) in extra deep drawing steel and reported a good correlation with different material parameters. But the limit strains in forming limit diagrams are many times reported higher due to overlap of the strain points

and large scatter in the measured strains with varying blank width (Katerina et al. 2021). For many practical applications, the measurement of cup/dome height at the point of necking or initiation of fracture under plane strain and biaxial stretching conditions is considered an acceptable criterion (Reddy et al 2019): These tests simulate the application specific synergistic interaction of mechanical properties of the steel grade, the stresses and loads existing during different processing operations. Examples of testing efficacy of a steel grade for deep drawing operation by earing test, stretch forming by Erichsen cupping test, stretch flanging by hole expansion ratio, and bending by bend test have also been reported by Manabu (2015).

Many previous studies (Andreas et al. 2000; Barrett et al. 2002) on ferritic rolling in low carbon steels have been aimed to produce thin gauge hot rolled coils with better deep drawability as a replacement of cold-rolled sheets to reduce the production cost. There are very limited studies which, followed ferritic hot rolling and subsequent cold rolling and annealing (Chang et al. 2020; Titto et al. 2004). These studies are also in laboratory mills and have never been tried in an industrial mill. Ferritic hot rolled coils after cold rolling and annealing develop different grain orientation and texture, compared to equiaxed grains in austenitic rolled coils (Chen et al 2009). Though having similar yield strength and ultimate tensile strength, the ferritic rolled and austenitic rolled sheets are expected to perform differently during application due to varying grains morphology and texture (Lei et al. 2019; Rajib et al. 2007). Formability is a critical requirement in interstitial free (IF) grade steels (Ghosh et al. 2009) used in many automotive components. Especially, with varying Δr , either positive or negative, the orientation of the sheet concerning the die or the part to be formed will be important (Goktug et al. 2006). This anisotropy may impact certain forming operations and must be studied in detail to avoid thinning or failure.

Though the bulk formability of the ferritic-rolled IF grade coils are reported to be good (Ghosh et al. 2008), but it may impact certain forming operations and must be studied in detail to avoid thinning or failure. Also, a detailed study of its formability behaviour for different applications after cold rolling and annealing has been less investigated. Due to the lack of availability of information on the formability behaviour of different ferritic temperature rolled steels, it is less produced and rarely utilized in industry (Hoile 2000). This work compares the fracture criterion, stretch-flangeability, deep drawability and stretch formability behaviour of the industrially produced, ferritic and austenitic hot rolled IF grade steel coils in the cold-rolled and annealed condition, for different formability

applications through specific tests, such as formability limit diagram, hole expansion ratio, earing test and Erichsen cupping tests. Their behaviour is compared based on mechanical properties, microstructure, and texture. Such processing – structure–formability comparison is never published. It is expected that this study will help in the selection of the ferritic rolled IF grade steels for specific applications. Customized size samples were cut from the central portion of the 3 sheets for each formability test.

6.1 Forming Limit Diagram (FLD)

The forming limit diagram (FLD) is the most commonly used and widely accepted fracture criterion for predicting the formability and safety limit of the material in sheet metal forming applications (Reddy et al. 2019). The forming limit diagram (FLD), also known as forming limit curve (FLC) provide a method for determining the process limitations in sheet metal forming through graphical representations of the material ability to sustain the strains underneath the forming limit curve without failure due to necking or fracturing (Sharbani 2011). The forming limit diagram can be determined for strain paths ranging from biaxial tension (as in stretch forming) to equal tension and compression (as in deep drawing). These are generated by failure points on a graph of two axes representing major and minor strains. The major strain is the strain in the direction of the maximum strain and the minor strain is the strain perpendicular to the major strain. In this work, the forming limit is determined by the Nakajima test (1968) in a bulging press using ARAMIS 3D deformation measurement system. The formability testing bulging press with optical 3D camera based measuring system is shown in Fig. 6.1. The Nakajima test is based on the principle of deforming sheet metal blanks of different geometries using a hemispherical punch until a fracture occurs. The forming limit curve in Nakajima test is determined using a 100 mm hemispherical cupping die. The die and the blank holder and its fixing is shown in Fig. 6.2. By varying the specimen width, different deep drawing and stretch forming conditions can be created on the sheet metal surface (from a regular biaxial deformation to a simple tensile load). In the present work, samples of sizes 250·250 mm, 250·200 mm, 250·150 mm, 250·130 mm, 250·110 mm, and 250·50 mm were cut by shearing operation. For evaluations with optical 3D measuring systems, e.g., Aramis by GOM, stochastic patterns are applied with a color spray, and the shift of the patterns under load are evaluated. A uniform thin layer of spray paint with a matt finish is applied on the sheets which form an arbitrary pattern of small black dots. These specimens are subjected to the

punch force till the fracture. 3D coordinates of the surface points are determined using the CCD cameras mounted on the top which measures the strain.



Fig. 6.1. Bulging press with 3D camera

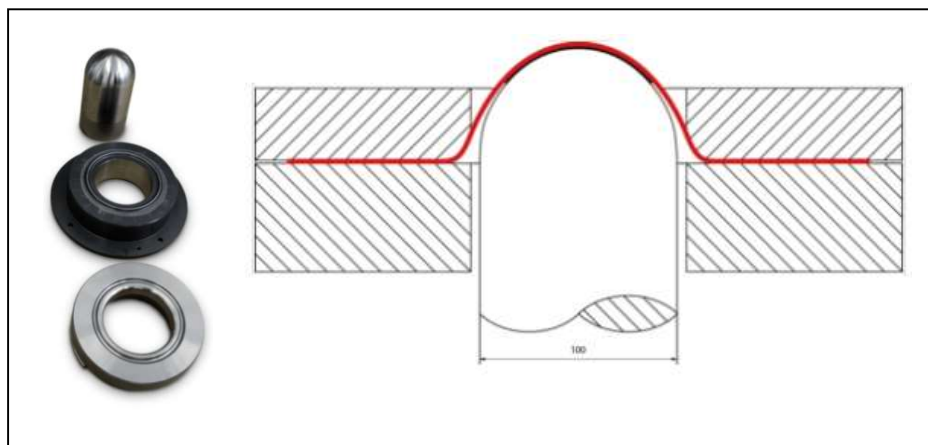


Fig. 6.2. Die and blank holder setup

The data is plotted as major and minor strain. Figure 6.3. shows the test samples before and after the formability limit testing. For each blank width, five specimens were tested to get the maximum number of data points for all the 3 samples (one austenitic rolled and two ferritic rolled).

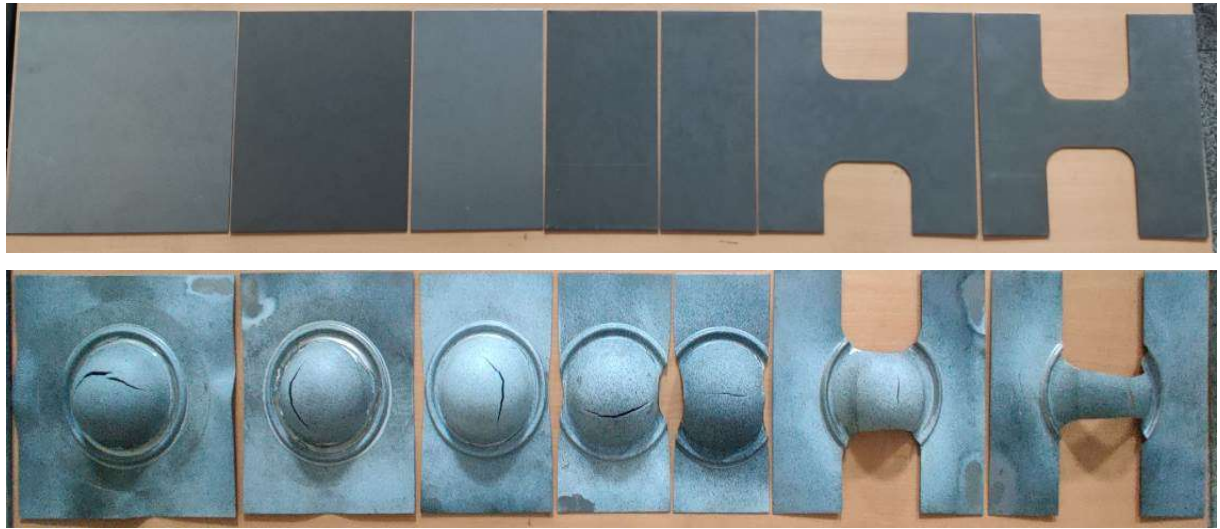


Fig. 6.3. Specimens before and after the FLD test

6.2 Hole Expansion Test

Stretch-flangeability is measured using hole expansion test (HET) and it represents the cut-edge formability of sheet materials or the ability of a material to form into a complex shaped component near the edges (Narayanasamy et al. 2010; Paul 2019). More precisely, it defines the ability to resist an edge crack during edge stretching deformation. Previous studies (Xinping et al. 2014; Jae Hyung et al. 2018) have reported varying correlations between HER (hole expansion ratio) and normal anisotropy (r-value), strain rate sensitivity (m-value), ultimate tensile strength (UTS), and yield ratio, etc.

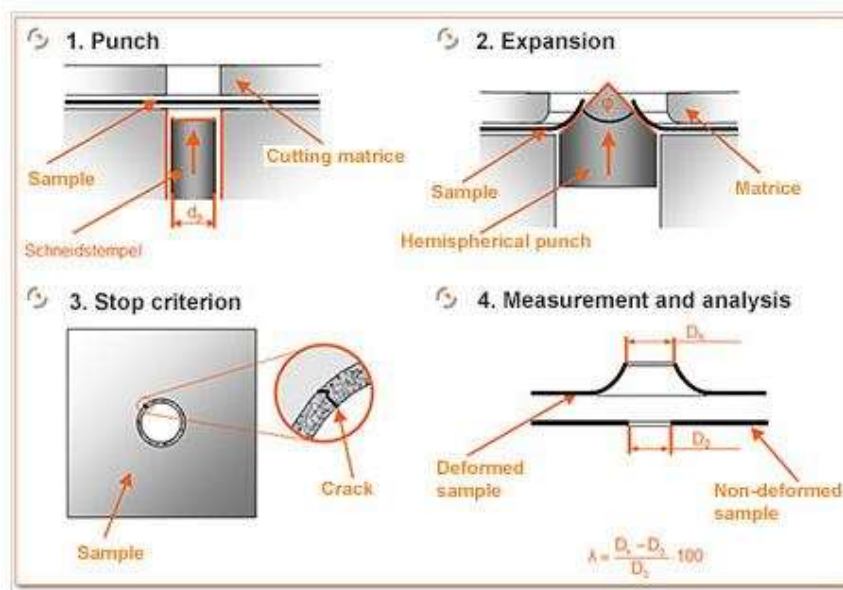


Fig. 6.4. Sequences of operations in the hole expansion test

Hole expansion tests were performed on all three samples in forming press (Zwick - BUP600) as per ISO 16630. A hole with a punching die diameter of $d_p = 10$ mm is first sheared into the sheet sample and was then expanded with a conical die. As soon as a crack that runs through the entire thickness of the plate was seen, the expansion was stopped and the resulting hole diameter D_h was determined. The process is shown pictorially in Fig. 6.4. The hole-expansion ratio is then defined as the ratio between the increase in the hole diameter ($D_h - D_0$) and the original hole diameter D_0 (Saikat et al.2011).

6.3 Earing Test

Earing tests are performed to evaluate the deep drawing ability of the sheet metal (Tajally et al. 2011, Adrienn et al. 2021). In the earing test, circular blanks are punched or inserted and drawn into cups. Due to different elongation in different directions or the crystallographic anisotropy, wavy cup rims are formed on the free edges of the cup. The top portion of these waves are called ears and generally, in low carbon steels, four ears are formed at the diagonal axis to the rolling direction (Liao et al 2018). The average height of the ear peaks (h_p) and valleys (h_v) is measured, and average earing in percentage is reported as the unit of measurement. Earing behaviour is normally very low in IF steels (Tajally et al. 2011), but it is an important test to determine the difference in ear height due to the textural differences in the austenitic and ferritic rolled sample. Earing test was conducted as per EN 1669 on a bulging press. A typical after test sample of an earing test is shown in Fig. 6.5.

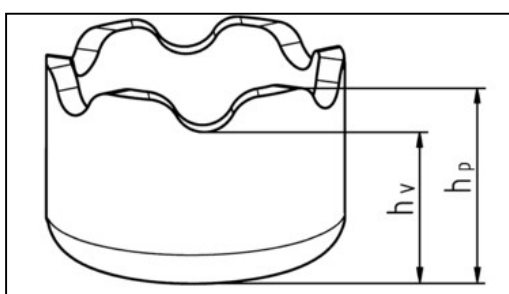


Fig. 6.5. Typical earing behaviour in sheet metals

6.4 Erichsen Cupping Test

Erichsen cupping test is used to evaluate the ability of metallic sheets to undergo plastic deformation in stretch forming (Salunkhe et al 2014, Sangkharat et al. 2019). In this test, a

hemispherical punch is pressed against a clamped sheet specimen placed between a die and a blank-holder until a fracture as shown in Fig. 6.6. The depth of the bulge or the dome height gives a measure of the ductility of the sheet in the plane of drawing under biaxial stress condition and is represented as the Erichsen cupping index (IE) (Kim et al 2011). All the three sheets were subjected to this test as per ISO 20482, at a constant force and drawing speed until a fine crack occurs that runs through-thickness of the specimen. Three samples were tested in each case, and the average value is indicated.

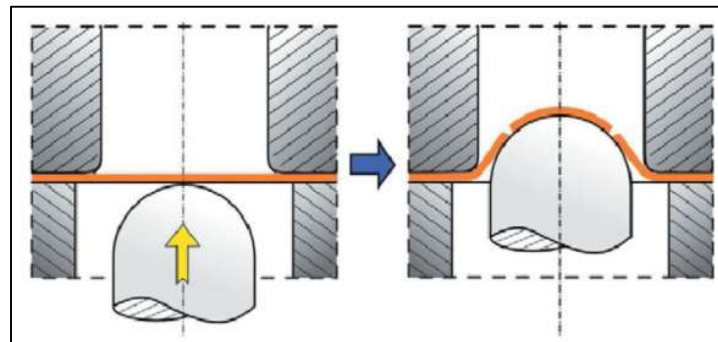


Fig. 6.6. Erichsen cupping test

CHAPTER 7

RESULTS AND DISCUSSION

In this section, the four simulations carried out in offline mode are referred as A, F1, F2, F3 and the three plant trials carried out are referred as AR, FR1 and FR2.

7.1 Thermo-Mechanical Simulation Results

Mean flow stress is an indicator of expected rolling loads and also helps in understanding the changes in microstructure taking place during hot rolling. Figure 7.1 shows the variation of flow stress in each stage of deformation during austenitic and ferritic rolling along with individual strain (ϵ) and strain rate ($\dot{\epsilon}$). The flow stress of the material continuously increased in all experimental cases up to the fifth stage of deformation due to strain hardening. It marginally reduced in the last strand deformation due to a significant reduction in strain in the last strand. The strain hardening effect is more pronounced in the deformations carried in the ferritic region compared to the austenitic region, for the same value of the strain and the strain rate. However, the absolute value of the flow stress for the ferritic rolling F1 (high temperature ferritic rolling) is always lower than that of the austenitic rolling (Kaspar 2012). Ferrite softens by dynamic recovery as it is having higher stacking fault energy (SFE) (Prasad et al. 1991; Longfei et al. 2006). In this case the softening or the flow stress reduction effect of the ferrite phase is higher than that of the hardening due to a decrease in temperature and applied strain, thereby keeping the flow stress or the deformation resistance lower. The absolute value of flow stress for the ferritic rolling F2 (medium temperature ferritic rolling) is lower than the austenitic rolling up to the 4th deformation step and is higher thereafter as the total strain increases. This is because dynamic recovery in ferrite is a function of temperature (Zhao et al. 2016)). It has been reported that lowering deformation temperature (above nose temperature in kinetic C-curve) shortens the incubation time for the onset of dynamic transformations and accelerates its kinetics (Priestner et al. 2002). At high temperature, the driving force and nucleation density for ferrite transformation are low, but the diffusivity of atoms is high. Therefore, the grain growth of dynamic transformed ferrite is rather dominant, resulting in a large grain size. In this case, hardening due to a decrease in temperature and applied strain increases with the number of deformations and equals the softening effect of the ferrite phase at the 4th deformation step and has reversed the effect thereafter. The absolute value of flow stress for the ferritic rolling F3 (low temperature ferritic rolling) is always higher than the austenitic rolling in all deformations. In this single phase region of ferrite,

hardening due to lower temperature is higher than the ferrite softening effect, which resulted in higher flow stress. A previous study (Pan and Lenard 1994) proved that deformation in austenite region exhibits typical work hardening and dynamic restoration behaviour but the deformation in ferrite shows quasi-linear increase in flow stress with small strain increments, because of Nb retarding the occurrence of dynamic recovery in ferrite and the presence of immobile dislocations. This behaviour is dominant at low temperatures as is in this case, where the flow stress increases significantly with increased strain.

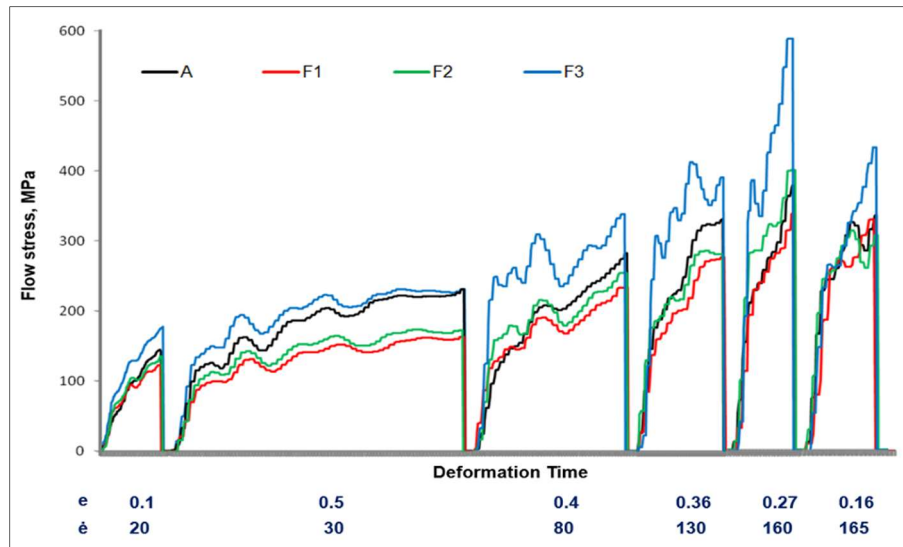


Fig. 7.1. Variation in flow stress with extent of deformation in Gleeble for IF steels

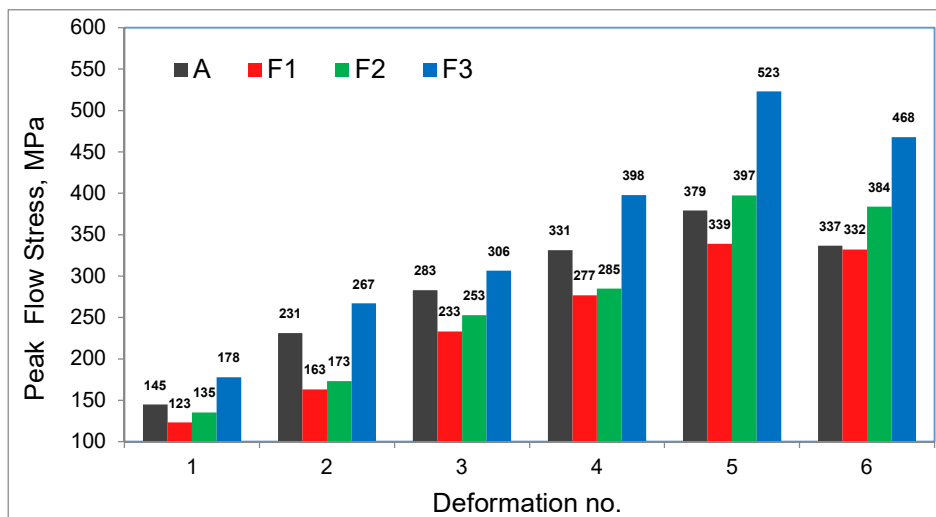


Fig. 7.2. Variation in peak flow stress with the extent of deformation in Gleeble for IF steels

If only the temperature effect is considered, the flow stress does not increase continuously. It has a non-uniform trend where it decreases first and then increases as we move down from Ar_1 . Figure 7.2 shows the variation in peak flow stress with deformation at each strand. The average flow

stress and the peak flow stress increases with reducing the temperature. Flow stress analysis shows that the strain hardening effect in the ferritic region is due to the combination of temperature, accumulated strain and does not have any linear relationship (Chuang et al. 2018). Based on the role of grain boundaries as an effective barrier to the movement of dislocations, the strain hardening and ultimate strength can be explained by the pile-up of dislocations at grain boundaries but the effect of the grain shape parameter not only affects the stress at grain boundary regions, but it also affects the stress distribution and strain localization making it non-linear (Chuang et al. 2018). Flow stresses are expected to be always lower if rolled in F1 temperature range on an industrial scale.

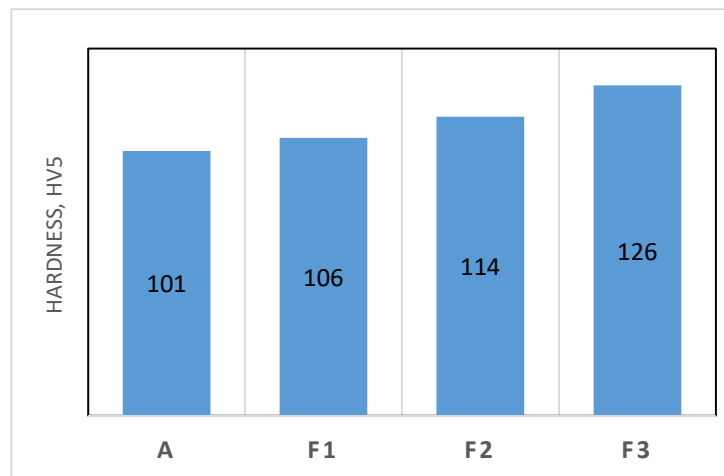


Fig. 7.3. Comparison of hardness on rolling simulated samples

Vickers hardness measurements (HV5) were performed on all four samples (5 kg) and the comparison of hardness (average of 5 readings) at the centre is shown in Fig. 7.3. The hardness of austenite simulated sample A is similar to the industrially rolled sample. However, the hardness of all ferritic rolled samples was found to be higher than that of the austenitic sample. The values for sample F1 is closest to the austenitic sample A. A comparison among the samples shows that hardness increased with a decrease in the experimental temperature. An increase in F1 can be attributed to finer grain size or increase of stored energy due to deformation, in spite of some amount of dynamic recovery in ferritic condition. It is well explained in the literature (Oliferuk et al. 2009; Kolupaeva and Semenov 2015) that a part of the energy consumed by plastic deformation of the metal is also absorbed, thereby increasing its internal energy. Stored energy is microstructurally associated with the accumulation of lattice defects and the significant part of this stored energy is the energy of statistically stored dislocations and their mutual interactions. It is also observed (Oliferuk et al. 2009) that the amount of stored energy increases, with lowering the temperature and increasing the degree of deformation. This phenomenon also imparts some

internal grain non-uniformity. An increase in F2 and F3, though having larger grains may be due to grain bands that restrict the dislocation movement. Banded structures have aligned grain boundaries which restrict the movement of dislocations thereby increasing the strength values. The range of hardness values indicates that there will not be a significant change in the YS and UTS of the ferritic-rolled sheets from the established existing austenitic-rolled sheets if rolled in F1 temperature range. Based on larger grain size and comparable hardness, the ferritic-rolled IF steel is expected to have higher % elongation and lower yield ratio (YS/UTS) than that of the austenitic-rolled steel if it is further annealed.

One of the key issues of ferritic rolling reported in the literature is non-uniformity in properties, along with thickness (Hoile 2000; Kiet et al. 2013). To study this behaviour, through thickness variation of grain morphology of austenitic and ferritic rolled samples were captured as shown in Fig. 7.4. In the austenitic temperature range rolled sample (A) the grain morphology is uniform with a thin chilled layer (200-400 μm) at the surface due to the contact with the dies. The high temperature ferritic-rolled sample (F1) also shows uniform grain morphology but with the presence of coarse grains along with certain bands (yellow line). The grain morphology variation is higher in the low temperature ferritic-rolled samples (F2 and F3), where a thicker band (white line) of highly deformed grains could be seen on both surfaces. The inhomogeneous distribution of the shear force along the thickness causes microstructural anisotropy which increases with a decrease in temperature in the ferritic region (Kiet et al. 2013). The shape of the grains is more uniform along with the central band and varies nonuniformly along thickness in A, F1 and F2 samples. The quarter band grains show a more elongated shape (indicated by darker arrows). The difference in grain size between the centre and surface band (indicated by white arrows) is highest in the lowest temperature rolled sample (F3) indicating an inconsistency in properties. This shows that very low temperature rolling can be detrimental to formability. Under ferritic rolling conditions, the hot rolling temperature of these coils governs the final properties. The temperature difference in hot rolled sheets generates the difference in the microstructure and texture of these fibre after cold rolling and annealing and variation in their formability behaviour (Vaish et al. 2003). Very low temperature rolling generates more of unwanted textures which reduces the percentage of favourable gamma fibre required for better formability. It is reported that (Chang et al. 2020) hot rolling texture is hereditary and formations of higher γ -fibre is after hot rolling, results in higher γ -fibre recrystallization texture after cold rolling and annealing.

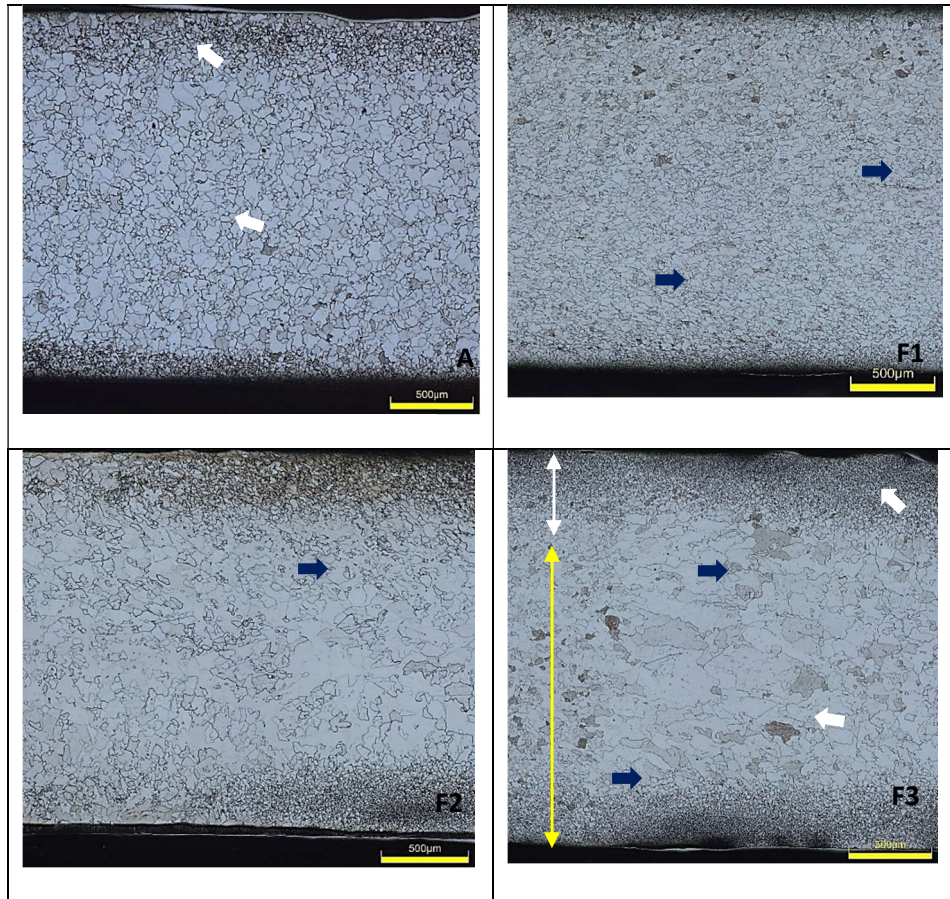


Fig. 7.4. Variation in grain morphology along with the thickness of the simulated samples

Small pieces were cut, polished and etched for microscopic analysis from the central part of the deformed samples. It was found that the microstructure along the thickness was homogeneous with a thin skin of deformed grains at the surface layer due to the chilling effect from the dies. Figure 7.5 shows the high magnification (500X) microstructures at the centre of the cross-section for the austenitic and three ferritic deformed samples which represents the experimental temperature profile of the simulation.

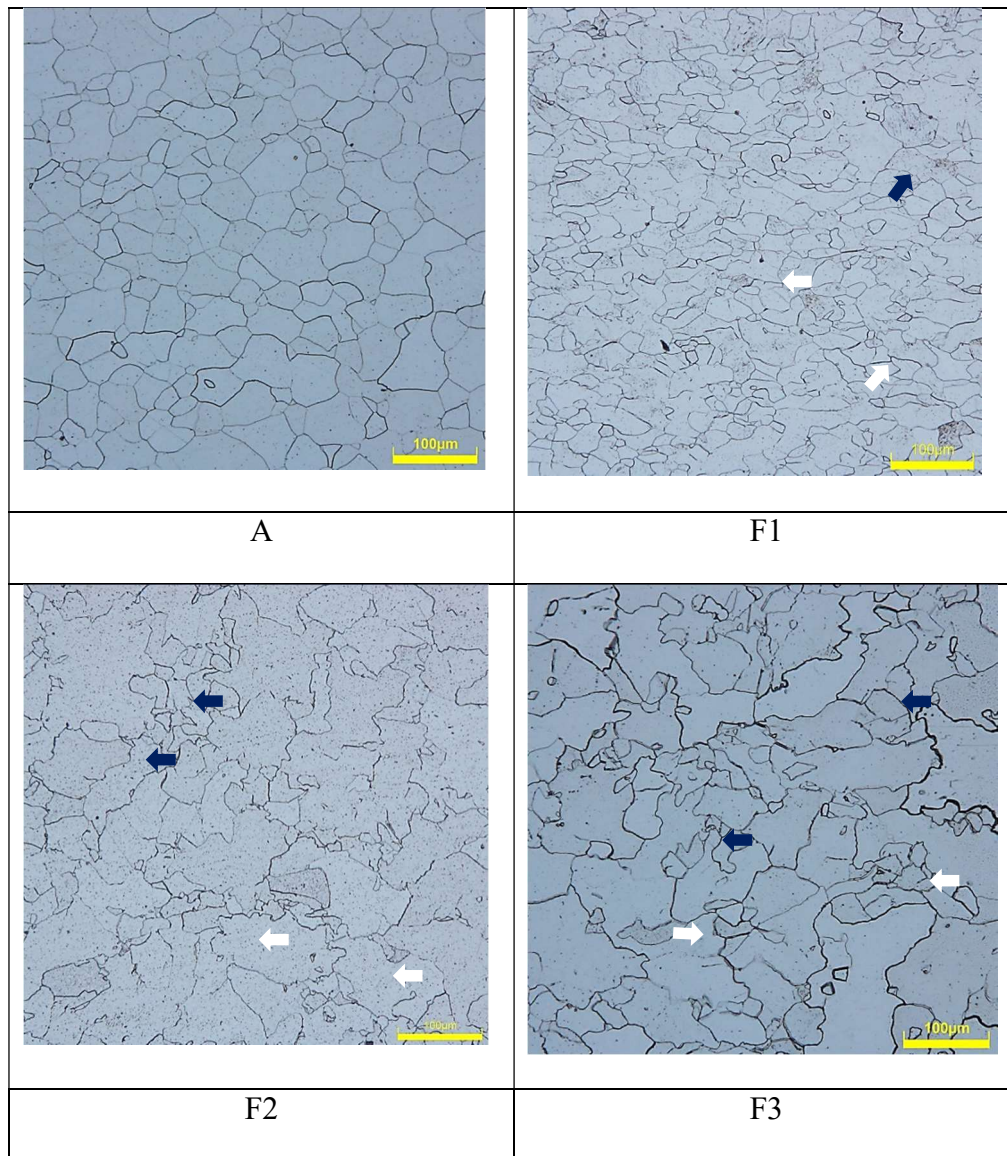


Fig. 7.5. Microstructures at the centre portion of the simulated samples

The microstructure of the austenitic rolled sample (A) having deformation start at 965 °C and finish at 920 °C was found similar to the industrially rolled microstructures of IF steel confirming the accuracy of the simulation. The austenitic rolled sample shows a predominantly polygonal ferrite structure with equiaxed fine grains of size ~ 30 µm. It is a completely recrystallized uniform grain structure. Ferritic rolling performed at high temperature in the ferrite region (F1) having deformation start at 865 °C and finish at 820 °C resulted in microstructure with partial recrystallization and grain size smaller than the austenitic sample. The mean intercept length of the grains was found to be 23 µm. Some of the newly formed small grains looks deformed and few have wavy boundaries indicating only recovery. These fine quasi-equiaxed ferrite grains

obtained could be explained by apparent dynamic recrystallization, which was assisted by dynamic recovery at high temperature (Huang et al. 2001). Rolling at relatively lower temperatures (F2) having deformation start at 800 °C and finish at 550 °C resulted in partially recovered and heterogeneous microstructure with duplex or bimodal grains. It shows a wide distribution of grain size having a mean intercept length of 32 μm . Some grains have bulged shape (indicated by dark arrows), due to deformation gradients and subsequent impending recovery.

The lowest temperature ferritic rolling (F3) having deformation start at 700 °C and finish at 655 °C resulted in a strained and non-recrystallized structure having large non-uniform, mostly deformed and few bulged grains of size $\sim 50 \mu\text{m}$. Grains in samples F2 and F3 show some clustering at certain locations. It is expected due to the interaction of uneven distribution of shear strain due to plain strain compression between the dies. None of the three ferritic rolled samples was found to be fully recrystallized. In comparison to austenitic rolling, the ferritic rolling microstructure at higher temperature exhibits smaller grain sizes but the size increased significantly as the temperature decreases indicating only recovery and no recrystallization. Huang et al. (2001) confirmed that in a Ti–Nb stabilized interstitial free (IF) steels, dynamic recovery was the dominant softening mechanism during axisymmetric compression deformation. Akbari et al. (1997) reported dynamic recovery as the operative restoration process during warm deformation. Original grain boundaries are clearly seen at all lower temperatures but the grain morphology changed due to the interaction of the micro-bands and shear bands formed resulting in small adjacent subgrains. It was also found that the subgrain and band boundaries become sharper at higher temperature resulting in higher fraction of elongated morphology as found in present experiments in F1 sample.

In F1 samples separate fine quasi-equiaxed grains are seen adjacent to large grains, and in F2 and F3 samples quasi-equiaxed grain clusters are seen. It is also found that the fraction of sharp edged non-uniform grains is higher in ferritic rolled samples (indicated by white arrows). This feature shows an increasing trend with decreasing temperature. It is due to a decrease in ultrafine polygonal ferrite and an increase in dislocations induced by ferritic rolling. Grains also became flattened with reducing the temperature in all the ferritic rolled samples. This increase in grains with low angle grain boundary and in-grain banding increases the strength of the material. It also indicates a higher degree of strain accumulation during ferritic rolling (Tao et al. 2007; Leilei et

al. 2021). This in-grain bands have significant impact on the recrystallization kinetics, grain size and ND fibre nucleation (Barnett and Jonas 1997).

Among all, F1 condition rolled microstructure is closest to the austenitic rolled microstructure and smallest in size. Hot-rolled grain size has a significant effect on the final grain size after cold rolling and annealing. Though a large grain in the final cold-rolled and annealed sheet is favourable for better formability (Lifeng et al. 2017), finer grains are required in the hot-rolled sheet. The development of finer grain morphology is due to the nucleation and grain growth during annealing by recrystallization and initial finer grain size provides more nucleation sites for recrystallization and grain growth. The mechanism of nucleation and grain growth from a deformed structure is shown in Fig. 7.6. Recovery results in thermally activated formation and re-organization of dislocation substructures in a deformed material before the onset of discontinuous nucleation phenomena known as recrystallization. Recrystallization starts when sufficient thermal activation is available to lead to nucleation and growth of strain free new grains in the plastically deformed matrix. The activation barrier is lower at the highly strained grain boundaries. After recrystallization, competitive capillary driven grain coarsening begins leading to increase in the average grain size and the associated reduction in Hall-Petch strengthening.

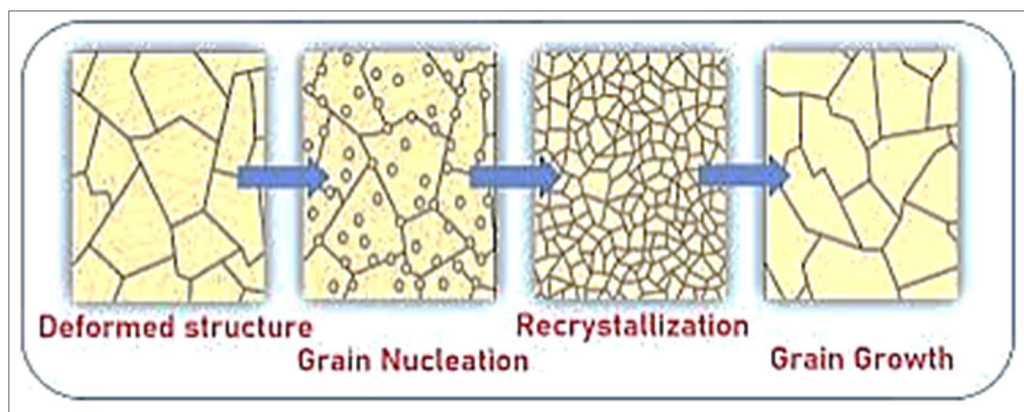


Fig. 7.6. Mechanism of nucleation and grain growth

The texture is the distribution of crystallographic orientations in a polycrystalline sample and it plays a significant role in the final properties of any rolled/deformed steel sheet (Chang et al. 2020; Leilei et al 2021). The texture of the steel sheet changes after each rolling or annealing step. In the present work, the $\phi_2 = 45^\circ$ orientation distribution function (ODF) sections of the Bunge's Euler space are used to display the textures. The ideal orientations of texture components for ϕ_2

= 45° ODF sections in BCC material along with its components and fibre nomenclature is shown in Fig. 7.7.

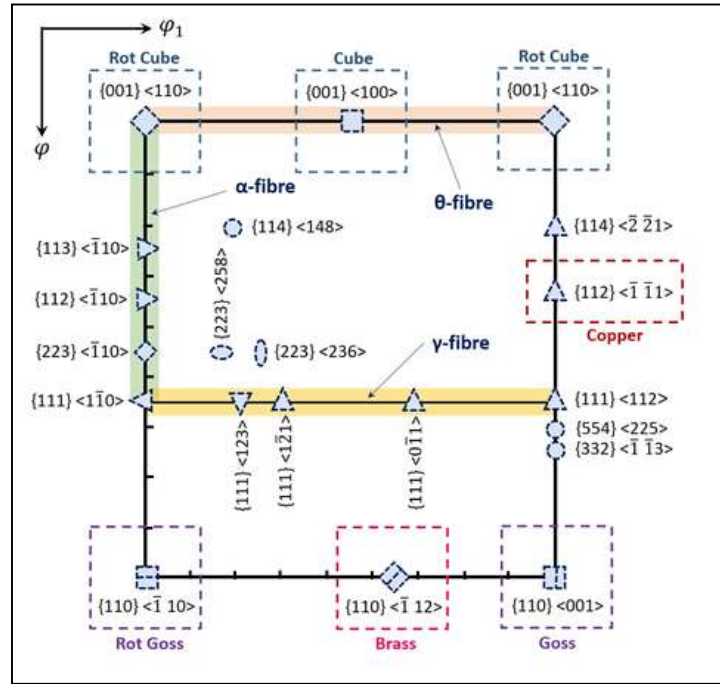


Fig. 7.7. Schematic illustration of important texture components for $\phi_2 = 45^\circ$ ODF sections in BCC material

For deep drawable steel sheets, alpha α -fibre ($\{110\} \parallel \text{RD}$) and gamma γ -fibre ($\{111\} \parallel \text{ND}$) are important (Ray et al. 1994; Hao et al. 2019). The higher the amount of these textures in hot rolled coils, the higher will be those textures in the final cold-rolled and annealed sheet (Hao et al. 2019). Additionally the ratio of γ -fibre ($\{111\} \parallel \text{ND}$) to theta θ -fibre($\text{RD} // \langle 100 \rangle$) should also be higher. Figure 7.8 shows the comparison of textures through the orientation distribution function map at $\phi_2=45^\circ$ for the austenitic and ferritic rolling simulated samples measured through bulk XRD on a PANalytical Empyrean machine. Since it is a plain strain compression simulation all samples show a lower texture index.

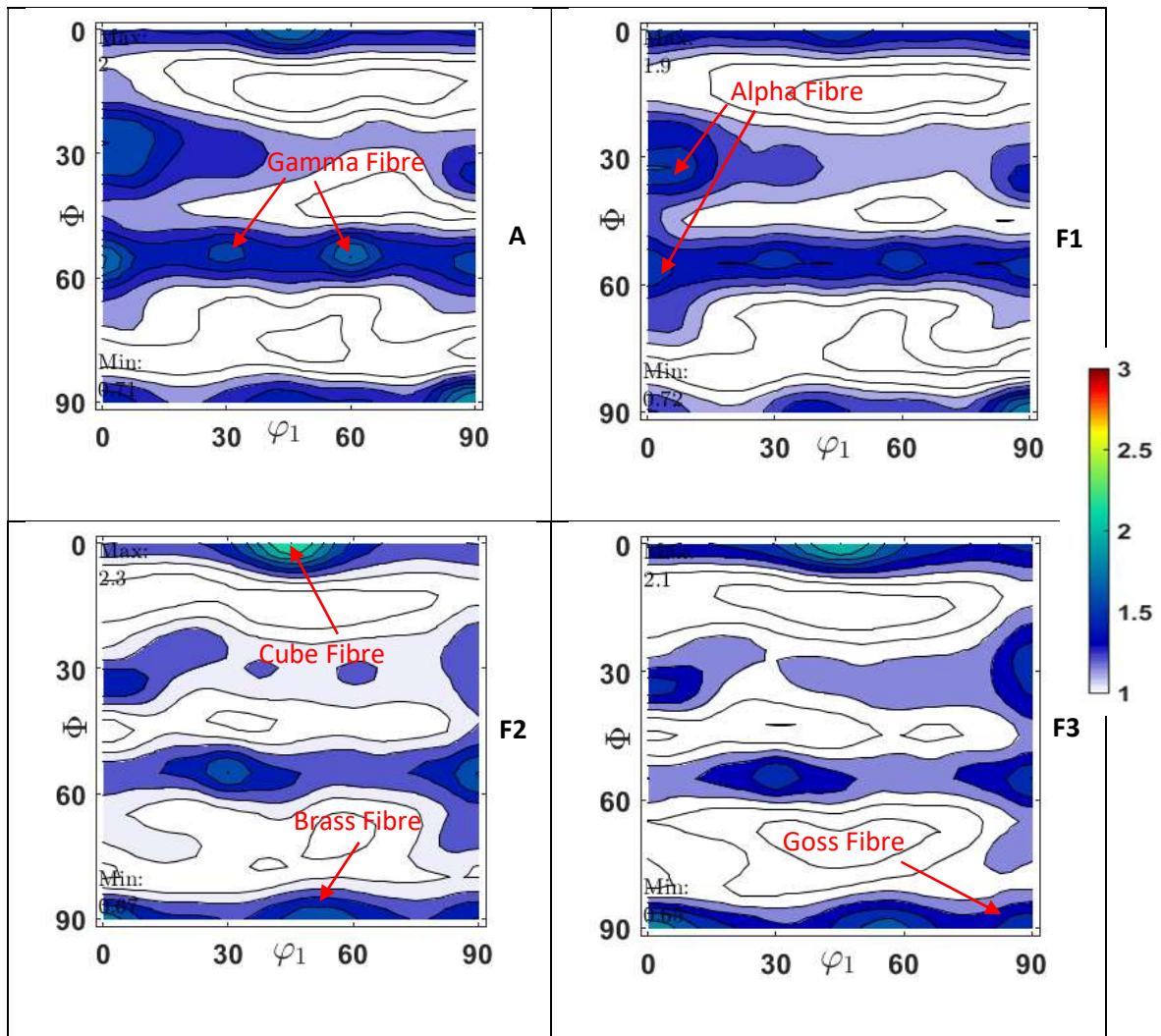


Fig. 7.8. Comparison of textures developed in rolling simulated samples

The austenitic regime rolled sample shows strong alpha fibre close to (113) and gamma fibre is uniformly distributed all along with $\langle 111 \rangle // \text{ND}$ in this sample. This can be linked to the randomising effect of the transformations in phases after deformation in the austenitic region. It has a random texture with varying alpha, gamma and cube texture with its maximum intensity at $113 \langle 110 \rangle$, $111 \langle 110 \rangle$ and $001 \langle 100 \rangle$ respectively. The lower temperature ferritic rolling samples show pronounced deformation texture with predominantly α -fiber texture and γ -fiber texture similar to that of the austenitic rolled samples but with varying intensities. This is due to the absence of phase transformation and softening after deformation (Hao et al. 2019).

Sample F1 processed at relatively higher temperatures shows the intensity of α -fiber and γ -fiber texture component maximum at (113) $\langle 110 \rangle$ and 111 $\langle 011 \rangle$ respectively. This sample has partial alpha fibre and well developed gamma fibre and lower theta θ -fibre (RD// $\langle 100 \rangle$) as compared to other ferritic samples. This sample also shows the highest ratio of gamma to theta fibre making it the most formable material among all. The low temperature ferritic sample F2 shows the development of unwanted cube fibre texture at 001 $\langle 100 \rangle$. It has a lower intensity of γ -fiber texture compared to F1 sample with a maximum at (111) $\langle 121 \rangle$. Low temperature rolling reduced the alpha fibre texture with presence only at 111 $\langle 110 \rangle$ in F2 sample. Sample F3 shows highest amount of cube 011 $\langle 100 \rangle$, goss (110) $\langle 001 \rangle$ and brass (110) $\langle 112 \rangle$ texture component among all the tested samples. The α -fibre and γ -fibre intensities are lowest in this sample among all. These initial textures may result in poor formability after cold rolling and annealing (Hao et al. 2019).

Previous studies (Hoile, 2000) suggest that, with the combination of finer grain, the $\langle 111 \rangle$ //ND texture is strengthened in the subsequent steps of cold rolling and annealing. With larger initial grains, the $\langle 110 \rangle$ texture is strengthened. This initial HR texture in F1 ferritic rolled samples is most favourable to the formation of higher recrystallization texture after cold rolling and annealing for better formability (Chang et al. 2020).

The above experiments have confirmed that it is feasible to produce steel under ferritic rolling conditions in an industrial hot strip mill and the regime must be designed taking temperature and reduction into account. Based on test results, the temperature ranges 850 °C to 800 °C is the most suitable for ferrite rolling with the lowest flow stress or load requirement under the existing austenitic strain and strain rates. Within this band, the finishing entry temperatures must be on the higher side for rolling lower thicknesses. It is concluded that ferritic rolled IF steels between the F1 and F2 temperature regime will result in homogeneous microstructure and is expected to give lower yield strength and a higher ductility compared to conventionally produced austenitic rolled coils. It will be a better input HR material for subsequent cold rolling and annealing than the existing austenitic rolled material. In industrially rolled coils it is expected to have improved deep drawing properties (Chang et al. 2020). Lowering of rolling temperature (120-150 °C) increases the possibility of energy savings and oxidation loss. Lower stress allows rolling of larger widths with less thickness and lowers shape defects thereby decreasing production costs and increasing productivity (Andreas et al. 2000; Chang et al. 2020).

7.2 HSMM (Hot Strip Mill Model) Simulation Results

The model was first validated for the existing austenitic rolling of IF grade steel. The predicted finishing temperature (FT), coiling temperature (CT) and the mechanical properties were found to be very close to the plant values and are shown in Table 2. It, therefore, confirms the accuracy of the configured model. The model was then run with the 3 different proposed ferritic rolling temperatures. It was found that by reducing the temperature in the model input, the model identifies the change in the microstructure from austenite to ferrite. It did not indicate any abnormal increase in the rolling loads or any abnormal change in the other process parameters for the first two conditions but showed a warning on load increase at the lowest temperature (F3). The predicted properties of the ferritic rolled samples show increased yield strength (YS), increased ultimate tensile strength (UTS) and decreased elongation with lowering the rolling temperatures as shown in Table 7.1. This increase is due to the strain hardening in absence of recrystallization and is in the expected range. The existing software simulates rolling feasibility and does not predict the texture, but the properties correlate to the development of deformed texture. This confirms that the proposed ferritic rolling regime can be applied in the existing mill under the ferritic rolling conditions 1 and 2 without any expected process issues if operated within these temperature limits.

Table 7.1. Comparison of process parameters and properties from the HSMM model

Condition	FT, °C	CT, °C	YS, MPa	UTS, MPa	% Elongation
Actual austenitic rolling parameters	920	641	201	295	48.5
Model output - austenitic rolling (A)	930	649	210.5	299.4	46.9
Model output - ferritic rolling -1 (F1)	840	640	222	312.5	41.4
Model output - ferritic rolling -2 (F2)	800	600	245	329	35.1
Model output - ferritic rolling -3 (F3)	750	570	276	345	28.2

7.3 Plant Hot Rolling Results

The details of the various measurements on the samples collected from both austenitic and ferritic rolled IF steel hot rolled coils are discussed below. The residual stress variation in the

surface layer is responsible for defects arising during the cutting and uncoiling process and also affects formability and fatigue life (Sasahara et al. 2005; Lokendra et al. 2017). Residual stress measurement was carried out on the head and the tail regions of coils. Magnetic Barkhausen Emission (MBE) measurements were carried out using Rollscan300 on top surfaces of the coils at a magnetizing field of 40kA/m by varying the frequency from 20-200Hz with 20Hz step. RMS voltage of the Magnetic Barkhausen Emission is the indirect measure of the residual stress in the steel sheet surface (Gatelier et al. 1995, Panda et al. 2020). The RMS voltage measured in millivolts, at different locations in the austenitic and both the ferritic rolled IF grade HR coils are shown in Figure 7.9. All the stresses are tensile as measured on the top surface of the coil. Variation of residual stresses is more in austenitic rolled samples and this variation causes the shape defects. This phenomenon is regularly seen in hot rolled coils due to narrow phase transformation bands and larger temperature gradients seen at high temperature rolling. The head end is under more tensile stress than the tail end. Variation of residual stress is less in ferritic rolled samples though the trend of stress having higher compressive stress at the tail remains same in both rolling regimes. This uniformity in residual stress is one of the key advantages of rolling in a single phase region.

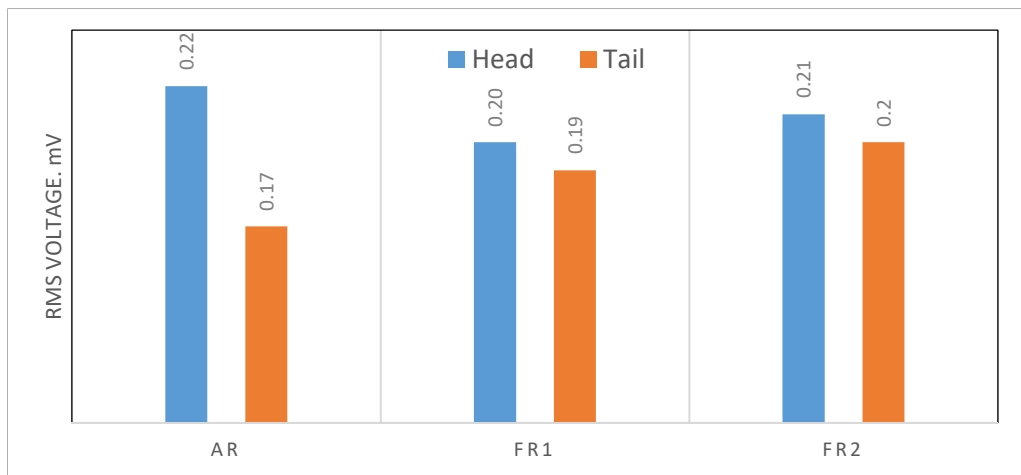


Fig. 7.9. Comparison of residual stress at different locations as measured using Magnetic Barkhausen Emission technique in hot rolled sheets

The strength of the rolled coils is measured using the tensile test and the formability is measured using the *r*-value (normal anisotropy parameter) and the hole expansion test. Tensile testing was carried out in a Zwick Z250 universal testing machine using ASTM E8 standard. Samples were cut in 3 directions, longitudinal, transverse and 45° to the rolling direction. Tensile testing was

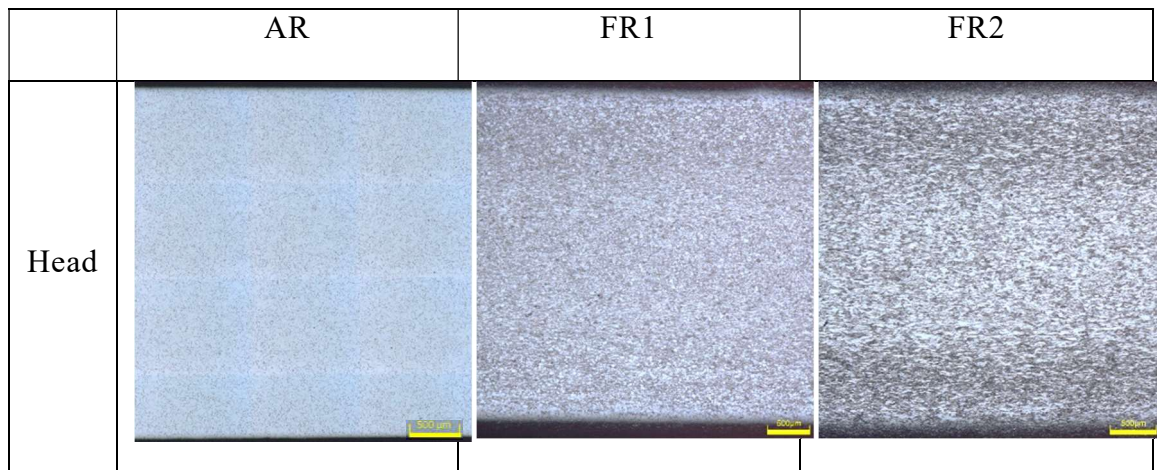
carried out in all 3 directions for the calculation of $\dot{\epsilon}$. The n (strain hardening exponent) value is obtained from the slope of the true stress and true strain curve. These values are presented in Table 7.2. The hardness of the samples was measured on the Vickers scale using a Zwick ZH μ micro-hardness tester. The load applied was 0.5 kg and the average of five indentation values were reported in HV. A hole expansion test was performed in forming press (Zwick - BUP600) using standard ISO 16630. In this test, a hole with a punching die diameter of $d_p = 10$ mm and a relative cutting clearance of 12% is sheared into the sheet sample. This hole is then expanded with a conical die. As soon as a crack that runs through the entire thickness of the plate was seen, the expansion is stopped and the resulting hole diameter D_h is determined. The hole-expansion ratio is then defined as the ratio between the increase in the hole diameter ($D_h - D_0$) and the original hole diameter D_0 . The comparison of the properties, microstructure and crystallographic texture and possible mechanisms are shown and discussed in the subsequent sections.

YS, UTS, % elongation and n -value is reported in both longitudinal (L) and transverse direction (T). YS, UTS and hardness of the ferritic rolled samples are higher than the austenitic rolled samples due to the deformation at lower temperatures and finer grain size. Table 7.2 shows the comparison of mechanical properties of the austenitic and the ferritic rolled IF grade HR coil at different locations. The non-uniform grain size distribution and banded structure acts as an additional barrier to dislocation movement and increases strength (Leilei et al. 2021). These plant recorded values are close to the HSMM predicted values. The comparison of HSMM model predicted values and actual plant rolled values of the tail end are compared in Table 7.3. The difference in values between the longitudinal and transverse direction is higher in ferritic rolled samples. This indicates a greater difference in grain orientation, which increases at the lower ferritic rolling temperature. Ferritic hot-rolled samples are similar to austenitic samples after cold rolling and could be compared to full hard condition and hence the elongation was found to be lower in both the ferritic rolled samples. Strength increases and elongation decreases with a decrease in finishing and coiling temperatures. Indices of formability $\dot{\epsilon}$ (\bar{r}) and hole expansion ratio in hot rolled condition decreases in ferritic rolled samples. Average plastic strain ratio or the normal anisotropy or the \bar{r} is a measurement of drawability (world auto steel 2021) and shows resistance to thinning in the thickness direction during deep drawing. Lower \bar{r} values are due to increased hardness and yield strength and reduced elongation (Toshio et al. 1981). Higher deformed structure without any recrystallization has stress concentration areas which initiate cracks at small deformation during the hole expansion test and result in lower formability. A

lower n value in ferritic samples indicates the presence of high residual stress in the samples. However, it is important to note that these coils are intermediate products and the formability is expected to improve after annealing.

Table 7.2. Comparison of the mechanical properties of ferritic and austenitic hot rolled coils

	Properties	AR				FR1				FR2			
		Head		Tail		Head		Tail		Head		Tail	
		L	T	L	T	L	T	L	T	L	T	L	T
1	YS, MPa	201	196	179	181	228	264	224	262	284	325	279	322
2	UTS, MPa	295	293	285	287	316	342	312	341	353	382	343	381
3	Elongation (%)	48.5	46.5	49.3	48.2	29.1	24.6	28.7	22.9	21.3	17.5	20.9	18.1
4	n	0.211	0.201	0.222	0.215	0.145	0.122	0.147	0.123	0.083	0.078	0.095	0.088
5	\bar{r}	0.96		0.98		0.69		0.78		0.93		0.97	
6	HER	152.8		153.2		131.35		135.25		112.6		114.4	
7	Hardness	100.6		92.2		101.3		108		115.3		119.3	



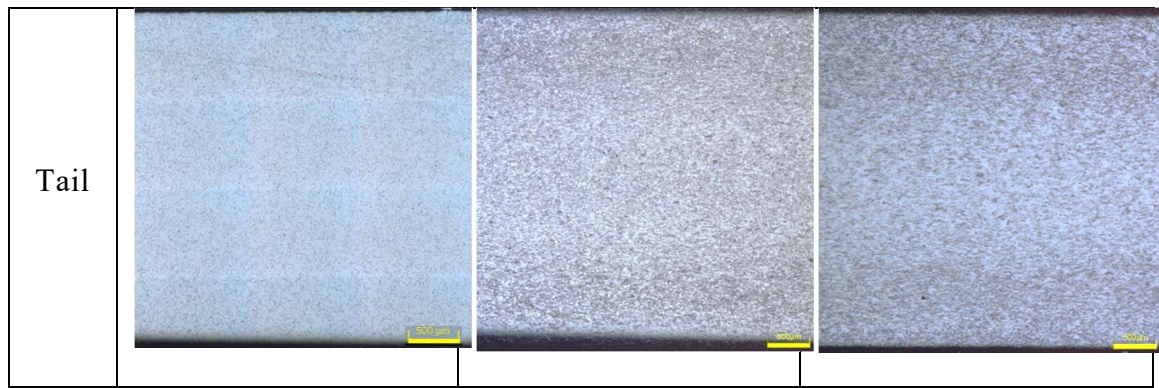


Fig. 7.10. Variation in grain morphology along the thickness in hot rolled sheets (scale – 500µm)

Table 7.3. Comparison of HSMM predicted and actual plant mechanical properties

	FR1		FR2	
	YS, MPa	UTS, MPa	YS, MPa	UTS, MPa
Model	222	312.5	245	329
Actual	224	312	279	343

Figure 7.10. shows the through thickness variation of grain morphology in a single image (captured through image stitching module) of austenitic and ferritic rolled samples at head and tail end along the rolling direction in 100X magnification. Grain morphology is very uniform in the austenitic temperature range rolled samples indicating uniform recrystallization. In the higher temperature ferritic rolled sample FR1, there is a thin layer of fine deformed grains or shear texture near both surfaces. The variation is higher in the FR2 samples where a thicker band of highly deformed, strained grains could be seen on both surfaces, especially at the head end. This shows that the through thickness microstructural anisotropy increases with a decrease in temperature in the ferritic region. The difference in the grain morphology between the surface and the mid-section is due to the additional shear friction between the material and the rolls and is non-homogeneously distributed along the thickness direction. This is a major drawback of ferritic rolling and affects the formability of the sheet (Barrett 1999). This is the reason for significantly reduced hole expansion values of the FR2 samples having lower FT and CT. This surface layer is expected to show shear texture ($\langle 110 \rangle // ND$) and lubrication is suggested (Barrett 1999; Keit et al. 2013), for its avoidance during ferritic rolling. However continuous use of lubrication during industrial rolling is not practically feasible. It is preferred to have optimum

rolling temperatures to avoid lubrication during industrial rolling. Nevertheless, it will become uniform after annealing (Zhao et al. 2019).

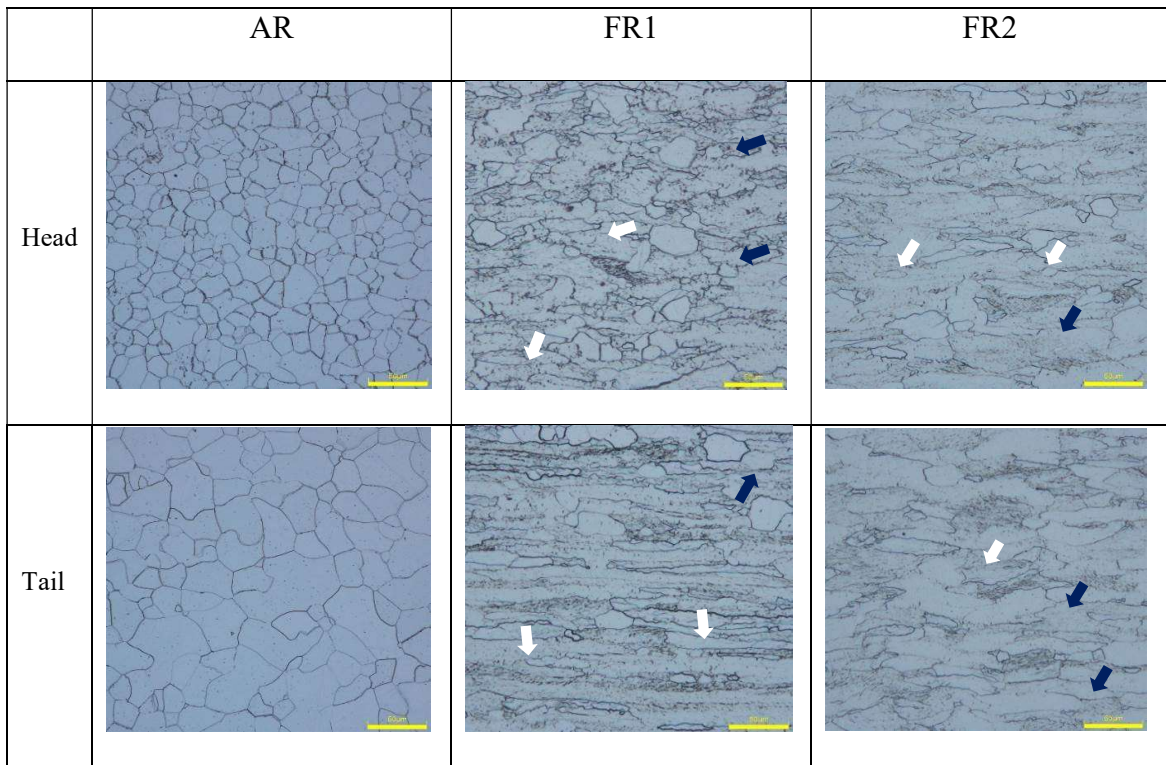


Fig. 7.11. Microstructures of austenitic and ferritic rolled samples in hot rolled sheets (scale – 50 μm)

Small steel samples were cut, mechanically polished and etched using 4% nital for grain size determination using optical microscopy. Figure 7.11 shows the comparison of the hot-rolled coil mid-section microstructure at the head and the tail end.

The optical microscopy of the IF grade steel hot rolled coil in austenitic conditions shows a typical ferritic microstructure with grain size varying between 30 – 40 μm . Variation in grain size and morphology can be seen between the head and the tail section. Grain size is finer in the head as compared to the tail regions of samples, presumably due to a higher cooling rate. At the tail portion, the ferritic microstructure is mostly recovered and some recrystallization has taken place which results in more equiaxed grains and marginally (5- 8%) lower properties especially elongation. Such non-uniformity of mechanical properties along the length and in the transversal direction is commonly reported in the literature (Ronan et al. 2014).

The ferritic rolled samples in FR1 also show completely ferritic microstructure but with elongated irregular grains of size varying between 15 – 30 μm . Ferrite rolling is not expected to have dynamic recrystallization (Ghosh et al. 2008), but recovery can be seen as the deformation is carried out close to transformation temperature. Under higher temperature ferritic rolling, at certain locations recovery has just initiated and this incipient recovery of the microstructure lead to saw-like or wavy edges (indicated by light arrows) on grains. Some of these grains are also having bulged shape (indicated by dark arrows), due to localised orientation gradients in the microstructure generated by the deformation and subsequent impending recovery. In the recovery process part of the dislocations are annihilated, but the remaining dislocations are stored in low-angle dislocation walls resulting in the formation of subgrains. It forms the subgrains in ferrite due to the “extended dynamic recovery”, which is similar to the “continuous recrystallization” (Cizek and Wyne 1997). Grains from ferritic rolling show wavy boundaries as ferrites absorbs more strain and carries most of the deformation (Fargas et al. 2008). The presence of combined bulged and wavy deformed grains showing misorientations in this sample is unique. The merging of dislocation walls in recovery leads to a gradual build-up of misorientations between neighbouring subgrains. This behaviour can also be attributed to the high stacking fault energy of ferrite which makes the static and dynamic recovery faster. Dynamic recovery is reported to be more dominant during the deformation in ferrite as dislocation climb occurs readily due to its high SFE, and also the diffusivity of iron atoms in ferrite is greater than in austenite for a given temperature (Langner et al. 1998). These sharp edge grains along with lower r-value and higher hardness indicates that the grains are in strained condition.

Compared to FR1, the low temperature ferritic rolled sample FR2 shows highly elongated deformed ferritic grains aligned along the rolling axis having non-uniform grain distribution. A higher level of undercooling at lower deformation temperatures drives the formation of higher amount of dynamically strain induced ferrite in FR2 sample (Hurley 2001). A large fraction of low-angle misorientations (indicated by light arrows) in FR2 samples indicate retained strain in the grains and hardened microstructure. In absence of dynamic recrystallization at lower temperature rolling, the morphology of the grains is more pancaked and strain is retained from hot rolling, which increases the strength and lowers elongation in FR2 coil. These un-recrystallized grains also degraded the r value. In FR2 samples deformed at a lower temperature, deformation bands or ingrain shear bands are also observed in many deformed grains (indicated by dark arrows) and is attributed to inhomogeneity of strain and

stress concentration in different grains. It is also reported (Jonas 1998) that in-grain deformation bands which are locations of high dislocation density are formed during the ferritic rolling which nucleates favourable gamma fibre ($\langle 111 \rangle // ND$). It is also supported by low carbon contents in this grade which results in low strain rate sensitivity favourable for such in-grain deformation bands (Jonas 1998). The morphology and size distribution are similar between the head and the tail end in the ferritic rolled samples. As the grains in ferritic rolling are strained, subsequent recrystallization annealing is required, to obtain the desired deep-drawing properties. Austenitic rolled samples show higher grain size as a result of dynamic recrystallization and/or metadynamic recrystallization.

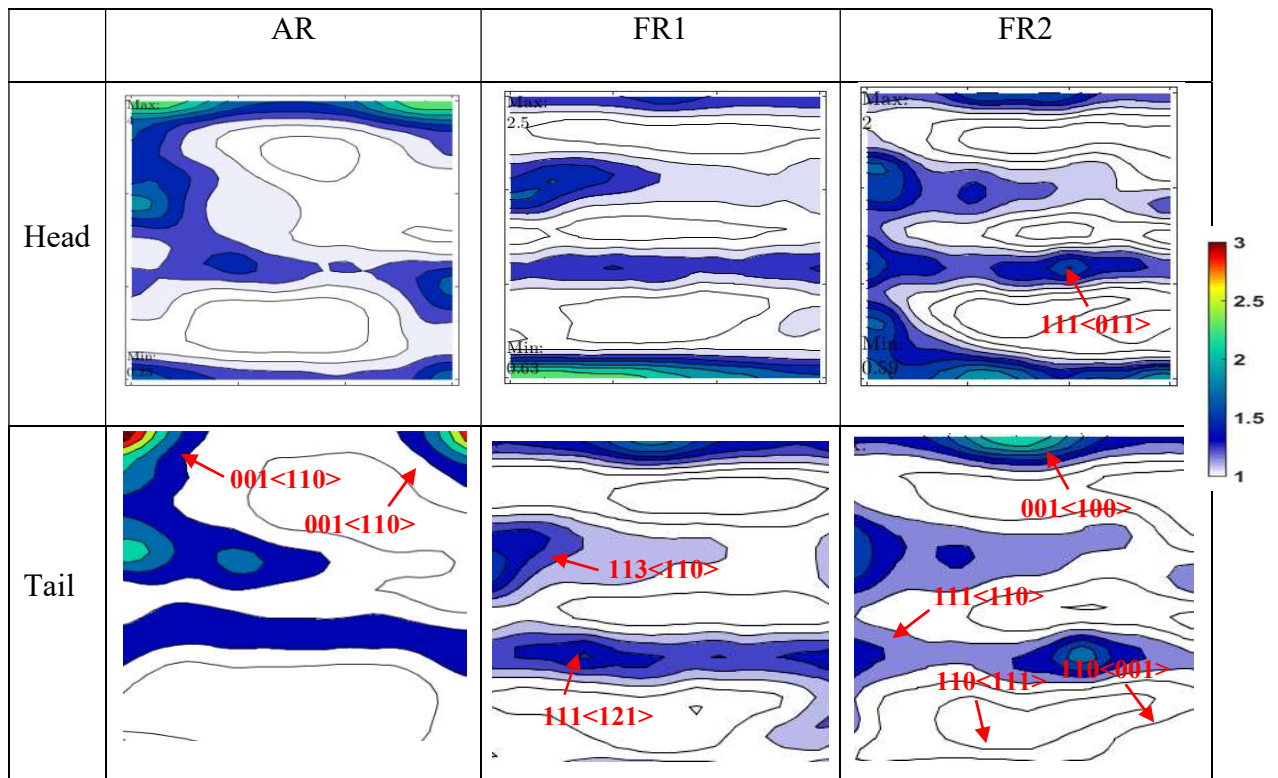


Fig. 7.12. Comparison of textures developed in austenitic and ferritic hot rolled sheets

Different hot band textures lead to different texture evolution during cold rolling and annealing. The deep drawing behaviour of steels depends basically on attaining the proper $\{111\}$ texture after each stage of hot rolling, cold rolling and annealing (Ray et al. 1994; Chang et al. 2020). Oriented nucleation mechanism is dominated in ferritic rolled samples compared to selective growth mechanism in austenitic rolled samples.

In oriented nucleation, first the strain free, low dislocation density regions are formed, which are

then free to grow into the deformed material (Gangali et al. 1995). Nucleation sites are the original grain boundaries, the deformation bands and the shear bands, all containing higher amounts of stored energy. As the boundary mis-orientation is the governing factor it is called oriented nucleation mechanism. Ferritic rolled samples have more boundary misorientations and stored energy and this mechanism is more prominent in FR1 and FR2 samples.

Once nucleation is complete, growth takes place, which may or may not be orientation dependent but the orientation changes occurring during growth can be described in terms of orientation dependent growth rates. Such changes correspond to orientation transformations (OTs) that involve particular pairs of $\langle hkl \rangle$ axes and angles (ω) or the planes (Aust and Rutter 1960). It was found that grain-to-grain misorientations are favoured for selective growth. In this mechanism selective growth takes along preferred planes and not dependent by the mis-orientation angle. This selective growth at particular orientations describes the grain growth in austenitic rolled samples. These mechanisms successfully predict the features of the final recrystallization texture.

Hence to obtain a beneficial recrystallization texture, the γ fibre should be the most prominent texture in the un-annealed condition. Coils having a higher amount of prior alpha and gamma fibre in hot rolled condition, are less susceptible to shear band formation during cold rolling and also helps in nucleating more gamma fibre during annealing. Higher gamma and alpha fibre are desired in hot rolled coils for improved formability after cold rolling and annealing (Wang et al. 2006; Chang et al. 2020).

The texture was measured on a Panalytical X-ray diffraction machine using texture goniometers. Samples were cut and prepared using chemical etching. Texture measurement was done in a mid-thickness section of RD-TD plane. Comparison of texture ODF along ϕ (0-90°), ϕ_1 (0-90°), ϕ_2 at 45° section for mid-section austenitic and ferritic rolled samples is shown in Fig. 7.12. Austenitic hot rolled coil (AR samples) shows nearly random texture at both the head and tail ends. It contains mostly cube and goss texture and weak recrystallization texture components corresponding to alpha fibre and gamma fibre. Both the head and tail sample have cube and rotated cube (theta fibre) with maxima at 001 \langle 110 \rangle . This is because, at high temperature rolling, where austenite is not recrystallized, the cube (001) \langle 100 \rangle texture of austenite transforms into the rotated cube (001) \langle 110 \rangle in the ferrite. Head sample shows maximum alpha fibre close to (001) whereas weak gamma fibre is uniformly distributed all along with \langle 111 \rangle //ND in this sample. This is attributed to the recovery processes. Recovery processes reduce the stored energy of \langle 111 \rangle

oriented grains and minimize their amount after recrystallization. The ratio of gamma/ theta fibre is ~ 0.4 . Similar results were also reported by Guo et al. (2014).

Ferritic rolled samples (FR1 and FR2) show more similarity in texture between head and tail, compared to the austenitic rolled sample (AR). More deformation texture and pronounced alpha and gamma texture is seen in the ferritic rolled samples compared to the austenitic samples. At lower temperature deformation, thermally activated dislocation movements (recovery) are restricted and complex multiple slipping dominates which leads to the formation of $\langle 111 \rangle$ oriented grains (Andreas et al. 2000; Zhao et al. 2019) with higher stored energy. With lowering deformation temperatures, the density of formation of the $\langle 111 \rangle$ oriented grains increases. No significant theta fibre is seen in both the ferritic rolled samples. The ratio of gamma/ theta fibre is > 1 under both conditions.

In FR1 sample austenite transforms towards gamma and alpha fibre and the cube texture is diminished. High temperature ferritic-rolled sample (FR1) shows gamma texture maximum at $111\langle 121 \rangle$ and alpha fibre texture maximum is at $113 \langle 110 \rangle$. By reducing the finishing temperature below $800\text{ }^\circ\text{C}$ and coiling temperature below $600\text{ }^\circ\text{C}$, in FR2 samples, a more distinctive gamma fibre component with the strong alpha fibre in the near $\langle 111 \rangle$ component could be observed. As the finishing rolling temperature decreases, more strain energy is accumulated in the material, which is favourable for the development of a recrystallization texture with a high $\langle 111 \rangle$ intensity or gamma texture. Low temperature ferritic rolled sample (FR2) shows gamma maxima at $111\langle 011 \rangle$ at both the ends which is the more stable orientation in this fibre texture. The relative proportion of alpha fibre is higher in FR2 sample compared to FR1 sample. Alpha fibre texture maxima is at $111\langle 110 \rangle$ in FR2 sample. But with reduced temperature rolling some unwanted cube fibre at $001\langle 100 \rangle$, goss fibre at $110\langle 001 \rangle$ and brass at $110\langle 111 \rangle$ also emerged in FR2 samples.

Present results are also in agreement with the previous work (Guo et al. 2014). Laboratory experiments from Guo et al. (2014) presents that by lowering the finishing temperature the deformation texture is improved with an increasing amount of $\{111\}$ oriented grains which supports the formation of a sharper $\{111\}$ recrystallized texture after coiling. Alpha orientation rotates to gamma orientation, leading to high intensity of gamma fibre texture during cold rolling and therefore FR1 sample having relatively higher alpha fibre is expected to yield higher gamma fibre before annealing. The presence of other unfavourable textures along with the alpha and gamma fibres in FR2 samples are expected to end up with more alpha fibres after annealing. It is

also important to note that there is also distinct texture characteristics along the thickness in FR2 samples rolled at lower FT and CT (finishing temperature and coiling temperature) where grains at different layers, experience different shear stress and thus orient differently.

Ferritic rolling experiments aimed to check the rollability within mill load limitations and the development of properties and texture under this condition. Comparison of rolling force values shows no increase in the load requirement during ferritic rolling. Variation of properties along the length was found to be higher in austenitic rolled samples due to phase transformation. Whereas, variation along the thickness was found to be higher in low temperature ferritic rolled samples. This initial HR texture especially in FR2 ferritic rolled samples is more favourable to the formation of higher final recrystallization texture after cold rolling and annealing but the formation of thicker shear texture at the surface, property variation along the thickness and significant increase in YS and UTS can move the final properties out of range. Better results are expected at lower FT and CT conditions with the use of lubrication during the rolling. Hence the FR1 rolling regime with finishing temperature at ~ 840 °C and coiling temperature at ~ 640 °C is more suitable for industrial rolling without any lubrication. The developed texture in FR1 was more favourable for achieving higher formability after cold rolling and annealing. Despite having a higher variation in temperature between the head and tail portion of the coil, the difference in residual stress, properties and texture is minimal. This is the key advantage of ferritic rolling which allows a higher flexibility in rolling and helps in reducing the shape defects. However, it requires optimization of cold rolling reduction and annealing temperatures concerning ferritic rolled coils for achieving improved properties compared to the conventional austenitic rolled coils.

7.4 Annealing Simulation Results

The sample size used for Gleeble simulation are smaller in size and bulk formability cannot be measured. Hence elongation measured through tensile test is considered as formability criterion in such simulated samples and higher elongation indicates higher formability. In this work, the annealed samples were subjected to tensile test and elongation for all three sheets were compared. Figure 7.13 shows the reduction in the UTS with an increase in temperature in annealing simulated samples. This confirms the softening of the material with increase in temperature. With increase in temperature, the recrystallization process and carbide dissolution moves towards completion resulting in decrease in strength and increase in elongation. Also, the increase in grain size and reduction in residual stresses at higher temperatures contributes to reduction in strength.

The rate of change of strength decreases at the higher temperature when the recrystallization is completed and residual stresses are all eliminated. Figure 7.14 shows the change in percentage elongation with an increase in soaking temperature. Increase in elongation indicates increase in expected formability in all the samples, though at different rates.

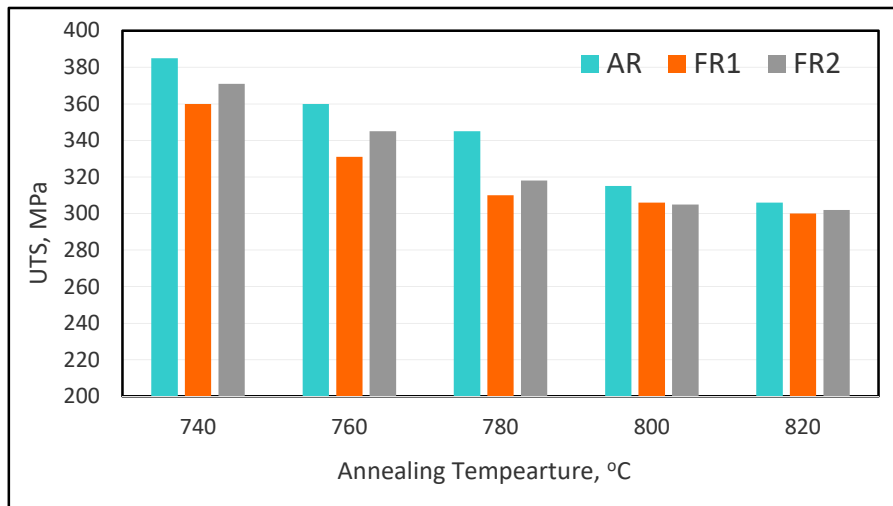


Fig. 7.13 Change in UTS with an increase in temperature in annealing simulated samples

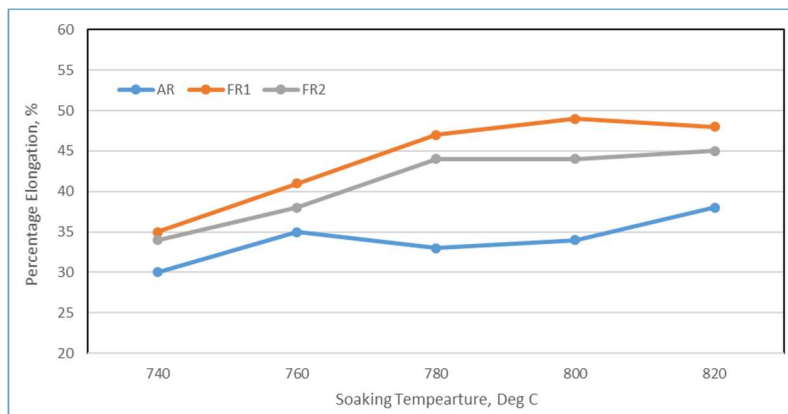


Fig. 7.14. Change in percentage elongation with an increase in temperature in annealing simulated samples


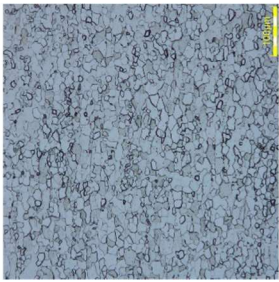
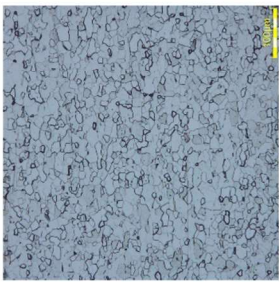







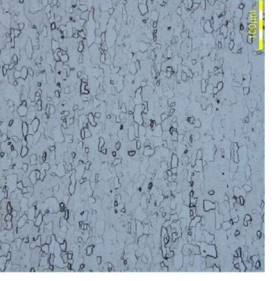
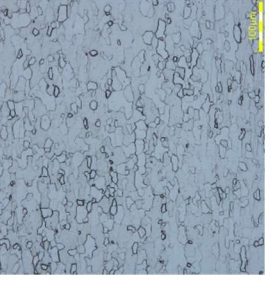
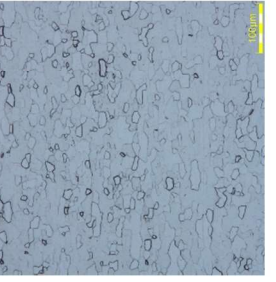
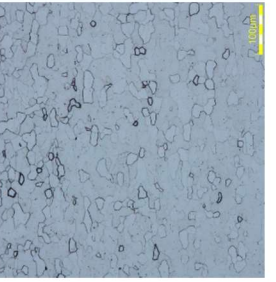
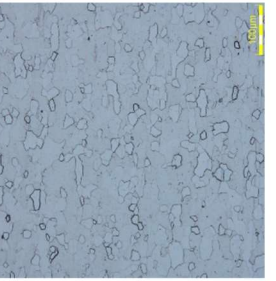
Soaking temperature	740 °C	760 °C	780 °C	800 °C	820 °C
AR					
FR1					
FR2					

Fig. 7.15 Comparison of microstructures and grain size of annealing simulated samples

The samples were also characterized through optical microscopy for the grain size measurements. Figure 7.15 shows the comparison of microstructures and grain size for the ferritic and austenitic rolled samples. The recrystallized grains formed in all samples have polygonal morphology. Increasing the temperature increases the elongation and grain size. However, beyond a certain temperature, its effect becomes constant. In industrial practice operating at higher soaking temperature is costly and difficult to maintain. It is always aimed to operate at the lowest possible temperature for achieving the desired properties. The comparison of elongation and microstructure indicates that temperatures above 780 °C should be sufficient for achieving complete recrystallization in ferritic rolled samples, compared to 800 °C required in the conventional austenitic rolled sheets. This can be related to higher stored energy which promotes faster nucleation and higher grain growth at lower temperatures. It is therefore planned to anneal the ferritic rolled samples between 780 – 800 °C soaking temperature during plant processing. This lower soaking temperature requirement is an advantage for the ferritic rolled samples.

7.5 Plant Cold Rolling (Full Hard) Sheet Results

Cold-rolled sheets, also called “full hard sheet” are the intermediate product. This requires subsequent annealing to achieve the desired properties. However, to study the property, microstructure and grain orientation transformation at each stage, characterization was carried out on the full hard sheet. The cut sheet was first subjected to residual stress measurement using Magnetic Barkhausen Emission (MBE) measurements at the head and at the tail end of the coils before the samples are cut for other characterization studies. RMS voltage of the Magnetic Barkhausen Emission measured at different locations in the austenitic and both the ferritic rolled IF grade HR coils are shown in Fig. 7.16. Since these sheets are in highly deformed conditions, it shows high residual stresses. Comparatively tail samples have higher stresses under all conditions. Ferritic rolled samples show marginally higher stresses due to more deformed and elongated grains compared to the austenitic rolled samples. The residual stress is expected to reduce after the continuous annealing process.

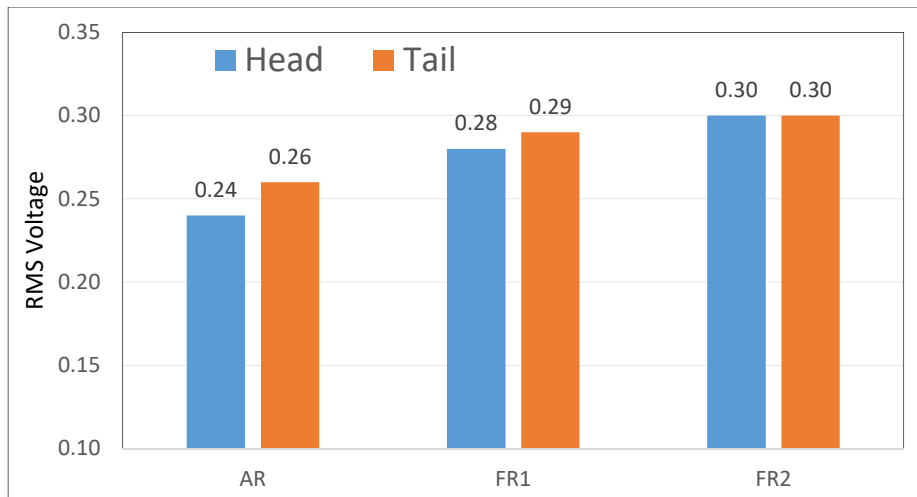


Fig. 7.16. Comparison of residual stresses at different locations as measured using Magnetic Barkhausen Emission technique

As these coils are highly work hardened, they exhibit high strength and has minimal ductility. Table 7.4. shows the comparison of mechanical properties for the conventional austenitic hot rolling and the ferritic regime rolled coils after cold rolling in full hard condition at the head and the tail location. Ferritic rolled coils have relatively higher tensile properties compared to austenitic rolled coils as observed in hot rolled coils. However, being highly deformed and with low elongation, the YS and UTS of all these coils are very close. Hardness is also higher for all these coils compared to coils in hot rolled condition. These coils are highly strained in this condition and many times results in holes and shape defect in CR sheets resulting from uneven stretching. In the present ferritic rolled coils no such defect was observed due to uniformity in HR coil properties along the length. As the cold-rolled sheet is having highly elongated grains in the rolling direction and very low elongation, its \dot{R} and n value are not comparable and are not measured.

Table 7.4. Comparison of mechanical properties of austenitic and ferritic rolled samples in full hard condition

	AR		FR1		FR2	
	Head	Tail	Head	Tail	Head	Tail
YS, MPa	630	613	640	632	642	640
UTS, MPa	644	632	658	648	650	655
%El	4.2	4.1	3.9	4.0	3.9	3.9
Hardness, (Hv -0.5)	207	209	211	215	214	216

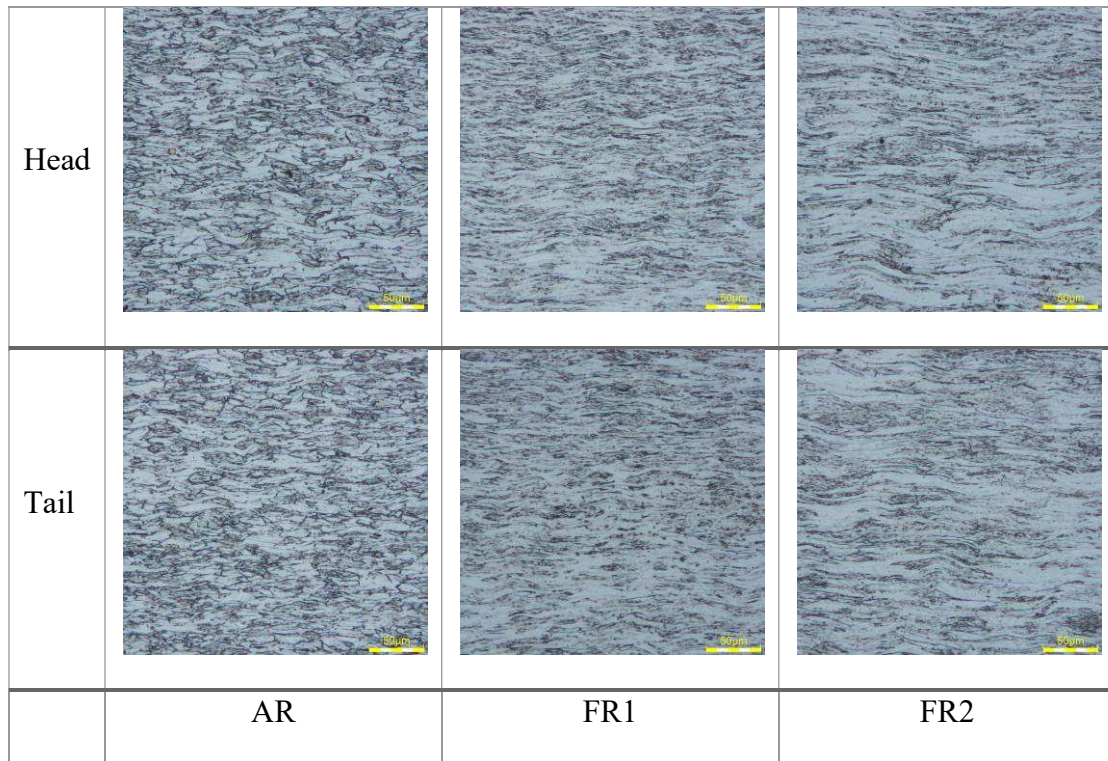


Fig. 7.17. Comparison of microstructures of austenitic and ferritic rolled sheets after cold rolling (scale – 50 μm)

The comparison of the microstructures is shown in Fig. 7.17. All samples show elongated grains of ferrite along the rolling direction. Microstructures show large strained, elongated fibrous grains with similar morphology in all three samples, both at head and tail. The microstructure is primarily homogeneous across the thickness in AR and FR1 samples. Some variation in grain morphology is seen in FR2 samples as was also observed in the hot-rolled stage. Comparatively, FR1 and FR2 samples show visibly more flattened or smaller grains due to their higher deformed structure at the hot-rolled stage. FR2 samples show relatively more strained grains and ribbon structure parallel to the rolling direction, compared to FR1 samples. The grain size is very small and non-uniform and hence not possible to measure the grain diameter by optical microscopy.

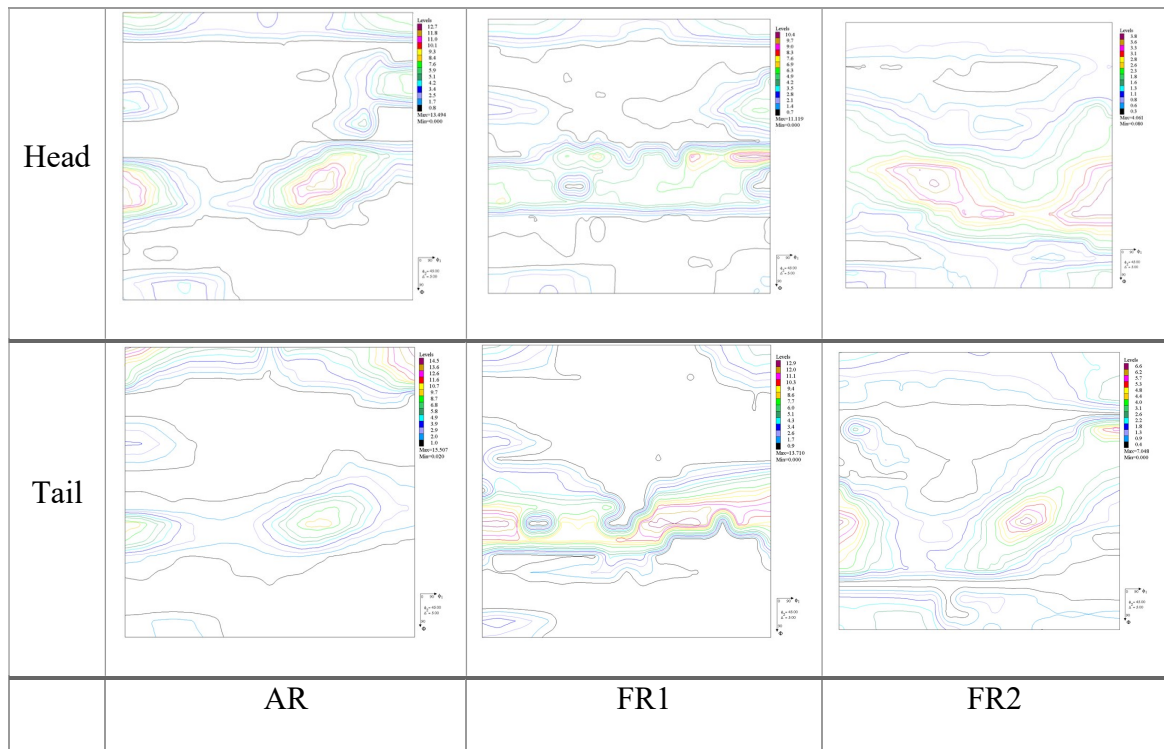


Fig. 7.18. Comparison of textures of austenitic and ferritic rolled sheets after cold rolling

The type and intensity of textures in cold rolled sheets (full hard condition) is influenced by the textures in hot rolled sheets. In these intermediate samples, no significant texture form variation has been found between the head and the tail samples, but texture proportion variation can be seen between the AR, FR1 and FR2 samples. Figure 7.18 shows the comparison of textures through the orientation distribution function map at $\phi_2=45^\circ$ for the austenitic and ferritic rolled sheets after cold rolling measured through the bulk XRD on the samples cut from the head and tail sections of the sheet. Since in the process of cold rolling, grains are deformed and elongated in the rolling direction, it has the uniform but unstable texture orientation and its evolution depends on the texture of the hot-rolled sheet. After cold rolling, the alpha texture $111\langle 110 \rangle$ and gamma texture at $111\langle 121 \rangle$ and $111\langle 011 \rangle$ strengthens and the $110\langle 110 \rangle$, $110\langle 111 \rangle$ and $110\langle 001 \rangle$ components diminish. The $001\langle 110 \rangle$ component is relatively stable and does not transform significantly and its presence can be seen in the cold rolled sheets also. The austenitic rolled samples (AR) show an equal amount of alpha texture and gamma texture. The low temperature ferritic rolled sample (FR2) also show the non-uniform combination of alpha texture and gamma texture. The gamma texture in this sample is more developed than the AR sample and has wide distribution between $111\langle 121 \rangle$ and $111\langle 112 \rangle$. The FR1 samples have predominantly gamma texture narrowly distributed between

111<121> and 111<011> but also has developed higher alpha texture during cold rolling compared to hot rolled condition.

7.6 Continuous Annealed Sheet Results

Similar to hot-rolled coils and the cold-rolled coils, cold-rolled and close (continuous) annealed sheets were also subjected to residual stress measurement using Magnetic Barkhausen Emission (MBE) measurements at the head and at the tail end of the coils before the samples are cut for various mechanical and formability tests. RMS voltage of the Magnetic Barkhausen Emission which is the indirect measure of the residual stress in the steel sheet surface measured at different locations in the austenitic and both the ferritic rolled IF grade HR coils are shown in Fig. 7.19. Ferritic rolled samples show marginally higher residual stresses, but no variation was found in the values between the head and tail end. The uniformity in stress is expected as the sheets are subjected to the continuous annealing process.

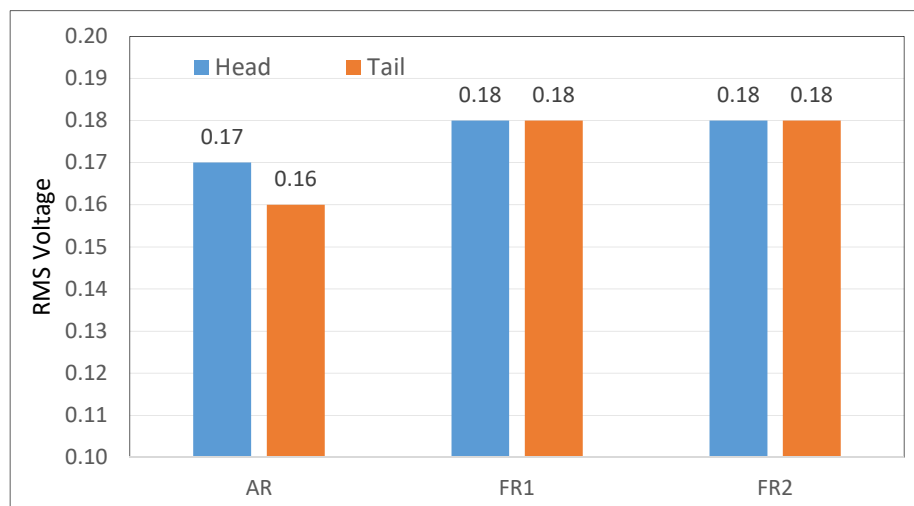


Fig. 7.19. Comparison of residual stresses at different locations as measured using Magnetic Barkhausen Emission technique in cold-rolled and annealed sheets

Table 7.5 shows the comparison of mechanical properties for the conventional austenitic hot rolling and the ferritic regime rolled coils after cold rolling and annealing at the head and the tail location. Since all the coils are continuously annealed, the properties difference between the head and the tail samples is very small. However, the variation is relatively low in both ferritic rolled samples compared to the austenitic rolled samples. No noticeable change is observed in yield strength and tensile strength of both the ferritic rolled coils when compared to the conventional austenitic hot rolling coils in both head and tail samples. However, elongation has increased

significantly in both the ferritic hot rolled coils. The key difference was observed in direct formability parameters \bar{r} – normal anisotropy, Δr - planar anisotropy, and n - strain hardening exponent. The properties were better than the austenitic rolled sheets.

Table 7.5. Comparison of mechanical properties of austenitic and ferritic rolled samples after cold rolling and annealing

	AR		FR1		FR2	
	Head	Tail	Head	Tail	Head	Tail
YS, MPa	158	167	148	149	152	156
UTS, MPa	299	291	286	283	285	287
%El	39.8	41.2	51.2	51.7	49.1	49.7
\bar{r} (r-bar)	2.10	2.12	2.15	2.14	1.92	1.93
Δr	0.12	0.13	0.10	0.10	0.06	0.06
n	0.23	0.22	0.26	0.25	0.24	0.25
Hardness, (Hv -0.5)	96	98	76	79	80	79

\bar{r} value which is a measure of average anisotropy variation in all directions (Ray et al. 1994; World auto steel 2017) was increased in FR1 samples but reduced in FR2 samples. In FR1 samples, the r values increased in rolling and diagonal directions but reduced in 90° direction, however, the overall effect in the \bar{r} is higher. In FR2 samples, the r values reduced in all three directions with not much significant variation among them, however the overall effect results in a reduced \bar{r} . Δr , the planar anisotropy measures variation of anisotropy with direction. Δr reduced in both the ferritic samples and was very low in FR2 samples. Higher \bar{r} results in reduced flow stress and is beneficial for deep drawing but higher Δr introduces earing and is not preferred (Tetsuro and Yoshikazu 2014).

n -value indicates material work hardening under plastic deformation and is more significant in stretch forming (Song at al. 2006; World auto steel 2017). n -value of both the ferritic rolled samples improved in comparison to the austenitic rolled samples. High strain hardening exponent (n -value) ensures that materials can be bent and stretched in a stamping die, whereas high normal anisotropy (\bar{r}) ensures that materials can be drawn in a stamping die. A higher n -value reduces wrinkling. It is understood that in ferritic rolling, the temperature plays an important role in the development of formability characteristics. Overall formability indicators show improved properties for ferritic

rolled samples but because of the differential trends in $\dot{\epsilon}$, Δr , and n -value, its combined effect on the formability behaviour must be experimentally studied under each condition.

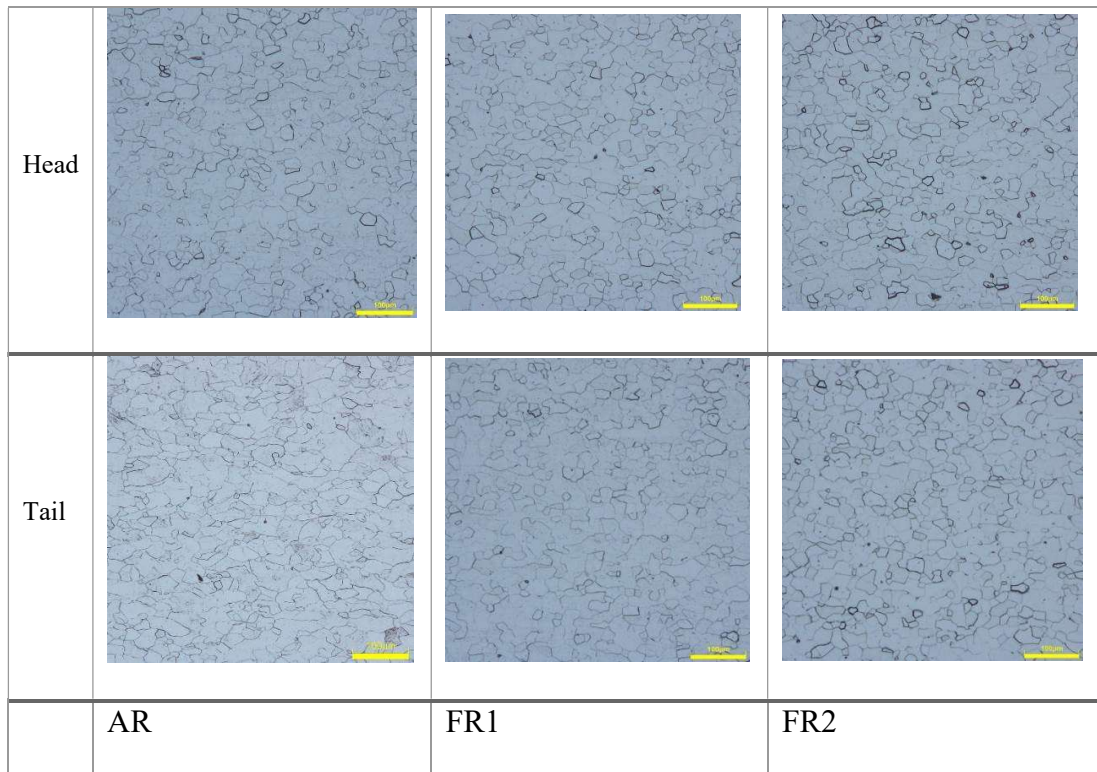


Fig. 7.20. Comparison of microstructures of austenitic and ferritic rolled sheets after cold rolling and annealing (scale – 100 μm)

The comparison of the microstructures is shown in Fig. 7.20. Microstructures show large ferritic grains with similar morphology in all three samples, both at head and tail ends. There is a good uniformity of grains in both the ferritic rolled sheets all along the coil. The average grain size of AR, FR1, and FR2 samples is 24.77 μm ($\pm 1\mu\text{m}$), 24.38 μm ($\pm 0.8\mu\text{m}$) and 21.93 μm ($\pm 0.8\mu\text{m}$) respectively in the head samples and 24.93 μm ($\pm 1.2\mu\text{m}$), 23.98 μm ($\pm 0.9\mu\text{m}$) and 21.55 μm ($\pm 1\mu\text{m}$) in the tail samples. Grains are marginally finer in FR2 samples compared to other two samples. It could be due to difference in initial microstructure resulting from different strain accumulation during hot rolling (Siciliano and Jonas 2000). Both the ferritic rolled samples FR1 and FR2 show recrystallized microstructure with rounded grains whereas the AR samples show polygonal morphology of the grains in both locations. Relatively higher roundness and uniform morphology of the gains in the FR2 sample should be the reason for lower planar anisotropy (Δr) (Hao et al. 2019).

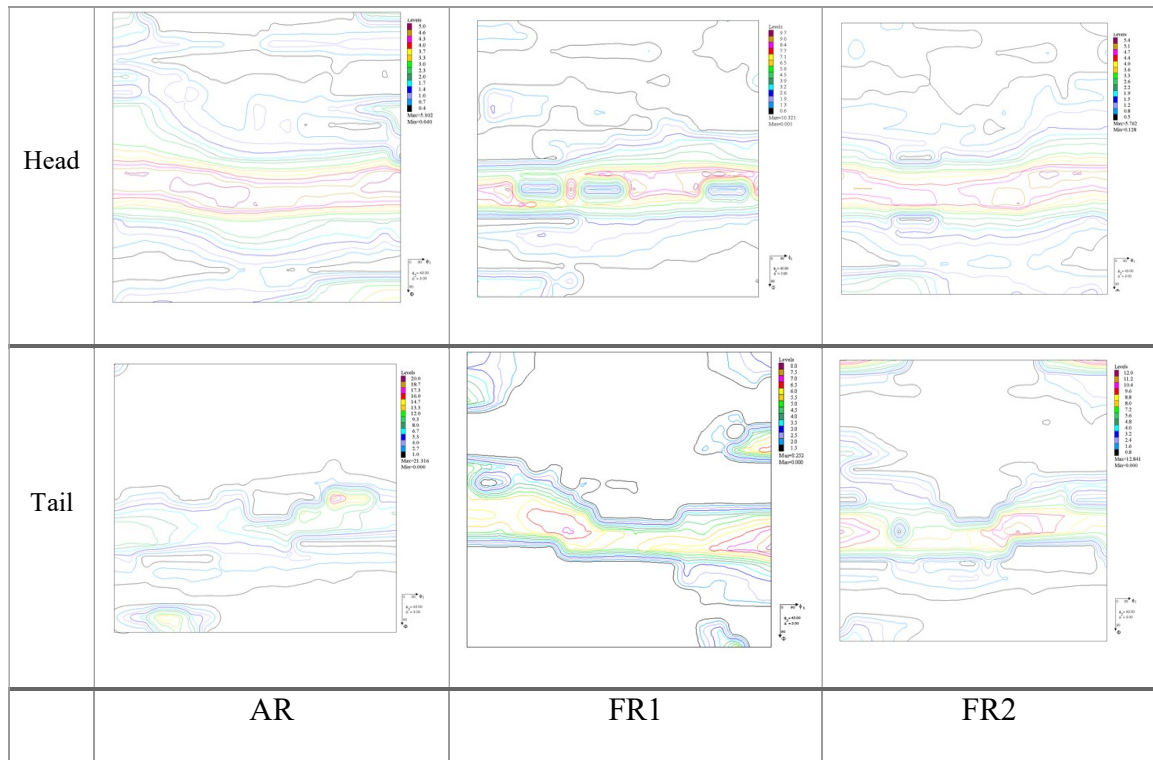


Fig. 7.21. Comparison of textures of austenitic and ferritic rolled sheets after cold rolling and annealing

Figure 7.21 shows the comparison of textures through the orientation distribution function map at $\phi_2=45^\circ$ for the austenitic and ferritic rolled sheets after cold rolling and annealing measured through the bulk XRD on the samples cut from the head and tail sections of the sheet. Compared to the cold-rolled samples the texture sharpens after annealing around the gamma texture. The intensities of $001 \langle 110 \rangle$ reduced significantly in annealed samples compared to cold rolled samples. No significant variation has been found between the head and tail samples on the prominent textures, but texture fraction variation can be seen between the AR, FR1 and FR2 samples. All three samples show a good amount of $\{111\}$ gamma texture stretching between $111 \langle 110 \rangle$ and $111 \langle 112 \rangle$ indicating good deep drawability behaviour for these steels. However, the relative difference in formability comes from the presence of alpha and cube textures and the ratio of its intensities with the gamma texture. Austenitic rolled samples after annealing show the combination of gamma and alpha fibre texture. Gamma fibre texture is uniformly distributed all along with $\langle 111 \rangle // ND$ in this sample with a maximum at $111 \langle 121 \rangle$. However, it also has widely distributed alpha fibre with maxima at $112 \langle 110 \rangle$. It also shows some cube texture at $001 \langle 110 \rangle$

inherited from the hot rolling stage. Ferritic rolled sample FR1 after annealing shows sharper texture with predominantly gamma fibre distributed all along $\langle 111 \rangle // \text{ND}$. It has maxima at $111\langle 121 \rangle$. No other fibre texture is present in major proportions. Ferritic rolled sample FR2 after annealing also shows the non-uniform distribution of gamma fibre and alpha fibre textures. Gamma fibre has maxima at $111\langle 011 \rangle$. It also shows distributed alpha fibre texture with unique maxima at $111\langle 110 \rangle$. It is concluded that with reducing the temperature in the ferritic region, the gamma fibre at $111\langle 121 \rangle$ distributes itself between a distinctive gamma fibre component $111\langle 112 \rangle$ and strong alpha fibre near $111\langle 110 \rangle$. These 111 components of gamma fibre contribute to high r-value and the lower relative difference of intensities between $111\langle 121 \rangle$ and $111\langle 110 \rangle$ components contributes to lower Δr in ferritic rolled samples, improving its formability (Chang et al. 2020).

The presence of a higher proportion of gamma fibre texture in FR1 ferritic rolled samples and better distribution of gamma fibre texture with alpha fibre texture in FR2 samples compared to the austenitic rolled samples, is expected to result in better formability characteristics (Chang et al. 2020). The presence of a more random texture or higher number of grains with random orientation in hot-rolled sheets of austenitic regime results in significant grains orienting towards alpha fibre texture as seen in AR samples. In low-temperature ferritic rolling, more strain energy is accumulated (Ray et al. 1994; Ahmed et al. 2017), which leads to the development of a recrystallization texture with a high $\{111\}$ intensity. But low-temperature rolling also imparts variation in through-thickness behaviour which increases with decreasing temperature. This phenomenon adds some unwanted alpha and cube textures in low temperature ferritic rolled coils after annealing as seen in FR2 samples. The phenomenon of texture development with temperature obtained for ferritic hot-rolled, cold-rolled, annealed sheets are different from the ferritic hot-rolled annealed cases studied previously. This is expected to impart variation in formability characteristics (Qiu et al. 2018).

This bulk XRD results were also confirmed by the volume fraction of textures calculated from the ODF using the LaboTex software. LaboTex sorts average ODF values for all symmetrically equivalent orientations of components from the database. The volume fractions of the three dominant fibre texture and the two most important components of the gamma fibre textures are shown in Table 7.6.

Table 7.6. Volume fractions of the three dominant fibres in austenitic and ferritic rolled samples

Sample	Texture index	Alpha fibre (RD//<110>), %	Gamma fibre (ND//<111>), %	Theta fibre (RD//<100>), %	$\{1\ 1\ 1\}$ <1 $\bar{2}$ 1>, %	$\{1\ 1\ 1\}$ <1 $\bar{1}$ 0>, %
AR (Head)	3.1	15.5	34.3	10.3	12.2	10.9
AR (Tail)	2.9	14.2	31.2	10.1	11.1	10.1
FR1 (Head)	5.2	12.2	45.8	7.2	19.1	10.2
FR1 (Tail)	5.3	10.2	45.1	5.1	18.5	9.1
FR2 (Head)	5.4	12.9	42.5	8.3	15.4	11.4
FR2 (Tail)	5.5	11.1	44.1	7.8	14.6	11.3

The volume fraction of textures shows that the proportion of gamma fibre texture is higher in the ferritic rolled samples and is maximum in FR1. Specifically, the $1\ 1\ 1\ \langle 1\ \bar{2}\ 1 \rangle$ component is higher in FR1 samples. Austenitic rolled samples show a higher fraction of the unwanted theta fibre texture. Among the ferritic rolled samples, the low temperature rolled sample FR2 has a higher fraction of alpha fibre component. Though the texture index is higher for the FR2 sample, the higher proportion of gamma fibre texture and specifically the $1\ 1\ 1\ \langle 1\ \bar{2}\ 1 \rangle$ component makes it highly formable. Studies by Guo et al. (2014) and Hao et al. (2019) also concluded the significant effect of α and γ texture in hot rolled coils during cold rolling and annealing in Ti-IF steel sheets.

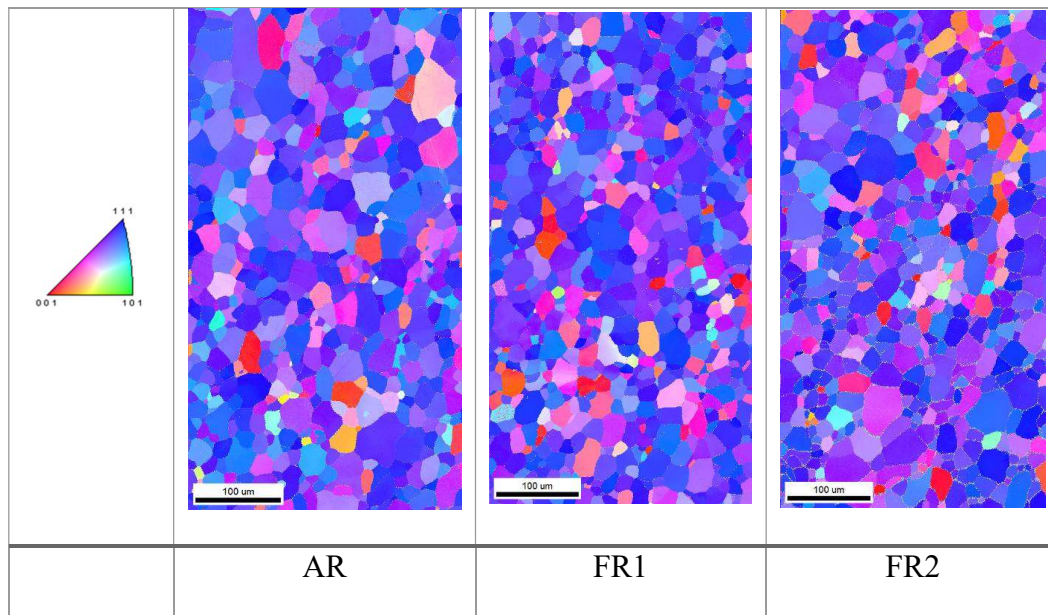


Fig. 7.22. Comparison of inverse pole figure maps from EBSD analysis for austenitic and ferritic rolled sheets

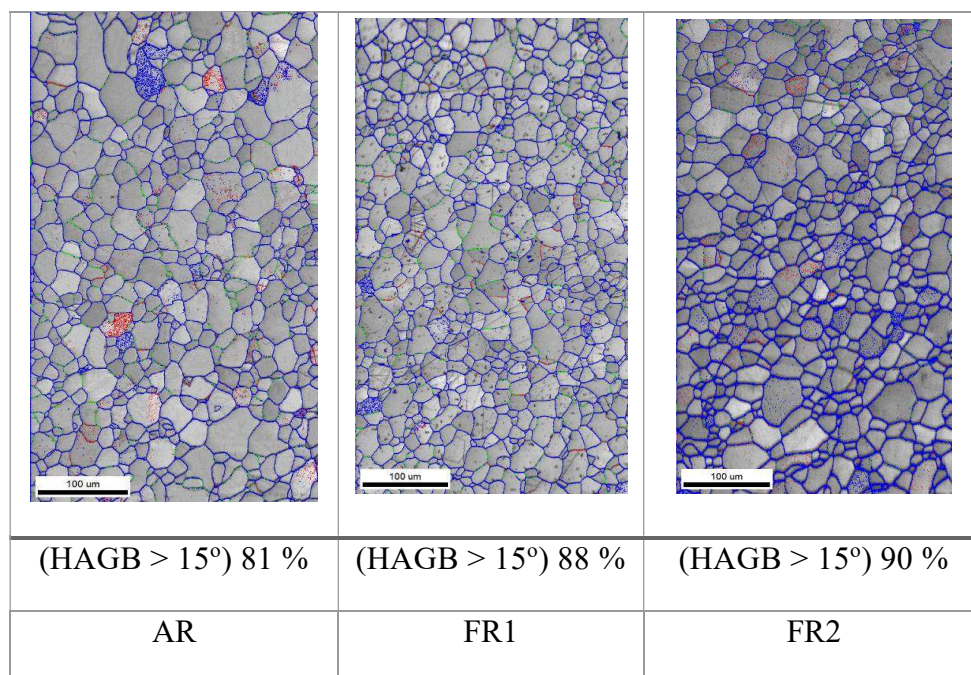


Fig. 7.23. Comparison of grain boundary mis-orientation from EBSD analysis for austenitic and ferritic rolled sheets

Electron Backscatter Diffraction (EBSD) analysis was also carried out on the cold-rolled and annealed samples rolled in both ferritic and austenitic regimes. Being a high end characterization tool, EBSD scanning was carried out only on one representative sample from each coil collected from the central portion of the head end. Figure 7.22 shows the comparison of inverse pole figure maps from EBSD analysis along with the standard stereo-triangle having three important textures

$\langle 111 \rangle$, $\langle 001 \rangle$ and $\langle 101 \rangle$. It is seen that all three samples (AR, FR1, and FR2) have predominantly gamma texture $\langle 111 \rangle$ indicated by a larger amount of blue coloured grains. AR sample shows a higher amount of other intermediate textures indicated by red and orange colour grains. Higher orientation towards the $\langle 111 \rangle$ or the gamma texture evolves from the in-grain shear bands and deformation bands resembling in-grain shear bands (Barnet et al. 1997) in the ferritic rolled sheets. Gamma texture oriented grains and grains of other orientation are of similar size in FR1 and FR2 samples whereas the other orientation grains are bigger in AR samples. This can be attributed to the difference in the recrystallization behaviour due to inherited hot rolled texture.

Figure 7.23. shows the comparison of grain boundary misorientation from EBSD analysis where high angle grain boundaries (HAGB $> 15^\circ$) are shown with blue lines. The high angle grain boundaries (HAGB $> 15^\circ$) are greater than 80% in all samples indicating that recrystallization process is fully completed. Ferritic rolled samples show higher amount of high angle grain boundaries, close to 90%. The higher amount of stored internal energy present in the deformed grains of cold-rolled steel of the ferritic regime provides the driving force for nucleation and recrystallization. Though the grain growth has been marginally higher in the austenitic rolled samples, higher amount of uniform nucleation leads to rounded grains in the ferritic rolled samples (Kohsaku 2020). This results in lower planar anisotropy (Δr) in FR1 and FR2 samples.

Based on the above results of bulk texture, texture fractions and EBSD results, it can be concluded that the evolution of the final texture after cold rolling and annealing depends on the hot-rolled texture of the coils which in turn depends on the hot rolling temperatures. The austenitic regime hot rolled coils which do not have any alpha and gamma texture transforms into strong alpha and weak gamma texture which subsequently after annealing converts into non-uniform gamma texture along with significant proportions of alpha texture. The high-temperature regime ferritic hot-rolled samples contain predominantly gamma texture. It forms some amount of alpha texture during cold rolling but later transforms to uniform gamma texture after annealing. The low-temperature regime ferritic hot-rolled samples containing higher alpha and lower gamma texture transforms to higher gamma and relatively much stronger alpha texture during cold rolling. It forms a nonuniform gamma texture with high intensity of the $\{111\} \langle 112 \rangle$ component after annealing. This difference in the texture components in the austenitic and ferritic rolled samples results in difference in the formability behaviour (Daniella et al. 2017).

There are different theories on the development of recrystallization textures in IF steels after annealing. The two prominent theories include oriented nucleation theory and oriented growth

theory (Magnusson et al. 2001; Kohsaku 2020). In the oriented nucleation theory, final texture is developed based on the formation of pre-oriented nuclei. Oriented growth theory proposes the formation of non-oriented nuclei or nuclei with a large variety of orientations, among which some with certain misorientation to the surrounding matrix will grow faster and dominate the final texture (Peter et al. 1995).

In FR1 samples, after annealing sharper homogeneous gamma fibre was formed with maxima at $111\langle 121 \rangle$ similar to the full hard samples with no other fibre texture present in major proportions. It indicates that it is governed by oriented nucleation, where initially oriented grains get nucleated more on gamma texture oriented grains. In FR2 samples maxima moved from $111\langle 121 \rangle$ to $111\langle 121 \rangle$ in gamma texture and alpha texture maxima also moved to $112\langle 131 \rangle$. Both these alpha and gamma textures moved their relative positions during the recrystallization. In this case, the final texture is affected by the surrounding matrix misorientations and grow in different components indicating the recrystallization is being governed by oriented growth. This suggests that there is a gradual transition of the recrystallization mechanism from oriented nucleation to oriented growth as the temperature of deformation in the ferritic region decreases. It can be attributed to the change in the grain morphology, especially the low angle grain boundaries which increases with reducing temperature resulting in lower nucleation sites (Fang et al. 2016). The heterogeneous substructures and higher initial stored energy in FR2 or the low temperature rolled samples, also promotes oriented growth recrystallization.

7.7 Formability Study Results

In the formability limit testing, it is found that the formability behaviour is different for the ferritic and austenitic rolled samples on either side of the plain strain axis. Figure 7.24 shows the comparison of major and minor strains for the tested samples. The FR1 sample shows the highest limits on the left-hand side representing the uniaxial tension or the tension-compression regime. On this side, the FR2 sample has lower limits than the AR sample. This behaviour can be correlated to the r values (Rees 2001; Paul 2019) which is lowest for the low temperature ferritic rolling. This indicates that for the deep drawing applications, high temperature ferritic rolled sheets would be more suitable. The FR2 sample shows the highest limits on the right-hand side of the FLD curve, which represents the biaxial tension or the tension-tension regime. The AR sample has the lowest limits on this side. This behaviour is correlated to the Δr which is highest and the n -value which is lowest for the austenitic rolled sample. This indicates that for the stretch forming applications, both the ferritic rolled sheets would be suitable.

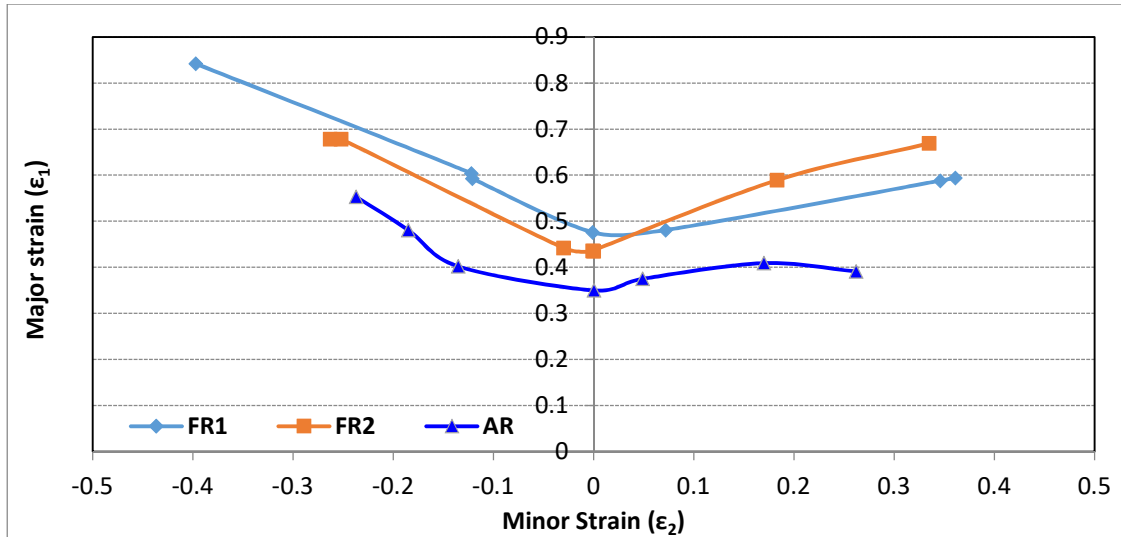


Fig. 7.24. Comparison of major and minor strains for austenitic and ferritic rolled sheets

The images of the HER test samples and their values are shown in Fig. 7.25. The hole expansion ratio of austenitic (AR) and ferritic rolled sheets (FR1 and FR2) were found to be $138 (\pm 4.5\%)$, $148 (\pm 3.0\%)$ and $142 (\pm 2.5\%)$ respectively. High temperature ferritic rolled samples show higher formability with increased HER. Five samples were tested in each case and the variation was also found lower in both the ferritic samples and FR2 sample being the least. The images of austenitic rolled samples with cracks show single penetrated cracks whereas ferritic rolled samples show uniform, small partial penetrated cracks in other directions also. As hole expansion test is sensitive to localized grain morphology variations, it is expected to show higher localized necking in austenitic-rolled samples and uniform small cracks in ferritic samples due to marginally higher through thickness grain morphology variations. However, it is also reported (Narayanasamy et al. 2010) that steels having a higher $n * \dot{\epsilon}$ value (product of the strain hardening exponent and the normal anisotropy) will have a higher hole expansion ratio value. Present results match with the previous studies (Narayanasamy et al. 2010). Due to relatively lower $\dot{\epsilon}$ values, the HER in FR2 samples is closer to AR samples. However, a lower value of Δr is expected to be the reason for lower HER variation in ferritic rolled samples and especially in low temperature rolled FR2 samples. The ferritic rolled samples can be used for stretch flanging application replacing the austenitic rolled samples and can have superior properties if the rolling temperatures are maintained in the upper ferritic band.


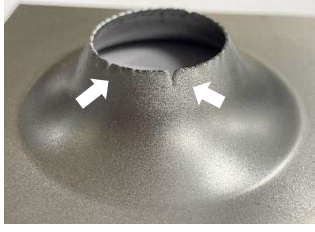
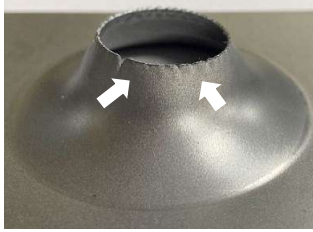
		
138 ($\pm 4.5\%$)	148 ($\pm 3\%$)	142 ($\pm 2.5\%$)
AR	FR1	FR2

Fig. 7.25. Comparison of HER for austenitic and ferritic rolled sheets

Earing behaviour is normally very low in IF steels but it is an important test to determine the difference in ear height due to the textural differences in austenitic and ferritic rolled samples. Four major ears were observed in all the tested samples, but the ferritic rolled samples show lower earring compared with the austenitic rolled samples. Austenitic rolled samples have the relatively irregular position of ears with skewed cup heights which can result from a higher amount of alpha fibre in the samples. The earring in the samples after the test is shown in Fig. 7.26. along with the average earring values. The height and positions of the ears relative to the rolling direction are reported to be dependent on the planar anisotropy. Hence FR2 samples with the lowest planar anisotropy (Δr), has the smallest ears (Liao et al 2018). The key difference is in the position of the ears. AR samples due to higher alpha fibres at specifically $112\langle 110\rangle$ show ears at 30° . FR1 samples with gamma fibre at $111\langle 121\rangle$ shows ears at close to 45° to the rolling direction. FR2 samples with gamma fibre at $111\langle 112\rangle$ and $554\langle 225\rangle$ shows ears at 60° w.r.t concerning rolling directions. Low ears and its formation at 45° to the rolling direction in FR1 sample is the most favourable condition.

		
10.2	8.9	8.1
AR	FR1	FR2

Fig. 7.26. Comparison of ear formation and average earing values for austenitic and ferritic rolled sheets

Erichsen cupping tested samples were sectioned along the specimen central axis passing through the crack as shown in Fig. 7.27. The variation in the thickness profile along the axis was measured using image analysis software in the opto-digital microscope. The morphologies and thickness variation of the bulged samples and the Erichsen index values are shown in Fig. 7.28. All the samples show crescent shaped crack around the central dome up to a certain arc length parallel to the rolling direction. But the length of the crack and the thinning at the opposite end are different. The thickness of the stretched sheet at different locations was measured and compared as shown in Fig. 7.28. The difference in dome height and thickness along the central line shows the variation in formability with the crystallographic orientation in differently processed materials.

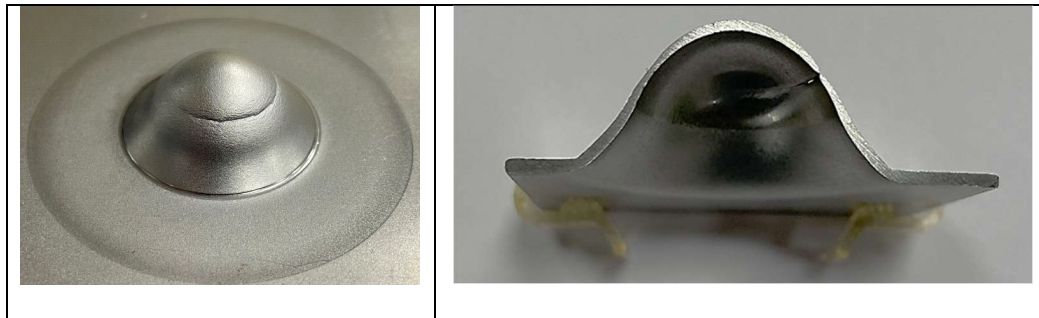


Fig. 7.27. Specimen after the cupping test

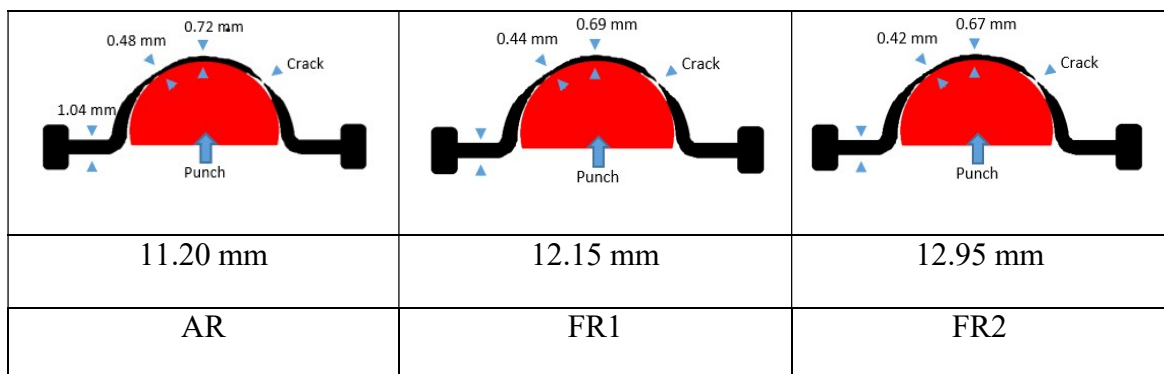


Fig. 7.28. Comparison of thickness variation after the test and Erichsen number values for austenitic and ferritic rolled sheets

It is found that FR1 and FR2 samples show higher Erichsen cupping index and lower final thickness compared to AR samples indicating higher stretch forming capability in ferritic rolled samples. The cup height increase could be correlated to higher strain hardening exponent in ferritic rolled

samples. Higher limits of major strain in the tension-tension region of FLD curve for FR2 samples results in relatively better formability in this test compared to FR1 sample. This is due to the delayed necking with higher strain hardening exponent values. Ferritic rolled samples are more formable for cupping type deformation applications with property improving with reducing rolling temperature.

Limitations of reduction to thin sheets and requirement of surface finish, restrict the direct use of hot-rolled coils processed under ferritic conditions. However, ferritic hot-rolled coils could be cold-rolled and annealed for having improved formability characteristics and could be implemented as industrial practice with no additional facilities. The present studies show that Nb-Ti IF grade ferritic rolled coils after cold rolling and annealing develop better elongation and strain hardening, exponent. A higher proportion of gamma fibre texture of $111\langle 121 \rangle$ gives better formability limits in the formability limit diagram. Present studies show that maintaining a higher ferritic rolling temperature gives better formability in hole expansion and earing tests. Industrial adaption of this ferritic hot rolling followed by cold rolling and annealing will give savings from reduced temperature and increases applications due to improved formability limits.

Austenitic rolling of IF steels is widely practiced in the steel industry. It has inherent issues of shape defects and lower yields. Recently, soft hot strip and hard hot strip produced through ferritic rolling are projected as a direct replacement to austenitic cold rolled sheets for many forming applications. However, existing industrial hot rolling mills, with higher final rolling thickness limitations cannot produce these thinner products. These products also have large property variations and reduced formability. Hence this process is not widely accepted. In the present work an intermediate process has been developed for producing high formability IF steels involving ferritic hot rolling and subsequent optimized cold rolling and annealing. The steel sheets developed through this new route can be produced in all the existing mills without any modifications, develops uniform properties all along the sheet, thereby increasing the yield, have better properties for all formability applications and lower cost due to reduced energy consumption. The temperature reduction of 150 °C in reheating furnace and 30 °C in annealing furnace gives 12-15 % energy savings in overall process compared to high temperature process being practised in austenitic rolling route. Developed IF steels can be used in the elements of the body structure and closures. It can also be an affordable material for deep drawing operations. It can be utilized for broad applications ranging from automotive body to electronic components as well as from enamel wares to house hold appliances.

CHAPTER 8

CONCLUSIONS

1. Nb-Ti stabilized IF grade steel was hot rolled in an industrial hot rolling mill at two different temperatures in the ferritic regime and subsequently cold-rolled and annealed, through offline optimization of parameters at each stage. Development of properties, microstructure and texture has been studied at each stage and compared with austenitic rolled IF grade steel. The annealed sheets were evaluated for different formability characteristics compared with austenitic regime rolled sheets which help in the application specific selection of this material. The work demonstrated that it is possible to industrially produce ferritic rolled IF grade steel sheets, with improved formability in an existing hot rolling and cold rolling line with no additional installations. The key conclusions at each stage of processing are enlisted below.
2. Hot rolling simulation and plant trials
 - i. Gleeble simulation of ferritic rolling (A_{r1} temperature varies between 875 – 851 °C) shows that flow stress of the steel decreases first and then increases as the rolling temperature is lowered below 700 °C. The strain hardening effect is more pronounced in the deformations carried in the ferritic region compared to the austenitic region for the same value of strain and strain rate which increased its hardness.
 - ii. Simulation samples show relatively more uniform microstructure at high temperature ferritic rolling (850 °C - 800 °C) and relatively heterogeneous microstructure with duplex grains and higher amount of low angle grain boundaries at low temperature rolling (< 800 °C). High temperature ferritic rolling transformed in to desired gamma and alpha fibres but unwanted cube, goss and brass textures increased at low temperature ferritic rolling.
 - iii. Deformation temperatures of 850 °C to 800 °C was found to be a most suitable working window for an industrial ferritic rolling process having reduced load requirement to achieve favourable grain morphology, texture and final mechanical properties.
 - iv. Based on simulation studies, industrial ferritic rolling was carried out in a seven stand hot strip mill under a ferritic regime at two different

temperatures. No increase in rolling load or shape variation has been found in the low temperature ferritic rolling.

- v. The ferrite rolled coils exhibits a strained microstructure, higher strength and lower elongation but with a desirable rolling texture having increased alpha fibre ($\langle 110 \rangle // RD$) and gamma fibre ($\langle 111 \rangle // ND$).
- vi. Variation of properties along the length was found to be greater in austenitic rolled samples, whereas variation along the thickness is greater in low temperature ferritic rolled samples. The variation in properties increased with decreasing the temperatures.
- vii. For non-lubricated ferritic industrial rolling, a finishing temperature of 840 °C and a coiling temperature of 640 °C is most suitable for achieving uniform properties and favourable initial texture for subsequent cold rolling and annealing.

3. Cold rolling and annealing simulations and plant trials

- i. Cold rolling was carried out at 75 % reduction in an industrial cold rolling mill and annealing simulation was carried out using the cold-rolled sheet samples in a Gleeble thermomechanical simulator to optimize the temperatures.
- ii. Annealing simulation shows that temperatures above 780 °C results in improved elongation and uniform microstructure. Based on the simulation results annealing was carried out for both the ferritic rolled coils in an industrial continuous annealing line in the temperature band of 780 – 800 °C.
- iii. In the plant annealed samples, the yield strength and tensile strength of both the ferritic rolled coils were similar to conventional austenitic hot rolling coils but has developed higher elongation. Compared to conventional austenitic hot rolled coils average anisotropy (\bar{r}) increased in high temperature ferritic rolled coils and decreased in low temperature ferritic rolled coils. Δr , the planar anisotropy reduced in both the ferritic samples and was very low in low temperature ferritic rolled coils. The strain hardening exponent (n -value) of both the ferritic rolled samples improved in comparison to austenitic rolled samples.

- iv. Both the ferritic rolled samples show recrystallized microstructure with rounded grains whereas the austenitic rolled samples show marginally bigger and polygonal morphology of the grains
- v. High temperature ferritic rolled coils shows sharper texture with predominantly gamma fibre texture distributed all along $\langle 111 \rangle // ND$ with maxima at $111 \langle 121 \rangle$. Low temperature ferritic rolled coils show nonuniform distribution of gamma fibre and alpha fibre textures with a gamma fibre maxima at $111 \langle 112 \rangle$. Austenitic rolled samples after annealing show the combination of gamma, alpha fibre and cube texture which makes it less formable. The variation in the final texture is due to the difference in the initial hot-rolled sheet texture and its evolution in subsequent processing steps.
- vi. There is a gradual transition of recrystallization mechanism from oriented nucleation to oriented growth as the temperature of deformation in the ferritic region decreases.

4. Formability studies

- i. Nb-Ti stabilized IF grade steel sheets show improved formability characteristics when rolled under ferritic regime compared to austenitic rolled sheets after cold rolling and annealing. However, the variation in formability behaviour was observed with a change in ferritic rolling temperature.
- ii. High temperature ferritic rolled sheets show higher forming limits for deep drawing applications and low temperature ferritic rolled sheets show higher forming limits for stretching applications under FLD curve. In the deep drawing side major strain varies between 0.5 - 0.85 and 0.4 – 0.7 for high temperature and low temperature ferritic rolled sheets respectively. In the stretching side major strain varies between 0.4 - 0.6 and 0.4 – 0.7 for high temperature and low temperature ferritic rolled sheets respectively.
- iii. Hole expansion ratio and average earing values are better for high temperature rolled sheets but the Erichsen cupping index is higher for low temperature ferritic rolled sheets.

- iv. The better formability characteristics of ferritic rolled sheets is due to higher elongation, higher strain hardening exponent, and pronounced gamma fibre texture of 111<121> component.
- v. The unique formability behaviour of low temperature ferritic rolled sheets is due to lower Δr , transformation to gamma fibre component at 111 <112> and relatively higher amount of alpha fibre component.
- vi. IF grade ferritic rolled steels are good low-cost replacement for austenitic rolled sheets in all forming applications. Considering benefits at different stages an approximate energy saving, can be in the range of 12 – 15 %.

LIST OF PUBLICATIONS

1. Satish Kumar D., Manjini Sambandam, Udaya Bhat K. (2020), “Development of an industrial ferritic rolling process for IF grade steel” *Ironmaking and Steelmaking*, Volume 47, Issue 6, 632-639. doi.org/10.1080/03019233.2020.1793290.
2. Satish Kumar D., Manjini Sambandam, Udaya Bhat K. (2021), “Thermomechanical Simulation of Ferritic Rolling Process”, *Materials Performance and Characterization* Vol. 10, No. 1. [doi:10.1520/MPC20210040](https://doi.org/10.1520/MPC20210040).
3. Satish Kumar D., Manjini Sambandam, Udaya Bhat K. “Optimization of Annealing Parameters for Ferritic Hot Rolled IF Grade Steel” *Metallography, Microstructure, and Analysis*, Issue 1/2022, [doi: 10.1007/s13632-022-00821-6](https://doi.org/10.1007/s13632-022-00821-6)
4. Satish Kumar D., Manjini Sambandam, Udaya Bhat K. “Formability Behaviour of Ferritic and Austenitic Rolled Nb-Ti Stabilized IF Grade Steel” *Metallurgical and Materials Engineering*, (under review).

REFERENCES

Adrienn Hlavacs, Mate Szucs, Valeria Mertinger, Marton Benke, (2021). “Prediction of Earing of Hot-Rolled Al Sheets from Pole Figures”, *Metals*, Vol 11, 99, 1-9.

Ahmad Ejaz, F Karim, K Saeed, Tanvir Manzoor, G H Zahid, (2014). “Effect of cold rolling and annealing on the grain refinement of low alloy steel”, *Materials Science and Engineering*, 60, 1-10.

Ahmed El-Kawas, Sabbah Ataia, Samir Ibrahim, (2017). “Industrial Production of Fine Grained Ferrite in Low-Carbon Steel”, *Journal of Petroleum and Mining Engineering*, Vol 19(1), 18-17

Allan Cramb, (2003). “Casting Volume” *The Making, Shaping and Treating of Steel*, 11th Edition, The AISE Steel Foundation, Pittsburgh.

Andreas, Tomitz and Radko, Kaspar (2000). “Deep drawable Thin-gauge Hot Strip of Steel as a Substitution for Cold Strip” *ISIJ International*, Vol. 40, No. 9, 927–931.

Andreas, Tomitz and Radko, Kaspar (2000). “Ferritic rolling to produce soft deep drawable thin hot strips” *Steel Research*, Volume 71, Issue 6-7, June, 233–238.

Andres C. G., Caballero F.G., Capdevila C., (2002). “Application of dilatometric analysis to the study of solid–solid phase transformations in steels” *Journal of Materials characterization*, 48, 101–111.

Animesh, T., Vinit, R.C., Kapish, M., Mukul, V., Athar, J., Mohit, K.S. (2013). “Formability Characteristics of Different Sheet Metals by Erichsen Cupping Testing with NDT Methods” *Journal on Material Science*, 1, 14-18.

Arbind Akela, Latchupatni Naidu, MarutiramKaza, Ashish Chandra and Prabhat Kumar Ghorui, (2016). “Study of earing defects in auto grade steel sheets based on anisotropic properties”, *Conference: AISP’ May 16*, Rourkela Steel Plant (RSP), Rourkela, 48 – 54.

Asensio, J., Romano, G., Martinez, V.J., Verdeja, J. I. and Pero-Sanz, J.A. (2001). “Ferritic steels - Optimization of hot-rolled textures through cold rolling and annealing” *Materials Characterization*, 47, 119 – 127.

Ashish Panda K. Mohapatra, J. N., Murugaiyan Premkumar, Roy Rajat K, Mitra Amitava, (2020). “Impact of Pre-formed Martensite on the Electromagnetic Properties and Martensitic Transformation Kinetics of Uniaxially Tensile Loaded 304 Stainless Steel”, *Journal of Materials Engineering and Performance*, Volume 29, Issue 11, 7141-7152

ASM Handbook, (2000). “Mechanical Testing and Evaluation”, Volume 8, Metals Park, Ohio: ASM International, USA

ASM Handbook, (2019). “Materials Characterization”, Volume 10, Metals Park, Ohio: ASM International, USA

Aust K.T. and J.W. Rutter, (1960). “Annealing twins and coincidence site boundaries in high-purity lead”, *Trans. of AIME*, 218, 1023-28.

Bunge, H. J. (1969). “Mathematische Methoden der Texturalanalyse” *Akademik-Verlag, Berlin*.

Barrett, C. J. and Wilshire, B. (2002). “The production of ferritically hot rolled interstitial-free steel on a modern hot strip mill.” *Journal of Materials Processing Technology*, 122, 56–62.

Barrett, C. J. (1999). “Influence of lubrication on through thickness texture of ferritically hot rolled interstitial-free steel”. *Ironmaking and Steelmaking*, 26(5), 393-397.

Barnett M. R. and Jonas J. J., (1999). “Distinctive aspects of the physical metallurgy of warm rolling” *ISIJ International*, Vol 39, No 9, 856 -873.

Barnett, M., R., Jonas. J., J. (1997). “Influence of ferrite rolling temperature on grain size and texture in annealed low C and IF steels” *ISIJ International*, Vol 37, 706 -714

Behrens B-A, D Rosenbusch, H Wester and M Dykiert, (2021). “Comparison of different testing approaches to describe the fracture behaviour of AHSS sheets using experimental and numerical investigations”, *40th International Deep-Drawing Research Group Conference (IDDRG 2021)*, June 21-July 2, Stuttgart Germany, 1157 -1167.

Chang Wengao, Wei Yu, Huan Yang, Zengqiang Man, Yunfei Cao, (2020). “Effect of Ferritic Hot Rolling Process on Microstructure and Properties of IF Steel” *Materials Science Forum*, Vol. 993, 505-512

Chen Ji-ping, Kang Yong-lin, Hao Ying-min, Guang-ming Liu, Ai-ming Xiong. (2009). “Experimental Study on Ti+ Nb Bearing Ultra-Low Carbon Bake Hardening Sheet Steel Hot-Rolled in the Ferrite Region”, *International Journal of Minerals, Metallurgy and Materials*, 16(5), 540 – 548.

Chuang Ren, Wenjiao Dan, Yongsheng Xu, Weigang Zhang, (2018). “Effects of Heterogeneous Microstructures on the Strain Hardening Behaviours of Ferrite-Martensite Dual Phase Steel”, *Metals*, 8, 824, 1-13.

Cizek P, B. P. Wyne (1997). “A mechanism of ferrite softening in a duplex stainless steel deformed in hot torsion”, *Materials Science and Engineering: A*, Volume 230, Issues 1–2, 1 July, 88-94.

Costa Viana, C. S. DA., Matheus, J. R. G., Lopes, A. M. and AlyelSharawy, H. H. (2000). “Microstructure and Texture of a warmed rolled IF steel”, *Textures and Microstructures*, Vol. 34, 243-253.

Daniella Gomes Rodrigues, Cláudio Moreira de Alcântara, Tarcísio Reis de Oliveira, Berenice Mendonc, Gonzalez, (2019). “The effect of grain size and initial texture on microstructure, texture, and formability of Nb stabilized ferritic stainless steel manufactured by two-step cold rolling”, *Journal of Material Research Technology*, Vol 8(5), 4151 – 4162.

David, H. Wakelin (1999), “Ironmaking Volume” *The Making, Shaping and Treating of Steel*. 11th Edition, The AISE Steel Foundation, Pittsburgh.

Dillamore, I. L. and Roberts, W.T. (1965). “Preferred orientations in wrought and annealed metals” *Metallurgical Reviews*, Vol 10, 271.

Duggan, B. J., Tse, Y. Y., Lam, G. and Quadir, M. Z. (2011). “Deformation and recrystallization of Interstitial Free (IF) Steel”, *Materials and Manufacturing Processes*, Vol 26, 51–57.

Dipak Mazumdar, (2015). First course in iron and steel making, University Press, India.

Elaheh Ghassemieh, (2011). “Materials in Automotive Application, State of the Art and Prospects” *New Trends and Developments in Automotive Industry*, InTechopen London

Elsner, A., Kaspar, R., Ponge, D., Raabe, D. and Van der Zwaag, S. (2004). “Recrystallization Texture of Cold Rolled and Annealed IF Steel Produced from Ferritic Rolled Hot Strip” *Materials Science Forum*, Vols. 467-470, 257-262.

Fang Xiaoying, Yin, Wenhong, Qin, Congxiang, Wang, Weiguo, Lo, K. H., Shek, C. H, (2016). “The interface character distribution of cold-rolled and annealed duplex stainless steel”, *Material Characterization*, June, 1-29.

Fargas G., Akdut N., Anglada M., Mateo A., (2008). “Microstructural Evolution during Industrial Rolling of a Duplex Stainless Steel”, *ISIJ International*, Vol. 48, No. 11, 1596–1602.

Fruehan, R. J. (1998). “Steelmaking and Refining Volume” *The Making, Shaping and Treating of Steel*. 11th Edition, The AISE Steel Foundation, Pittsburgh.

Felker Caleb A., John. G. Speer, Emmanuel De Moor, Kip O. Findley, (2020). “Hot Strip Mill Processing Simulations on a Ti-Mo Microalloyed Steel Using Hot Torsion Testing”, *Metals*, Vol 10, 334, 1-19.

Gangali Peter, John J Jonas, Toshiaki Urabe, (1995). “A Combined Model of Oriented Growth for the Recrystallization Nucleation and Selective of Interstitial-Free Steels”, *Metallurgical and Materials Transactions A*, Vol 26A, Sept, 2399 -2406.

García-Sesma Leire, Beatriz López, Beatriz Pereda, (2020). “Effect of High Ti Contents on Austenite Microstructural Evolution During Hot Deformation in Low Carbon Nb microalloyed Steels”, *Metals*, 10, 165, 1-24.

Ghosh, P., Ghosh, C. and Ray, R. K. (2008). “Precipitation Behavior and Texture Formation at Different Stages of Processing in an Interstitial Free High Strength Steel” *Scripta Materialia*, 59, 276 -281.

Ghosh P, B. Bhattacharya, R.K. Ray. (2007), “Comparative study of precipitation behavior and texture formation in cold rolled-batch annealed and cold rolled-continuous annealed interstitial free high strength steels” *Scripta Materialia*, 56, 657 - 660.

Gatelier C-Rothea, J. Chicois, R. Fougères, P. Fleischmann. (1998). “Characterization of pure iron and carbon-iron binary alloy by Barkhausen noise measurements: Study of the influence of stress and microstructure” *Acta Materialia*, 46(14).

Göktuğ Çınar. (2006). “Effects Of Anisotropy On Formability In Sheet Metal Forming”, M.Sc. Thesis, *Istanbul Technical University*, Institute of Science and Technology, June.

Großheim, H., Schotten, K. and Bleck, W. (1996). “Physical simulation of hot rolling in the ferrite range of steels” *Journal of Materials Processing Technology*, 60, 609 – 614.

Guang Xu, Chen Zhenye, Liu Li, Yu Shengfu. (2008). “Deformation Behaviour of Ultra-Low Carbon Steel in Ferrite Region during Warm Processing”, *Journal of Wuhan University of Technology-Mater*, Sci. Ed. Feb., 29-32.

Guo Yan-hui., Wang Zhao-dong, Zou Wen-wen, Liu Xiang-hua, Wang Guo-dong, (2008). “Textures and Properties of Hot Rolled High Strength Ti-IF Steels” *Journal of Iron and Steel Research International*, 15 (5), 70-76.

Guo, Yan-hui., Zhang Xing-yao. and Jing, Xiao-rong. (2014). “Evolution of Hot rolled Texture during Cold Rolling and Annealing in Ti-IF Steel”, *Advances in Materials Science and Engineering*, Vol. 1, No. 1, 19-25.

Hai-liang Yu, Kiet Tieu, Cheng Lu, Guan-yu Deng, Xiang-hua Liu, (2013). “Occurrence of surface defects on strips during hot rolling process by FEM”, *International Journal of Advanced Manufacturing Technology*, 67, 1161–1170.

Hao Lei-lei., Lang Li, Chen-yang Qiu, Jian-gong Wang, Xun Zhou, Yong-lin Kang, (2019). “Texture development and properties of Ti-IF steels produced by different hot-rolling processes” *Journal of Iron and Steel Research International*, Vol 26, 310–320.

Hashimoto O., Satoh S., Irie T., Ohashi. N., (1982). “Ultra-low c-nb-p steel sheet with high strength and excellent deep drawability” *Proceedings of an International Conference on Advances in the Physical Metallurgy and Applications of Steels*, Liverpool, England, 95–104.

Harlet, Ph., Beco, F., Cantineaux, P., Bouquegneau, D., Messien, P. and Herman, J. C. (1993). “New Soft Steel Grades Produced by Ferritic Rolling at Cockerill Sambre” *Int. Symposium on Low-Carbon Steels for the 90's, The Minerals, Metals and Materials Society, Pittsburgh, USA* 389–396.

Held, F. J. (1965). *Mechanical Working and Steel Processing Conference, ISS, Warrendale, PA*, 3.

Helong, Cai., Junsheng, Mou. and Ziyong, Hou. (2015). “Microstructure, Texture and Property of Interstitial-Free (IF) Steel after Ultra-fast Annealing”, *Advanced Materials Research*, Vols.

1120-1121, 1003-

1007.

Herman, J.C., Cantineaux, P. and Langlais, J. M. (1992). “Future Prospects of Ferritic Hot- Rolled Thin Strip Steel: A new "Low Cost" approach for steel sheet production” *Steel World*, February, 48–54.

Hoile S. (2000). “Processing and properties of mild interstitial free steels - A Review” *Materials Science and Technology*, Vol 16, 1079-1093.

Huang C., E. B. Hawbolt, X. Cen, T. R. Medowcraft, D. K. Matlock, (2001). “Flow stress modelling and warm rolling simulation behaviour of two Ti-Nb Interstitial free steels in ferrite region”, *Acta mater.* 49 1445–1452.

Hurley, P. J., Hodgson, P. D. (2001). “Effect of process variables on formation of dynamic strain induced ultrafine ferrite during hot torsion testing”, *Materials Science and Technology*, 17(11), 1360–1368.

Hutchinson, B. (1994). “Practical aspects of texture control in low carbon steels”, *Material Science Forum*, 157–162, 1917–1928.

Jae Hyung Kim, Young Jin Kwon, Taekyung Lee, Kee-Ahn Lee, Hyoung Seop Kim, and Chong Soo Lee (2018). “Prediction of Hole Expansion Ratio for Various Steel Sheets Based on Uniaxial Tensile Properties”, *Metallurgical and materials International*, Vol. 24, No. 1, 187 – 194.

Jonas. J.J, (1998). “Modern LC and ULC Sheet Steels for Cold Forming: Processing and Properties”, Int. Symp. On forming of steels, Aachen, March, 73-84.

Katerina Rubešová, Martin Rund, Sylwia Rzepa , Hana Jirková, Štěpán Jeníček, Miroslav Urbánek, Ludmila Kučerová, Pavel Konopík, (2021). “Determining Forming Limit Diagrams Using Sub-Sized Specimen Geometry and Comparing FLD Evaluation Methods”, *Metals*, 11, 484, 1-11.

Katoh, H., Takechi, H., Takahashi, N. and Abe, M. (1985). “Technology of continuously annealed cold-rolled sheet steel” (ed. R. Pradhan), *Warrendale, PA, AIME*, 37-60.

Kiet Tieu A, Hongtao Zhu, Qiang Zhu (2013). “Effects of Lubrication in Ferrite Rolling

of Interstitial Free Steel”, *Materials Science Forum*, November, Volumes 773-774, 186-191.

Kim Y.I., J.H. Kim, Y. Kim, M.Y. Lee, Y.H. Moon, D. Kim (2011). “Formability evaluation of tailor-welded blanks of boron steel sheets by Erichsen cupping test at elevated temperature”, *Transactions of Materials Processing*, 20, 568 - 574.

Kino, N., Yamada, M., Tokunaga, Y. and Tsuchiya, H. (1990). “Metallurgy of vacuum degassed steel products” (ed. R. Pradhan), *Warrendale, PA, TMS*, 197-214.

Kolupaeva S, M Semenov, (2014). “The stored energy of plastic deformation in crystals of face-centered cubic metals”, *Materials Science and Engineering*, 71, 1-7.

Kohsaku Ushioda, (2020). “Advances in research on deformation and recrystallization for the development of high-functional steels”, *Science and Technology of Advanced Materials*, Vol. 21, No. 1, 29–42.

Kong Ning, Kiet Tieu , Hongtao Zhu, Qiang Zhu, Peter Gandy, (2014). “Effects of Lubrication in Ferrite Rolling of Interstitial Free Steel”, *Materials Science Forum*, Vol 773-774, 186-191.

Langner, H. and Bleck, W. (1998). “Fundamentals of Softening Processes during Ferrite Hot Rolling” *Proceedings of 40th MWSP Conference*, ISS, Warrendale, V.35, .345 – 349.

Lankford, W. T., Snyder, S. C. and Bauscher, J. A. (1950). “New Criteria for Predicting the Press Performance of Deep Drawing Sheets” *Trans. ASM* 42, 1197–1232.

Leilei Li, Zhen Cai, Shuize Wang, Huibin Wu, Yuhui Feng, Yongqian Liu, Xinping Mao (2021). “Texture Evolution with Different Rolling Parameters of Ferritic Rolled IF Steel”, *Metals* 2021, 11(9), 1341 – 1352.

Liao Lu-hai, Xiao-fei Zheng, Yong-lin Kang, Wei Liu, Yan Yan, and Zhi-ying Mo.

(2018). “Crystallographic texture and earing behaviour analysis for different second cold reductions of double-reduction tinplate”, *International Journal of Minerals, Metallurgy and Materials*, Volume 25, Number 6, 652 – 662.

LifengLV, Liming, Fu., Sohail, Ahmad., Aidang, Shan. (2017). “Effect of heavy warm rolling on microstructures and mechanical properties of AISI 4140 steel” *Materials Science & Engineering A*, 704, 469 – 479.

Llewellyn, D. T. and Hudd, R. C. (1998). “Steels. metallurgy and applications” *3rd edn*, *Butterworth-Heinemann*, London 39.

Lokendra Kumar, Shrabani Majumdar, Raj Kumar Sahu, (2017). “Measurement of the Residual Stress in Hot Rolled Strip using Strain Gauge Method”, *AIP Conference Proceedings*, July, 1-5.

Longfei Li, Yang Wangyue, Sun Zuqing, (2006). “Dynamic Recrystallization of Ferrite in a Low-Carbon Steel”, *Metallurgical and Materials Transactions A*, Vol 37A, March, 609 – 619.

Loveday M.S., G.J. Mahon, B. Roebuck, A.J. Lacey, E.J. Palmiere, C.M. Sellars and M.R. van der Winden (2006). “Measurement of flow stress in hot plane strain compression tests” *Materials at High Temperatures*, 23(2), 85-118.

Magnusson, H. Juul Jensen, D. and Hutchinson, B. (2001). “Growth Rates for Different Texture Components During Recrystallization of IF Steels” *Scripta Materialia*, 44(3), 435–441.

Majumdar, Shrabani, (2011). “Formability limit diagram of high strength steel sheet (DP 590)” *International Journal of Mechanical Engineering*, Aug 2011, Vol 1, No 2, 114-118.

Manabu, T. (2015). “Sheet Steel Technology for the Last 100 Years: Progress in Sheet Steels in Hand with the Automotive Industry” *ISIJ International*, Vol. 55, No. 1, 79–88.

Messien, P. and Herman, J. C. (1993). “r-Value improvement of steel using hot rolling lubrication” *Int. Symposium on Low-Carbon Steels for the 90's*, The Minerals, Metals and Materials Society, Pittsburgh, USA, 383-388.

Miklós Tisza. (2020) “Development of Lightweight Steels for Automotive Applications”, *Engineering Steels and High Entropy-Alloys*, InTechopen London

Millitzer M., E.B. Hawbolt and T.R. Meadowcroft. (2000). “Microstructural Model for Hot Strip Rolling of High Strength Low-Alloy Steels”, *Metallurgical and Materials Transactions A*, Volume 31A, 1247 – 1259.

Mohrbacher, Hardy. (2007). “Niobium microalloyed automotive steels – Higher strength and better functionality” *International Conference on Microalloyed Steels: Emerging technologies and applications*, Kolkata, India, 9-11 March.

Nakazima, K., Kikuuma, T., Hasuka, K. (1968). “Study on the formability of steel sheets” *Yawata technical report no.264*. 41–154.

Narayanasamy, R., Sathiya Narayanan C. (2005). “Forming limit diagram for interstitial free steels: part I. Material Science Engineering A”, 399(1), 292–307.

Narayanasamy R., C. Sathiya Narayanan. (2006). “Forming limit diagram for Indian interstitial free steels” *Materials and Design*, Vol 27, 882–899.

Narayanasamy, R., Sathiya, Narayanan, C., Palani, Padmanabhan., Venugopalan, T. (2010). “Effect of mechanical and fractographic properties on hole expandability of various automobile steels during hole expansion test”. *International Journal of Advanced Manufacturing Technology*. 47, 365–380.

Nourani Mohamadreza, Hossein Aliverdilu, Hossein Monajati Zadeh, Hamid Khorsand, Ali Shokuhfar, Abbas S Milani, (2010). “A Study on the Formability of IF and Plain Carbon Mild Steels”, *ASME 2010 International Design Engineering Technical Conference & Computers and Information in Engineering Conference*, August 15-18,

Montreal, Quebec, Canada, 1-8.

Okuda, Kaneharu. and Seto, Kazuhiro. (2013). “Recrystallization Behaviour of IF Steel Sheets

Immediately after Hot-rolling in Ferrite Region” *ISIJ International*, Vol. 53, No. 1, 152–159.

Oliferuk W, Maj M (2009). “Stress-strain curve and stored energy during uniaxial deformation of polycrystals”, *European J. of Mechanics A/Solids*, Vol 28, 266–272.

Paepet, A. de, Herman, J.C. and Leroy, V. (1997). “Deep drawable ultra low carbon Ti IF steels hot rolled in the ferrite region” *Steel Research*, 68(11), 479–486.

Paepe, A De., Autesserre, P., Vasseur, E., (2002). “Development of optimal rolling schedules for ferritic rolling, European Commission, Directorate-General for Research and Innovation”, Final report, Publications Office, Luxembourg.

Pan, Y., Lenard, J. G., (1994). “Dynamic recovery in Nb-Ti IF steels during hot and warm rolling”, *Steel Research*, 65(6), 248-253.

Parakka A P, David Jiles, H. Gupta, M. Zang. (1997). “Barkhausen effect in steels and its dependence on surface condition”, *Journal of Applied Physics*, 81(8), 5085-5086

Pawan, Kumar., Banerjee, M. K., Peter, Hodgson. and Amit, Roy Choudhary. (2016). “Warm working characterization of low carbon steel in hot rolling” *Materials Today: ICEMS 2016, Proceedings*, 4, 9505–9508.

Perera, M., Saimoto, S. and Boyd, D. (1991). “Interstitial free steel sheet. processing, fabrication and properties” (ed. L. E. Collins and D. L. Baragar), *Ottawa, CIM/ICM*, 55-64.

Pero-Sanz, J., Ruiz-Delgado, M., Martinez, V. and Verdeja, J. I. (1999). “Annealing Textures for Drawability: Influence of the Degree of Cold Rolling Reduction for Low-

Carbon and Extra Low-Carbon Ferritic Steels” *Materials Characterization*, 43, 303 – 309.

Poyraz Okan, Bilgehan Ogel, (2020). “Recrystallization, grain growth and austenite formation in cold rolled steels during inter-critical annealing”, *Journal of Materials Research and Technology*, Vol 9, Issue 5, Sept –Oct, 11263 – 11277.

Prasad Y V R K and Ravichandran N, (1991). “Effect of stacking fault energy on the dynamic recrystallization during hot working of FCC metals: A study using processing maps”, *Bull. Mater. Sci.*, Vol 14, No. 5, October, 1241-1248.

Priestner, R., Al-Horr, Y. M., Ibraheem, A. K. (2002). “Effect of strain on formation of ultrafine ferrite in surface of hot rolled microalloyed steel”, *Mater. Sci. Technol.* 18, 973–980.

Qiu Chen-Yang, Lang Li, Lei-lei Hao, Jian-gong Wang, Xun Zhou, Yong-lin Kang, (2018). “Effect of continuous annealing temperature on microstructure and properties of ferritic rolled interstitial-free steel”, *International Journal of Minerals, Metallurgy and Materials*, Volume 25, Number 5, 536 – 546.

Radko Kaspar, Andreas Tomitz, (2012), Metal-2012, 21st International Conference on Metallurgy and Materials, May 23 - 25, Hotel Voroněž I, Brno, Czech Republic.

Rajib Saha, R.K. Ray and D. Bhattacharjee. (2007). “Attaining deep drawability and non-earing properties in Ti + Nb interstitial-free steels through double cold rolling and annealing”, *Scripta Materialia*, 57, 257 - 260.

Ravi Kumar D. (2002). “Formability analysis of extra deep drawing steel” *J Material Process Technology*. 130, 31–41.

Ray, R. K. and Haldar, A. (2002). “Texture Development in Extra Low Carbon (ELC) and Interstitial Free (IF) Steels during Warm Rolling” *Materials and Manufacturing Process*, Vol.17, No. 5, 715–729.

Ray, R. K., Jonas, J. J. and Hook, R. E. (1994). “Cold rolling and annealing textures in low carbon and extra low carbon steels” *International materials reviews.*, 39, (4), 129-172.

Rees, DWA. (2001). “Factors influencing the FLD of automotive sheet metal” *Journal of Material Process Technology*, 118(1), 1–8.

Reddy A C S, Rajesham S, Reddy P R, and Uma Maheswar A C, (2019), “Formability: A Review on Different Sheet Metal Tests for Formability”, *International Conference on Multifunctional Materials (ICMM-2019)*, Hyderabad, India, 1 -10

Roberto, Gerardo Bruna. (2011). “Effects of hot and warm rolling on microstructure, texture and properties of low carbon steel” *Metallurgy and Materials*, 64(1), 57- 62.

Ronan Jacolot, Didier Huin, Artem Marmulev, Eliette Mathey, (2014). “Hot rolled coil property heterogeneities due to coil cooling: impact and Prediction”, *Key Engineering Materials*, September, 622 – 629

Saikat Kumar De., Anjana, Deva., Siddhartha, Mukhopadhyay., Bimal, Kumar, Jha. (2011). “Assessment of Formability of Hot-Rolled Steel through Determination of Hole-Expansion Ratio” *Materials and Manufacturing Processes*. 26, 37–42.

Sakai, T., Saito, Y. and Kato, K. (1988). “Texture formation in low carbon Ti-bearing steel sheets by high speed rolling in ferrite region” *Trans. ISIJ*, 28, 1036-1042.

Salunkhe Ujwala Sunil, K. Baba Pai (2014). “Investigation of formability of CRCA Steel sheet by Erichsen Cupping Test analysis” *IOSR Journal of Mechanical and Civil Engineering (IOSR-JMCE)*, Volume 11, Issue 2, 52 – 55.

Samarasekera I.V., D.Q. Jin and J.K. Brimacombe. (1997). “The Application of Microstructural Engineering to the Hot Rolling of Steel”, *38th Mechanical Working and*

Steel Processing Conference Proceedings, Vol. XXXIV, Iron and Steel Society, 313-327.

Sangkharat, T. Dechjarem, S. (2019). “Using image processing on Erichsen cup test machine to calculate anisotropic property of sheet metal”. *Procedia Manuf.* Vol 29, 390–397.

Sam K. Chang and Hee J. Kang, (1995). “Hot direct rolling in ferrite region in extra low-carbon steel”, *Steel research*, 66, No. 11, 463-470.

Sasahara, H. (2005). “The effect on fatigue life of residual stress and surface hardness resulting from different cutting conditions of 0.45%C steel”, *International Journal of Machine Tools and Manufacture*, 45, 131–136.

Sarkar B., Anjana Deva, S. Mukhopadhyay, B.K. Jha, D. Mukerjee, A.S. Mathur, (2010). “ Processing and Application of Interstitial Free (IF) Grade Steel: Prospects in SAIL”, *International Conference on Interstitial free Steels: Manufacturing and Applications, IF STEEL 2010*, Feb, Jamshedpur, India, 1-19.

Schey, J. A. (1992). “Formability determination for production control” *J Mater Process Technology*. 32, 207–221.

Sellars, C. M. (1986). “Modelling of structural evolution during hot working process” *Annealing processes-recovery, recrystallization and grain growth*. Rise National Laboratory, Roskilde, Denmark, 167-184.

Siciliano, F., Jonas, J.J. (2000). “Mathematical modeling of the hot strip rolling of microalloyed Nb, multiply-alloyed Cr-Mo, and plain C-Mn steels”, *Metall Mater Trans A* 31, 511–530.

Siciliano Fulvio, Samuel Filgueiras Rodrigues, Clodualdo Aranas Jr, John Joseph Jonas, (2020). “The dynamic Transformation of ferrite above Ar₃ and the consequences on hot rolling of steels”. *Technol. Metal. Mater. Miner.*, São Paulo, v. 17, n. 2, 90-95.

Song, Y. Q., Guan, Z. P., Ma, P. K., Song, J. W. (2006). “Theoretical and experimental standardization of strain hardening index in tensile deformation” *Acta Metallurgica Sinica*, 42, 673–680.

Sushant Rath, (2016). “Computer Simulation of Hot Rolling of Flat Products”, *Software Engineering*, 4(6), 75-81.

Tajally M., Emaddodin E., Fathallah Qods, (2011). “An experimental study on earing and planar anisotropy of low carbon steel sheets” *World Applied Sciences Journal*, 15(1), 1 – 4.

Tao, HanFu., Wang, Zuo-cheng. and Jing, Cai-nian. (2007). “Mechanical Properties and Microstructures of Ferritic-Rolled Ultra-Low Carbon (ULC) and Ti-Stabilized Interstitial-Free (Ti-IF) Steels”, *Key Engineering Materials*, 353-358.

Tetsuro Ohwue, Yoshikazu Kobayashi, (2014). “Analysis of earing in circular-shell deep-drawing of bcc and hcp sheet metals”, *Procedia Engineering*, 81, 887 – 892.

Tiitto K.M, Jung C., Wrav P., Garcia C.I., and Deardo A.J. (2004). “Evolution of Texture in Ferritically Hot Rolled Ti and Ti + Nb Alloyed ULC Steels during Cold Rolling and Annealing”, *ISIJ International*, 44, 404-413.

Tokunaga, Y, and Yamada, M., (1985). “Method for the production of cold rolled steel sheet having super deep drawability” US patent 4,504,326.

Toshio Irie, Susumu Satoh, Koichi Hashiguchi, Isao Takahashi, Osamu Hashimoto, (1981). “Metallurgical Factors Affecting the Formability of Cold-rolled High Strength Steel Sheets”, *Transactions ISIJ*, Vol 21, 693 – 801.

Tsunoyama, K., Sakata, K., Obara, T., Satoh, S., Hashiguchi, K. and Irie, T. (1988). “Hot and cold rolled sheet steels” (ed. R. Pradhan and G. Ludkovsky), *Warrendale, PA, TMS*, 155-165.

Vaish A.K. Humane M.M., P.K. De, Mahto B, Ravi Kumar B., (2003). “Effect of texture formation on formability of cold rolled and annealed extra deep drawing and interstitial free steel sheets”, *Journal of Metallurgy and Materials Science*, Vol. 45, No. 1, January-March, 1-10.

Vegas MI, Medina S. F., Chapa M, Ouispe A., (1999). “Determination of Critical Temperatures (T_{nr} Ar3 Ar1) in Hot Rolling of Structural Steels with Different Ti and N Contents”, *ISIJ International*, Vol. 39, No. 12, 1304-1310.

Vladimir B. Ginzburg, (2001), “Flat Products Volume” *The Making, Shaping and Treating of Steel*, 11th Edition, The AISE Steel Foundation, Pittsburgh.

Wang Fan, Peng Tian, Yonglin Kang, Jingtao Zhu, Zhe Qin, Liang Chen., (2019). “Simulation Experimental Study on Ferrite Rolling Process of Low-Carbon Steels” *Materials Science Forum*, Vol. 944, 329-336.

Wang, Z. D., Guo, Y. H., Sun, D.Q., Liu, X. H. and Wang, G. D. (2006). “Texture comparison of an ordinary IF steel and a high-strength IF steel under ferritic rolling and high-temperature coiling” *Materials Characterization*, 57, 402–407.

Wang, Zhao-dong., Guo, Yan Hui., Zhao, Zhong., Liu, Xiang-hua. and Wang, Guo-dong. (2006). “Effect of Processing Condition on Texture and Drawability of a Ferritic Rolled and Annealed Interstitial-Free Steel” *Journal of Iron and Steel Research, International*, 13(6), 66– 65.

Wilson, D.V. J. (1966). “Plastic anisotropy in sheet steels” *Journal of the Institute of Metals*, 94, 84 -88.

Wilshynsky, Dresler. D. O., Matlock, D. K. and Krauss, G. (1995). *ISS Mech. Work. Steel Process. Conf.*, Vol 33, 927-40.

World steel. (2011), “Steel in Automotive” <https://www.worldsteel.org/steel-by-topic/steel-markets/automotive.html>, (July 18, 2021).

World auto steel, Advanced High-Strength Steels Application Guidelines, Version 6.0, April 2017

Xinping Chen, Haoming Jiang, Zhenxiang Cui, Changwei Lian, Chao Lu, (2014). “Hole expansion characteristics of ultra-high strength steels, *Procedia Engineering*”, Vol 81, 718 – 723.

Yamada, T., Oda, M. and Akisue, O. (1995). “Effects of Properties Copper, Nickel, Chromium and Tin of Titanium-bearing Extra low-carbon on Mechanical Steel Sheets”, *ISIJ International*, 35, (11), 1422-1429.

Yazheng Liu, Xuewen Hu, Guoning He, Bo Jiang, Chaolei Zhang. (2019), “The deformation behavior of steel SPHC during ferrite rolling in CSP process” *Procedia Manufacturing*, Vol 29, 498–503.

Ye-Jin Yang, Jian-Xun Fu, Ren-Jie Zhao and Yan-Xin Wu. (2015). “Dilatometric Analysis of Phase Fractions during Austenite Decomposition in Pipeline Steel”, *3rd International Conference on Material, Mechanical and Manufacturing Engineering (IC3ME 2015)* Guangzhou, China, June 27-28.

Yong-hwan Cho, Jaeun Lee, Donguk Kim, Juseok Kang, Wung Yong Choo, Heung Nam Han, (2017). “Ferrite phase analysis based on low-angle grain boundary density in low carbon linepipe steel”, *Proceedings of the 5th International Symposium on Steel Science (ISSS 2017)* Nov. 13-16, 2017, Kyoto, Japan, 203 – 207.

Zerovnik P, Janez Grum, Zerovnik G. (2010). “Determination of Hardness and Residual-Stress Variations in Hardened Surface Layers With Magnetic Barkhausen Noise”, *IEEE Transactions on Magnetics*, April, 46(3), 899 – 904.

Zhao Hu., Pengfei Cheng, Xun Zhou, (2019). “Microstructure and Mechanical Properties of Ferritic Rolling Low Carbon Steel” *Materials Science Forum*, Vol. 944, 278-282.

Zhang Jian, Chen Deng-Fu, Hwang Weng-Sing, Han Ming-Rong, (2015). “The effects of heating/cooling rate on the phase transformations and thermal expansion coefficient of C–Mn as-cast steel at elevated temperatures”, *J. Mater. Res.*, Vol. 30, No. 13, 2081-2091.

Zhang Peng, Yan-hui Guo, Wang Zhao-dong, Wang Guo-dong, Liu Xiang-hua, (2010). “Texture Evolution in Ferritic Rolled Ti-IF Steel During Cold Rolling”, *Journal of Iron and Steel Research, International*, Volume 17, Issue 1, 44-48.

Zhao Lijia, Nokeun Park, Yanzhong Tian, Akinobu Shibata, Nobuhiro Tsuji, (2016). “Combination of dynamic transformation and dynamic recrystallization for realizing ultrafine-grained steels with superior mechanical properties”, *Nature, Sci. Rep.* 6, 39127, 1-11.

PUBLISHED
PAPERS



Development of an industrial ferritic rolling process for IF grade steel

D. Satish Kumar^a, Manjini Sambandam^a and Udaya Bhat^b

^aResearch and Development, JSW Steel Ltd, Vijayanagar Works, Bellary, India; ^bNational Institute of Technology Karnataka, Surathkal, India

ABSTRACT

Interstitial free (IF) grade steels have high transformation temperatures and often results in non-uniform rolling and lower yields. In the present work, industrial ferritic rolling process is developed, where finish rolling is carried out below the Ar₁ temperature for the IF grade steel. Offline simulation was carried out using a hot strip mill model (HSMM) software and full-scale ferritic rolling was carried out in a seven-stand hot strip mill under two different finishing and coiling temperatures and compared with austenitic rolling. Furnace drop-out temperature, mill speed and inter-stand cooling were controlled to achieve the desired low rolling temperatures. Both ferritic rolled coils had strained elongated grains and well-developed alpha (<110>//RD) and gamma (<111>//ND) textures. The lower finishing and coiling temperature processed coil shows higher microstructural and textural variation along with the thickness. This work established the optimum parameters for the industrial ferritic rolling process for IF grade steel.

ARTICLE HISTORY

Received 12 May 2020
Revised 30 June 2020
Accepted 1 July 2020

KEYWORDS

Ferritic rolling; hot strip mill model; IF steel

Introduction

Interstitial free (IF) steels are ultra-low carbon automotive steels used for outer body applications and are texture sensitive. These grades have rolling issues when rolled in the austenitic region. Significant shape and property changes are observed when the temperature of some parts of the coil falls into its narrow transformation band. Recently, a new strategy of warm rolling or ferritic rolling [1–4] is extensively investigated to mitigate hot rolling defects and develop a cheap, soft and ductile hot rolled strip as a substitute for the conventional cold rolled and annealed strip. Many laboratory and pilot studies [3–5] have been conducted on the ferrite-region-rolling, and the results show that hot rolling in the ferrite region is feasible, and the finished materials have pronounced {111} < 110 > annealing texture and have good deep drawability, as required for this grade [6]. It has also gained interest as a means of cutting down costs due to lower temperature and extending the application range of hot rolled products. Ferritic rolling introduces the possibility of producing three different products [2] (i) Soft hot strip – thinner hot rolled coils for direct deep drawing applications, (ii) hard hot strip – thinner hot rolled coils for deep drawing applications after annealing and (iii) hard cold strips – thicker hot rolled coils for deep drawing applications after cold rolling and annealing. Studies [7–9] showed that the process of hot rolling in the ferrite region followed by recrystallisation annealing results in a much stronger γ -fibre texture (// ND) than the conventional austenite rolling process. Thicker ferritic rolled material after cold rolling and annealing achieves better formability [10]. Therefore, the optimisation of hot rolling process parameters for rolling IF steel in ferritic regime is of great interest to steel producers. However, in spite of several claimed benefits, ferritic rolling is not in wide practice in the industry as rolling in ferritic zone or lower temperatures possess many operational problems. Industrial production of thinner hot rolled coils (<1.5 mm) as a direct replacement of CR coils or after annealing is not

feasible from the angle of reduction ratio limitations in a hot strip mill and requirement of surface finish. It is also reported that higher reduction ferritic rolling requires higher mill power and rolling loads due to low-finish rolling temperatures. Some previous works [8,9] have claimed poor deep drawability properties caused by a detrimental shear structure formed during rolling at the final finishing stands. The results found in the literature for the mill loads and properties of ferritic rolled hot strips are diverse and not consistent even for similar steel grades [10]. This is due to the fact that the mill rolling parameters, such as re-heating furnace exit temperature, roughing reductions, roughing temperatures, finishing reductions, finishing entry and exit temperatures, run on table (ROT) cooling pattern and coiling temperatures, strongly influence the results obtained. Most of these previous studies have been done in a lab-scale rolling mill or in a simulator which does not simulate the end-to-end industrial rolling process taking all parameters into account. Moreover, due to practical strain limitations of a smaller sample size, the number of deformations was also limited in the published studies. Industrial rolling experiences different strain and stain rates in each stand in a particular sequence. The accumulated strain from the previous stands influences the microstructure development in subsequent stands and on the ROT. Also, the temperature difference between the head and the tail end in an industrially hot rolled coil results in the property variation along the length of the coil. This impact is lower in the fully austenitic region. Maximum allowed temperature difference between the head and the tail needs to be studied for ferritic rolling. Low-temperature rolling increases the friction between the roll and the steel surface and hence lubrication has also been reported as key parameter [11] in achieving better texture. Therefore, the ferritic rolling can only be developed for a particular mill configuration, only by plant trials, so as to achieve the targeted hot rolled properties and texture for subsequent cold rolling and annealing operations. In this work, full-scale low-temperature industrial hot rolling has been carried out for

Table 1. Elemental range of selected IF grade steel, wt-%.

C	Mn	Si	Al	S	P	Ti	Nb	B	N
0.001–0.003	0.15–0.18	0.006–0.0012	0.030–0.040	0.01 max	0.02 max	0.02–0.03	0.01–0.015	0.0003 max	0.004 max

an IF grade steel based on the hot strip mill model simulation, which establishes the process parameters for industrial ferrite rolling. The difference in mechanical properties, microstructure and texture was studied for ferritic and austenitic rolled samples. It is aimed to develop favourable ferritic rolled HR coil for subsequent cold rolling and annealing useful for deep drawing applications.

Offline simulation

The study has been carried out for an Nb–Ti stabilised IF grade steel. This grade is currently rolled in the hot strip mill in the austenitic region. It is a high formability grade steel and has low yield during conventional austenitic rolling due to surface defects associated with high temperature rolling. The chemical composition (wt-%) range of the selected grade is shown in Table 1.

wDevelopment of gamma fibre all along the coil in an HR coil is a function of temperature and rolling regime [8]. Hence, optimised finishing and coiling temperature need to be identified. During industrial rolling, there is also a wide variation in temperature (50–80°C) along the width and length of the coil, which leads to the deformation of the strip in the two-phase region particularly closer to the edge of the strip or at the tail end. For the design of the rolling temperature schedules, to keep the complete deformation in the ferrite region, the determination of the exact γ - α transformation temperatures, which are high in this grade, becomes very important. Upper transition temperature, Ar_3 and lower transition temperature, Ar_1 were measured using phase transformation measurement in a DSC (Differential Scanning Calorimetry) equipment. For simulation, the samples were collected from the transfer bar produced during the austenitic rolling at hot strip mill. From the thermal changes in the DSC curve, the Ar_3 and Ar_1 were found to be ~ 905 and $\sim 871^\circ\text{C}$, respectively, for the industrial cooling rates of $3\text{--}5^\circ\text{C s}^{-1}$ for the selected IF grade steel.

Direct plant trails are risky and costly and hence the proposed rolling schedules were studied and validated offline. Recently, such offline simulations are being carried out by many researchers [12,13] and steel companies are using commercial simulation packages, such as Hot Strip Mill Model (HSMM). The HSMM software can be used to effectively determine the optimum processing conditions to achieve the desired product properties in the hot rolling process. The HSMM model performs a series of calculations to simulate the physical process of rolling steel in a hot strip mill. In the model, the mechanical and thermodynamic processes are modelled based on the first principles and established rolling equations from the literature. In the present work, HSMM V6.5 is used to simulate the existing austenite rolling

process and the proposed ferritic rolling process. The objective of HSMM simulation is to study the effect of temperatures in the ferritic zone on the flow stress and final properties. The HSMM model was first configured for hot strip mill – 2 of JSW steel, Vijayanagar works, India, where the existing austenitic rolling is being carried out and ferritic rolling is proposed. The model is completely linked to simulate the processing of the steel slab from the reheating furnace dropout to the down coiler. Configuration process includes data input on the furnace area, roughing area (mills, edgers, sprays), heat retention area (coil box, panels), finishing area (mills, edgers, sprays), run out table and mill exit area. It also requires a specific set of coefficients to be used for the grade of steel being processed via a specific rolling mill schedule. Based on the inputs, model calculates the finishing and coiling temperatures and tracks the properties at the head, middle and tail points along the length of the coil. The model was first validated for the existing austenitic rolling of IF grade steel. The model predicted finishing temperature (FT), coiling temperature (CT) and the mechanical properties were found to be very close to the plant values and are shown in Table 2. It, therefore, confirms the accuracy of the configured model. The model was then run with the three different proposed ferritic rolling temperatures. It was found that by reducing the temperature in the model input, the model identifies the change in the microstructure from austenite to ferrite. It did not indicate any abnormal increase in the rolling loads or any abnormal change in the other process parameters for the first two conditions but showed warning on load increase at the lowest temperature (ferritic rolling – 3). The predicted properties of the ferritic rolled samples show increased yield strength (YS) and ultimate tensile strength (UTS) and decreased elongation with lowering the rolling temperatures as shown in Table 2. This increase is due to strain hardening in absence of recrystallisation and is in the expected range. The existing software simulates rolling feasibility and does not predict the texture, but the properties correlate to the development of deformed texture. This confirms that the proposed ferritic rolling regime can be applied in the existing mill under the ferritic rolling conditions 1 and 2 without any expected process issues if operated within these temperature limits.

Plant trials

The hot rolling is a complex process and the microstructure evolution during rolling is a function of static, dynamic and metadynamic recrystallisation and grain growth. These processes are interdependent and must be studied in an integrated manner to derive logical conclusions. Based on the

Table 2. Comparison of process parameters and properties from the HSMM model.

Condition	FT, °C	CT, °C	YS, MPa	UTS, MPa	% Elongation
Actual Austenitic Rolling Parameters	920	641	201	295	48.5
Model Output – Austenitic Rolling	930	649	210.5	299.4	46.9
Model Output – Ferritic Rolling –1 (FR1)	840	640	222	312.5	41.4
Model Output – Ferritic Rolling –2 (FR2)	800	600	245	329	35.1
Model Output – Ferritic Rolling –3 (FR3)	750	570	276	345	28.2

HSMM results, ferritic rolling-1 and ferritic rolling-2 regimes were considered for plant trials. For establishing the ferritic rolling, full-scale plant trials were conducted in a 2-Hi, 2 stand roughing and 7 stand finishing hot rolling mill. Two coils were rolled at two different target conditions, namely FR-1 (FT-840°C, CT-640°C) and FR-2 (FT-800°C, CT-600°C). The industrial trials started with a continuously cast 220 mm thick and 1470 mm wide IF grade slabs. Slabs were reheated in a gas-fired re-heating furnace for 160 min to achieve the drop out temperature of 1130°C. It was followed by descaling, two stand roughing and stand finishing to produce a HR coil of 4 mm thickness. Speed of the slab movement was kept lower at 60 mpm (metres per minute) to obtain lower ferritic temperatures. After furnace exit, slab was descaled and rolled in two stand reversing roughing mill with 3 passes in each stand. During industrial rolling, it is not feasible to significantly lower re-heating furnace temperatures to ferritic range and hence the furnace exit temperature was lowered by 100–150°C. This restricts the rolling temperatures and therefore the rough rolling is carried in austenite phase above A_{r3} and the slab is held thereafter to cool down through the two-phase region before it enters the finishing stands on the transfer table. The finish rolling is carried out in the ferrite phase below A_{r1} . The roughing mill exit thickness was maintained at about 44 mm and temperature at 930°C to ensure all roughing deformations being carried out, above A_{r3} temperature. The FR-1 and FR-2 transfer bars were then held and air cooled to 840°C and 800°C, respectively, before entering into finishing stands for ferritic rolling. The speeds were controlled to match the finishing entry temperatures. The intermediate bars were then rolled in seven passes to 4 mm thickness in the finishing mill. The actual finish rolling temperature achieved was 825°C and 780°C, marginally lower than the targeted values. The rolled coils were then cooled on the run-out table (ROT) and the coiling temperatures achieved were 625 and 575°C in FR-1 and FR-2, respectively. This shows that whole rolling has been carried in two temperature bands, FR1 at higher temperatures and FR2 at lower temperatures in the ferrite region. This helps in studying the effect of these critical rolling temperatures on the microstructure development. The cooling pattern was kept similar to the IF grade austenitic rolling. All the rolling data and the samples for a similar section austenitic rolling named as AR were also collected from the plant for detailed characterisation and process comparison. The comparison of process parameters for the austenitic and both the ferritic rolling coils in the hot strip mill is shown in Table 3.

No process abnormality or alarms were observed during the ferritic rolling. During each rolling pass, the strain is imparted to the material which causes an increase in dislocation density

Table 3. Comparison of key hot rolling parameters.

S. No	Parameters	AR	FR1	FR2
1	Re-heating furnace exit temperature, °C	1247	1130	1128
2	Roughing mill 1 Passes, Nos	3	3	3
3	Roughing mill 2 Passes, Nos	3	3	3
4	Roughing mill exit temperature, °C	1052	930	910
5	Roughing mill exit thickness, mm	44.1	44.6	44.5
6	No of finishing passes, Nos	7	7	7
7	Finishing mill entry temperature, °C	964	860	820
8	Finishing temperature, °C	920	825	780
9	Coiling temperature, °C	641	625	575
10	Final coil thickness, mm	4.1	4.05	4.05

Table 4. Comparison of rolling force in each stand (kN).

Stand	F1	F2	F3	F4	F5	F6	F7
AR	22,650	23,795	21,036	18,464	14,608	12,228	10,660
FR1	20,023	22,249	19,586	17,138	14,457	12,221	10,470
FR2	20,077	22,307	19,631	17,176	14,498	12,267	10,542

and consequently results in work hardening. But simultaneously static and dynamic recrystallisation also takes place. The finish rolling parameters also have a strong impact on the microstructure and texture evolution. As it is not possible to measure the microstructural differences of the coil between the stands, it is indirectly compared by measuring the change in the rolling force exerted in each stand. No significant change in rolling force in the finishing stands was observed between austenitic and ferritic rolling. Rolling forces in ferritic rolling were marginally lower than the austenitic rolling. Table 4 shows the comparison of rolling force (MPa) in each stand in the finishing mill. At the selected temperatures, the softening effect of phase transformation or ferrite phase is equal to the hardening effect due to a decrease in temperature and applied strain, which keeps the roll force or the deformation resistance close to austenitic rolling conditions. The shape of the fish tail was also normal and similar to the austenitic rolling hence did not affect the head and tail shear. Temperature difference between the head end and tail was ~50°C, marginally higher than the austenitic rolled coils, which is attributed to the slower speeds and resulting in a difference in physical properties.

Full-width samples were collected from both the head end and the tail end of the hot-rolled coil after cooling as shown in Figure 1. To map the variation of properties, samples were cut from the centre at both head and tail ends. The full-width sample was first subjected to residual stress measurement to quantify the relative difference of stresses between the selected areas. This is done on the as-received samples to avoid stress relieving due to cutting. After the residual stress measurement, from each full-width sample, the surface was marked for various testing from the similar locations as shown in Figure 2. Complete characterisation was carried out at two locations in each coil to map the variations in the properties. Customised samples were cut for tensile testing, hole expansion ratio, phase analysis and microscopy. Since the temperature difference between the head and tail is much higher than the centre and the width, the comparative analysis has been carried out between the head and the tail samples in all the coils.

Comparison of austenitic and ferritic rolled coils

The details of the various measurements on the samples collected from both austenitic and ferritic rolled IF steel hot rolled coils are discussed below. The residual stress variation in the surface layer is responsible for defects arising during cutting and uncoiling process and also effects formability



Figure 1. Sampling locations in the coil.

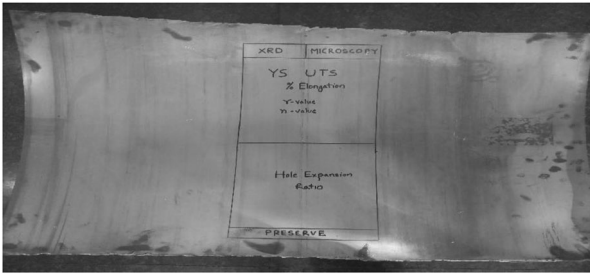


Figure 2. Markings for sample testing on HR coil.

and fatigue life [14]. Residual stress measurement was carried out on the head and the tail regions of coils. Magnetic Barkhausen Emission (MBE) measurements were carried out on top surfaces of the coils at a magnetising field of 40 kA/m by varying the frequency from 20 to 200 Hz with 20 Hz step. RMS voltage of the MBE is the indirect measure of the residual stress in the steel sheet surface [15]. The RMS voltage measured in millivolts, at different locations in the austenitic and both the ferritic rolled IF grade HR coils, is shown in Figure 3. All the stresses are tensile as measured on the top surface of the coil. Variation of residual stresses is more in austenitic rolled samples and this variation causes the shape defects. The head end is under more tensile stresses than the tail end. Variation of residual stresses is less in ferritic rolled samples though the trend of stresses having higher compressive stresses at the tail remains the same in both rolling regimes. This uniformity in residual stresses is one of the key advantages of rolling in a single-phase region.

Strength of the rolled coils is measured using tensile test and the formability is measured using r value (normal anisotropy parameter) and hole expansion test. Table 5 shows the comparison of mechanical properties of the austenitic

and the ferritic rolled IF grade HR coil at different locations. Tensile testing was carried out in a Zwick Z250 universal testing machine using ASTM E8 standard. Samples were cut in three directions, longitudinal, transverse and 45° to rolling direction. Tensile testing was carried out in all three directions for the calculation of r -bar. The n (strain hardening exponent) value is obtained from the slope of the true stress and true strain curve. Hardness of the samples was measured on Vickers scale using a Zwick ZH μ micro-hardness tester. Load applied was 0.5 kg and the average of five indentation values was reported in HV. Hole expansion test was performed in forming press (Zwick – BUP600) using standard ISO 16630. In this test, a hole with a punching die diameter of $d_p = 10$ mm and a relative cutting clearance of 12% is sheared into the sheet sample. This hole is then expanded with a conical die. As soon as a crack that runs through the entire thickness of the plate was seen, the expansion is stopped and the resulting hole diameter D_h is determined. The hole expansion ratio is then defined as the ratio between the increase in the hole diameter ($D_h - D_0$) and the original hole diameter D_0 . The comparison of the properties, microstructure and crystallographic texture and possible mechanisms are shown and discussed below.

YS, UTS, % elongation and n -value are reported in both longitudinal (L) and transverse direction (T). YS, UTS and hardness of the ferritic rolled samples are higher than the austenitic rolled samples due to the deformation at lower temperatures and finer grain size. The non-uniform grain size distribution and banded structure acts as an additional barrier to dislocation movement and increases the strength. These plant recorded values are close to the HSMM predicted values. The difference in values between the longitudinal and transverse directions is higher in ferritic rolled samples. This indicates a greater difference in grain orientation, which

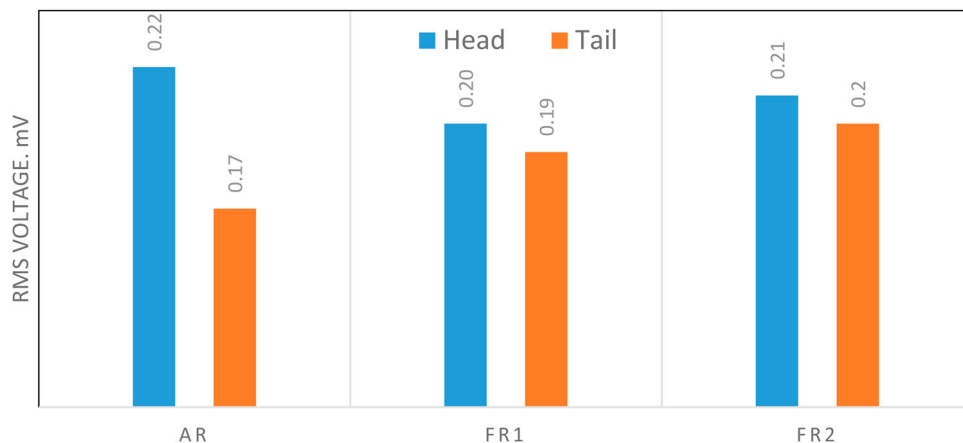


Figure 3. Comparison of residual stresses at different locations as measured using Magnetic Barkhausen Emission technique.

Table 5. Comparison of mechanical properties.

S. No	Properties	AR				FR1				FR2			
		Head		Tail		Head		Tail		Head		Tail	
		L	T	L	T	L	T	L	T	L	T	L	T
1	YS, MPa	201	196	179	181	228	264	224	262	284	325	279	322
2	UTS, MPa	295	293	285	287	316	342	312	341	353	382	343	381
3	Elongation (%)	48.5	46.5	49.3	48.2	29.1	24.6	28.7	22.9	21.3	17.5	20.9	18.1
4	n	0.211	0.201	0.222	0.215	0.145	0.122	0.147	0.123	0.083	0.078	0.095	0.08
5	r bar	0.96		0.98		0.69		0.78		0.93		0.97	
6	HER	152.8		153.2		131.35		135.25		112.6		114.4	
7	Hardness	100.6		92.2		101.3		108		115.3		119.3	

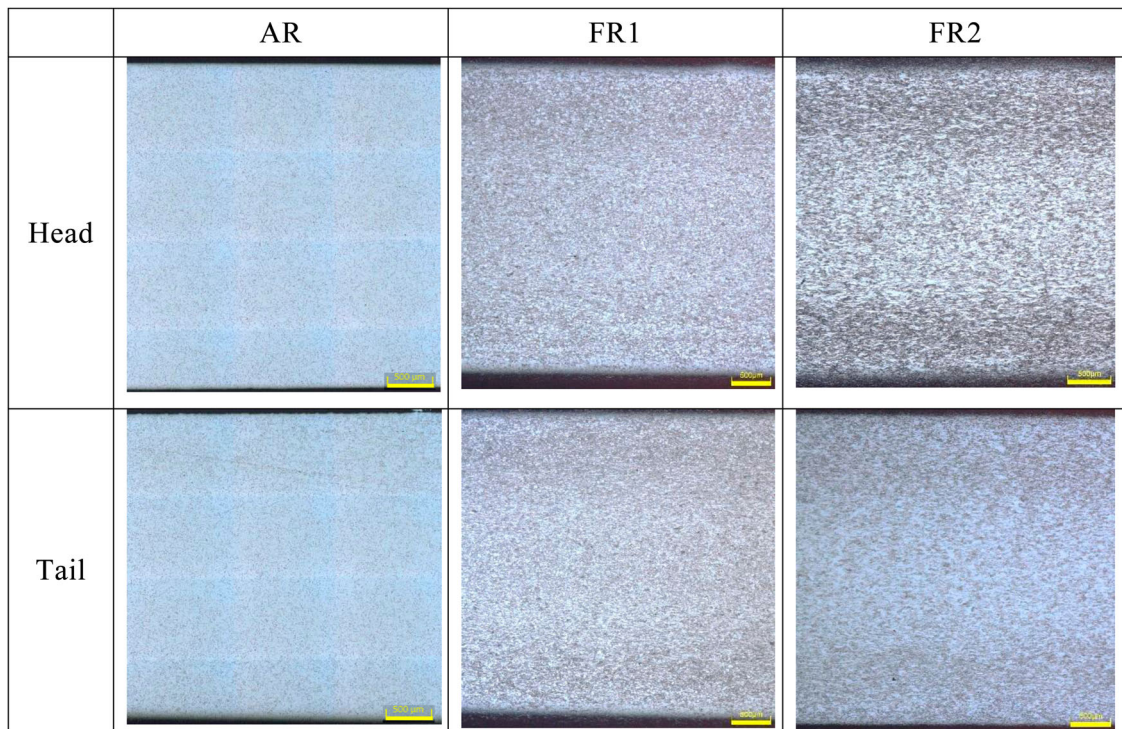


Figure 4. Variation in grain morphology along the thickness.

increases at the lower ferritic rolling temperature. Ferritic hot rolled samples are similar to austenitic samples after cold rolling and could be compared to full hard condition and hence the elongation was found to be lower in both the ferritic rolled samples. Strength increases and elongation decreases with a decrease in finishing and coiling temperatures. Indices of formability r -bar and hole expansion ratio in hot rolled condition decrease in ferritic rolled samples. Average plastic strain ratio or the normal anisotropy or the r -bar is a measurement of drawability and shows resistance to thinning in the thickness direction during deep drawing. Lower r -bar values are due to increased hardness and yield strength and reduced elongation. Higher deformed structure without any recrystallisation has stress concentration areas, which initiate cracks at small deformation during the hole expansion test and result in lower formability. Lower n value in ferritic samples indicates the presence of high residual stress in the samples. However, it is important to note that these coils are intermediate products and the formability is expected to improve after annealing.

Figure 4 shows the through-thickness variation of grain morphology in a single image (captured through image stitching module) of austenitic and ferritic rolled samples at head and tail end along the rolling direction in 100 \times magnification. Grain morphology is very uniform in the austenitic temperature range rolled samples indicating uniform recrystallisation. In the higher temperature ferritic rolled sample FR1, there is a thin layer of fine deformed grains or shear texture near both the surfaces. The variation is higher in the FR2 samples where a thicker band of highly deformed strained grains could be seen on both the surfaces, especially at the head end. This shows that the through thickness microstructural anisotropy increases with a decrease in temperature in the ferritic region. The difference in the grain morphology between the surface and the mid-section is due to the additional shear friction between the material and the rolls and is inhomogeneously distributed along the thickness

direction. This is a major drawback of ferritic rolling and affects the formability of the sheet [11]. This is the reason for significantly reduced hole expansion values of the FR2 samples having lower FT and CT. This surface layer is expected to show shear texture ($\langle 110 \rangle // ND$) and lubrication is suggested [11] for its avoidance during ferritic rolling. However, continuous use of lubrication during industrial rolling is not practically feasible. It is preferred to have optimum rolling temperatures to avoid lubrication during industrial rolling. Nevertheless, it will become uniform after annealing.

Small steel samples were cut, mechanically polished and etched using 4% nital for grain size determination using optical microscopy. Figure 5 shows the comparison of the hot rolled coil mid-section microstructure at the head and the tail end.

The optical microscopy of the IF grade steel hot rolled coil in austenitic conditions shows typical ferritic microstructure with grain size varying between 30 and 40 μm . Variation in grain size and morphology can be seen between the head and the tail section. Grain size has been found to be finer in the head as compared to tail regions of samples, presumably due to a higher cooling rate. At the tail portion, ferritic microstructure is mostly recovered and some recrystallisation has taken place which results in more equiaxed grains and marginally lower properties.

The ferritic rolled samples in FR1 also show completely ferritic microstructure but with elongated irregular grains of size varying between 15 and 30 μm . Ferrite rolling is not expected to have dynamic recrystallisation, but recovery can be seen as the deformation is carried out close to transformation temperature. Under higher temperature ferritic rolling, at certain locations, recovery has just initiated and this incipient recovery of the microstructure leads to saw like or wavy edges (indicated by light arrows) on grains. Some of these grains are also having bulged shape (indicated by dark arrows) due to localised orientation gradients

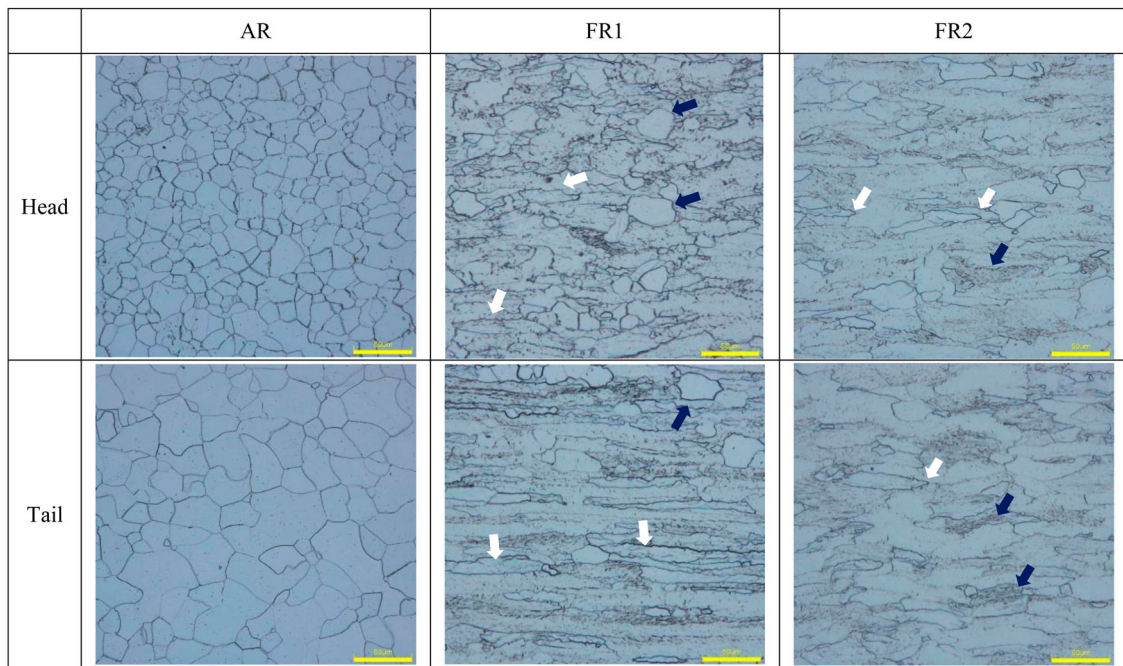


Figure 5. Microstructures of austenitic and ferritic rolled samples.

in the microstructure generated by the deformation and subsequent impending recovery. The presence of combined bulged and wavy deformed grains in this sample is unique and this behaviour can be attributed to high stacking fault energy of ferrite which makes the static and dynamic recovery faster. Dynamic recovery is reported to be more dominant during the deformation in ferrite as dislocation climb occurs readily due to its high SFE and also the diffusivity of iron atoms in ferrite is greater than in austenite for a given temperature [16]. These sharp edge grains along with lower r value and higher hardness indicate that the grains are in strained condition.

Compared to FR1, the low-temperature ferritic rolled sample FR2 shows highly elongated deformed ferritic grains aligned along the rolling axis having non-uniform grain distribution. Higher level of undercooling at lower deformation temperatures drives the formation of higher amount of dynamic strain-induced ferrite in FR2 sample [17]. Large fraction of low-angle mis-orientations (indicated by light arrows) in FR2 samples indicates retained strain in the grains and hardened microstructure. In the absence of dynamic recrystallisation at lower temperature rolling, the morphology of the grains is more pancaked and strain is retained from hot rolling, which increases the strength and lowers the elongation in FR2 coil. These un-recrystallised grain also degraded the r values. In FR2 samples deformed at a lower temperature, deformation bands or ingrain shear bands are also observed in many deformed grains (indicated by dark arrows) and is attributed to inhomogeneity of strain and stress concentration in different grains. Jonas [18] reported that in-grain deformation bands which are locations of high dislocation density are formed during the ferritic rolling which nucleates favourable gamma fibre ($\langle 111 \rangle // ND$). It is also supported by low carbon contents in this grade which results in low strain rate sensitivity favourable for such in-grain deformation bands. The morphology and size distribution are similar between the head and the tail end in the ferritic rolled samples. As the grains in ferritic rolling are

strained, subsequent recrystallisation annealing is required, to obtain the desired deep drawing properties.

Different hot band textures lead to different texture evolution during cold rolling and annealing. The deep drawing behaviour of steels depends basically on attaining the proper $\{111\}$ texture after each process of hot rolling, cold rolling and annealing [7]. Oriented nucleation mechanism is dominated in ferritic rolled samples compared to selective growth mechanism in austenitic rolled samples. Hence, to obtain a beneficial recrystallisation texture, the γ fibre should be the most prominent texture in the un-annealed condition. Coils having higher amount of prior alpha and gamma fibre in hot rolled condition are less susceptible to shear band formation during cold rolling and also help in nucleating more gamma fibre during annealing. Higher gamma and alpha fibre is desired in hot rolled coils for improved formability after cold rolling and annealing [8].

Texture was measured on a Panalytical X-ray diffraction machine using texture goniometers. Samples were cut and prepared using chemical etching. Texture measurement was done in a mid-thickness section of RD-TD plane. Comparison of texture ODF along φ ($0-90^\circ$), φ_1 ($0-90^\circ$), φ_2 at 45° section for mid-section austenitic and ferritic rolled samples is shown in Figure 6.

Austenitic hot rolled coil (AR samples) shows nearly random texture at both the head and tail ends. It contains mostly cube and goss texture and weak recrystallisation texture components alpha fibre and gamma fibre. Both the head and tail sample has cube and rotated cube (theta fibre) with maxima at $001\langle 110 \rangle$. This is because, at high temperature rolling, where austenite is not recrystallised, the cube $(001)\langle 100 \rangle$ texture of austenite transforms into the rotated cube $(001)\langle 110 \rangle$ in the ferrite. Head sample shows maximum alpha fibre close to (001) whereas weak gamma fibre is uniformly distributed all along $\langle 111 \rangle // ND$ in this sample. This can be attributed to the recovery process in these high-temperature rolled and coiled samples,

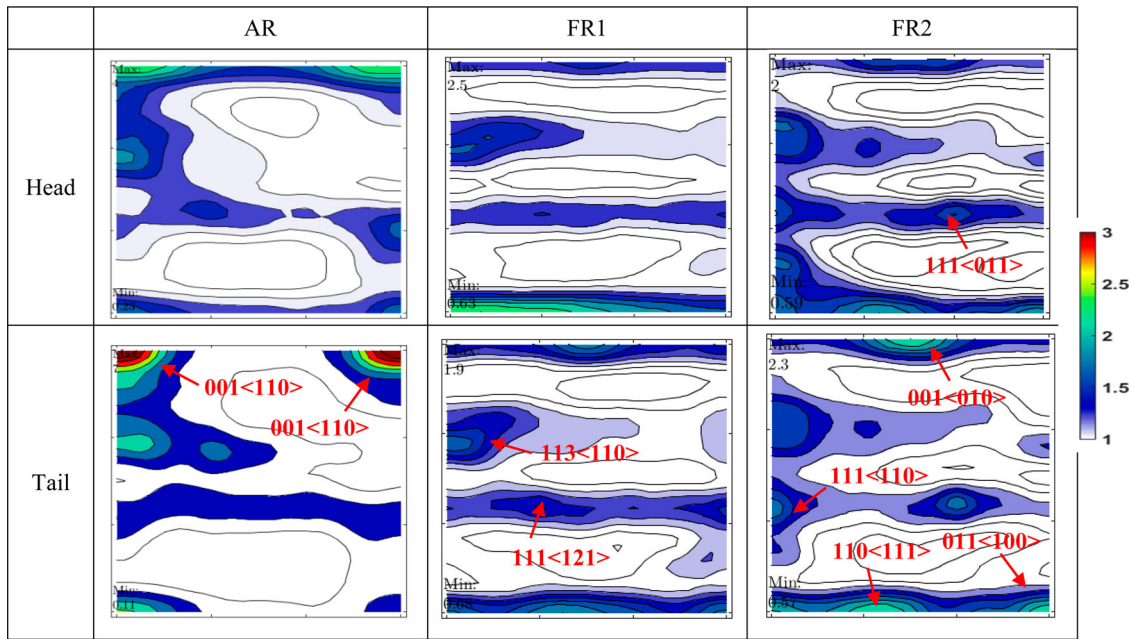


Figure 6. Texture ODF of austenitic and ferritic rolled samples.

reduces the stored energy of $\langle 111 \rangle$ oriented grains and minimises their amount after recrystallisation. Ratio of gamma/theta fibre is ~ 0.4 .

Ferritic rolled samples (FR1 and FR2) show more similarity in texture between head and tail compared to austenitic rolled sample (AR1). More deformation texture and pronounced alpha and gamma texture is seen in ferritic rolled samples compared to austenitic samples. At lower temperature deformation, thermal-activated dislocation movements (recovery) are restricted and complex multiple slipping dominates which leads to the formation of energy-rich $\langle 111 \rangle$ oriented grains [1]. With lowering deformation temperatures, the density of the formation of the $\langle 111 \rangle$ oriented grains increases. No significant theta fibre is seen in both the ferritic rolled samples. Ratio of gamma/theta fibre is > 1 under both the conditions.

In FR1 sample, austenite transforms towards gamma and alpha fibre and the cube texture is diminished. High temperature ferritic rolled sample (FR1) shows gamma texture maximum at $111\langle 121 \rangle$ and alpha fibre texture maxima is at $113\langle 110 \rangle$. By reducing the finishing temperature below 800°C and coiling temperature below 600°C , in FR2 samples, a more distinctive gamma fibre component with the strong alpha fibre in the near $\langle 111 \rangle$ component could be observed. As the finishing rolling temperature decreases, more strain energy is accumulated in the material, which is favourable for the development of a recrystallisation texture with a high $\langle 111 \rangle$ intensity or gamma texture. Low temperature ferritic rolled sample (FR2) shows gamma maxima at $111\langle 011 \rangle$ for both the ends which is the more stable orientation in this fibre texture. The relative proportion of alpha fibre is higher in FR2 sample compared to FR1 sample. Alpha fibre texture maxima is at $111\langle 110 \rangle$ in FR2 sample. But with reduced temperature rolling, some unwanted cube fibre at $001\langle 010 \rangle$, goss fibre at $011\langle 100 \rangle$ and goss/brass at $110\langle 111 \rangle$ also emerged in FR2 samples.

Present results are also in agreement with the previous work [19] from laboratory experiments that the lowering finishing temperature improves the deformation texture

with an increasing amount of $\{111\}$ oriented grains which supports the formation of a sharper $\{111\}$ recrystallised texture after coiling. Alpha orientation rotates to gamma orientation, leading to a high intensity of gamma fibre texture during cold rolling and therefore FR1 sample having relatively higher alpha fibre is expected to yield higher gamma fibre before annealing. The presence of other unfavourable textures along with the alpha and gamma fibres in FR2 samples is expected to end up with more alpha fibres after annealing. It is also important to note that there are also distinct texture characteristics along the thickness in FR2 samples rolled at lower FT and CT where grains at different layers experience different shear stress and thus orient differently.

The aim of ferritic rolling experiments was to check the rollability within mill load limitations and development of properties and texture under this condition. Comparison of rolling force values shows no increase in the load requirement during ferritic rolling. Variation of properties along the length was found to be higher in austenitic rolled samples due to phase transformation. Whereas variation along the thickness was found to be higher in low temperature ferritic rolled samples. This initial HR texture specially in FR2 ferritic rolled samples is more favourable to the formation of higher final recrystallisation texture after cold rolling and annealing but the formation of thicker shear texture at the surface, property variation along the thickness and significant increase in YS and UTS can move the final properties out of range. Better results are expected at lower FT and CT conditions with the use of lubrication during the rolling. Hence the FR1 rolling regime with finishing temperature at $\sim 840^\circ\text{C}$ and coiling temperature at $\sim 640^\circ\text{C}$ is more suitable for industrial rolling without any lubrication. The developed texture in FR1 was more favourable for achieving higher formability after cold rolling and annealing. In spite of having higher variation in temperature between the head and tail portion of the coil, the difference in residual stress, properties and texture is minimal. This is the key advantage of ferritic rolling which allows a higher flexibility in rolling and helps in reducing the shape defects. However, it requires optimisation of cold

rolling reduction and annealing temperatures with respect to ferritic rolled coils for achieving improved properties compared to conventional austenitic rolled coils.

Conclusions

In the present work, industrial ferritic rolling process has been developed for the IF grade steel through offline simulation using HSMM software and plant trials in a seven-stand hot strip mill under ferritic regime for producing an intermediate product, a hard cold strip for subsequent cold rolling and annealing. No increase in rolling load or shape variation has been found in the low temperature ferritic rolling. The ferrite rolled coils exhibit a strained microstructure, higher strength and lower elongation but with a desirable rolling texture having increased alpha fibre ($\langle 110 \rangle // RD$) and gamma fibre ($\langle 111 \rangle // ND$). When compared with austenitic rolled coils, a variation of properties along the length was found to be greater in austenitic rolled samples, whereas variation along the thickness is greater in low-temperature ferritic rolled samples. The variation in properties increased with decreasing the temperatures. For non-lubricated ferritic industrial rolling, finishing temperature of 840°C and coiling temperature of 640°C are most suitable for achieving uniform properties and favourable initial texture for subsequent cold rolling and annealing.

Disclosure statement

No potential conflict of interest was reported by the author(s).

References

- [1] Andreas T, Radko K. Deep drawable thin-gauge hot strip of steel as a substitution for cold strip. *ISIJ Int.* 2000;40(9):927–931.
- [2] Elsner A, Kaspar R, Ponge D, et al. Recrystallization texture of cold rolled and annealed IF steel produced from ferritic rolled hot strip. *Mater Sci Forum.* 2004;467–470:257–262.
- [3] Herman JC, Cantineaux P, Langlais JM. Future prospects of ferritic hot-rolled thin strip steel: a new 'low cost' approach for steel sheet production. *Steel World.* 1992;2(Feb):48–54.
- [4] Paepet AD, Herman JC, Leroy V. Deep drawable ultra low carbon Ti IF steels hot rolled in the ferrite region. *Steel Res.* 1997;68(11):479–486.
- [5] Roberto GB. Effects of hot and warm rolling on microstructure, texture and properties of low carbon steel. *Metall Mater.* 2011;64(1):57–62.
- [6] Barrett CJ, Wilshire B. The production of ferritically hot rolled interstitial-free steel on a modern hot strip mill. *J Mater Process Technol.* 2002;122:56–62.
- [7] Ray RK, Jonas JJ, Hook RE. Cold rolling and annealing textures in low carbon and extra low carbon steels. *Int Mater Rev.* 1994;39(4):129–172.
- [8] Wang ZD, Guo YH, Sun DQ, et al. Texture comparison of an ordinary IF steel and a high-strength IF steel under ferritic rolling and high-temperature coiling. *Mater Charact.* 2006;57:402–407.
- [9] Hiroshi T. Metallurgical aspects on interstitial free sheet steel from industrial viewpoints. *ISIJ Int.* 1994;34(1):1–8.
- [10] Barnett MR, Jonas JJ. Distinctive aspects of the physical metallurgy of warm rolling. *ISIJ Int.* 1999;39(9):856–873.
- [11] Barrett CJ. Influence of lubrication on through thickness texture of ferritically hot rolled interstitial-free steel. *Ironmaking Steelmaking.* 1999;26(5):393–397.
- [12] Rath S. Computer simulation of hot rolling of flat products. *Softw Eng.* 2016;4(6):75–81.
- [13] Millitzer M, Hawbolt EB, Meadowcroft TR. Microstructural model for hot strip rolling of high strength low-alloy steels. *Metall Mater Trans A.* 2000;31A:1247–1259.
- [14] Sasahara H. The effect on fatigue life of residual stress and surface hardness resulting from different cutting conditions of 0.45% C steel. *Int J Mach Tools Manuf.* 2005;45:131–136.
- [15] Gatelier C-R, Chicois J, Fougères R, et al. Characterization of pure iron and carbon-iron binary alloy by Barkhausen noise measurements: study of the influence of stress and microstructure. *Acta Mater.* 1998;46(14):4873–4882.
- [16] Langer H, Bleck W. Fundamentals of softening processes during ferrite hot rolling. 40th Mechanical Working and Steel Processing Conference, Vol. 35. Warrendale: ISS; 1998. p. 345–359.
- [17] Hurley PJ, Hodgson PD. Effect of process variables on formation of dynamic strain induced ultrafine ferrite during hot torsion testing. *Mater Sci Technol.* 2001;17(11):1360–1368.
- [18] Jonas JJ. Modern LC and ULC sheet steels for cold forming: processing and properties. International Symposium, Aachen. March 1998. p. 73–84.
- [19] Guo Y-H, Xing-yao Z, Jing X-R. Evolution of hot rolled texture during cold rolling and annealing in Ti-IF steel. *Adv Mater Sci Eng.* 2014;1(1):19–25.

D. Satish Kumar,¹ S. Manjini,² and Udaya Bhat Kuruveri³

Thermomechanical Simulation of Ferritic Rolling of Titanium-Niobium Interstitial-Free Steel

Reference

D. Satish Kumar, S. Manjini, and U. B. Kuruveri, "Thermomechanical Simulation of Ferritic Rolling of Titanium-Niobium Interstitial-Free Steel," *Materials Performance and Characterization* 10, no. 1 (2021): 569–584. <https://doi.org/10.1520/MPC20210040>

ABSTRACT

Austenitic or two-phase rolling of ultra-low carbon steels face temperature control issues and generate shape defects. Ferritic rolling has been developed as a solution, and ferritic hot-rolled sheets are used as final products, replacing hot-rolled followed by cold-rolled sheets. However, it is not in regular industrial production because of mill limitations. Hence, ferritic hot rolling must be optimized for developing a ferritic cold-rolled and close-annealed sheet through subsequent processing. In this work, industrial ferritic rolling process was simulated for a titanium-niobium interstitial-free steel using a thermomechanical simulator. Multi-hit plane strain compression tests were carried out at three different regimes below the lower transformation temperature (A_{r1}). Steels were processed under high strain and strain rates as experienced during industrial hot rolling operation, and the results were compared with the conventional austenitic rolling. The flow stress of the material in the ferritic regime decreased with decreasing deformation temperatures but increased at temperatures below 700°C. Nonuniformity in grains and texture also increased with decreasing temperatures. High-temperature rolling in ferritic condition close to A_{r1} temperature does not differ significantly from the austenitic condition, whereas the low-temperature ferritic rolled material had through-thickness microstructural nonuniformity and unwanted goss and brass fibers. The intensity of gamma-fiber $\{111\}$ || normal direction (ND) required for formability was highest in the intermediate temperature zone. Deformation between temperatures of 850°C and 800°C was found to be ideal. Based on simulation studies, full-scale plant rolling was carried out under the optimized ferritic regime. The microstructure and texture matched closely with the simulation results. This work provides a working window for ferrite rolling in an industrial hot strip mill for developing ferritic cold-rolled close-annealed products.

Manuscript received December 3, 2020; accepted for publication July 7, 2021; published online August 27, 2021. Issue published August 27, 2021.

¹ Research and Development, JSW Steel Ltd., R&D Building, Vijayanagar Works, Toranagallu, Vidyanagar, Bellary, Karnataka 583275, India (Corresponding author), e-mail: satishkumar.dabburu@jsw.in, <https://orcid.org/0000-0002-2538-6582>

² Research and Development, JSW Steel Ltd., R&D Building, Vijayanagar Works, Toranagallu, Vidyanagar, Bellary, Karnataka 583275, India

³ Department of Metallurgical and Materials Engineering, National Institute of Technology Karnataka, National Highway 66, Srinivasnagar, Surathkal, Mangalore, Karnataka 575025, India

Keywords

ferritic rolling, Gleeble, interstitial-free steel, hot deformation, texture

Introduction

Various ultra-low carbon steels are being used in automobiles after 1990s. These steels are industrially produced by hot rolling, cold rolling, and annealing. Hot rolling is generally done at high temperatures, either in austenite or two-phase state. During the industrial hot rolling of interstitial-free (IF) steels, the issues of load variation, hunting, buckling, and shape defects arise, which results in edge slivers and holes during the subsequent cold rolling. This requires double trimming of the cold-rolled sheets, which reduces the product yield and increases the cost. During the 1990s, ferritic rolling was promoted as a possible solution to overcome this problem.¹ In the ferritic rolling strategy, the finish rolling is carried out below the two-phase region.² This low rolling temperature practice is expected to present an improved rolled product quality³ with fewer surface defects as two-phase rolling is completely avoided. It is expected to produce sheets with higher drawability, required for making automobile panels.¹

In the literature, two different ferritic rolling strategies have been suggested,⁴ producing a “soft” hot strip and a “hard” hot strip. The “soft” hot strip is rolled at higher temperatures just below the lower transformation temperature (A_{r1}), ensuring full or partial recrystallization of the strip, and the “hard” hot strip is rolled and coiled at the much lower temperatures in the ferritic region, resulting in a strained microstructure requiring subsequent annealing. Soft hot strips are used directly, whereas hard hot strips are used after customized annealing in annealing furnaces. Both these products can be used as a cheaper substitute for cold strip for some applications (Barrett et al.).⁵ Several studies have been published where microstructure and texture have been optimized for achieving r -value or the deep-drawability in the hot strips comparable to that of a cold strip produced through conventional austenitic rolling.

Despite several claimed benefits,^{1,5} ferritic rolling is not in wide practice in the industry for multiple reasons. One of the major limitations reported in many studies^{5–8} is the formation of poor $\{111\}$ texture, which reduces drawability. One method to produce a strong $\{111\}$ texture is to encourage extensive shear band formation during rolling. This concept requires major changes in the hot rolling mill to incorporate thinner sheet rolling capability. It is suspected and also reported many times^{9,10} that ferritic rolling requires higher mill-power and rolling loads because of low finish rolling temperatures. A detailed review by Hiroshi¹¹ also confirmed that both the metallurgical and the industrial viewpoints for a particular steel plant or the mill configuration together govern the economics of the ferritic rolling process. Because of these reasons, ferritic rolling is not used much industrially.

Therefore, for ferritic rolling to be used industrially, it must yield products with fewer defects (or better yield) and improved texture, without considerable change in the rolling load. The use of fully soft and fully hard hot strips for subsequent cold rolling and annealing may not be the ideal intermediate products and is also less investigated. These studies were mostly carried out in laboratory mills and have occasionally been tried in an industrial mill. Additionally, the optimization of hot rolling parameters for cold-rolled close-annealed (CRCA) ferritic-rolled product is not found in the literature.

The applications of IF steels require good formability, which is achieved by attaining a high fraction of gamma (γ)-fiber $\{111\}$ || normal direction (ND) texture.¹² Chang et al.¹³ studied the effect of the ferritic hot rolling process of titanium micro-alloyed IF steel and reported a strong impact of hot rolling finishing temperature (FT) and developed texture on the final properties after cold rolling and annealing. It is also found that higher hot-rolled gamma texture develops into higher gamma texture in the final sheet. The ferritic hot rolling parameters must be studied and optimized to achieve good grain orientation and texture suitable for subsequent cold rolling and annealing.¹⁴

The effect of various hot rolling parameters under ferritic condition is studied extensively on specific physical metallurgy aspects, such as recrystallization and texture, but very few studies simulated the actual process including rolling mill conditions. The combined effect of key parameters, such as deformation temperature, rolling reduction, the resistance to deformation, and cooling rate, which are important for its control on an industrial

scale, is less studied. Guo¹⁵ rolled a high-strength titanium-IF steel at a fixed FT of 760°C and coiling temperature (CT) of 740°C. The study reported higher values in properties and texture in ferritic-rolled samples but with larger variations between the surface and the center. This is attributed to low-temperature deformation and lower cooling on run-out-table (ROT).

The laboratory studies on the effect of finishing or deformation temperatures by Jeong¹⁶ also reported a significant decrease in mean *r*-value because of the formation of stronger {100} <011> texture along with a recrystallization texture near {554} <225> with decreasing temperatures. This lowers the formability characteristics.

Matsuoka¹⁷ studied the variations along with the thickness and linked it to nonuniform recrystallization texture formed because of the additional shear strain introduced by the frictional force between the rolls and the material resulting in <110>//ND recrystallized grains near the surface, and <111>//ND being formed at the midplane. Barrett,¹⁸ through his laboratory studies, showed that the use of ester oil lubrication during ferritic hot rolling results in total suppression of the detrimental (110) shear texture to give a strong (222) dominated texture throughout the thickness of the strip. This lubrication requirement during rolling is also responsible for less acceptance of ferritic rolling in industries, where such addition is difficult in a continuous rolling mill and therefore must be looked at alternatively through temperature optimization.

Akbari¹⁹ studied the microstructural evolution of an IF steel during warm working in the temperature range of 500°C–800°C through the wedge-shaped slab at max 50 % deformation and reported the formation of microbands independent of strain, temperature, and initial grain orientations but also found shear bands at lower temperature and higher strain rates. Okuda and Seto²⁰ conducted one-pass ferritic hot rolling with different rolling temperatures and rolling reductions for 0.016 % niobium and 0.023 % titanium IF steels separately and also found different recrystallization behaviors and kinetics. During industrial rolling, the material experiences multiple deformation steps and different strain and strain rates in each stand. The flow behavior in each stand is dependent on the accumulated strain and the applied stress²¹ at that particular temperature and the extent of inter-stand recrystallization. Hence the individual deformation study on the effect of strain and temperature will not be able to predict the combined effect and properties during the industrial rolling. This phenomenon must be studied in actual rolling conditions where deformation is much higher.

There are also some inconsistencies in the results presented in the literature. Roberto⁹ reported bigger grain sizes with irregular shape under the ferritic rolling process, whereas Okuda and Seto²⁰ showed finer grains at a higher reduction level in the hot rolling. Harlet et al.²² reported a more homogeneous microstructure, lower yield stress, and higher ductility for high temperature ferritic-rolled coils compared to conventional austenitic-rolled coils but in a specific temperature range, which is not studied extensively by the other researchers. These variations are attributed to different strain and strain rates applied in simulation, making them an important variable and dependent on mill configurations. Tiitto²³ also found that ferritic hot rolling seems to be beneficial only if it contributes to the development of a strong intensity of the γ -fiber texture and a uniform and small grain size during annealing.

In this work, it is therefore decided to simulate the full industrial ferritic rolling process with similar strain, strain rates, and cooling in a thermomechanical simulator. This work aims at developing an intermediate ferritic product for subsequent cold rolling and annealing, which can attain improved formability comparable to conventional austenitic-rolled sheets. In the present study, rolling simulation is carried out at three different temperatures in the ferritic zone and compared with the austenitic rolling for the change in flow stress, strain hardening effect, hardness, microstructure, and texture. The simulation results were further validated through the plant trials for the optimized parameters.

Grade Selection and Dilation Studies

The steel used in this study is a niobium-titanium-stabilized IF-grade steel having a composition as shown in **Table 1**. The unique feature of this grade is low levels of carbon and nitrogen remaining in the ferrite, achieved by

TABLE 1

Composition of the selected IF grade (wt. %)

C	Mn	Si	Al	S	P	Ti	Nb	B	N	Fe
0.002	0.17	0.006	0.036	0.007	0.011	0.027	0.011	0.0001	0.0025	Balance

using both niobium and titanium. Because of the combined effect of these two elements, complete stabilization is being achieved at a much lower weight percentage. The selected IF grade is one of the most consumed materials and is prone to many surface and shape defects during the austenitic rolling; hence, it is the best composition for comparison in ferritic rolling.

In industrial ferrite rolling, rough rolling or roughing is carried out in the austenite phase above A_{r3} temperature and the finish rolling is carried out in the ferrite phase below A_{r1} temperature. The slab is held on the intermediate roller table between the roughing and finishing stands to cool down through the two-phase region and to facilitate complete phase transformation. The ferrite rolling process requires the finish rolling temperature to be controlled below A_{r1} temperature all along the length of the coil. Additionally, IF steels have a higher and narrower transformation band; therefore, precise determination of the A_{r3} and A_{r1} temperatures, which gives the range of the γ - α transformation temperatures for the experimental cooling rates, is important. The knowledge of the recrystallization behavior of ferrite in the absence of a second phase in IF steels is also important to set the ferritic rolling process parameters. For this study, the upper transition temperature, A_{r3} , and the lower transition temperature, A_{r1} , were measured using dilation studies using a contact-type thermal dilatometer in a thermo-mechanical simulator. For simulation, the samples were collected from the transfer bar produced during the austenitic rolling in a hot strip mill. Cylindrical samples of the IF grade steel (85 mm long with 10-mm diameter) were heated to 1,200°C at the rate of 1°C/s and soaked for 60 s for homogenization. These specimens were then cooled at different controlled cooling rates (1°C/s, 2°C/s, 5°C/s, 10°C/s, 15°C/s, 20°C/s, 25°C/s, and 30°C/s) to study the effect of cooling rate. The transformation of phases results in the change of volume during cooling and was recorded using a contact-type thermal dilatometer by measuring the dilation in the test specimen. The different transition temperature points or the beginning and the end temperatures of the transformed phase were obtained by taking the tangential point of the dilation curve. The change in the A_{r3} and A_{r1} temperatures at different cooling rates are shown in **Table 2**. The phase transition temperature decreases with increasing the cooling rate, but the difference between A_{r3} and A_{r1} increases with increasing the cooling rate.

The industrial cooling rates vary between 2°C/s and 5°C/s, and therefore the transformation temperatures were measured at 2°C/s and 5°C/s. A_{r3} and A_{r1} temperatures at a cooling rate of 2°C/s were found to be 906°C and 871°C, respectively, and similarly, at a cooling rate of 5°C/s, temperatures were found to be 902°C and 868°C, respectively. Hence, the temperatures of the transfer bar head must be maintained at 30°C–40°C below this temperature for having the full coil rolling in the ferritic region.

TABLE 2

Effect of the cooling rate on transformation temperatures

Cooling Rate, °C/s	A_{r3} , °C	A_{r1} , °C	Temperature Difference
			$(A_{r3}-A_{r1})$, °C
1	911	875	36
2	906	871	35
5	902	868	34
10	886	851	35
15	883	837	46
20	873	830	43
25	877	813	64
30	874	807	67

Thermomechanical Simulation

Rolling load is a critical limitation in any mill and it depends on the temperature of deformation, applied strain in a stand, and the corresponding strain rate. Therefore, before the industrial rolling, it is necessary to calculate and compare the flow stress of IF grade at the operating temperatures. The knowledge of the plastic flow behavior of IF steel at lower temperatures is also required to adjust the reduction ratios in various stages during rolling. Generally, the flow stress values decrease with increasing the temperature and vice versa. In ferritic rolling, at lower temperatures, it is expected to have an increase in the flow stress and requires higher mill loads. It is also established that the deformation resistance varies nonuniformly with the decrease in rolling temperatures.²⁴ Therefore, it is important to choose the range of least deformation resistance for minimizing the rolling pressure, which brings process stability and will also improve the rolling mill availability and productivity during the industrial rolling.

It also becomes imperative to study the impact of low-temperature phase transformation on the flow stress values and optimize the ferritic rolling temperatures for industrial rolling. In the present time, design and optimization of hot deformation processes are no more attempted using costly and time-consuming industrial trials.²⁵ Mathematical modelling packages have advantages over the plant trials and are regularly used for such simulations, but their prediction accuracy is limited to the conditions, where correlations between the strain-controlled deformation and the microstructure evolution are known. For the new and complex deformation conditions, flow stress behavior and microstructural changes can only be experimentally identified using thermomechanical simulators.¹⁰ It is well established through many previous studies^{26,27} that the hot rolling characteristics of steels can be accurately predicted using hot compression tests in Gleeble-thermomechanical simulator. In the present work, hot compression or deformation tests under plane strain conditions were performed in the Gleeble-3800 thermomechanical simulator for simulating the hot rolling of IF grade steel in the austenitic and ferritic temperatures. The simulator can simulate the exact strain and strain rates in each stand and the inter-stand times at the set temperatures. As the cast structure suffers from structural in-homogeneities and segregations, the samples were collected from an austenitic-rolled IF steel transfer bar from the hot strip mill for obtaining a homogeneous initial structure. The samples were cut into smaller pieces and machined into a 30 by 26 by 15-mm cuboid shape for the simulations. Multi-hit plane strain compression tests were carried out using the hydra-wedge module of Gleeble to measure the flow stress values for the selected IF grade under three different ferritic temperature regimes. The existing austenitic rolling was also simulated for comparison. The strain and strain rates in each deformation pass during the ferritic rolling were kept similar to the values experienced during the industrial austenitic hot rolling.

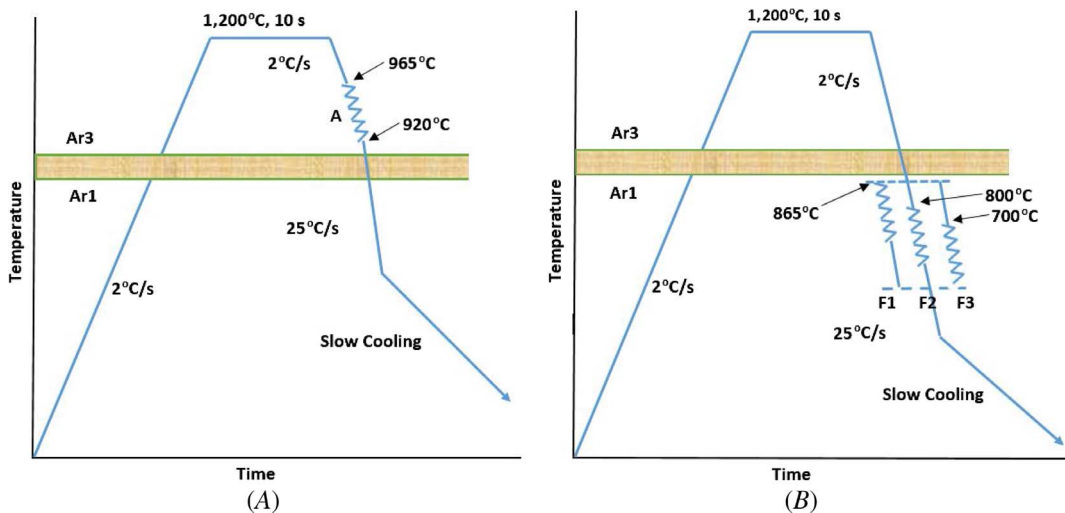
The deformation was carried out in a vacuum using the tungsten carbide deformation dies and nickel paste lubricant to avoid sticking and to ensure uniform deformation along the contact surface during hot compression tests. The temperature of the specimens was monitored using a chromel-alumel thermocouple. The transfer bar samples were collected after rough rolling, which is always carried out at a temperature above the recrystallization temperature, and the finish rolling, ROT cooling, and CTs are simulated. They have a direct impact on the final properties. The strain, strain rates, FT, and CT programmed for each pass during all four experiments are shown in [Table 3](#). Because of the strain limitation in Gleeble, all seven finishing passes of the hot strip mill could not be simulated. Consequently, a total of six passes (deformation passes 2–7) were simulated under plane strain condition (with pass 2 being partially simulated). A maximum strain of 0.5 was given in stand 3, and a minimum strain of 0.16 was given in stand 7. During rolling, the strip speed is lowest in the initial stands and hence corresponding strain rate of 20 s^{-1} was maintained in the first stand and the highest strain rate of 165 s^{-1} was given in stand 7 where the strip speed is maximum.

The schematic temperature-time plots indicating the simulating conditions is shown in [figure 1](#). The specimens were heated to $1,100^\circ\text{C}$ at a rate of 2°C/s and held for 10 s for homogenization. Ar_3 and Ar_1 temperatures were taken corresponding to a cooling rate of 2°C/s . Thereafter, the sample was control cooled to the first deformation temperature. A 3-s holding time was given to homogenize the temperature in the sample before the deformation in each deformation cycle. The strain and strain rates of each six deformation steps are different and

TABLE 3

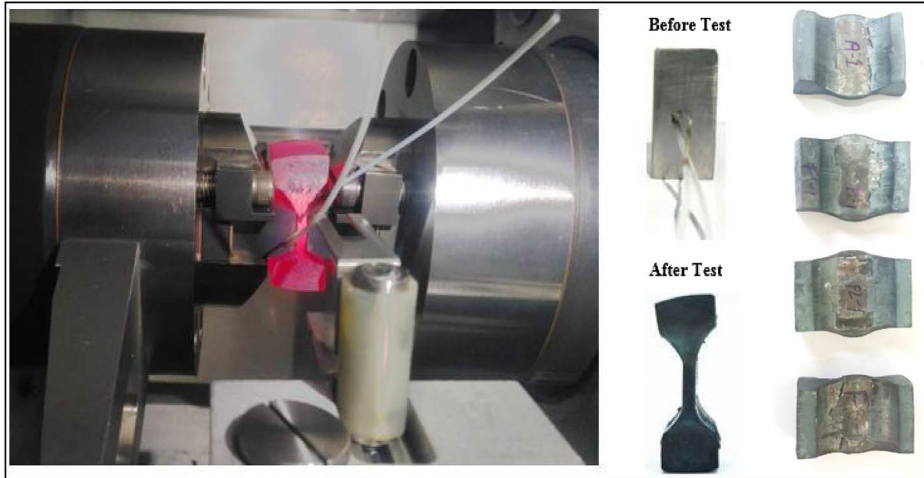
Rolling simulation plan and temperatures

Finishing Pass	Strain	Strain Rate, s ⁻¹	Austenitic Rolling (A) Temperature, °C	Ferritic Rolling (F1) Temperature, °C	Ferritic Rolling (F2) Temperature, °C	Ferritic Rolling (F3) Temperature, °C
1	0.65	10	965	865	800	700
2	0.60	20	969	869	804	704
3	0.50	30	973	873	808	708
4	0.40	80	974	874	809	709
5	0.36	130	943	843	778	678
6	0.27	160	933	833	768	668
7	0.16	165	923	823	758	658
FT, °C	920	820	755	655
CT, °C	640	640	600	550

FIG. 1 Schematic temperature-time plots indicating simulating conditions: (A) austenitic rolling and (B) ferritic rolling.

are similar to the values set in the austenitic industrial rolling of an IF steel. A delay period of 2–4 s was given between each deformation step based on the rolling speed. This is to simulate the time taken for the movement of material between each stand. A total of four finishing and ROT cooling sequences were simulated: (1) austenitic rolling—“A” with finishing start at 965°C, (2) high-temperature ferritic rolling representing soft hot strip—“F1” with finishing start at 865°C, (3) medium temperature ferritic rolling—“F2” with finishing start at 800°C, (4) low-temperature ferritic rolling representing hard hot strip—“F3” with finishing start at 700°C. F1 simulated the industrial rolling just below Ar₁ temperature to see the effect of partial recrystallization, whereas F2 and F3 trials simulated complete ferritic rolling at lower temperatures within practically possible limits of an industrial rolling setup. ROT cooling of the strip was simulated by spraying mist through the specially designed nozzles onto the specimen surface to provide a cooling rate of 25°C/s down to the CT. CTs were varied between 640°C and 550°C based on the FTs. The specimens were then slowly cooled to room temperature in the simulator itself in 30 min to simulate the slow cooling of the coil surface after the coiling. The deformation dies, initial sample, and the final sample after deformation are shown in [figure 2](#). The temperature of the specimen, flow stress, time, and strain for each deformation was recorded continuously. The measured sample temperatures during the continuous rolling and the cooling cycle closely matched with the programmed temperatures.

FIG. 2 Hot deformation simulation in the thermomechanical simulator.

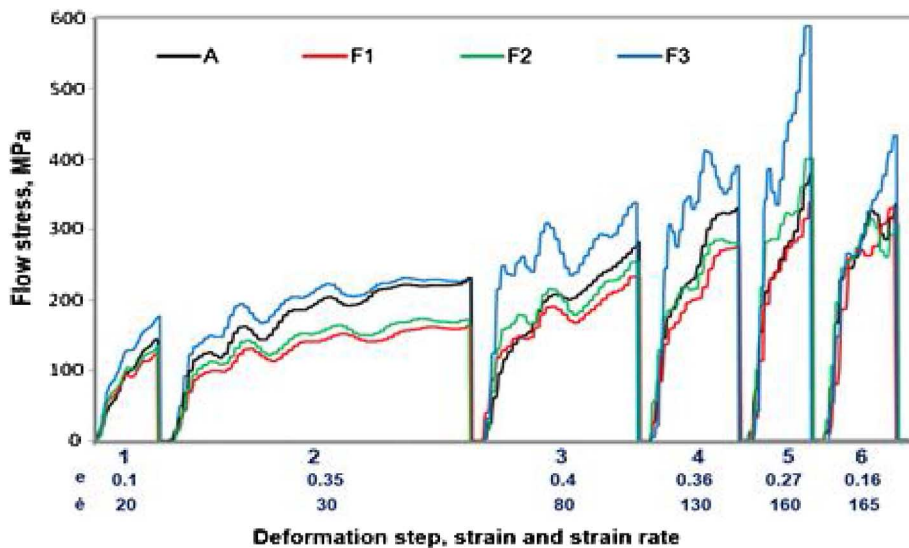


Five samples were repeated under each condition, and the best three samples having a uniform shape and contact thickness were selected for flow stress mapping and characterization. From these dumbbell-shaped samples, a rectangular piece was cut from the central axis as shown in [figure 2](#). The precisely cut, center parts of the deformed samples were used for further characterization studies.

Results and Discussion

Mean flow stress is an indicator of expected rolling loads. It also helps in understanding the changes in microstructure taking place during the hot rolling. [Figure 3](#) shows the variation of flow stress in each deformation during the austenitic and ferritic rolling along with the individual strain (ϵ) and strain rate ($\dot{\epsilon}$). The flow stress of

FIG. 3 Variation in flow stress with the extent of deformation between austenitic and ferritic rolled samples.



the material continuously increased in all experimental cases up to the fifth deformation because of strain hardening. It marginally reduced in the last stand deformation because of a significant reduction in strain in the last stand. The strain hardening effect is more pronounced in the deformations carried in the ferritic region compared to the austenitic region for the same value of the strain and the strain rate. However, the absolute value of the flow stress for the ferritic rolling F1 (high-temperature ferritic rolling) is always lower than the austenitic rolling. Ferrite softens by the dynamic recovery as it is having higher stacking fault energy. In this case, the softening or the flow stress-reduction effect of the ferrite phase is higher than that of the hardening because of a decrease in temperature and applied strain, thereby keeping the flow stress or the deformation resistance lower. The absolute value of the flow stress for the ferritic rolling F2 (medium temperature ferritic rolling) is lower than the austenitic rolling up to the fourth deformation step and is higher thereafter as the total strain increases. This is because dynamic recovery in ferrite is a function of temperature.²⁸ In this case, hardening that is due to a decrease in temperature and applied strain increases with the number of deformations and equals the softening effect of the ferrite phase at the fourth deformation step and has reversed the effect thereafter. The absolute value of flow stress for the ferritic rolling F3 (low-temperature ferritic rolling) is always higher than the austenitic rolling in all deformations. In this single-phase region of ferrite, hardening that is due to lower temperature is higher than the ferrite softening effect and it resulted in the higher flow stress. In this case, the flow stress increases significantly with the increased strain.

If only the temperature effect is considered, the flow stress does not increase continuously. It has a non-uniform trend where it decreases first and then increases as we move down from Ar_1 temperature. **Figure 4** shows the variation in the peak flow stress with deformation at each stand. The rate of increase of average flow stress and the peak flow stress increases with reducing the temperature for the similar reduction regime. Flow stress analysis shows that the strain hardening effect in the ferritic region is due to the combination of temperature and the accumulated strain and does not have any linear relationship. These results are different in this full rolling simulation when compared to previously published work²⁴ where rolling was simulated partially (single deformation). Flow stresses are expected to be always lower if rolled only in the F1 ferritic temperature range on an industrial scale and not at lower temperatures. At lower temperatures, hardening effect becomes stronger.

Vickers hardness measurements (HV5) were performed on all four cut samples, and the comparison of hardness (average of five readings) at the center is shown in **figure 5**. The hardness of simulated sample A

FIG. 4 Variation in peak flow stress of austenitic and ferritic rolled samples.

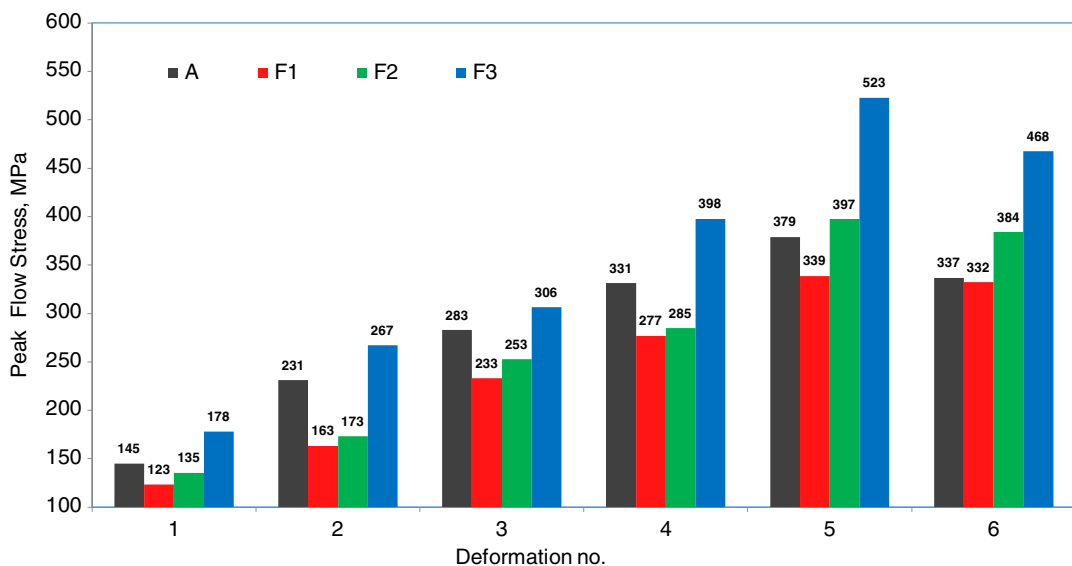
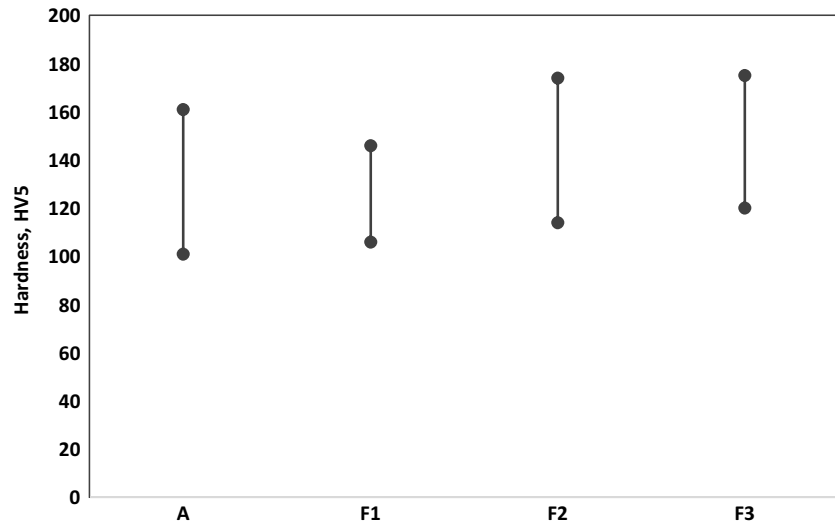


FIG. 5

Comparison of the hardness of austenitic and ferritic rolled samples.



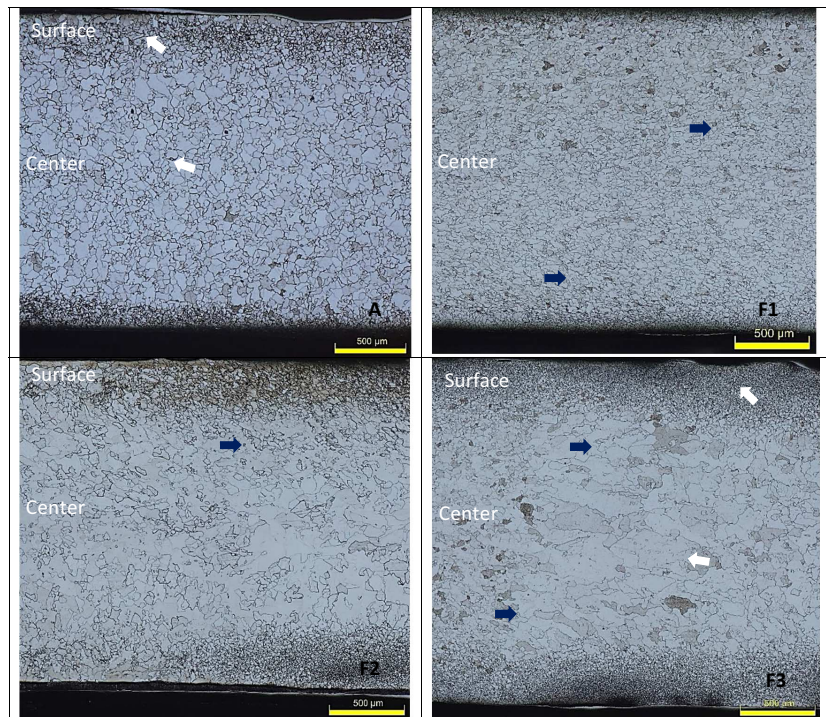
(austenitic) is similar to the industrially rolled sample. However, the hardness of all ferritic-rolled samples was found to be higher than the austenitic sample. The hardness values of sample F1 is closest to the austenitic sample A. A comparison among the samples shows that hardness increased with a decrease in the experimental temperature. An increase in hardness in the F1 sample can be attributed to the finer grain size or increase in strain energy because of the deformation, despite some amount of dynamic recovery in ferritic condition. An increase in hardness in F2 and F3 samples, although having larger grains, may be due to the microstructural bands that restrict the dislocation movement. The range of hardness values indicates that the yield strength and ultimate tensile strength of the ferritic rolled sheets will be higher and elongation will be lower than the austenitic-rolled sheets in hot-rolled condition.

One of the key issues of ferritic rolling reported in the literature is the nonuniformity in properties along with the thickness.²¹ To study this behavior, through-thickness variations of the grain morphology of austenitic- and ferritic-rolled samples were captured as shown in **figure 6**. For this purpose, small pieces were cut, polished, and etched for microscopic analysis from the central part of the deformed samples. In the austenitic temperature range rolled sample (A), the grain morphology is uniform with a thin chilled/fine-grained layer at the surface, which is due to the contact with the dies. The high-temperature ferritic-rolled sample (F1) also shows uniform grain morphology but with the presence of coarse grains along with certain microstructure bands. The grain morphology variation is higher in the low-temperature ferritic-rolled samples (F2 and F3) where a thicker band of highly deformed grains could be seen on both surfaces. The inhomogeneous distribution of the shear force along the thickness causes microstructural anisotropy,¹⁷ which increases with a decrease in temperature in the ferritic region. The shape of the grains is more uniform along with the central portion and varies nonuniformly along with the thickness (quarter band) in A, F1, and F2 samples. The quarter band grains show a more elongated shape (indicated by darker arrows in **fig. 6**). The difference of grain size between the center and surface (indicated by white arrows in **fig. 6**) is highest in the lowest temperature-rolled sample (F3). It is an indication of inconsistency in properties. This shows that very low-temperature rolling results in through-thickness variation in microstructure, and it could be detrimental for formability in the cold-rolled stage.

Figure 7 shows the high-magnification (500X) optical microstructures at the center of the cross section for the austenitic and three ferritic deformed samples, which represents the experimental temperature profile of the simulation. The microstructure of the austenitic-rolled sample (A) having the deformation start at 965°C and the

FIG. 6

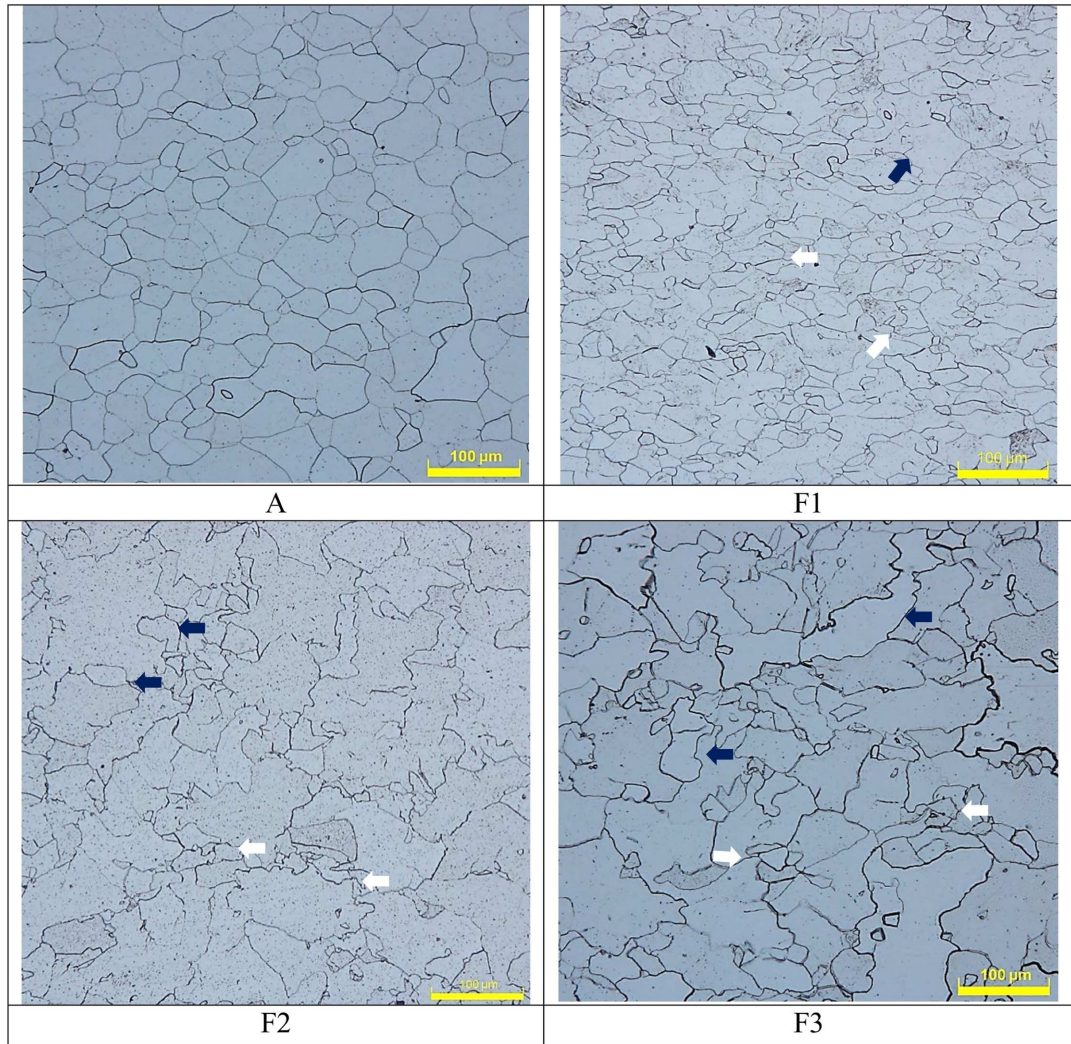
Variation in grain morphology along the thickness of austenitic and ferritic rolled samples.



finish at 920°C was found to be similar to the industrially (austenitic) as-rolled microstructures of the IF steel. It confirms the accuracy of the simulation. The austenitic-rolled sample shows predominantly the quasi-polygonal ferrite structure with equiaxed fine grains of size $\sim 30 \mu\text{m}$. It is completely recrystallized uniform grain structure. Ferritic rolling performed at high temperatures in the ferrite region (F1) representing soft hot strip, having the deformation start at 865°C and the finish at 820°C, resulted in microstructure with partial recrystallization and grain size is smaller than the austenitic sample.

The mean intercept length of the grains was found to be $23 \mu\text{m}$. Some of the newly formed grains are deformed, and a few have wavy boundaries, indicating the only recovery. Rolling at relatively lower temperatures (F2) representing an intermediate condition, having the deformation start at 800°C and the finish at 655°C, resulted in partially recovered and heterogeneous microstructure with duplex grains. It shows a wide distribution of grain size having a mean intercept length of $32 \mu\text{m}$. Some grains have a bulged shape (indicated by dark arrows in [fig. 7](#)) because of deformation gradients and the subsequent impending recovery. This behavior indicates the occurrence of multiple softening mechanisms. At such high strain and strain rates, interpass softening effect of titanium and niobium by solute drag effect is not visible. No bulk dynamic recrystallization is seen in the samples, but a few small grains could be seen on certain grain boundaries. Such behavior of ferrite can be linked to both the low stored energy mechanisms of strain-induced precipitation and strain-induced boundary migration.

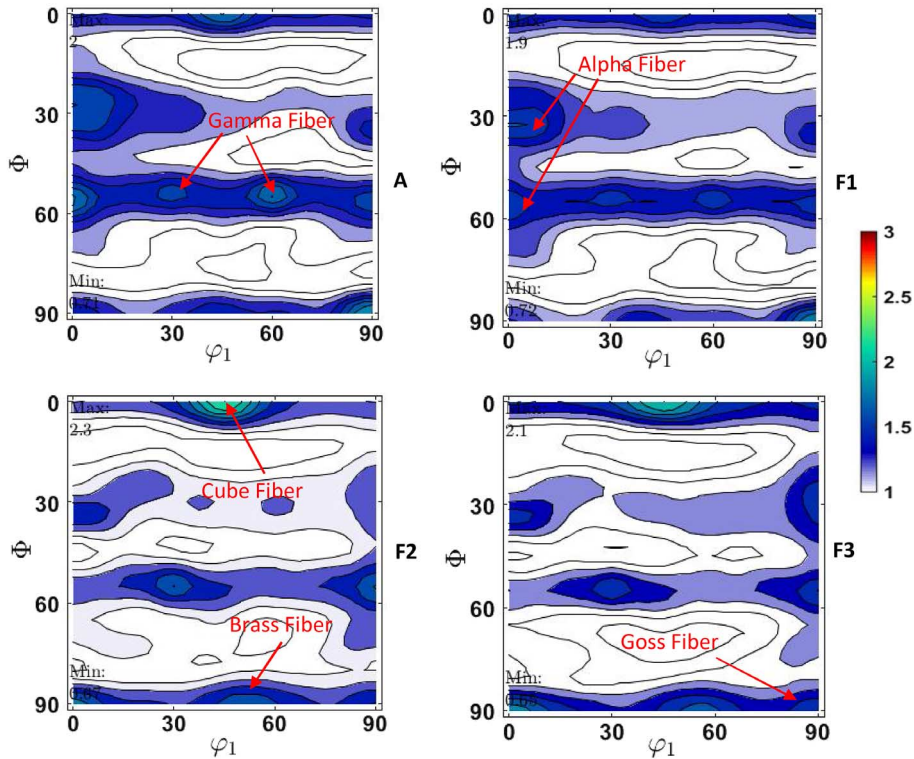
The lowest temperature ferritic rolling (F3) (representing hard hot strip) having the deformation start at 700°C and the finish at 655°C resulted in a strained and nonrecrystallized structure having large nonuniformly deformed grains of size $\sim 50 \mu\text{m}$. Grains in samples F2 and F3 show some clustering at certain locations. It is expected because of the interaction of uneven distribution of shear strain that is due to the plain strain compression between the dies.²⁹ None of the three ferritic-rolled samples was found to be fully recrystallized. In comparison to the austenitic rolling, the ferrite rolling microstructure at higher temperature exhibits smaller grain sizes, but the size increased significantly as the temperature decreased, indicating only recovery and no recrystallization.

FIG. 7 Microstructures at the center portion of austenitic and ferritic rolled samples.

It is also found that the fractions of grains with irregular and distorted boundary (indicated by white arrows in [fig. 7](#)) are higher in the ferritic-rolled samples. In the electron backscatter diffraction, they are expected to show higher amounts of low-angle grain boundaries. This fraction of visible grains with low-angle grain boundary shows an increasing trend with decreasing temperature. It is due to a decrease in fine polygonal ferrite and an increase in dislocations induced by the ferritic rolling.⁹ Grains also became flat with reducing the temperature in all the ferritic-rolled samples. This increase in grains with low-angle grain boundary increases the strength of the material because of a higher degree of strain accumulation. F1 condition-rolled microstructure is closest to the austenitic-rolled microstructure.

For deep-drawable steel sheets, the α -fiber ($\langle 110 \rangle \parallel$ rolling direction (RD)) and the γ -fiber ($\{111\} \parallel$ ND) are important.¹² If they are higher in the initial hot-rolled coils, the fraction will be higher in the final cold-rolled and the annealed sheet. Additionally, the ratio of γ -fiber ($\{111\} \parallel$ ND) to θ -fiber (RD/ $\langle 100 \rangle$) should also be higher. [Figure 8](#) shows the comparison of textures through the orientation distribution function map at $\phi_2 = 45^\circ$ for the austenitic and ferritic rolling simulated samples measured through the

FIG. 8 Comparison of textures of austenitic and ferritic rolled samples.



bulk x-ray diffraction. Because it is the plane strain compression simulation, all samples show a lower texture index. The major texture fibers are also shown in [figure 8](#).

The austenitic regime-rolled sample shows strong α -fiber texture close to (113), and γ -fiber texture is uniformly distributed all along with $\langle 111 \rangle // \text{ND}$ in this sample. This can be linked to the randomizing effect of the transformations in phases after deformation in the austenitic region. It has a random texture with varying alpha, gamma, and cube texture with its maximum intensity at 113 $\langle 110 \rangle$, 111 $\langle 110 \rangle$, and 001 $\langle 010 \rangle$, respectively. The lower temperature ferritic rolling samples show pronounced deformation texture with predominantly α -fiber texture and γ -fiber textures. It is similar to that of the austenitic-rolled samples but with varying intensities. This is due to the absence of phase transformation and the softening after deformation.

Sample F1 processed at relatively higher temperatures shows the intensity of α -fiber and γ -fiber texture component maximum at (113) $\langle 110 \rangle$ and 111 $\langle 011 \rangle$, respectively. This sample has partial α -fiber, well-developed γ -fiber, and lower θ -fiber (RD// $\langle 100 \rangle$) texture as compared to other ferritic samples. This sample also shows the highest ratio of γ - to θ -fiber texture, making it the most formable material among all. The low-temperature ferritic sample F2 shows the development of unwanted cube fiber at 001 $\langle 010 \rangle$. It has a lower intensity of γ -fiber texture compared to the F1 sample with a maximum at (111) $\langle 121 \rangle$. Low-temperature rolling has reduced the α -fiber texture with presence only at 111 $\langle 110 \rangle$ in the F2 sample. Sample F3 shows the highest amount of cube 011 $\langle 010 \rangle$, goss (110) $\langle 100 \rangle$, and brass (110) $\langle 112 \rangle$ texture component among all the tested samples. The α -fiber and γ -fiber intensities are lowest in this sample among all. These initial textures²³ may result in poor formability after the cold rolling and the annealing.

The results match the findings of Tiitto²³ where hot deformation of niobium- and titanium-alloyed steels at a high temperature (870°C) in the ferritic region leads to higher {111} $\langle 110 \rangle$ intensities and higher r values in the

annealed condition than hot deformation at a low temperature (800°C). This initial hot-rolled texture in the F1 ferritic-rolled samples is the most favorable to the formation of higher final recrystallization texture after the cold rolling and the annealing for formability.¹² The above experiments have confirmed that it is feasible to produce steel under ferritic rolling conditions in an industrial hot strip mill, and the regime must be designed, taking temperature and reduction into account. Contrary to previous understanding,²⁰ which was based on single deformation steps or constant strain rate, present multiple deformation steps with high strain, and strain rates, it is concluded that the temperature range of 850°C to 800°C is the most suitable for ferrite rolling in an industrial hot strip mill, with the lowest flow stress or load requirement under the existing austenitic strain and strain rates rather than having fully soft or hard strips.

Plant Trials and Validation

Based on the simulation results, the full-scale plant trials of ferritic rolling were conducted in a 2-Hi, 2 stand roughing, and 7 stands finishing hot rolling mill. An IF-grade steel slab on 220-mm thickness was rolled in ferritic regime below A_{r1} temperature in the optimized range of 850°C to 800°C to the final thickness of 4.05 mm. The slab was taken out of the furnace at 1,130°C, and the finishing strand reductions were carried out between 835°C and 810°C. The finishing and CTs obtained were 810°C and 610°C, respectively. Samples were collected from the central portion of the tail end of the coil. For comparative study, samples were also collected from the conventional austenitic-rolled coils of a similar thickness, where the furnace exit temperature was 1,250°C, reduction carried out between 960°C and 930°C (above A_{r3}), and the achieved finishing and CTs were 920°C and 640°C, respectively. During the ferritic rolling in the optimized temperature band, the loads and currents were lower than the austenitic rolling values because of the softening effect of ferrite phase transformation.

Figure 9 shows the through-thickness variation of grain morphology of austenitic- and ferritic-rolled samples along the rolling direction in 100X magnification. In the austenitic-rolled sample that is due to complete recrystallization, the grain size or morphology is uniform along the thickness. In the ferritic-rolled sample, a thin layer of finely deformed and elongated grains was found on both the surfaces because of additional friction between the rolls and the steel at low-temperature rolling. However, this layer is very small at the optimized temperature regime without lubrication compared to the shear layer seen in the rolling simulated samples and could have been higher at further lower temperatures. The central portion shows uniform grain distribution, although slightly different morphology from the austenitic-rolled samples.

FIG. 9

Through-thickness grain size variation in austenitic and ferritic rolled samples.

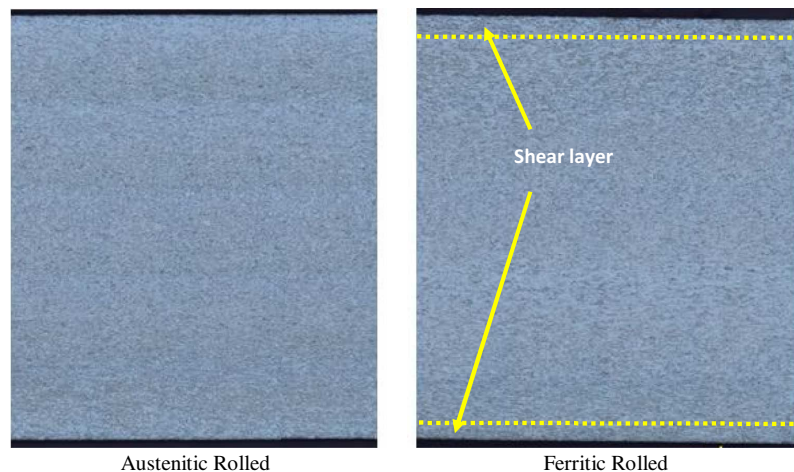


Figure 10 shows the comparison of grain morphology at a central plane in austenitic- and ferritic-rolled samples. Both the samples show a complete ferrite structure, but with different morphology. The austenitic-rolled sample shows typical equiaxed grains with size varying between 30 and 40 μm , resulting from complete recrystallization. Ferritic-rolled samples, in the absence of recrystallization, show elongated, deformed ferrite grains aligned along the rolling axis. It has nonuniform grain distribution with grain size varying between 10 and 30 μm . A small portion of grains has grown and bulged because of expected recovery, which is also found in F2 and F3 samples in the simulation trials. This strained microstructure also shows in-grain deformation or shear bands. These are locations of high dislocation density, which are formed during the ferritic rolling and nucleates favorable γ -fiber texture ($\langle 111 \rangle // \text{ND}$). The optimum temperature deformation resulted in an optimum combination of grain morphology with a mix of grains as seen in the F1 and F2 samples of the simulation study.

The texture was also measured using an x-ray diffractometer, and the comparison of texture orientation distribution function along ϕ (0° – 90°), ϕ_1 (0° – 90°), ϕ_2 at 45° section for the mid-section of the Rolling Direction - Transverse Direction plane in austenitic- and ferritic-rolled samples is shown in **figure 11**. Austenitic hot-rolled coil (austenitic rolled samples) shows nearly random texture with weak recrystallization texture components of α -fiber and γ -fiber along with cube and goss texture components. Austenite-rolled samples

FIG. 10

Comparison of grain morphology at a central plane in austenitic and ferritic rolled samples.

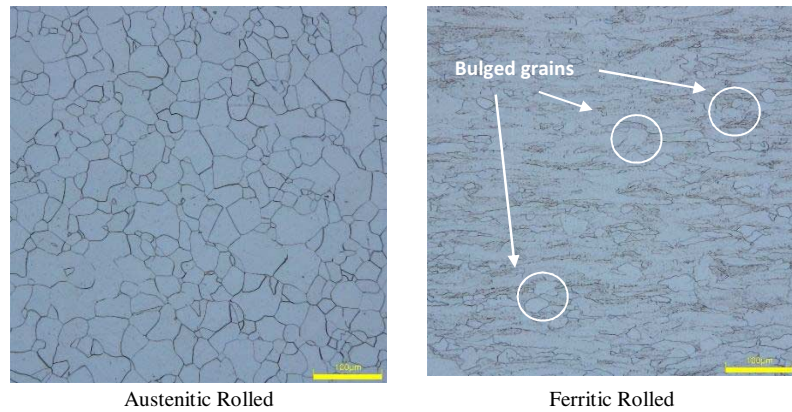
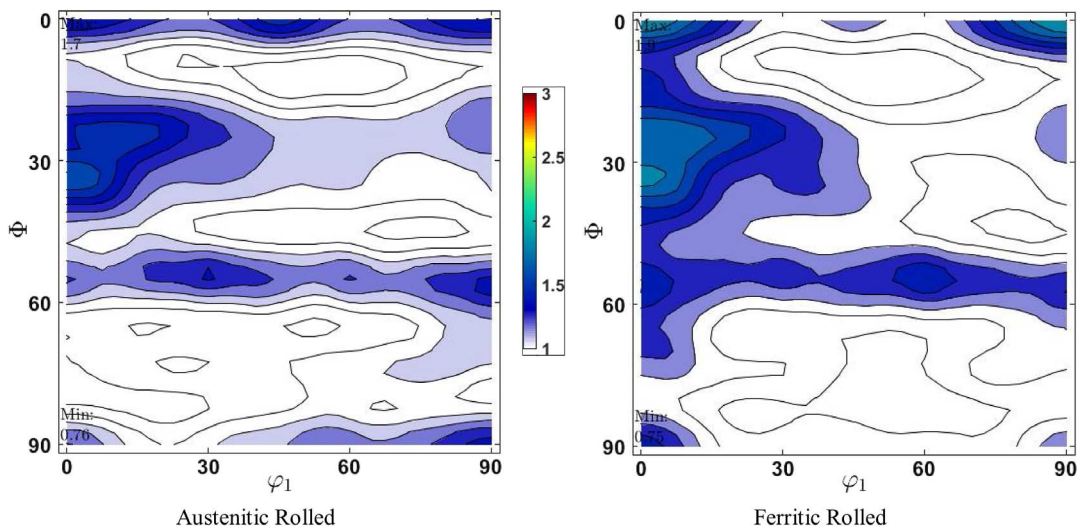


FIG. 11 Comparison of texture at the central plane in austenitic and ferritic rolled samples.



show predominantly alpha texture at $112\langle 110 \rangle$. Weak γ -fiber texture is uniformly distributed all along at $\langle 111 \rangle // ND$ in this sample. Ferritic-rolled samples show pronounced alpha and gamma texture compared to the austenitic samples. Other texture components are reduced at optimized ferritic rolling temperature. Gamma texture maximum was found at $111\langle 011 \rangle$, which contributes directly to the formability. The alpha texture maxima at $112\langle 110 \rangle$ also strengthens gamma texture after cold rolling and annealing. This texture distribution at the hot-rolled stage is most suited for achieving higher $\{111\}$ gamma-oriented grains and improved formability, after cold rolling and annealing compared to the austenitic rolled sheets. Orientation of grains from a randomized texture to sharper $\{111\}$ gamma texture in plant-rolled coil matches the simulation results. Plant trial results have validated the findings of the simulation experiments and establish that the assumptions and program used in the thermomechanical simulator matched the plant rolling.

Rolling at higher ferritic temperature regimes ($>850^\circ\text{C}$) results in the development of soft strip for direct usage, but because of prior recrystallization, these are very similar to austenitic coils and do not provide any advantage. Rolling at lower ferritic temperature regimes ($<800^\circ\text{C}$) results in the development of a hard strip for usage after direct annealing but found to have higher through-thickness variations and result in unwanted textures. Both the soft and the hard strips were found not suitable; rather, the semi-soft strips are the best intermediate product for subsequent cold rolling and annealing application. It is concluded that the ferritic-rolled niobium-titanium stabilized IF steels between the F1 and F2 temperature regime (deformation between 850°C – 800°C) will result in inhomogeneous microstructure and are expected to give a lower yield strength and a higher ductility compared to the conventionally produced austenitic-rolled coils. It will be a better input hot-rolled material for subsequent cold rolling and annealing than the existing austenitic-rolled material. The presently developed semi-soft hot strip can be utilized by all the existing hot strip mills and develop CRCA ferritic sheets with improved formability. This route not only eliminates the austenitic rolling issues in the existing mill but also provides an improved product compared to the austenitic-rolled material. In industrially rolled coils, it is expected to have improved deep drawing properties. Lowering of rolling temperature (120°C – 150°C) increases the possibility of energy savings and oxidation loss. Lower stress allows rolling of larger widths with less thickness and lowers shape defects, thereby decreasing the production costs.

Conclusions

Ferritic hot-rolled soft and hard strips are not suitable for production in the existing mills. Hence, for the existing mills, where subsequent cold rolling and annealing are to be carried out, the hot rolling temperature must be optimized. In the present work, the feasibility of producing niobium-titanium-stabilized IF-grade steel strip under the full ferritic rolling conditions with high strain and strain rates in an industrial hot strip mill is explored. The mill has been studied using a thermomechanical simulator. The flow stress of the material first decreased and then increased as the ferritic deformation temperature is lowered. High-temperature ferritic-rolled material ($>850^\circ\text{C}$) shows equiaxed microstructure and random texture, whereas low-temperature rolled material ($<800^\circ\text{C}$) resulted in duplex grains with an unwanted cube and goss texture components. A deformation temperature range of 850°C to 800°C was found to be the most suitable working window for ferrite rolling, which produces a semi-soft product having reduced load requirement and achieving a favorable grain morphology and texture with higher intensity of gamma and alpha texture required for higher formability. This was validated through plant trials, which confirmed the simulation results.

References

1. A. Tomitz and R. Kaspar, "Ferritic Rolling to Produce Soft Deep Drawable Thin Hot Strips," *Steel Research* 71, nos. 6–7 (June 2000): 233–238.
2. S. Hoile, "Processing and Properties of Mild Interstitial Free Steels," *Materials Science and Technology* 16, no. 10 (October 2000): 1079–1093.
3. A. de Paepe, J. C. Herman, and V. Leroy, "Deep Drawable Ultra Low Carbon Ti IF Steels Hot Rolled in the Ferrite Region," *Steel Research* 68, no. 11 (1997): 479–486.

4. A. Elsner, R. Kaspar, D. Ponge, D. Raabe, and S. van der Zwaag, "Recrystallization Texture of Cold Rolled and Annealed IF Steel Produced from Ferritic Rolled Hot Strip," *Materials Science Forum* 467–470 (October 2004): 257–262.
5. C. J. Barrett and B. Wilshire, "The Production of Ferritically Hot Rolled Interstitial-Free Steel on a Modern Hot Strip Mill," *Journal of Materials Processing Technology* 122, no. 1 (March 2002): 56–62.
6. P. Messien and J. C. Herman, "r-Value Improvement of Steel Using Hot Rolling Lubrication" (presented at the International Symposium on Low-Carbon Steels for the 90's, Pittsburgh, PA, October 18–21, 1993).
7. A. O. Humphreys, D. Liu, M. R. Toroghinejad, E. Essadiqi, and J. J. Jonas, "Warm Rolling Behavior of Low Carbon Steels," *Materials Science and Technology* 19, no. 6 (June 2003): 709–714.
8. T. Sakai, Y. Saito, and K. Kato, "Texture Formation in Low Carbon Ti-Bearing Steel Sheets by High Speed Rolling in Ferrite Region," *Transactions of the Iron and Steel Institute of Japan* 28 (1988): 1036–1042.
9. R. G. Bruna, "Effects of Hot and Warm Rolling on Microstructure, Texture, and Properties of Low Carbon Steel," *Metallurgy and Materials* 64, no. 1 (March 2011): 57–62.
10. H. Grobheim, K. Schotten, and W. Bleck, "Physical Simulation of Hot Rolling in the Ferrite Range of Steels," *Journal of Materials Processing Technology* 60, nos. 1–4 (June 1996): 609–614.
11. H. Takechi, "Metallurgical Aspects on Interstitial Free Sheet Steel from Industrial Viewpoints," *ISIJ International* 34, no. 1 (1994): 1–8.
12. R. K. Ray, J. J. Jonas, and R. E. Hook, "Cold Rolling and Annealing Textures in Low Carbon and Extra Low Carbon Steels," *International Materials Reviews* 39, no. 4 (1994): 129–172.
13. W. Chang, W. Yu, H. Yang, Z. Man, and Y. Cao, "Effect of Ferritic Hot Rolling Process on Microstructure and Properties of IF Steel," *Materials Science Forum* 993 (May 2020): 505–512.
14. M. Ferry, D. Yu, and T. Chandra, "Influence of Hot Deformation Conditions on the Annealing Behaviour of Cold Rolled Ultra Low Carbon Steel," *ISIJ International* 41, no. 8 (2001): 876–882.
15. Y. Guo, Z. Wang, W. Zou, X. Liu, and G. Wang, "Textures and Properties of Hot Rolled High Strength Ti-IF Steels," *Journal of Iron and Steel Research International* 15, no. 5 (September 2008): 70–76, [https://doi.org/10.1016/S1006-706X\(08\)60252-6](https://doi.org/10.1016/S1006-706X(08)60252-6)
16. W. C. Jeong, "Effect of Hot-Rolling Temperature on Microstructure and Texture of an Ultra-Low Carbon Ti-Interstitial-Free Steel," *Materials Letters* 62, no. 1 (January 2008): 91–94, <https://doi.org/10.1016/j.matlet.2007.04.081>
17. S. Matsuoka, M. Morita, O. Furukimi, and T. Obara, "Effect of Lubrication Condition on Recrystallization Texture of Ultra-Low C Sheet Hot-Rolled in Ferrite Region," *ISIJ International* 38, no. 6 (1998): 633–639, <https://doi.org/10.2355/isijinternational.38.633>
18. C. J. Barrett, "Influence of Lubrication on Through Thickness Texture of Ferritically Hot Rolled Interstitial Free Steel," *Ironmaking & Steelmaking* 26, no. 5 (1999): 393–397, <https://doi.org/10.1179/030192399677176>
19. G. H. Akbari and C. M. Sellars, "Microstructure Development during Warm Rolling of an IF Steel," *Acta Materialia* 45, no. 12 (December 1997): 5047–5058, [https://doi.org/10.1016/S1359-6454\(97\)00170-5](https://doi.org/10.1016/S1359-6454(97)00170-5)
20. K. Okuda and K. Seto, "Recrystallization Behaviour of IF Steel Sheets Immediately after Hot-Rolling in Ferrite Region," *ISIJ International* 53, no. 1 (January 2013): 152–159.
21. M. X. Jia, Y. P. Lü, L. F. Xu, and Y. P. Song, "The Influence of Friction on the Texture Formation of an IF Steel during Hot Rolling in the Ferrite Region," *Steel Research International* 84, no. 8 (April 2013): 761–765, <https://doi.org/10.1002/srin.201200260>
22. P. H. Harlet, F. Beco, P. Cantineaux, D. Bouqueneau, P. Messien, and J. C. Herman, "New Soft Steel Grades Produced by Ferritic Rolling at Cockerill Sambre," in *International Symposium on Low-Carbon Steels for the 90's*, ed. G. Tither and R. Asfahant (Pittsburgh, PA: The Minerals, Metals and Materials Society, 1993), 389–396.
23. K. M. Tiitto, C. Jung, P. Wrav, C. I. Garcia, and A. J. Deardo, "Evolution of Texture in Ferritically Hot Rolled Ti and Ti + Nb Alloyed ULC Steels during Cold Rolling and Annealing," *ISIJ International* 44, no. 2 (2004): 404–413, <https://doi.org/10.2355/isijinternational.44.404>
24. X. Guang, C. Zhenye, L. Li, and Y. Shengfu, "Deformation Behaviour of Ultra-Low Carbon Steel in Ferrite Region during Warm Processing," *Journal of Wuhan University of Technology—Materials Science Edition* 23 (February 2008): 29–32, <https://doi.org/10.1007/s11595-006-1029-6>
25. V. Kumar, "Thermo-mechanical Simulation Using Gleeble System - Advantages and Limitations," *Journal of Metallurgy and Materials Science* 58, no. 1 (January–March 2016): 81–88.
26. R. A. Morgridge and P. Karjalainen, "Hot-Rolling Simulation and Modelling Using Gleeble 1500," *Steel Research* 63, no. 7 (July 1992): 297–303, <https://doi.org/10.1002/srin.199200520>
27. W. Fan, P. Tian, Y. Kang, J. Zhu, Z. Qin, and L. Chen, "Simulation Experimental Study on Ferrite Rolling Process of Low-Carbon Steels," *Materials Science Forum* 944 (January 2019): 329–336, <https://doi.org/10.4028/www.scientific.net/MSF.944.329>
28. R. Z. Wang and T. C. Lei, "Dynamic Recrystallization of Ferrite in a Low Carbon Steel during Hot Rolling in the (F+A) Two-Phase Region," *Scripta Metallurgica et Materialia* 31, no. 9 (November 1994): 1193–1196, [https://doi.org/10.1016/0956-716X\(94\)90575-4](https://doi.org/10.1016/0956-716X(94)90575-4)
29. B. Tang, L. Xiang, L. Cheng, D. Liu, H. Kou, and J. Li, "The Formation and Evolution of Shear Bands in Plane Strain Compressed Nickel-Base Superalloy," *Metals* 8, no. 2 (February 2018): 141, <https://doi.org/10.3390/met8020141>



Optimization of Annealing Parameters for Ferritic Hot-Rolled IF Grade Steel

D. Satish Kumar¹ · S. Manjini¹ · K. Udaya Bhat²

Received: 20 November 2021 / Revised: 21 January 2022 / Accepted: 21 January 2022
© ASM International 2022

Abstract

Ferritic hot rolling of low carbon steel is now widely adopted by steelmakers for reducing energy costs and increasing the yield. These ferritic hot-rolled coils carry forward different grain morphology and texture which result in variation in properties after cold rolling and annealing compared to austenitic hot-rolled coils. These ferritic hot-rolled coils require different annealing treatments based on the hot rolling temperature for better results. In the present work, a Nb–Ti stabilized interstitial free (IF) grade steel was hot rolled at two different temperatures in the ferritic regime in an industrial hot strip mill and was subsequently cold rolled. These cold-rolled sheets were subjected to different continuous annealing cycles with soaking temperatures varying from 740 to 820 °C on a thermo-mechanical simulator for optimization of temperatures and study its effect on microstructure and properties. These coils were compared with simulated conventional austenitic hot-rolled coils. Ferritic rolled coils show better elongation and a higher percentage of equiaxed grains indicating better formability. The optimum continuous annealing temperature was found to be a function of hot rolling temperature in the ferritic regime. Elongation and grain size increased with an increase in temperature in all the samples, but the ferritic rolled coils show faster change due to higher stored energy. Comparison of elongation and microstructure indicates that temperatures above 780 °C should be sufficient for achieving complete recrystallization in ferritic rolled samples, compared to 810 °C required in the conventional austenitic rolled sheets which is an industrial advantage. Based on simulation studies, full-scale plant continuous annealing was carried out under the optimized temperature conditions where microstructure and properties matched closely with the simulation results and electron backscatter diffraction (EBSD) analysis confirmed improved texture.

Keywords Carbon steels · Ferritic rolling · Light microscopy · Microstructure

Introduction

The low carbon and IF grade steels have good formability and are extensively utilized for automotive and other complex shape applications. Due to stringent surface finish and quality requirements, these are low yield and high-cost products. Low carbon composition restricts the process parameters during re-heating to be maintained in a higher temperature range. Thin gauge ferritic hot-rolled IF steels,

either directly or after an annealing treatment, have been presented as a low-cost replacement of cold-rolled sheets to reduce the production cost [1]. Though these materials have been reported to have good formability characteristics on a laboratory scale, industrial production was rarely adopted due to practical difficulties [2]. In some recent studies [3, 4], these hot ferritic hot-rolled coils were subjected to subsequent cold rolling and annealing similar to conventional austenitic rolling and were found to have improved characteristics. Such a processing route saves on the cost of processing, improves yield and can be adopted in existing rolling mills without any changes. However, ferritic hot rolling involves deformation below A_{r1} temperature, which changes the grain morphology and orientation in the hot-rolled sheet compared to the austenitic hot-rolled sheet [4]. Their subsequent processing through cold rolling and annealing is expected to further vary the final microstructure and texture. This may result in variation in the formability

✉ K. Udaya Bhat
udayabhatk@gmail.com

D. Satish Kumar
satishkumar.dabbiru@jsw.in

¹ Research and Development, JSW Steel Ltd, Vijayanagar Works, Bellary 583275, India

² Department of MME, National Institute of Technology Karnataka, Surathkal 575025, India

characteristics of the final product. Formability is an important requirement in interstitial free (IF) grade steels for various direct and indirect applications. Even the perforation in the sheets affects the final formability where diameter, layout of the punched holes and material characteristics and is reported to have significant effect [5]. It is reported [6] to be a function of final grain orientations and texture developed through previous processing steps. Even with similar yield strength and ultimate tensile strength, the difference in the grain orientations and texture was found after cold rolling and annealing in previous studies [7–9]. Steel sheets hot rolled under ferritic regime closer to A_{r1} temperature results in "soft" hot strips and when rolled at temperatures much lower than A_{r1} temperature results in "hard" hot strips. Studies on varying cold reduction in IF grade ferritic rolled "soft" or "hard" hot strips show that "soft" hot strips result in the highest mean r -values, whereas "hard" hot strips result in improved planar anisotropy when processed under similar annealing conditions [8]. Conventional austenitic hot-rolled coils show intermediate values, which indicates the importance of ferritic rolling temperature. Microstructural changes during annealing, not only releases much larger amounts of stored energy but larger new grains are also formed by the nucleation of strain-free grains and the coalescence of many smaller grains to form larger ones. This change is dependent on inherent stresses which is a function of ferritic rolling temperature [9]. In ferritic hot-rolled IF grade coils, the distribution of texture and grain morphology also varies non-uniformly along with the thickness and its severity increases with a decrease in temperature and lubrication [10]. This factor must also influence the annealing temperature. In these steels, the major orientation textures found include gamma and alpha, with gamma being most preferred texture for better formability. During continuous annealing, alpha orientation components increase first but latterly the gamma orientation components increase with the increase in annealing temperature but the strain hardening exponent n value and r value continuously increase with temperature [11]. A combination of these parameters in ferritic rolled coils must be optimized. Compared to low carbon steels, the IF steel behaviour is reported to be more dependent [12] on the annealing temperature due to its low carbon and more oriented grains in developing $\langle 111 \rangle$ texture suitable for formability. It is found that more γ -fibre recrystallization texture is formed after cold rolling and annealing in coils having higher γ -fibre after hot rolling [3]. The amount of γ -fibre in a hot-rolled sheet is again a function of temperature and hot rolling conditions. In one of the previous studies [4] about Ti-IF steel, ferritic hot-rolled at 791 °C and with 86% cold reduction, the yield strength (YS), ultimate tensile strength (UTS), and yield ratio decreased and r value and n value increased with increasing annealing temperature from 730 to 820 °C which was related to the sizes of TiN and TiS

precipitates which did not change but the sizes of Ti_4C_2S and TiC precipitates increased with the increase in annealing temperatures. From the studies mentioned previously, it is clear that the final properties of ferritic rolled sheets depend on the cold rolling and annealing parameters. Hence, the cold rolling and more specifically annealing parameters must be optimized to have fixed properties for ferritic rolled sheets. The cold-rolled sheets are continuously annealed for controlled recrystallization and relieving stresses. The continuous annealing heating cycle plays an important role as it develops the microstructure which determines the final mechanical properties [13]. The continuous annealing heating cycle in an annealing furnace is divided into several sub-sections. The coil is first passed into preheating section, then heating section, soaking section followed by slow cooling section, rapid cooling section, overageing section and fast cooling in the end. In spite of many sections, the key property controlling parameters of any continuous annealing heating cycle are inter-critical annealing temperature, soaking duration and cooling rate. These continuous annealing heating cycle parameters are in turn dependent on composition and thickness. The development of strength in these processes is by phase transformation and precipitation and is controlled by line speed and strip temperatures [11, 14]. Improper control of these parameters results in microstructures and texture variations which result in changes in properties required for desired applications. Hence, it is important to develop the process parameters specific to different compositions to achieve the desired properties in the final sheet. Since the ferritic rolled sheets have a different stress distribution and grain morphology, the annealing cycle must be selected different from the conventional cycles, followed for austenitic rolled sheets. Change or optimization of furnace temperatures during continuous annealing in plant is costly and not feasible. In the present work, offline experiments were carried out to simulate the existing continuous annealing line in a thermo-mechanical simulator (Gleeble). Gleeble system is an efficient, fast and accurate simulator for complex heating cycles involving multistep heating and cooling steps. Gleeble has been regularly used for such simulations due to its versatility and precise controlling capabilities. In Nb or Ti stabilised steels, the formability is reported not sensitive to heating rate but to the soaking temperature [5]. This work also aims to find an optimized annealing temperature regime for an IF grade cold-rolled sheet, produced from industrially ferritic hot-rolled coils and compare it with austenitic hot-rolled sheets.

Table 1 Composition of selected IF grade, wt.%

C	Mn	Si	Al	S	P	Ti	Nb	B	N
0.002	0.17	0.006	0.036	0.007	0.011	0.027	0.011	0.0001	0.0025

Materials Processing and Simulation

Processing of Austenitic and Ferritic Rolled Steel

IF grade steels are the most commonly used high formability material, regularly produced under austenitic rolling conditions which requires high annealing temperatures ($>800\text{ }^{\circ}\text{C}$) after cold rolling for complete recrystallization. Hence, in the present study, an Nb–Ti stabilized IF grade hot-rolled steel was been selected for simulation studies and industrial trials. The chemical composition (wt.%) of the selected grade is shown in Table 1.

Two slabs of the continuously cast IF grade were selected for industrial ferritic rolling in a 2-Hi, 2 stand roughing and 7 stands finishing hot rolling mill. Transformation start temperature Ar_3 and transformation finish temperature Ar_1 temperatures for the above composition were ~ 905 and $\sim 871\text{ }^{\circ}\text{C}$, respectively. To study the effect of low-temperature deformation in the ferritic regime, 220-mm-thick slabs were hot rolled at two different temperatures below the Ar_1 temperature up to 4 mm thickness. For the upper ferritic temperature regime rolling, coil (namely FR1) was processed at a finish rolling temperature of $825\text{ }^{\circ}\text{C}$ and coiling temperatures of $625\text{ }^{\circ}\text{C}$. For the lower ferritic temperature regime rolling, coil (namely FR2) was processed at a finish rolling temperature of $780\text{ }^{\circ}\text{C}$ and coiling temperature of $575\text{ }^{\circ}\text{C}$. Conventional austenitic rolling takes place at a finish rolling temperature of $920\text{ }^{\circ}\text{C}$ and coiling temperature of $640\text{ }^{\circ}\text{C}$. Ferritic rolled coils were found to be in good shape and had no rolling issues. These two ferritic rolled coils along with austenitic rolled coils were subsequently cold rolled in an industrial cold rolling mill. These hot-rolled coils were first pickled in hydrochloric acid to remove the oxide layer and subsequently cold rolled in a 5 stand tandem cold rolling mill. The total 76% reduction was given to achieve the final coil thickness of 1 mm. The two different temperature ferritic hot rolled coils are expected to develop different grain morphology and orientations [3], which on subsequent cold rolling and annealing is expected to give differences in properties compared to conventional austenitic rolled coils. Before further processing through continuous annealing and skin pass mill, these full-hard cold-rolled sheets (2 ferritic rolled coils, FR1 and FR2 and a representative austenitic rolled coil AR) were kept aside, and samples were cut for offline annealing simulation.



Fig. 1 Specimens for strip annealing simulations in Gleeble

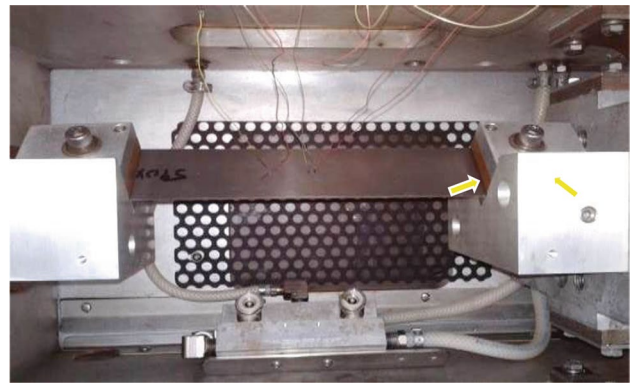


Fig. 2 Thermocouple arrangements during strip annealing simulations set-up in Gleeble

Annealing Simulation

Representative cold-rolled full hard sheets of both the ferritic rolled coils and the one austenitic rolled coil of similar thickness were collected and cut from the tail end of the coil, due to ease of sampling. These sheets were further cut to experimental dimensions of $240 \times 50\text{ mm}$ size with 5 mm diameter holes on either side (for fixing in the simulator), as shown in Fig. 1. All the samples were cleaned with acetone to remove any dirt or scale.

On these samples, chrome–alumel thermocouple wires were welded and then fixed inside pocket jaw module with strip annealing grips. Figure 2 shows the arrangement for strip annealing simulation in Gleeble 3800 thermo-mechanical simulator. The continuous annealing process was broadly divided into four stages, heating section, soaking section, rapid cooling section and the overageing section. These sections were programmed into the simulator in a time-temperature plot.

In annealing, the soaking temperature is the most critical parameter. Other parameters are optimised as per the production requirement. Hence, in this work, simulations were carried out to study the effect of soaking temperature on the ferritic rolled samples compared to the austenitic rolled

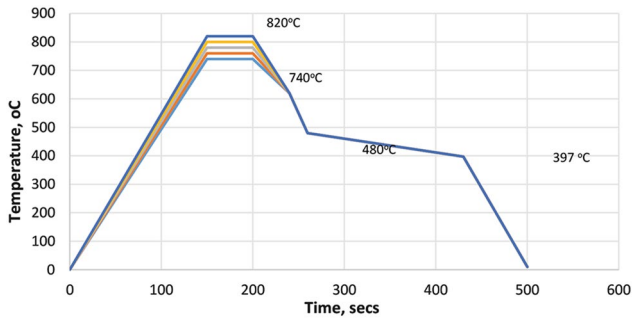


Fig. 3 Simulated annealing cycles



Fig. 4 Strip sample after annealing simulation in Gleeble

samples and to identify the optimized temperature band. The conventional austenitic rolled sheet was annealed at 800–820 °C during the actual production. The samples from all three coils were subjected to soaking temperatures of 740, 760, 780, 800 and 820 °C. The heating rate was programmed at 5 °C/s, and the soaking time was kept for 45 s. In the rapid cooling section, the strip was cooled at the rate of 14 °C/s till 480 °C. The final overaging was done at 397 °C before cooling to room temperature at a speed of 5 °C/s. Other than the soaking temperature all other parameters were kept similar to the conventional austenitic annealing cycle. The annealing cycles simulated are shown in Fig. 3.

Characterisation

Three samples were tested under each cycle. Figure 4 shows the condition of the sample after annealing simulation. The samples did not show any excessive oxidation and uniform surface near the central portion. These Gleeble simulated samples were tested in an (universal testing machine) UTM for mechanical properties and checked under an optical microscope for microstructure to find the optimized cycle producing the largest grains and highest elongation. The samples for the tensile test samples were precisely cut out of the simulated specimens as shown in Fig. 5 and subjected to the tensile test for strength and elongation. Two samples were subjected to tensile test, and one sample was used for the microscopy study after polishing and etching.

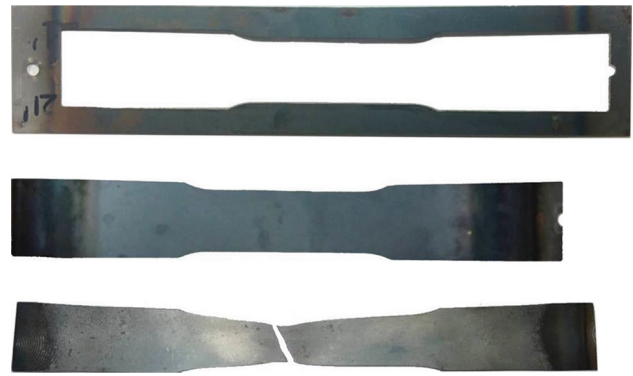


Fig. 5 Tensile test specimen punched out and tested from the annealed sample

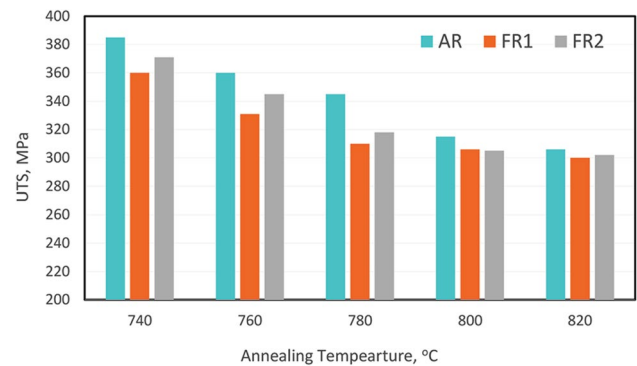


Fig. 6 The comparison of ultimate tensile strength in annealing simulated samples

Results and Discussion

Cold rolling is a basic strengthening process. The steel sheets after cold rolling have high ultimate tensile strength (UTS) and low elongation. However, during the annealing process, due to stress relieving and recrystallization, the strength decreases and the elongation increases. Figure 6 shows the comparison of the ultimate tensile strength (UTS) in simulated annealed samples. The UTS values (average of two samples values) in all samples are within the grade acceptable limits, confirming the accuracy of the annealing cycles. The UTS values are relatively higher for the AR samples due to incomplete recrystallization compared to the FR samples. The ultimate tensile strength decreases with increasing annealing temperature in all samples. This confirms the softening of the material with increase in temperature. With increase in temperature, the recrystallization process and carbide dissolution move towards completion resulting in decrease in strength and increase in elongation. Also, the increase in grain size and reduction in residual

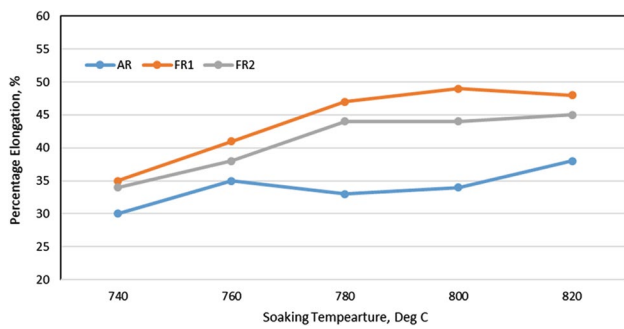


Fig. 7 Change in percentage elongation with an increase in temperature in annealing simulated samples

stresses at higher temperatures contributes to reduction in strength. The rate of change of strength decreases at the higher temperature when the recrystallization is completed and residual stresses are all eliminated.


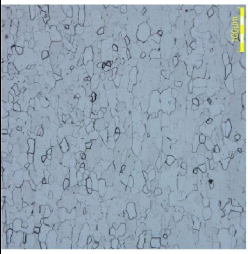
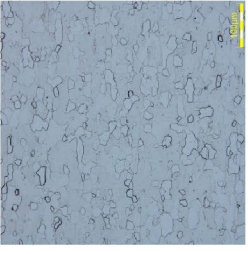
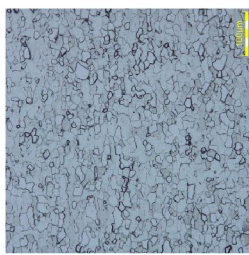
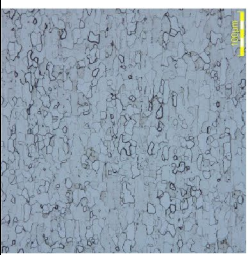

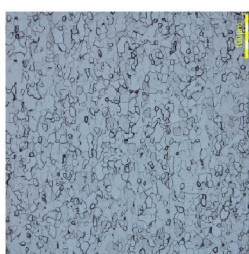
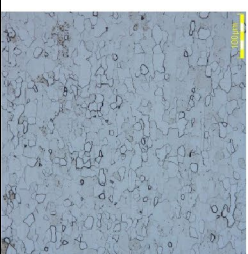
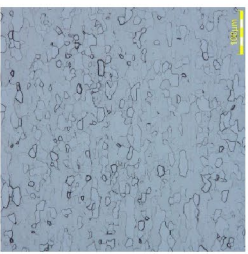
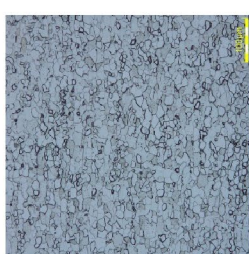
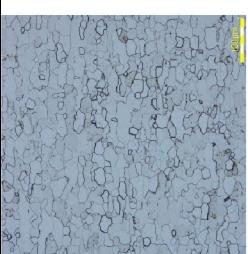
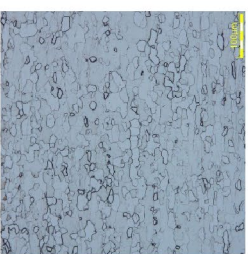
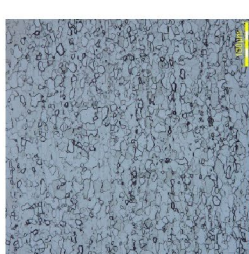
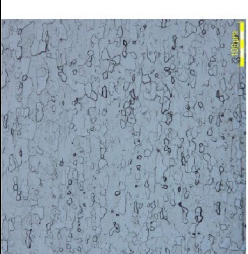
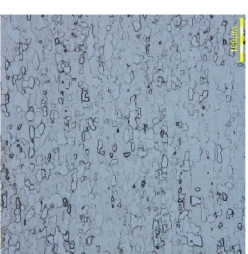
In addition to strength, formability is also an important requirement in these grades. The sample size used for Gleeble simulation is smaller in size and bulk formability cannot be measured. Hence, elongation measured through tensile test is considered as formability criterion in such simulated samples and higher elongation indicates higher formability [15]. Figure 7 shows the change in percentage elongation with an increase in soaking temperature. The elongation increased continuously with an increase in annealing temperature in all the samples. FR1 sample achieved greater than 40 % elongation, (normally desired in these grades) at annealing temperatures between 760 and 780 °C and FR2 samples at 780°C. This can be related to higher stored energy which promotes faster nucleation and higher grain growth at lower temperatures. The bulk of the energy generated during the hot rolling process or the deformation of steel is dissipated as heat. A small fraction of this energy stored in the material, which act as the driving force for recrystallization during annealing. This stored energy comes from lattice strains and the crystalline imperfections generated during the rolling process which again is a function of temperature [16]. Lower temperature deformations or rolling as in FR1 and FR2 generates more strains and imperfections raising the stored energy. The presence of higher deformation heterogeneity and in-grain shear bands in low temperature deformed material creates preferential sites for start of recrystallization nucleation. Higher stored energy gradient also increases the growth rate [17]. AR samples achieved close to 40 % elongation when annealed beyond 800 °C. Among the two ferritic hot-rolled samples, high-temperature sample FR1 shows marginally improved properties due to comparatively better through-thickness uniformity in hot-rolled stage sheets. There is no significant increase in elongation in ferritic rolled samples beyond 800 °C, whereas the

AR samples may require higher temperature annealing to reach grain size stability.

The microstructures of the samples were characterized through optical microscopy for the study of grain size and grain size distribution. Table 2 shows the comparison of microstructures and grain size for the ferritic and austenitic rolled samples. The elongated and the deformation bands of the cold-rolled samples are expected to get converted into uniform polygonal grains during annealing. The ferritic recrystallized grains forming in all samples have predominantly polygonal morphology. All the low-temperature annealing simulated samples show a small amount of deformed ferrite, with a relatively higher proportion in AR samples. The microstructure shows that at 740 °C, the stress relieving is completed and recrystallization or the nucleation of new grains has started but did not reach its completion. The grains in AR samples are smaller compared to FR samples at all the experimental temperatures indicating slower recrystallization in AR samples. The high-temperature ferritic rolled FR1 samples show a marginally higher grain size than for the low temperature rolled FR2 samples. The grains in the sample annealed at 780 °C are in the range of 10–15 μm in AR samples and 14–18 μm in both FR samples. The grains increased in size when annealed at 820 °C and are in the range of 20–24 μm in AR samples and 22–26 μm in both the FR samples. The grains in both the AR and FR samples continuously increased in size with the increase in annealing temperature. The increase in the size of grains becomes negligible, after 780 °C in FR1 samples and after 800 °C in FR2 samples, but have a higher increase in AR samples even at 820 °C. The percentage of the non-uniform morphological grains is higher in FR2 samples and can be correlated with initial higher stained elongated grains higher deformation and higher stored energy in FR2. In this process, the growth of individual grains is a function of grain boundary free energy and grain features, which is again affected by temperature and composition [18]. Higher stored energy makes the nucleation rate of the new grains faster than the nucleated grains growth rate. In such materials, newly formed grains sweep the deformation microstructure discontinuously [19]. The grains in AR samples are expected to grow bigger and rounded at further higher temperatures.

Results show that increasing the annealing temperature increases the elongation and grain size. However, beyond a certain temperature, its effect becomes constant. In industrial practice operating at higher soaking temperature is costly and difficult to maintain. It is always aimed to operate at the lowest possible temperature for achieving the desired properties. The comparison of elongation and microstructure indicates that temperatures above or equal to 780 °C should be sufficient for achieving complete recrystallization at the existing speeds in ferritic rolled samples, compared to 800 °C required in the conventional austenitic rolled sheets.

Table 2 Comparison of microstructures and grain size of annealing simulated samples

820 °C			
800 °C			
780 °C			
760 °C			
740 °C			
Soaking temperature	AR	FR1	FR2

It is therefore planned to anneal the ferritic rolled samples between 780 and 800 °C soaking temperature during plant processing. This lower soaking temperature requirement is an advantage for the ferritic rolled samples.

Plant Trials and Validation

To validate the simulation results, the cold-rolled sheets were processed through continuous annealing and skin pass

in an industrial continuous annealing mill. In the heating stage, the ferritic coils were heated from room temperature to soaking temperature of 780 °C, which was lower than the conventional austenitic rolling carried out at 820 °C. All other parameters were maintained similar to conventional austenitic rolling. The heating rate was maintained at 5 °C/s, and the soaking time was 45secs. In the rapid cooling section, all the coils were cooled to 480 °C at the rate of 14 °C/s. The final step overageing was done at 397°C before cooling to room temperature at a speed of 5 °C/s. The used annealing cycles for both ferritic rolled coils and the austenitic rolled coils are shown in Fig. 8. These annealed coils were subjected to skin pass reduction of 0.9%.

For comparative study, full-width samples were collected from the tail portion of both the ferritic rolled coils (FR1 and FR2) and a representative austenitic rolled coil (AR)

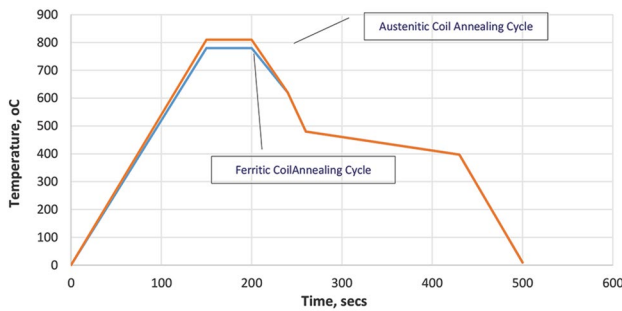


Fig. 8 Annealing cycle followed for the experimental coils

Table 3 Comparison of mechanical properties of austenitic and ferritic rolled samples

	AR	FR1	FR2
YS, MPa	155–159	145–150	150–160
UTS, MPa	290–305	280–300	280–300
%El	39–40	51–53	49–51
\bar{r} (r -bar)	2.10	2.15	1.93
n	0.23	0.26	0.25

rolled to a similar thickness. Customized samples were cut for tensile testing and microscopy.

Table 3 shows the comparison of mechanical properties for the conventional austenitic hot-rolled sheets (810 °C annealed) and the ferritic regime optimized annealing temperature rolled coils (780 °C, annealed) after cold rolling and annealing. The yield strength and tensile strength of both ferritic rolled coils were found in a similar range when compared to the conventional austenitic hot-rolled coils. Elongation has increased significantly in both the ferritic hot-rolled coils. The formability characteristics \bar{r} —normal anisotropy shows increased values in the FR1 sample but marginally reduced in FR2 samples. This can be attributed to a greater fraction of elongated grains in the initial structure resulting from the low-temperature rolling. The n —strain hardening exponent increased in both the FR1 and FR2 samples. Higher \bar{r} results in reduced flow stress and is beneficial for deep drawing, and a higher n -value reduces wrinkling. This establishes that ferritic rolled IF steels annealed at lower temperatures can yield better formability characteristics compared to conventional austenitic rolled coils.

Samples were cut from the coil, polished and etched using nital for microscopic analysis. The comparison of the microstructures observed under an optical microscope is shown in Fig. 9 Microstructure observation shows large ferritic grains in all three samples. Both the ferritic rolled samples FR1 and FR2 samples show recrystallized microstructure with rounded grains, whereas the AR samples show polygonal morphology of the grains. Comparatively higher roundness and uniformity in the grains found in the FR2 sample. The grains in AR, FR1 and FR2 samples varied in the size ranges of 23.5–24.5 μm , 23–24 μm and 22.5–23.5 μm , respectively. Grains are marginally finer in the FR1 and FR2 samples resulting from final grains in the initial structure and should be the reason for lower planar anisotropy (Δr).

Texture is an important characteristic for determining the formability. Metals are polycrystalline material, and the mass orientation of these crystals is called textures. During deformation, the ease of material flow is determined by glide of loops on crystallographic planes in crystallographic

Fig. 9 The comparison of the microstructures after cold rolling and annealing

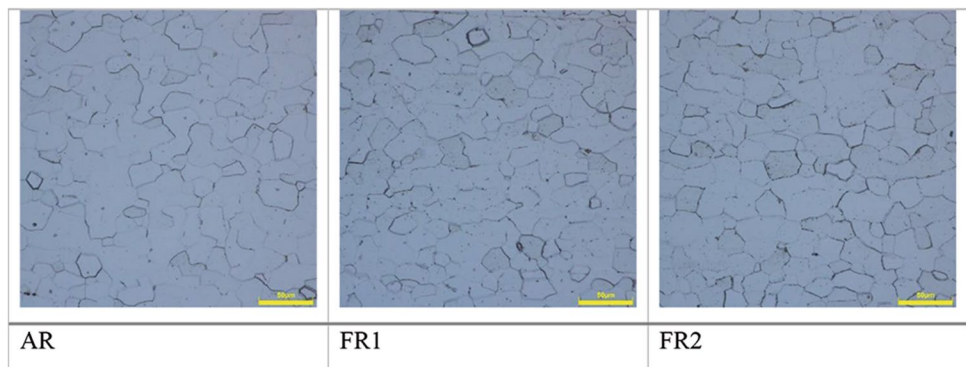
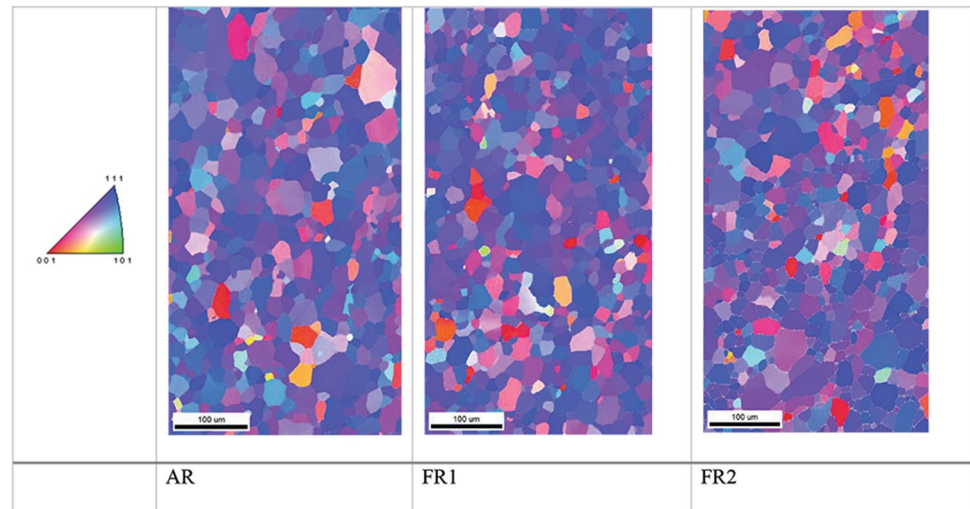


Fig. 10 The comparison of inverse pole figure maps from EBSD analysis



directions [20]. The mass orientation of these slip planes in a particular direction is measured as textures for defining particular property. For better formability, the slip movement should be uniform in all directions and is possible when $\langle 111 \rangle$ crystallographic plane is parallel to the sheet plane. This $\langle 111 \rangle$ orientation of grains parallel to normal direction (ND) is called the gamma texture and should be predominantly present for higher formability [20]. Electron backscatter diffraction (EBSD) analysis was also carried out on the cold-rolled and annealed samples hot rolled in both ferritic and austenitic regimes for texture analysis. Figure 10 shows the comparison of inverse pole figure maps from EBSD analysis along with the standard stereo-triangle having three important textures $\langle 111 \rangle$, $\langle 001 \rangle$ and $\langle 101 \rangle$. It is seen that all three samples (AR, FR1, and FR2) have predominantly gamma texture $\langle 111 \rangle$ indicated by a larger amount of blue coloured grains. AR sample shows a higher amount of other intermediate textures indicated by red and orange colour grains. Higher orientation towards the $\langle 111 \rangle$ or the gamma texture evolves from the in-grain shear bands and deformation bands resembling in-grain shear bands [21] in the ferritic rolled sheets. Gamma texture-oriented grains and grains of other orientations are of similar size in FR1 and FR2 samples, whereas the other orientation grains are bigger in AR samples. This can be attributed to the difference in the recrystallization behaviour due to inherited hot rolled texture. This confirms that optimized low temperature annealing does not affect the formability of the ferritic rolled sheets.

The grain size and morphology in the plant rolled samples matched closely with the simulated samples and hence authenticated the findings of the simulation experiments. It validates the assumptions and programme used in the thermo-mechanical simulator matched the plant rolling. Though the ferritic rolling temperature does not make a significant difference in properties, a high-temperature rolling

regime should be preferred. This work establishes that ferritic hot-rolled coils can be subsequently cold and annealed to achieve better properties at lower annealing temperatures, giving energy savings.

Conclusions

A Nb–Ti stabilized IF grade steel was hot rolled in austenitic and ferritic conditions for developing a product to be used in cold-rolled and annealed conditions. The cold-rolled sheets were simulated for optimization of annealing temperatures in a thermo-mechanical simulator before the plant processing. High-temperature ferritic rolled coils show better formability properties than low-temperature ferritic rolled and austenitic rolled coils. Ferritic rolled coils can be annealed at 780 °C by achieving complete recrystallization compared to 810 °C required in the conventional austenitic rolled sheets, which results in significant energy savings. Continuous annealing of cold-rolled sheets in an industrial mill validated the simulation results. This new processing will help in the wider adoption of the ferritic rolling process on an industrial scale for developing high formability sheets in cold-rolled and annealed conditions.

References

1. A. Tomitz, R. Kaspar, Ferritic rolling to produce soft deep drawable thin hot strips. *Steel Res.* **71**(6–7), 233–238 (2000)
2. T. Hiroshi, Metallurgical aspects on interstitial free sheet steel from industrial viewpoints. *ISIJ Int.* **34**(1), 1–8 (1994)
3. C. Wengao, W. Yu, H. Yang, Z. Man, Y. Cao, Effect of ferritic hot rolling process on microstructure and properties of IF steel. *Mater. Sci. Forum.* **993**, 505–512 (2020)

4. C.-Y. Qiu, L. Li, L.-L. Hao, J.-G. Wang, X. Zhou, Y.-L. Kang, Effect of continuous annealing temperature on microstructure and properties of ferritic rolled interstitial-free steel. *Int. J. Min. Metall. Mater.* **25**(5), 536–546 (2018)
5. M. Sehhath, A. Mahdianikhotbesara, M. Hadad, Formability Investigation for Perforated Steel Sheets. SAE MobilityRxiv. Preprint. submitted September 28, (2021). <https://doi.org/10.47953/SAE-PP-00182>
6. R.K. Ray, J.J. Jonas, R.E. Hook, Cold rolling and annealing textures in low carbon and extra low carbon steels. *Int. Mater. Rev.* **39**(4), 129–172 (1994)
7. P. Ghosh, C. Ghosh, R.K. Ray, D. Bhattacharjee, Precipitation behavior and texture formation at different stages of processing in an interstitial free high strength steel. *ScriptaMaterialia*. **59**(3), 276–278 (2008)
8. A. Elsner, R. Kaspar, D. Ponge, D. Raabe, S. Vander Zwaag, Recrystallization texture of cold rolled and annealed IF steel produced from ferritic rolled hot strip. *Mater. Sci. Forum.* **467–470**, 257–262 (2004)
9. A.-H. Bui, H. Le, Strength and microstructure of cold-rolled if steel. *Acta MetallurgicaSlovaca*. **22**(1), 35–43 (2016)
10. Z.-D. Wang, Y.H. Guo, Z. Zhao, X.-H. Liu, G.-D. Wang, Effect of processing condition on texture and drawability of a ferritic rolled and annealed interstitial-free steel. *J. Iron Steel Res. Int.* **13**(6), 60–65 (2006)
11. H. Pan, X. Shen, D. Li, Y. Liu, J. Cao, Y. Tian, H. Zhan, H. Wang, Z. Wang, Y. Xiao, Effect of annealing process on microstructure, texture, and mechanical properties of a Fe-Si-Cr-Mo-C deep drawing dual-phase steel. *Curr. Comput.-Aided Drug Des.* **10**, 777–793 (2020)
12. J. Pero-Sanz, M. Ruiz-Delgado, V. Martinez, J.I. Verdeja, Annealing textures for drawability: influence of the degree of cold rolling reduction for low-carbon and extra low-carbon ferritic steels. *Mater. Charact.* **43**, 303–309 (1999)
13. S. Hoile, Processing and properties of mild interstitial free steels: a review. *Mater. Sci. Technol.* **16**, 1079–1093 (2000)
14. K. Zheng, Z. Jie, L. Hongbo, K. Ning, Effects of continuous annealing process parameters on the microstructure and mechanical properties of dual phase steel. *Steel Res. Int.* **89**(8), 1800034 (2018)
15. A.C.S. Reddy, S. Rajesham, P.R. Reddy, A.C. Uma Maheshwar, Formability: a review on different sheet metal tests for formability, in *International Conference on Multifunctional Materials (ICMM-2019)*, Hyderabad, India. 19–21 Dec, pp. 1–5 (2019)
16. K.K. Alaneme, E.A. Okotete, Recrystallization mechanisms and microstructure development in emerging metallic materials: A review. *J. Sci.: Adv. Mater. Dev.* **4**(1), 19–33 (2019)
17. P.R. Rios, F. Siciliano Jr., H.R. Sandim, R.L. Plaut, A.F. Padilha, Nucleation and growth during recrystallization. *Mater. Res.* **8**(3), 225–238 (2005)
18. J. Hu, X. Wang, J. Zhang, J. Luo, Z. Zhang, Z. Shen, A general mechanism of grain growth: I. Theory. *J. Materiomics*. **7**, 1007–1013 (2021)
19. J. Wang, J. Li, X. Wang, X. Mi, S. Zhang, Rapid heating effects on grain-size, texture and magnetic properties of 3% Si non-oriented electrical steel. *Bull. Mater. Sci.* **34**(7), 1477–1482 (2011)
20. M. Holscher, D. Raabe, K. Lucke, Rolling and recrystallization textures of body centered cubic steels. *Steel Res.* **62**(12), 567–576 (1991)
21. M.R. Barnett, J.J. Jonas, Influence of ferrite rolling temperature on grain size and texture in annealed low C and IF steels. *ISIJ Int.* **37**, 706–714 (1997)

Publisher's Note Springer Nature remains neutral with regard to jurisdictional claims in published maps and institutional affiliations.

D. Satish Kumar

E-mail : dabbirusk@gmail.com

Phone : 91 – 09449598273

Years of Experience : +17 Years

Current Position : General Manager – R&D, JSW Steel Ltd, India

Personal Information

Date of birth : 11th July' 1979

Father's Name : Late Shri. D. Govind Rao

Present Address : R3/8, Vidyanagar, JSW Steel Township, Toranagallu, Dist - Bellary, (Karnataka) 583275

Academia

B.E. (Hons.): Metallurgical Engineering,
National Institute of Technology, Raipur, CG, India (2001)

M.Tech: Materials and Metallurgical Engineering,
Indian Institute of Technology, Kanpur, India (2003)

IPR

Patents : 17

Copyrights : 9

Journal Publications : 55

Conference Proceedings : 90

Awards and Honors

National Young Metallurgist of the Year, NMD ATM - 2007 - Awarded by Ministry of Steel, Govt. of India

Sail Gold Medal – Co-Author, NMD ATM – 2012 - Awarded by Indian Institute of Metals

Golden Peacock Innovative Product/Service Award' - 2016 (JSW Steel) for Conversion of Granulated Blast Furnace Slag into Fine Aggregate

Editor's Choice Article – 2018 - Journal of Failure Analysis and Prevention

National Energy Efficiency Innovation Award - 2021 - Awarded by Ministry of Power, Govt. of India